**Universidade de Aveiro** Departamento de Engenharia Mecânica
**Ano 2013**

**Bruno Cardoso Lamas**

# Desenvolvimento e caracterização de nanofluidos para intensificação de transferência de calor

# Nanofluids development and characterization for heat exchanging intensification

**Universidade de Aveiro** Departamento de Engenharia Mecânica
**Ano 2013**

**Bruno Cardoso Lamas**

# Desenvolvimento e caracterização de nanofluidos para intensificação de transferência de calor

Tese apresentada à Universidade de Aveiro para cumprimento dos requisitos necessários à obtenção do grau de Doutor em Engenharia Mecânica, realizada sob a orientação científica do Doutor Nelson Amadeu Dias Martins, e da Doutora Mónica Sandra Abrantes de Oliveira Correia, Professores Auxiliares do Departamento de Engenharia Mecânica da Universidade de Aveiro

Apoio financeiro da FCT e do FSE no âmbito do III Quadro Comunitário de Apoio.

“*I cannot teach anybody anything. I can only make them think.*” - Socrates

**o júri**

presidente

Prof. Doutor Fernando Manuel Bico Marques
professor catedrático da Universidade de Aveiro

Prof. Doutor Mário Manuel Gonçalves da Costa
professor associado com agregação do Instituto Superior Técnico da Universidade de Lisboa

Prof. Doutor Vítor António Ferreira da Costa
professor associado com agregação da Universidade de Aveiro

Prof. Doutor Abel Gomes Martins Ferreira
professor auxiliar da Faculdade de Ciências e Tecnologia da Universidade de Coimbra

Prof. Doutor Nelson Amadeu Dias Martins
professor auxiliar da Universidade de Aveiro

**agradecimentos**

I express my gratitude to my supervisors Dr Nelson Martins, and Dr. Mónica Oliveira, Assistant Professors at the Department of Mechanical Engineering from the University of Aveiro, for their valuable guidance, assistance and inspiration.

I am also very grateful to Dr. Maria Fonseca, and MSc. Bruno Abreu, Research fellows at the Department of Mechanical Engineering from the University of Aveiro, for their assistance during the nanofluids engineering and thermal conductivity assessment.

In addition, I want to express my sincere acknowledge to Dr. Helena Nogueira, and Dr. Celeste Azevedo from University of Aveiro for their support with the spectroscopic studies (FTIR), to Dr. Sandra Magina from University of Aveiro for her support with the thermo gravimetric analysis (TGA), and to Eng. Pedro Prazeres for his assistance with the analytical centrifuge measurements.

I also acknowledge Fundação para a Ciência e Tecnologia (FCT) and Fundo Social Europeu (FSE), for the financial support through the individual grant (SFRH/BD/6445/2009).

**palavras-chave**

nanofluidos, condutividade térmica, nanotubos de carbono, estabilidade coloidal, teoria do meio efetivo, teoria do meio efetivo diferencial

**resumo**

A desmaterialização da economia é um dos caminhos para a promoção do desenvolvimento sustentável na medida em que elimina ou reduz a utilização de recursos naturais, fazendo mais com menos. A intensificação dos processos tecnológicos é uma forma de desmaterializar a economia. Sistemas mais compactos e mais eficientes consomem menos recursos. No caso concreto dos sistemas envolvendo processo de troca de calor, a intensificação resulta na redução da área de permuta e da quantidade de fluido de trabalho, o que para além de outra vantagem que possa apresentar decorrentes da miniaturização, é um contributo inegável para a sustentabilidade da sociedade através do desenvolvimento científico e tecnológico.

O desenvolvimento de nanofluidos surge no sentido de dar resposta a estes tipo de desafios da sociedade moderna, contribuindo para a inovação de produtos e sistemas, dando resposta a problemas colocados ao nível das ciências de base. A literatura é unânime na identificação do seu potencial como fluidos de permuta, dada a sua elevada condutividade, no entanto a falta de rigor subjacente às técnicas de preparação dos mesmos, assim como de um conhecimento sistemático das suas propriedades físicas suportado por modelos físico-matemáticos devidamente validados levam a que a operacionalização industrial esteja longe de ser concretizável.

Neste trabalho, estudou-se de forma sistemática a condutividade térmica de nanofluidos de base aquosa aditivados com nanotubos de carbono, tendo em vista a identificação dos mecanismos físicos responsáveis pela condução de calor no fluido e o desenvolvimento de um modelo geral que permita com segurança determinar esta propriedade com o rigor requerido ao nível da engenharia. Para o efeito apresentam-se métodos para uma preparação rigorosa e reprodutível deste tipo de nanofluido assim como das metodologias consideradas mais importantes para a aferição da sua estabilidade, assegurando deste modo o rigor da técnica da sua produção. A estabilidade coloidal é estabelecida de forma rigorosa tendo em conta parâmetros quantificáveis como a ausência de aglomeração, a separação de fases e a deterioração da morfologia das nanopartículas.

Uma vez assegurado o método de preparação dos nanofluídos, realizou-se uma análise paramétrica conducente a uma base de dados obtidos experimentalmente que inclui a visão central e globalizante da influência relativa dos diferentes fatores de controlo com impacto nas propriedades termofísicas. De entre as propriedades termofísicas, este estudo deu particular ênfase à condutividade térmica, sendo os fatores de controlo selecionados os seguintes: fluido base, temperatura, tamanho da partícula e concentração de nanopartículas. Experimentalmente, verificou-se que de entre os fatores de controlo estudados, os que maior influência detêm sobre a condutividade térmica do nanofluido, são o tamanho e concentração das nanopartículas.

Com a segurança conferida por uma base de dados sólida e com o conhecimento acerca da contribuição relativa de cada fator de controlo no processo de transferência de calor, desenvolveu-se e validou-se um modelo físico-matemático com um caracter generalista, que permitirá determinar com segurança a condutividade térmica de nanofluidos.

**keywords**

nanofluids, thermal conductivity, carbon nanotubes, colloidal stability, effective medium theory, differential effective medium theory

**abstract**

The economy dematerialization is a means to promote sustainable development as it eliminates or reduces the use of natural resources. Hence, the intensification of technological processes is a way to dematerialize the economy. More compact and efficient systems require fewer resources. In what concerns technological systems involving heat exchange processes, intensification results in the reduction of the exchanging area and amount of working fluid, which in addition to other advantages inherent to systems' miniaturization, is a direct contribution of the scientific and technological development to a more sustainable society.

The development of nanofluids is a response to such challenges of contemporary society, contributing to the innovation of products and systems by solving fundamental questions raised at the level of basic sciences. The available literature is unanimous identifying nanofluids potential as an engineering thermal fluid due to their thermo-physical properties, namely a high thermal conductivity. However, the lack of rigorous preparation techniques as well as of a systematic knowledge of their thermo-physical properties, supported by validated physical-mathematical models, are serious constrains to their use in engineering applications.

In this work, the thermal conductivity of carbon nanotubes, water based nanofluids were systematically studied. The governing physical mechanisms for heat conduction in the nanofluid were established as the basic condition for the development of a general model able to securely determine this property with the precision required in engineering applications. For this purpose the methodologies to correctly prepare such nanofluids in a reproducible way as well as to measure their long term stability are presented. The colloidal stability is accurately established and quantified taking into account parameters such as the absence of agglomeration, separation of phases and deterioration of the morphology of the nanoparticles.

A parametric analysis was developed through appropriate DOE methodologies in order to build a comprehensive data base of the nanofluid physical properties as a function of control factors, previously identified variables considered to have the greatest impact on the variability of thermo-physical properties. Among the latter, this work gives particular attention to the acquisition of thermal conductivity data against the selected control factors: base fluid, temperature, size and concentration of nanoparticles. It was verified experimentally that amongst these control factors, those that hold the greatest influence on the thermal conductivity of the nanofluid are the size and concentration of nanoparticles.

A solid database and the awareness about the relative contribution of each mechanism controlling the heat transfer process in nanofluids successfully supported the development and validation of a general physical-mathematical model to determine the thermal conductivity of nanofluids.

# TABLE OF CONTENTS

# LIST OF FIGURES

## Appendix

# LIST OF TABLES

Appendix

# NOMENCLATURE

| | |
|---|---|
| $A$ | Area [m²] |
| $a$ | Radius [m] |
| $A_{cs}$ | Cross section area [m²] |
| Al | Aluminium |
| $Al_2O_3$ | Alumina |
| Au | Gold |
| $B$ | Average number of particles in contact to a given particle (collisions) |
| $C_d$ | Drag coefficient |
| CNT | Carbon nanotube |
| C-TWN | Coated transient hot-wire |
| Cu | Copper |
| CuO | Cupric oxide |
| $c_v$ | Specific heat [kJ/kg K] |
| $d$ | Diameter [m] |
| $D$ | Diffusion coefficient [m²/s] |
| DW | Distilled water |
| EDEMT | *Extended differential effective medium theory* |
| EG | Ethylene glycol |
| EMT | *Effective medium theory* |
| EO | Engine oil |
| EVT | *Excluded volume theory* |
| $F$ | Force [N] |
| $f_{error}$ | Fractional error |
| Fe | Iron |
| $G$ | Interfacial thermal conductance [W/m² K] |
| $g$ | Gravitational acceleration constant [m/s²] |
| $\Delta G$ | Variation of the free energy of Gibbs [kJ] |
| $h$ | Convection coefficient [W/m²K] |
| $H_{BM}$ | Hindered Brownian rate [mm/day] |
| $H_{ratio}$ | Hindered ratio |
| $k$ | Thermal conductivity [W/mK] |
| $k_B$ | Boltzmann constant 1.38x10$^{-23}$ [m² kg/ s²] |
| $k^{eq}$ | Equivalent thermal conductivity [W/m K] |
| $L_{ii}$ | Depolarization factors of the particle along the *ii* axes |
| $l$ | Length [m] |
| $m$ | Mass [kg] |
| $m_c$ | constant of proportionality achieved in the phase separation rate analysis |
| *mse* | Mean square error |
| MWCNT | Multi-walled carbon nanotube |
| $n$ | Number |
| $Pr$ | Prandtl number |
| $Q$ | Heat [W] |
| $R$ | Resistance [m² K/W] |
| $Re$ | Reynolds number |
| S | Surface |

| | |
|---|---|
| $SiO_2$ | Silicon dioxide |
| SWCNT | Single-walled carbon nanotube |
| $T$ | Temperature [K] |
| $t$ | Time [s] |
| $TiO_2$ | Titanium dioxide |
| TWN | Transient hot-wire |
| $v$ | Relative velocity [m/s] |
| V | Volume |
| $v_s$ | Settling velocity [m/s] |
| $\langle V_{ex} \rangle$ | Total excluded volume of a suspension inside a control volume |
| $\langle V \rangle$ | Excluded volume of a suspended particle |

*GREEK SYMBOLS*

| | |
|---|---|
| $\Delta$ | Difference |
| $\alpha$ | Bending angle [rad] |
| $\beta$ | Dynamic friction [kg/s] |
| $\delta$ | Nano-layer thickness [m] |
| $\zeta$ | Zeta potential |
| $\vartheta$ | Colatitude angle of the spherical coordinates |
| $\kappa$ | Bending buckling [rad/Å] |
| $\mu$ | Dynamic viscosity [Pa s] |
| $\xi$ | Displacement of the particle [m] |
| $\rho$ | Mass density [kg/m³] |
| $\sigma$ | Standard deviation |
| $\varphi$ | Azimuth angle of the spherical coordinates |
| $\phi$ | Volume fraction [%] |
| $\chi$ | Sphericity of the particle |

*SUBSCRIPTS*

| | |
|---|---|
| *bf* | Base fluid |
| *c* | Critical or at the percolation threshold |
| *cl* | Cluster |
| *cv* | Control volume |
| *d* | Drag |
| *eff* | Effective |
| *eq* | Equivalent |
| *K* | Kapitza |
| *layer* | Interfacial layer solid particle-medium |
| *p* | Particle |
| *s* | Stochastic |
| *xx* | Transverse axis of the elongated particles |
| *yy* | Transverse axis of the elongated particles |
| *zz* | Longitudinal axis of the elongated particles |
| $\alpha$ | Bending angle |

# 1 INTRODUCTION

## 1.1 CHAPTER SYNTHESIS

Nanofluids are suspensions of nanoparticles in conventional base fluids. With the appropriate nanoparticle size and volume fraction, nanofluids present an enhancement in the effective heat transfer coefficient when comparing with the base fluid. The main objective of this work is to develop and characterize carbon nanotube based nanofluids for thermal engineering applications. A literature survey focus on recent research developments on nanofluids for thermal applications, showed that there are controversial theories to explain measured anomalous thermal conductivity enhancement of nanofluids, namely Brownian motion, nanoparticles agglomeration and nano-layering ordering, thus further work is required to understand and predict nanofluids thermal properties. In this Chapter, the research objectives and contribution of the thesis are outlined supported by a comprehensive literature review.

## 1.2 BACKGROUND AND MOTIVATION

Sustainable development usually requires system dematerialization, which leads to processes intensification and particularly to heat transfer intensification. High performance thermal fluids, such as nanofluids, are a practical way to intensify heat transfer processes in compact (dematerialized) systems, thus it may be claimed that thermal nanofluids research is a need for humankind sustainable development. An example is the continuous advances on electronic devices which increased the demand for new engineering solutions to improve the effectiveness of heat transfer, mainly in what concerns to compact or miniaturized systems. It is well known that the performance of many of these systems or devices strongly depends on their cooling technology. Therefore, the intensification of the heat transfer rate in compact cooling systems is a key factor for the continuous development of these systems.

Regarding the *Newton's law of cooling* (Equation 1.1), such improvements can be achieved through the increase of the temperature difference ($\Delta T$), heat exchanger area ($A$), and convective coefficient ($h$) (INCROPERA et al., 2006).

$$Q = h \cdot A \cdot \Delta T \qquad 1.1$$

with

$$h = \frac{Nu \cdot k}{L} \qquad 1.2$$

where $Q$ is the heat flow, $Nu$ is the flow Nusselt number, $k$ is the fluid heat transfer conductivity and $L$ is a characteristic dimension of the system.

The increase on temperature difference may be limited by the process or materials constrains. Therefore, a common strategy is through the maximization of the exchange surface area (for a given geometry and boundary conditions). However, this maximization generally leads to the increase of the overall volume of the heat exchanger, that may be limited by miniaturization or intensification constrains. Some new technologies in this field are being developed, *e.g*. the microchannel heat exchangers with improved surface-to-volume ratio, phase change devices such as heat pipes, vortex generators, among others (KHAN et al., 2011, MOHAMMED et al., 2011, SIDDIQUE et al., 2010).

Another method is through the increase of the heat transfer coefficient of the operant fluid. This is usually achieved by a significant increase of fluid velocity, acting on the Nusselt number (*Nu*), which produces a rise on the required pumping power. However, the poor thermal properties of conventional working fluids (*e.g.* water, ethylene glycol and a typical dielectric fluid, such as polyalphaolefin) are still major barriers for the innovation on the geometry of heat exchangers and their miniaturization. In Table 1.1, thermo-physical properties of conventional working fluids are presented.

Table 1.1: Thermo-physical properties of water and ethylene glycol at room temperature (ASHRAE, 2005, INCROPERA et al., 2006).

| Thermo-physical property | Water | Ethylene glycol | Polyalphaolefin |
|---|---|---|---|
| Thermal conductivity [W/m·K] | 0.613 | 0.252 | 0.145 |
| Dynamic viscosity [Pa·s] | 0.001 | 0.016 | 0.999 |
| Density [g/cm³] | 0.997 | 1.114 | 0.890 |
| Specific heat capacity [kJ/kg·K] | 4.179 | 2.415 | 1.868 |

An additional strategy for heat transfer intensification is through increasing the thermo-physical properties of conventional fluids, to enhance their convective coefficient, independently of the fluid flow characteristics. It is a fact that fluids present considerably lower thermal conductivity than solid materials, as can be depicted from Figure 1.1. It seems quite evident that the mixture of conductive solid particles in conventional fluids may improve the conduction of the suspension.

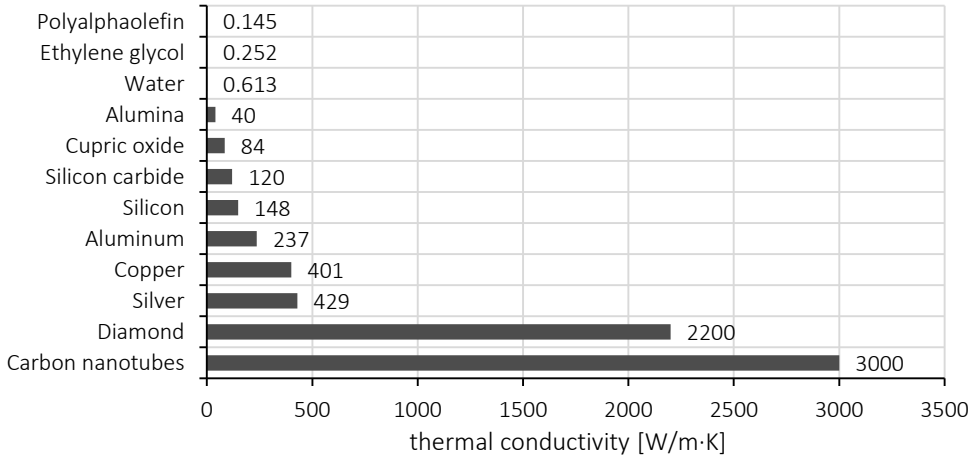


Figure 1.1: Thermal conductivities of common solids and liquids, at room temperature (EASTMAN et al., 2004).

Theoretical and experimental studies on increasing conduction properties of liquids, by suspending millimetre or micrometre sized particles, have been conducted by Maxwell more than a century ago. From his work emerged the *effective medium theory* (EMT), the classical theory, suggesting the thermal diffusion in both phases as the main mechanism governing the thermal conductivity enhancement (MAXWELL, 1873).

As the theory of Maxwell only reflects on very dilute suspensions of non-interacting spherical particles, several models based on the EMT were proposed by different authors. These upgraded classical models add to the EMT the effect produced by the particle shape, their possible interaction for higher concentrations, and a thermal interface resistance at the solid particles surface (BRUGGEMAN, 1935, DAVIS, 1986, FRICKE, 1924, HAMILTON et al., 1962, HASHIN et al., 1962, HASSELMAN et al., 1987, JEFFREY, 1973).

However, the incorporation of micro sized particles present a rapid sedimentation due to their high volume or size. This causes clogging of the flow channels, surface abrasion, increased pressure drop, and a fast decay of the engineered thermo-physical properties(HAMILTON et al., 1962, MAXWELL, 1873).

In 1995, Choi *et al.* reported that an innovative class of heat transfer fluids could be engineered by suspending nanoparticles in conventional fluids, appearing for the first time the word *nanofluid*. They reported a dispersion of metallic nanoparticles in the base fluid with exciting improvements on the effective thermal conductivity at very low concentrations (CHOI et al., 1995). This is an important issue, since a small amount of particles produces a relatively low enhancement on the viscosity, leading to minor pressure drop penalty. Since then, theoretical and experimental

researches on nanofluids have gained considerable interest. Some of the advantages announced for the application of nanofluids include the following (DING et al., 2006):

1. Increased thermal conductivity (probably higher than that predicted through classical theories);
2. Possibility to achieve good stability conditions;
3. Low pressure drop penalty;
4. Low probability of heat exchange surface abrasion;
5. Possibility to be introduced in current thermal systems technologies.

Among the thermo-physical properties of nanofluids, thermal conductivity is, perhaps, the most studied over the past years. This is referred by several researchers as anomalously high, and not described by the EMT (CHOI et al., 2001, EASTMAN et al., 2001). Several theories have been recently proposed in an attempt to model the thermal conductivity for these next-generation engineering fluids, but, apparently, without success (LEE et al., 2010). As expected, divergences on the proposed theories resulted on the publication of several predictive models with different premises, causing unrelated results, and lack of confidence on the effective thermo-physical properties predicted.

Particles at nanoscale may exhibit physical properties different from those of the corresponding bulk solids. In addition, chemical composition, size, shape and surface characteristics also play an important role on their effect on the respective nanofluid physical properties. At the nanoscale, the percentage of atoms at the surface of the material becomes significant, presenting a high surface-to-volume ratio. This provides a superior thermal, mechanical, optical, magnetic, and electric properties when comparing to those of the corresponding bulk solids (DUNCAN et al., 1989, XUAN et al., 2000). Furthermore, a strong interaction of the surface of non-agglomerated nanoparticles with the solvent may overcome density differences, making it possible to produce stable suspensions (HILDING et al., 2003, NASIRI et al., 2011).

For these reasons, it is expected that nanofluids come to be a new class of heat transfer fluids. These are formed by dispersed nanoparticles in conventional fluids, and present significant improvements in the effective thermo-physical properties comparing with those of the base fluid. A stable suspension of nanoparticles in a conventional fluid significantly reduces the severe clogging problems evidenced using micrometre particles (CHOI, 1998). A successful employment of nanofluids will support the current trend toward component miniaturization and sustainable

development by enabling the design of smaller and lighter heat exchangers, and improving the energy efficiency in industrial processes and systems development.

## 1.3 STATEMENT OF THE PROBLEM

At present, the known literature does not present a consensual and robust model capable of predicting the thermal conductivity of a generic nanofluid with an acceptable level of accuracy for engineering purposes. Furthermore, from the experimental results of many researchers, it is known that the thermal conductivity of nanofluids may depend on several parameters, including the nanoparticles geometry and spatial distribution, their volume fraction, base fluid type, and temperature. However, given the lack of an experimental parametric assessment to this property, the need for further work into this promising research field is emphasised.

A comprehensive experimental research programme, supported by a well-designed parametric study is a pre-condition to experimentally identify the mechanisms responsible for heat conduction phenomena in nanofluids, being the basis for the definition and validation of a general physical model able to assess thermal conductivity of nanofluids.

It is of utmost importance the availability of reliable predictive models of nanofluids physical properties, namely for thermal conductivity, in order to support their introduction towards industrial applications. Such models are also essential to accelerate the production of nanofluids without the need of a strong support of experimental work.

A reliable predictive model of nanofluids thermo-physical properties is a fundamental requirement to support the engineering and integration of nanofluids in the future energy systems.

## 1.4 THESIS OBJECTIVES AND RESEARCH QUESTIONS

The main objective of this work is to develop and characterize carbon nanotubes based nanofluids useful for thermal engineering applications.

The available literature reports that the addition of conductive nanoparticles to conventional fluids produces significant increases in their heat conduction capacity. However, sample preparation is not an easy or straight-forward task, and requires the application of specific techniques to ensure acceptable stability levels. This feature is recognized by the scientific community as essential to ensure the quality of the thermo-physical properties' assessment. Therefore, the development of

an adequate methodology to produce carbon nanotubes based nanofluids with confirmed long term stability is a primary objective of this work

In addition, it is intended to identify the inherent mechanisms responsible for heat conduction in nanofluids, and a physical predictive model for the effective thermal conductivity will also be developed and experimentally validated. To this end, on a first analysis, the nanofluids will be designed and tailored through the use of available theoretical models. Thermal characterization of nanofluids will be achieved through experimental parametric analysis where special attention will be given to the base fluid type, nanoparticles size and geometry, volume fraction of nanoparticles, and temperature.

The proposed research work contributes to the worldwide scientific knowledge answering to the following questions:

1. What are the stability conditions to achieve long-term CNT based nanofluids for thermal applications?
2. What are the most important inherent physical mechanisms responsible for the effective thermal conductivity improvement showed by such CNT based nanofluids?
3. Is it possible to predict the thermal conductivity of CNTs based nanofluids through a general physical-mathematical model?

Therefore, the ultimate aim of this research work is the development and validation of a physical based mathematical model representative of CNTs based nanofluids thermal conductivity as a function of the different parameters affecting this thermal property. The acquired experimental data and knowledge regarding the heat transfer mechanisms in nanofluids will contribute to their dissemination in engineering applications, both at the fundamental and engineering levels.

## 1.5 LITERATURE REVIEW

In the following Sections, it is presented a literature survey of the subjects in the preparation of nanofluids and their stability, and the most important researches on their thermal conductivity behaviour.

### 1.5.1 PREPARATION OF NANOFLUIDS

As previously stated, nanofluids are suspensions of nanoparticles in conventional thermal base fluids. With the appropriate nanoparticle size and volume fraction, they can show an enhancement

in the effective heat transfer coefficient of the mixture (CHOI et al., 2001, CHOI et al., 1995, EASTMAN et al., 1997, EASTMAN et al., 2001).

Several nanoparticles have been documented in the literature for the preparation of nanofluids for thermal management. Among them, the most common are copper (Cu), cupric oxide (CuO), alumina ($Al_2O_3$), gold (Au), iron (Fe), titanium dioxide ($TiO_2$), silicon dioxide ($SiO_2$), and carbon nanotubes (CNTs). The typically studied base fluids are the distilled water (DW), ethylene glycol (EG), and engine oil (EO).

CNTs are allotropes of carbon with cylindrical nanostructure, exhibiting extraordinary strength and unique electrical and thermal properties (IIJIMA, 1991). These are usually categorized as single-walled nanotubes (SWCNTs) and multi-walled nanotubes (MWCNTs), as schematically represent in Figure 1.2. Since their discovery in 1991, research on growth, characterization, and application development has exploded (MEYYAPPAN, 2004). A well-known CNTs synthesis is the catalytic chemical vapour deposition (CCVD). Through this method, it is possible to synthesize CNTs with controlled lengths and diameters, respectively through the manipulation of the chemical reaction time, and on the molecular entity used in the synthesis process. Furthermore, this method also enables the production of high quantities of pure CNTs (JOSE-YACAMAN et al., 1993). Other synthesis approaches have been extensively researched, including arc-discharge, laser ablation, pyrolysis and enhanced plasma vapour deposition. The arc-discharge technique is usually applied for the production of CNTs with significantly lower diameters, as the SWCNTs, despite being an expensive technique due to smaller production quantities (HERNADI et al., 1996, KEIDAR et al., 2004, MERCHAN-MERCHAN et al., 2010, SCHNITZLER et al., 2008).

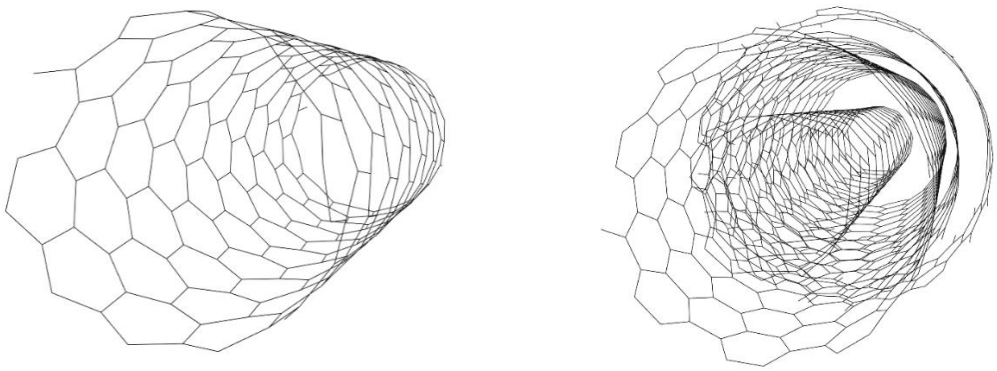

a) b)

Figure 1.2: Schematic representation of a SWCNT a) and a MWCNT b).

The methods for nanofluids production are generally summarized into two categories, *one-step* approach and *two-step* method. The first involves the formation of the nanoparticles from molecular entities directly within the base fluid. The *two-step* approach consists on the fragmentation of massive particles into smaller ones, being then dispersed in a second process step (DAS et al., 2008, GOPALAKRISHNAN, 1995, RAAB et al., 2011).

#### *1.5.1.1 ONE-STEP METHOD*

The one-step method consists in the formation of nanofluids through physical or chemical reactions. In this, the nanoparticles are created directly within the base fluid, *i.e.* the nanoparticles are simultaneously produced and dispersed in the fluid. Therefore, it is avoided the process of drying, storage, and transport, thereby minimizing agglomeration of the nanoparticles (LI et al., 2009).

Eastman *et al.* has established a physical method in which Cu vapour was directly condensed into nanoparticles by contact with a flowing low-vapour-pressure liquid, producing stable CuO-DW and Cu-EG nanofluids (EASTMAN et al., 1997, EASTMAN et al., 2001). In 2004, Zhu *et al.* presented a method consisting on microwave irradiation, through which obtained a non-agglomerated and stable Cu-EG nanofluid by the hydrothermal chemical reduction of salts (ZHU et al., 2004). Nanofluids stable for over a month, consisting of monodispersed silver nanoparticles on mineral oil were also prepared by this method (BÖNNEMANN et al., 2005). Another method, based on a vacuum submerged arc nanoparticle synthesis has been applied to produce nanofluid with non-agglomerated nanoparticles of different shapes. Lo *et al.* prepared CuO, $Cu_2O$, and Cu based nanofluids with this technique (LO et al., 2005). Yu *et al.* presented another *one-step* method for the preparation of graphene oxide colloids through a phase transfer approach (YU et al., 2011). CNTs based nanofluids may also be obtained via a one-step technique, namely through the carbon plasma-discharge directly in water (HSIN et al., 2001).

The major advantage of the *one-step* approach relies in the nanoparticles agglomeration minimization. This is essential to ensure better stability of the sample. However, this technique has limitations on the sample size, making this method expensive for mass production. Particle size control is also an issue when employing this technique. Furthermore, usually some residual reactants are left in the nanofluids due to incomplete reaction. These are noise effects that prevent an accurate characterization of the thermo-physical properties and, moreover, may limit the applicability of the nanofluids (LEE et al., 2010).

#### *1.5.1.2 TWO-STEP METHOD*

In the *two-step* method, the preparation of nanofluids is processed by suspending previously synthetized nanoparticles, into base fluids in a second processing step. Since this method requires the isolate preparation of nanoparticles, agglomeration may take place in both steps, *i.e.* nanoparticle synthesis and/or dispersion step. Therefore, to avoid agglomeration, it is necessary an earlier separation of the nanoparticles. This can be achieved through physical or chemical techniques (DAS et al., 2008).

Commonly, the first step is designated by *nanoparticles stabilization*, and the second by *nanoparticles dispersion*. When used, *nanoparticles stabilization* requires the application of specific techniques, described in the following Section. On the other hand, *nanoparticles dispersion* is, generally attained by the application of low periods of ultrasonication and/or magnetic-stirrer mixing. (DAS et al., 2008).

Compared with the *one-step* method, this approach has been more commonly used by researchers in the nanofluid field. Since the nano-powder synthesis techniques have already been scaled up to industrial production levels, the *two-step* method is seen as the most economical to produce nanofluids in large scale. The major disadvantage of this method is that the addition of dispersants or stabilizers, used for colloidal stability improvement, may affect the thermal conductivity of the nanofluid. CNTs nanofluids are typically tailored via the two-step method (NASIRI et al., 2011).

### 1.5.2 NANOFLUIDS STABILITY

The production of a stable suspension of nanoparticles is still a technical challenge. The high surface-to-volume ratio of the nanoparticles induces strong van der Waals interparticle interactions (CAO, 2004, GHADIMI et al., 2011a, MEYYAPPAN, 2004). These interactions, associated with the Brownian movement, cause the aggregation of the nanoparticles, which begin to behave as micrometre particles. This will result in the settlement and clogging of the channels, but also in the decreasing of the thermal conductivity of the nanofluid (FEDELE et al., 2011, MEIBODI et al., 2010). Therefore, the research on nanofluids stability is of major importance for their thermo-physical properties assessment.

#### 1.5.2.1 MODES OF NANOPARTICLES STABILIZATION

Particle agglomeration may be prevented by balancing the interparticle attractive forces through electrostatic or steric repulsion (BOTHA, 2007, MISSANA et al., 2000, POPA et al., 2010).

Electrostatic repulsions may be induced through physical methods, such as ultrasonication, ball milling or high speed shearing (DAS et al., 2003a, DAS et al., 2003b, EASTMAN et al., 1997, XUAN et al., 2000). These methods induce electric charges on the nanoparticle surface, guaranteeing kinetic stability. However, these are recognized by the destruction that they cause to the nanoparticles. For instance, when subjecting CNTs to high ultrasonication periods, their average length could be reduced by 65%. Moreover, ball-milling and high-speed shear cause the opening of CNT the sidewalls. Shorter CNTs are less suitable to entangle (HILDING et al., 2003).

On the other hand, steric repulsions may be employed through chemical methods. These include both surfactants and covalent functionalization techniques, that cause a hydrophobic-to-hydrophilic conversion of the surface of the nanoparticles (GHADIMI et al., 2011b, JIN et al., 2009, WONG et al., 2002, XUAN et al., 2000). It should be noted that both methods may change the pH value of the samples.

Surfactants, or dispersants, are easy and economic methods for nanoparticles stabilization enhancing the stability of nanofluids. These are positioned at the interface of the two phases, inducing a higher degree of continuity between the nanoparticles and fluid, therefore, improving the nanoparticles wettability (VAISMAN et al., 2006). Although surfactant additions are an effective way to improve the stability of nanofluids, it use might cause several problems. Their use influences the final properties of the mixture as it forms an interfacial layer between the two phases that may limit the thermal conductivity enhancement (CHEN et al., 2008, NASIRI et al., 2011). Furthermore, nanofluids are subjected to heat and cooling routine processes, leading to the degradation of the dispersant or the formation of foams (NASIRI et al., 2011). Nguyen *et al.* found that the viscosity of nanofluids may have hysteresis behaviour, possibly by the surfactant degradation which culminates in the agglomeration of the nanoparticles (NGUYEN et al., 2007).

The use of covalent functionalized nanoparticles, a surfactant-free technique for nanoparticle stabilization, is a promising approach to produce nanofluids. The most common covalent functionalization techniques are the oxidative treatments which are capable of to attach to the nanoparticles surface, oxygenating functional groups such as carboxylic and alcohol groups. This

may be achieved through chemical treatment, such as boiling nitric and sulphuric acid, or through a dielectric barrier discharge plasma. The carboxylic groups (COOH) behave as weak acids and possess ion-exchange properties, having both hydrogen acceptors and hydrogen donors. This will improve the CNTs wettability, due to a more hydrophilic surface structure, and reduce agglomeration by increasing the electrostatic repulsions that counter-balance with the Van der Waals attraction forces. However, this will also change the isoelectric point (pH) of the dispersion, producing a pH value lower than that of the base fluid. Moreover, both carboxyl and alcohol groups have polar properties, contributing for the solubility of the CNTs in polar solvents, such as distilled water and ethylene glycol (ESUMI et al., 1996, NASEH et al., 2010, XIE et al., 2011, XIE et al., 2003).

Despite being a common method to enhance their stability in base fluids, chemical treatment may cause the shortening of the CNTs. The length reduction of the CNTs depends on the extent and intensity of the reaction, and the new size distribution should always be determined after the functionalization procedure by scanning electron microscope (SEM) or transmission electron microscopy (TEM) in order to characterize the resulting CNTs (BALASUBRAMANIAN et al., 2005, BANERJEE et al., 2005, NASEH et al., 2010, WEPASNICK et al., 2010, YUDIANTI et al., 2011).

#### *1.5.2.2 METHODS FOR STABILITY ASSESSMENT*

The simplest and consistent method to evaluate the colloidal stability of nanofluids is the phase separation rate measurement. In this, the concentration of the nanoparticles is obtained through a specific experimental apparatus, considering the stability point when the concentration keeps constant. To test the concentration variation of the nanoparticles, sedimentation photograph, and UV-visible spectrophotometry were typically used.

The sedimentation photograph method consists of a set of cameras that photograph the nanofluids, registering the sedimentation of the nanoparticles with the time (LI et al., 2007, LISUNOVA et al., 2006).

UV-visible spectrophotometer measures the absorption or transmittance percentage of a solution or dispersion. The absorption is the ratio of the radiant flux absorbed by the nanoparticles, which is proportional to the concentration, as stated by the Beer-Lambert law (INGLE et al., 1988, RUSSEL et al., 1989). The variation of nanoparticles concentration with time can be obtained by the measurement of the absorption of nanofluids, if the nanoparticles have characteristic absorption bands in the wavelength 190-1100nm. This is a reliable method to evaluate quantitatively the

stability and concentration of nanofluids. However, the major disadvantage of this method is the long periods of measuring time required (INGLE et al., 1988, RUSSEL et al., 1989).

Another method to assess the colloidal stability of nanofluids is the Zeta potential analysis. This measures the repulsions, or zeta potential of charged particles. Since colloidal systems are stabilized by repulsion, the larger the repulsive forces between particles, the less likely they will be to come together and form an aggregate. In general, nanofluids with high absolute zeta potential (*>25mV*) are stabilized, while nanofluids with lower absolute zeta potential (*<25mV*) tend to coagulate or flocculate (LI et al., 2007, RUSSEL et al., 1989).

### 1.5.3 THERMAL CONDUCTIVITY

Among the thermo-physical properties of nanofluids, the thermal conductivity is that gathering more attention from the research community. Experimental studies to the thermal conductivity enhancement of nanofluids have been carried out during the past years. The results achieved are described as anomalously higher than the predicted by the classical models. This extraordinary property contributed the exponential interest in experimental and theoretical research on nanofluids observed in the past few years.

The classical understanding of the thermal conductivity of mixtures originates from the *effective medium theory* (EMT), which normally involves only the particle shape, volume fraction, both conductivity of the pure materials that compose the mixture, and the Kapitza resistance (BRUGGEMAN, 1935, DAVIS, 1986, HAMILTON et al., 1962, HASHIN et al., 1962, HASSELMAN et al., 1987, JEFFREY, 1973). Although this method can give good effective thermal conductivity predictions for micrometre or lager-size solid/fluid mixtures, it was reported that may fail for nanosized particles.

#### *1.5.3.1 MEASUREMENT METHODS*

The measurement of the thermal conductivity of liquids or solutions may be a difficult task, since it is necessary to establish a steady one-dimensional temperature field. To overcome this, several techniques have been presented and applied in the measurement of this property in nanofluids. The techniques for measuring the thermal conductivity can be classified into two broad categories, the *steady-state* and *transient*.

The *steady-state* method performs a measurement when the temperature of the material measured does not change with time. The disadvantages of steady-state methods are that the heat lost cannot be quantified and may give a considerable inaccuracy. Also, the free convection may set in, giving higher apparent values of the thermal conductivity. Many researchers have reported experimental studies with steady-state parallel plate method. For instance, Wang *et al.*, measured the thermal conductivity of $Al_2O_3$ in DW, EG and EO with steady-state parallel plate, registering a 12% enhancement with an absolute error less than 3% (WANG et al., 1999).

The transient techniques are preferred over the steady-state ones, since they minimize the effects of radiation, free convection and heat losses. Among the various methods available, highlights the transient hot-wire technique (THW), and temperature oscillation technique.

The THW, the most widely used method, consist of a thin metallic wire used as both a heater source and a temperature sensor inside of the electrically non-conducting liquid. The system normally involves a high thermal conductive wire, suspended symmetrically in a liquid in a vertical cylindrical container. The wire is heated by sending a current through it, and the temperature increase of the fluid, measured by the same wire, depends on the liquid thermal conductivity, which is easily calculated from the temperature-time profile of the wire. To the common sense based on the equation of Fourier, the higher the thermal conductivity, the lower the temperature rise will be detected. In this method, the effect of free convection along the wire is minimized through very short timeframe measurements, increasing the accuracy of the apparatus. Both theory and application of the modern THW technique were developed by Castro *et al.*, Kestin *et al.*, and Roder (CASTRO et al., 1976, KESTIN et al., 1978, RODER, 1981). The main drawback of this technique is the requirement for a chemical wire coating for measurements in electrically conductive fluids (NAGASAKA et al., 1981, PENAS et al., 2008).

In electrically conductive fluids, the electrical current flows through these, and the heat generation of the wire becomes ambiguous. Therefore, traditional THWs are unsuitable for measuring nanofluids composed of metal nanoparticles, since it is expected that these nanofluids become electrically conductive. Eastman *et al.* used a coated transient hot wire (C-THW) to measure the thermal conductivity of a Cu-EG reporting an enhancement up to 40%, and reproducing literature values for the base fluid with an absolute deviation less than 1.5% (EASTMAN et al., 2001).

This method is widely used by the research community of nanofluids, through the commercial analysers *KD2* and *KD2-Pro*, which have acceptable accuracy. Furthermore, these analysers have

the hot wire encapsulated in a needle, allowing the measurement of electrically conductive fluids (BUONGIORNO et al., 2009, DECAGONDEVICES, 2013).

The temperature oscillation method is based on the propagation of a temperature oscillation inside a cylindrical liquid volume. Assuming that the nanofluid is isotropic and the thermo-physical properties are uniform and constant with time, it is possible to accurately measure the thermal diffusivity and thermal conductivity. Das *et al.* measured the thermal conductivity and thermal diffusivity of $Al_2O_3$ and CuO suspension in DW with this method. The results highlight a thermal conductivity enhancement of 2% to 36% with a maximum uncertainty of 2.11% (DAS et al., 2003b).

#### *1.5.3.2 EXPERIMENTAL STUDIES*

As mentioned above, there are several types of nanoparticles used in the investigations of nanofluids. These can be categorized through their physical properties, metallic, metallic oxide, and non-metallic, or through their shape, (quasi-)spherical and non-spherical (or elongated). The latter categorization lies upon the EMT, which describes the thermal conductivity as a function of the conductivity of the pure materials who compose the mixture, and shape of the dispersed particles. According to these models, particles with higher conductivity and non-spherical shape, lead to a greater increase in the effective conductivity (BRUGGEMAN, 1935, DAVIS, 1986, HAMILTON et al., 1962, HASHIN et al., 1962, HASSELMAN et al., 1987, JEFFREY, 1973).

##### Nanofluids based on (quasi-)spherical nanoparticles

Copper and aluminium are common metal materials known for their high thermal conductivity. However, the heat transfer capacity is significantly reduced with their oxidation (*e.g.* cupric oxide and alumina), as it can be depicted from Figure 1.1. Usually, these nanoparticles are considered as quasi-spheres. Due to being less expensive, these have been the most studied nanoparticles. In Table 1.2, it is presented a summary of the highest effective thermal conductivity enhancement reported by several authors, for cupric, cupric oxide and alumina nanoparticles (as mentioned, these are generally categorized as quasi-spherical).

Table 1.2: Summary of experimental studies of thermal conductivity in metal and metal oxide spherical particles based nanofluids.

| Researchers | Particle | Base fluid | Measurement method | Stabilization and dispersion method | $\phi$ | $\frac{k_{eff}}{k_{bf}}$ |
|---|---|---|---|---|---|---|
| (EASTMAN et al., 1997) | CuO | DW | C-THW | vacuum evaporation | 5.0% | 1.60 |
| (WANG et al., 1999) | $Al_2O_3$ | DW | steady-state | ultrasonication | 3.0% | 1.12 |
| (WANG et al., 1999) | $Al_2O_3$ | EG | steady-state | ultrasonication | 8.0% | 1.40 |
| (WANG et al., 1999) | CuO | DW | steady-state | ultrasonication | 9% | 1.34 |
| (WANG et al., 1999) | CuO | EG | steady-state | ultrasonication | 15% | 1.55 |
| (XUAN et al., 2000) | CuO | DW | C-THW | surfactant | 5.0% | 1.56 |
| (XUAN et al., 2000) | Cu | EO | C-THW | surfactant | 5.0% | 1.28 |
| (EASTMAN et al., 1997) | Cu | EG | C-THW | one-step | 1.0% | 1.40 |
| (XIE et al., 2002) | $Al_2O_3$ | DW | C-THW | ultrasonication | 5.0% | 1.20 |
| (XIE et al., 2002) | $Al_2O_3$ | EG | C-THW | ultrasonication | 5.0% | 1.29 |
| (DAS et al., 2003b) | $Al_2O_3$ | DW | T. oscillation | surfactant | 4.0% | 1.10 |
| (DAS et al., 2003b) | CuO | DW | T. oscillation | surfactant | 4.0% | 1.16 |
| (LI et al., 2006) | $Al_2O_3$ | DW | steady-state | ultrasonication | 10% | 1.30 |
| (LI et al., 2006) | CuO | DW | steady-state | ultrasonication | 10% | 1.52 |
| (VENERUS et al., 2006) | $Al_2O_3$ | DW | optical | surfactant | 2.5% | 1.50 |
| (HWANG et al., 2006b) | CuO | DW | C-THW | surfactant | 1.0% | 1.05 |
| (HWANG et al., 2006b) | CuO | EG | C-THW | surfactant | 1.0% | 1.09 |
| (LIU et al., 2006) | Cu | DW | C-THW | c. functionalization | 0.2% | 1.24 |
| (ZHANG et al., 2006) | $Al_2O_3$ | DW | C-THW | ultrasonication | 15% | 1.20 |
| (YOO et al., 2007) | $Al_2O_3$ | DW | C-THW | ultrasonication | 1.0% | 1.04 |
| (LEE et al., 2008) | $Al_2O_3$ | DW | C-THW | ultrasonication | 0.3% | 1.44 |
| (OH et al., 2008) | $Al_2O_3$ | DW | C-THW | surfactant | 4.0% | 1.13 |
| (OH et al., 2008) | $Al_2O_3$ | EG | C-THW | surfactant | 4.0% | 1.10 |
| (YU et al., 2010) | Cu | EG | C-THW | ultrasonication | 0.5% | 1.46 |

Many of the researchers that studied these particles reported an almost linear increase of the heat conductivity with the volume fraction (EASTMAN et al., 2001, LEE et al., 2008, OH et al., 2008, WANG et al., 1999, XIE et al., 2002, XUAN et al., 2000, YOO et al., 2007). In contrast, other researchers observed a non-linear thermal conductivity enhancement with the volume fraction rise, describing it as an anomalous behaviour (LI et al., 2006, ZHANG et al., 2006).

Some anomalous behaviours when comparing to the EMT were also reported. Wang *et al.* measured the thermal conductivity of $Al_2O_3$ and CuO nanoparticles dispersed in distilled water (DW), ethylene glycol (EG) and engine oil (EO). The increase was different for each base fluid, suggesting a dependency on the base fluid thermo-physical properties. They suggested that the Brownian motion of the nanoparticles, which is higher for fewer viscous fluids, may describe the

observed results (WANG et al., 1999). Xuan *et al.* studied the thermal conductivity enhancement of Cu nanofluids dispersed through the application of surfactants, reporting a maximum increase of 56% for volume fractions of 5%. In this study, the results demonstrated a dependency on the base fluid and size of the nanoparticles, being suggested once again the Brownian motion may be a relevant factor affecting the heat conductivity enhancement (XUAN et al., 2000). Other authors also suggested this particle random motion to explain some of the anomalous behaviour observed regarding heat conductivity enhancement (LI et al., 2006, PATEL et al., 2003, YU et al., 2010, ZHANG et al., 2006).

Keblinski *et al.* stated that the thermal conductivity enhancement could also be explained by the fluid nano-layer at the liquid-particle interface, the thermal property of the nanoparticle and nanoparticle clustering (EASTMAN et al., 2004, KEBLINSKI et al., 2002). In the following sections, these heat conduction mechanisms will be described in detail.

Xie *et al.* investigated the effects of pH value of the suspensions, the specific surface area of the nanoparticles and the thermal conductivity of the base fluid on the resulting nanofluid heat conductivity. The observed enhancement seemed to increase with the decrease of pH values, and with the increase of nanoparticles specific surface area. Moreover, the enhancement appeared to be higher for less conductive base fluids, a contrasting behaviour from the results observed by Wang *et al.* and Xuan *et al.* (XIE et al., 2002). The pH values of the samples are associated with the interface particle-base fluid bonding, suggesting that a strengthen interface provides higher enhancement on the thermal conductivity (GHADIMI et al., 2011b, JIN et al., 2009, LEE et al., 2006).

Das *et al.* investigated the influence of the temperature on the enhancement of thermal conductivity of nanofluids of $Al_2O_3$ and CuO. The experimental results shown that the thermal conductivity rise with an increase on temperature (DAS et al., 2003b). This behaviour was also observed by other researchers (LI et al., 2006, YU et al., 2010, ZHANG et al., 2006). In contrast to these results, Venerus *et al.* measured the thermal conductivity of $Al_2O_3$-DW nanofluids, reporting no anomalous enhancement, since the observed results comply with the EMT (VENERUS et al., 2006).

In order to demystify the reported intriguing observations, several worldwide researchers participated on an international benchmark project designated as the *International Nanofluid Property Benchmark Exercise* (INPBE). Each group synthesized nanofluids of metal and metal oxide nanoparticles, according to a given dispersion methodology. The samples were then measured

through different approaches, and after data normalization, they stated that these were within the suggested upper and lower bounds of the EMT (BUONGIORNO et al., 2009). Nevertheless, the results do not disclose the mechanisms that govern the heat conduction in nanofluids, since the dispersion methodology was kept constant through the groups and, therefore, it is not expected a relevant divergence of the results. Furthermore, no predictive model was validated and the considered bonds of the EMT are referred to a perfect interfacial thermal resistance ($0\,m^2K/W$) and the existence of a thermal resistance of $10^{-7}\,m^2K/W$. As it will be shown in the next Chapter, these bonds provide a large interval where the results can certainly fit. In addition, other researchers found that nanofluids produced with such nanoparticles show a heat conductivity within EMT boundaries (CHERKASOVA, 2009, EAPEN et al., 2007, EAPEN et al., 2010, KEBLINSKI et al., 2008).

### Nanofluids based on carbon nanotubes (non-spherical or elongated nanoparticles)

Some authors experimentally compared the effective thermal conductivity of nanofluids based on spherical particles with ones based on CNTs (CHOI et al., 2001, EASTMAN et al., 2001, HWANG et al., 2006b, LIU et al., 2011, ZHANG et al., 2006). The results, summarized in Table 1.3, showed that CNTs produce higher enhancements on the conductivity when compared with the other particles.

Table 1.3: Comparison of the thermal conductivity experimentally observed between spherical particles and CNTs.

| Researchers | Particle | Base fluid | $\phi$ | $\frac{k_{eff}}{k_{bf}}$ |
|---|---|---|---|---|
| (EASTMAN et al., 2001) | Cu | EG | 1% | 1.40 |
| (CHOI et al., 2001) | MWCNT | EO | 1% | 2.50 |
| (ZHANG et al., 2006) | $Al_2O_3$ | DW | 15% | 1.20 |
| (ZHANG et al., 2006) | MWCNT | DW | 0.9% | 1.40 |
| (HWANG et al., 2006b) | CuO | DW | 1% | 1.05 |
| (HWANG et al., 2006b) | MWCNT | DW | 0.5% | 1.07 |

Such results may be explained by CNTs thermal conductivity, which has been reported as ballistic, and to the elongated shape of them, which according to the EMT produces higher enhancements (HAMILTON et al., 1962, HONE, 2002). These suggestions have been raising the interest on these nanoparticles for the production of nanofluids. In Table 1.4, it is presented a summary of the highest effective thermal conductivity reported in the literature, for CNTs based nanofluids.

Table 1.4: Summary of experimental studies of thermal conductivity in CNTs based nanofluids.

| Researchers | Base fluid | Measurement Method | Stabilization and dispersion method | $\phi$ | $\frac{k_{eff}}{k_{bf}}$ |
|---|---|---|---|---|---|
| (CHOI et al., 2001) | EO | C-THW | not specified | 1.0% | 2.50 |
| (XIE et al., 2003) | DW | C-THW | c. functionalization | 1.0% | 1.08 |
| (XIE et al., 2003) | EG | C-THW | c. functionalization | 1.0% | 1.12 |
| (XIE et al., 2003) | EO | C-THW | c. functionalization | 1.0% | 1.20 |
| (ASSAEL et al., 2005) | DW | C-THW | surfactant | 0.6% | 1.34 |
| (HWANG et al., 2006a) | DW | C-THW | ultrasonication | 1.0% | 1.11 |
| (HWANG et al., 2006a) | EG | C-THW | ultrasonication | 1.0% | 1.30 |
| (LIU et al., 2005) | EG | C-THW | ultrasonication | 1.0% | 1.12 |
| (LIU et al., 2005) | EO | C-THW | ultrasonication | 2.0% | 1.30 |
| (HWANG et al., 2006b) | DW | C-THW | surfactant | 1% | 1.07 |
| (HWANG et al., 2006b) | EO | C-THW | surfactant | 0.5% | 1.09 |
| (ZHANG et al., 2006) | DW | C-THW | surfactant | 0.9% | 1.40 |
| (DING et al., 2006) | DW | C-THW | surfactant | 1.0% | 1.80 |
| (HWANG et al., 2007) | DW | C-THW | ultrasonication | 1.0% | 1.07 |
| (HWANG et al., 2007) | EO | C-THW | ultrasonication | 0.5% | 1.08 |
| (CHEN et al., 2008) | EG | C-THW | c. functionalization | 1.0% | 1.18 |
| (WEITING et al., 2009) | R113 | transient plane source | ultrasonication | 0.2% | 1.35 |
| (WEITING et al., 2009) | DW | transient plane source | ultrasonication | 0.2% | 1.13 |
| (XIE et al., 2009) | EG | C-THW | c. functionalization | 1.0% | 1.27 |
| (GARG et al., 2009) | DW | C-THW | surfactant | 1.0% | 1.20 |
| (NASIRI et al., 2011) | DW | C-THW | c. functionalization | 0.3% | 1.10 |
| (NASIRI et al., 2011) | DW | C-THW | surfactant | 0.3% | 1.05 |
| (HARISH et al., 2012) | EG | C-THW | surfactant | 0.3% | 1.15 |

In general, all authors have reported a non-linear thermal conductivity enhancement with CNTs volume fraction, describing it as an anomalous behaviour (CHOI et al., 2001, DING et al., 2006, HARISH et al., 2012, LIU et al., 2005, WEITING et al., 2009, XIE et al., 2003, ZHANG et al., 2006). Still, some authors have reported this trend as almost linear (CHEN et al., 2008, HWANG et al., 2006a).

A large number of mechanisms have been proposed to clarify the anomalous thermal conductivity improvement of CNTs based nanofluids. It is described by the literature that the performance of the nanofluid critically depends upon size, volume fraction, and aspect ratio of the nanoparticles (CHOI et al., 2001, NAN et al., 2003, SHENOGIN et al., 2004b). In 2001, Choi *et al.* produced the first MWCNTs suspension, reporting an unusual thermal conductivity enhancement of more than 150% for 1%vol., suggesting the formation of a solid-like structure of the liquid at the interface that

enhances the heat conduction through the mixture, as previously stated for spherical particles suspensions (CHOI et al., 2001). This was also suggested by Xie *et al.,* which dispersed MWCNTs in DW and EG. It was as well verified that the size and shape of the nanotubes play key roles in the non-linear enhancement with volume fraction raising (XIE et al., 2003).

Zhang *et al.* studied the effect of temperature on the thermal conductivity of MWCNTs based nanofluids. In this study, it was found that the conductivity of nanofluids has the same slope of the base fluid conductivity with temperature (ZHANG et al., 2006). However, other authors have observed a temperature dependence of the thermal conductivity, suggesting that this may be explained by the increased Brownian movement of the nanoparticles (AMROLLAHI et al., 2008, GARG et al., 2009, LIU et al., 2005, NASIRI et al., 2011, WEITING et al., 2009, XIE et al., 2009).

Some authors also claim that the elongated geometry of CNTs allows the easily formation of local percolation structures, due to aggregation, even for lower volume fractions (BIERCUK et al., 2002, DENG et al., 2009, SHENOGINA et al., 2005, ZHONG et al., 2006). It should be noted that, percolation theory describes the degree of connectivity of chaotic systems, like suspensions of nanoparticles. This predicts the existence of a critical particle concentration threshold, characterized by the formation of a spanning cluster, even if exists some isolated nanoparticles (STAUFFER, 1979). Therefore, due to the higher aspect ratio of the CNT, a decreased percolation threshold is highly probable, originating a continuous phase even for the dispersed solid phase. Nevertheless, Cahill's research group and others researchers proved experimentally the existence of a thermal discontinuity even at volume fractions above percolation threshold (BIERCUK et al., 2002, HUXTABLE et al., 2003). This thermal discontinuity was attributed to a thermal resistance at the interface, known as Kapitza resistance, described in the following Section.

#### *1.5.3.3 ANOMALOUS HEAT CONDUCTION ENHANCEMENT MECHANISMS*

As previously stated, several authors reported unexplained or anomalous effective thermal conductivity enhancements on nanofluids. As result, different theories have been proposed to describe the observed experimental results. From these, it may be highlighted the Brownian motion, the nano-layer structure and the nanoparticles clustering or aggregation.

Table 1.5 presents a summary of the main researcher works proposing these alternative mechanisms to explain the anomalous effective thermal conductivity observed.

Table 1.5: Resume of the proposed mechanism and respective researches.

| Proposed Mechanism | Researchers |
|---|---|
| Brownian motion | (DAS et al., 2003b, DING et al., 2007, JANG et al., 2004, KEBLINSKI et al., 2008, KOO et al., 2004, KUMAR et al., 2004, LI et al., 2006, LIU et al., 2005, PATEL et al., 2003, PATEL et al., 2005, PRASHER et al., 2005, WANG et al., 1999, XIE et al., 2002, YU et al., 2003, YU et al., 2010) |
| Nano-layer structure | (CHEN et al., 2008, CHOI et al., 2001, DING et al., 2006, DING et al., 2007, EASTMAN et al., 2004, EVANS et al., 2008, HONG et al., 2005, KEBLINSKI et al., 2002, PATEL et al., 2003, XIE et al., 2005, XIE et al., 2003, XIE et al., 2002, XUE et al., 2003, YU et al., 2003) |
| Nanoparticle aggregation/percolation | (CHOI et al., 2001, EVANS et al., 2008, LI et al., 2007, PRASHER et al., 2006, WANG et al., 1999, WANG et al., 2003b, XIE et al., 2002, XUAN et al., 2003, ZHU et al., 2004) |

### Brownian motion

As seen, one of the intriguing behaviours reported by several researchers is the strong temperature dependence of the effective thermal conductivity of nanofluids, which has been attributed to the Brownian motion of the nanoparticles (AMROLLAHI et al., 2008, DAS et al., 2003b, GARG et al., 2009, LI et al., 2006, LIU et al., 2005, NASIRI et al., 2011, WANG et al., 1999, WEITING et al., 2009, XIE et al., 2009). The contribution of the Brownian motion to increase heat conduction in nanofluids can be classified into two categories: (1) collisions between Brownian particles, and (2) Nanoscale convection induced by the Brownian particles.

Regarding collisions, the developed theory states that during the Brownian diffusion of the particles, it is produced interparticle collisions. When two particles collide, the solid-solid heat transfer mode could increase the effective thermal conductivity of the nanofluids. This mechanism is particularly interesting because it helps explain the experimental observations that suggest an increase in thermal conductivity with temperature. It is expected that with a rise on temperature, *i.e.* with a higher Brownian diffusion of the particles, the number or collisions increase, resulting in a higher heat conduction enhancement.

Keblinski *et al.* analytically estimated the characteristic time scale of the Brownian diffusion and compared with that of thermal diffusion of the fluid. The results suggested that the thermal diffusion is much faster than the Brownian diffusion, even for extremely small particles. Thus, they proposed that the Brownian motion may be neglected (EASTMAN et al., 2004, KEBLINSKI et al., 2002).

Later, Jang *et al.* and Prasher *et al.* suggested that during Brownian diffusion of the particles, nanoscale convention may occur, enhancing the thermal conductivity of the nanofluids. This was a mechanism neglected in the study of Keblinski *et al.*. Through the comparison of the time scale of the Brownian diffusion with that of convection during Brownian motion, they found that the effect of convection may be almost instantaneously when compared with the diffusion of the nanoparticles (JANG et al., 2004, PRASHER et al., 2006). Jang *et al.* and Prasher *et al.* also developed an effective thermal conductivity model, considering this heat conduction mechanism (see Section 1.5.3.4).

Nevertheless, some researchers observed that the dependence of thermal conductivity enhancement on temperature is negligible, since they simple follow the temperature behaviour of the base fluid. This suggest that the Brownian motion plays a negligible role in the heat conduction enhancement in nanofluids (EVANS et al., 2008, KEBLINSKI et al., 2008, KOUSHKI et al., 2013, ZHANG et al., 2006).

### Nano-layer structure

The molecular-level layering theory states that the molecules of a liquid near a solid surface become more organized than the bulk liquid, forming a solid-like layer structure. This solid-like layer can extent up to several molecular distances, for sufficient strong interaction between the atoms of the liquid and the solid surface. These structural changes of the liquid have been shown to have significant effects on various properties, such as thermal transport and viscosity (SNOOK et al., 1978).

It is known that phonons are responsible for the highly efficient heat transfer mechanism in solids. They have the ability to travel over long distances before being scattered, known as phonon mean free path. Therefore, the formation of the solid-like layer may produce an enhancement on the heat conduction through the liquid near the solid particle.

In 2003, Yu *et al.* proposed that this nano-layer structure act as a thermal bridge between the nanoparticles and the bulk liquid (YU et al., 2003). Based on this mechanism, they developed two models, for spherical and non-spherical particles. Since then, many other models were developed taking into account the effect of this mechanism (see Section 1.5.3.4).

Nevertheless, through non-equilibrium molecular dynamics, Xue *et al.* verified that the nano-layer solid structure does not produce impact on the effective thermal conductivity enhancement (XUE et al., 2004). In addition, Evans *et al.* studied the thermal conductivity of ordered molecular water through molecular dynamics, suggesting a minor effect for typical molecule ordering that probably might be observed in nanofluids. The study also suggests that a significant enhancement is only possible in crystalline order, such as ice. They stated that the latter is unlikely to be induced by the hydrophilic surfaces of nanofluids, since this are only formed, at room temperature, with very high electrical fields (EVANS et al., 2007).

### Nanoparticle aggregation/percolation

The nanoparticles aggregation is another proposed mechanism to explain the anomalous thermal conductivity enhancement of nanofluids. This theory assumes that the nanoparticles clusters form local percolation-like paths with lower thermal resistance, increasing the overall thermal conductivity and viscosity of nanofluids (KEBLINSKI et al., 2002, PRASHER et al., 2006, WANG et al., 2003a). However, according to Xuan *et al.*, the aggregation of the nanoparticles may also produce a negative impact on the enhancement of the thermal conductivity, since the Brownian motion will be slower (XUAN et al., 2003).

Regarding non-spherical particles, such as CNTs, several authors suggested that the elongated geometry of CNTs allows the easily formation of a continuous solid network structures, or percolation structure, even for lower volume fraction (BIERCUK et al., 2002, DENG et al., 2009, KYRYLYUK et al., 2008, SHENOGINA et al., 2005, ZHONG et al., 2006). Through the measurement of the effective electrical conductivity, Biercuk *et al.* found experimentally that the CNTs have an extremely low percolation threshold. However, the results shown that, for the same volume fraction, the thermal conductivity presents discontinuity in the dispersed phase (BIERCUK et al., 2002). These results can be explained by a thermal resistance at the solid-medium boundary, also known as Kapitza resistance.

In 1941, Kapitza found an interfacial thermal resistance when heat flows from a solid to a fluid medium, which became known as Kapitza resistance. For instance, consider a particle suspended in a liquid medium subjected to a given heat flux. In the case of a perfect interface, the temperature of the particle is equal to that of the liquid, at the particle surface. However, according to Kapitza, there is an interfacial thermal resistance that leads to a finite temperature discontinuity at the surface of the particle, limiting the effective thermal conductivity enhancement. This heat barrier is associated with the differences among the phonon spectra of the two phases. This resistance exists even at atomically perfect interfaces and differs from contact resistance (KAPITZA, 1941).

Huxtable *et al.* experimentally verified the magnitude of these Kapitza resistances in CNTs based composites. They measured the Kapitza resistance of sodium dodecyl sulphate encapsulated SWCNT suspensions in heavy water, through a transient absorption method. The results alluded that the thermal resistance of the interface solid-solid is a factor of order ≈2 higher than that of the medium-solid interface. They also argued that the Kapitza resistance does not depend critically on the surfactant, as long as this is not covalently bonded to the CNTs (HUXTABLE et al., 2003).

Later, through molecular dynamics simulation, various authors have shown that the Kapitza resistance depends on the strength of the bonds between the medium and the CNTs (SHENOGIN et al., 2004a, SHENOGINA et al., 2005, XUE et al., 2003). Furthermore, Shenogin *et al.* suggested that functionalization also drop the thermal conductivity of the CNTs (SHENOGIN et al., 2004a). Other researchers also suggested that an increase in the degree of functionalization of the CNTs reduce the thermal resistance of the interface (CLANCY et al., 2006, HAIBO et al., 2007, ZHONG et al., 2006). More recently, Nasiri *et al.* experimentally confirmed these results by comparing the effective thermal conductivity of CNTs suspensions dispersed by surfactants and covalent functionalization techniques. The samples dispersed by covalent functionalization techniques presented the higher enhancement of thermal conductivity (NASIRI et al., 2011).

#### *1.5.3.4 THEORETICAL STUDIES*

Throughout the years, several models were developed to predict the results observed experimentally. In this document, these are categorized by classic models, models for nanofluids of spherical nanoparticles, and models for nanofluids of non-spherical particles. This categorization lies in the ability of the models to predict the effect of the nanoparticles size and shape, since all of them predict the influence of the both thermal conductivities of the pure materials that form the mixture.

## Classical models

The classical models are generally characterized as static models, with the assumption of motionless particles and heat conduction (diffusion) in both continuous matrix phase and dispersed phase. The input parameters for these models are the volume fraction, shape and size of the particles and, only for concentrated suspensions, the particle-particle interaction.

The simplest model based on the EMT was developed by Maxwell. The model considers a heterogeneous system consisting of a diluted suspension of non-thermally interacting spherical particles (MAXWELL, 1873). The effective thermal conductivity can be expressed as:

$$k_{eff}=\frac{k_p+2k_{bf}+2\phi(k_p-k_{bf})}{k_p+2k_{bf}-\phi(k_p-k_{bf})}\cdot k_{bf} \qquad 1.3$$

The main limitation of the Maxwell model is that it only predicts the conductivity of suspensions with low volume fractions, an essential premise to ensure that the particles do not thermally interact. To address this constraint, Bruggeman proposed an iterative model that predicts the thermal conductivity for thermally interacting particles. For low volume fractions, the predictions from the Bruggeman model and the Maxwell model are identical (BRUGGEMAN, 1935). However, they show discrepancies for higher volume fractions. The model of Bruggeman is given by:

$$\left(\frac{k_p-k_{eff}}{k_p-k_{bf}}\right)\cdot\left(\frac{k_{bf}}{k_{eff}}\right)^{\frac{1}{3}}=(1-\phi) \qquad 1.4$$

Nevertheless, these two models do not account for the effects of particle shape. The first model for effective thermal conductivity prediction for non-spherical particles was derived by Fricke, using a method similar to Maxwell's approach (FRICKE, 1924, 1925). The model predicts the effective thermal conductivity of suspensions of thermally non-interacting and randomly oriented spheroidal particles. The model can be expressed as:

$$k_{eff}=\frac{k_p+(N-1)k_{bf}-\phi(N-1)(k_{bf}-k_p)}{k_p+(N-1)k_{bf}-\phi(k_p-k_{bf})}\cdot k_{bf} \qquad 1.5$$

where $N$ is a dimensionless parameter that depends on the shape particles and upon the ratio of the conductivities of the two phases.

Later, Hamilton and Crosser proposed a simple equation for $N$, that could be applied to other shapes (HAMILTON et al., 1962). The Hamilton and Crosser shape factor can be written as:

$$N=\frac{3}{\chi} \tag{1.6}$$

where $\chi$ is the sphericity of the particle and is defined as the ratio of the surface area of an equivalent sphere, to the real surface area of the particle. When $\chi=1$, the Fricke's model is reduced to the Maxwell's model (HAMILTON et al., 1962).

Based on the assumption that the effective thermal conductivity depends on other parameters rather than volume fraction and both thermal conductivity of the materials that compose the mixture, Hashin and Shtrikman derived theoretical bounds for the effective thermal conductivity of mixtures (HASHIN et al., 1962):

$$k_{bf}\cdot\left(\frac{k_p+2k_{bf}+2\phi(k_p-k_{bf})}{k_p+2k_{bf}-\phi(k_p-k_{bf})}\right)\leq k_{eff}\leq k_{bf}\cdot\left(1+\frac{3(1-\phi)\left(k_p-k_{bf}\right)}{3k_p+\phi\left(k_p-k_{bf}\right)}\right) \tag{1.7}$$

According to the authors, the heterogeneous systems that meet the EMT exhibit thermal conductivity ranging within this interval.

As mentioned in the Section 1.5.3.3, in 1941, Kapitza founded the interfacial thermal resistance in suspensions of solid particles (KAPITZA, 1941). Taking this thermal boundary resistance into account, Hasselman and Johnson derived an expression for the effective thermal conductivity of suspensions (HASSELMAN et al., 1987). They found that the effective thermal conductivity depends on the volume fraction, and size and shape of the dispersed particles. The resulting expression for spherical particles can be arranged as:

$$k_{eff}=\frac{k_p\cdot(1+2\kappa_K)+2k_{bf}+2\phi(k_p(1-\kappa_K)-k_{bf})}{k_p\cdot(1+2\kappa_K)+2k_{bf}-\phi(k_p(1-\kappa_K)-k_{bf})}\cdot k_{bf} \tag{1.8}$$

and for non-spherical particles can be expressed as:

$$k_{eff}=\frac{k_p\cdot(1+2\kappa_K)+(N-1)\cdot k_{bf}+(N-1)\cdot\phi\cdot(k_p\cdot(1-\kappa_K)+k_{bf})}{k_p\cdot(1+2\kappa_K)+(N-1)\cdot k_{bf}-\phi(k_p\cdot(1-\kappa_K)-k_{bf})}\cdot k_{bf} \tag{1.9}$$

where $\kappa_K$ is a dimensionless parameter defined as:

$$\kappa_K=\frac{a_K}{a_p} \tag{1.10}$$

where $a_K$ is the Kapitza radius, or the equivalent thickness of the base fluid, with the same thermal conductivity, over which is caused the equivalent temperature drop at the interface. This is defined as:

$$a_K = R_K \cdot k_{bf} \tag{1.11}$$

As observed in the previous Section, other heat transfer mechanism were suggested for nanofluids, namely the Brownian motion, liquid layering at the liquid-particle interface, and the effects of particle clustering. Such considerations were subsequently employed in several theoretical models, formulated for nanofluids.

### Models for nanofluids of spherical nanoparticles

Wang *et al.* proposed a fractal model in order to predict the thermal conductivity of nanofluids. This model, based on the EMT and the fractal theory, seeks to introduce into the model of Maxwell the effect of the nanoparticles clustering or agglomeration. The fractal theory describes the disorder and stochastic process of clustering and polarization of nanoparticles within the mesoscale limit. The thermal conductivity can be calculated as (WANG et al., 2003a):

$$k_{eff} = \frac{(1-\phi) + 3\phi \int_0^{\infty} \frac{k_{cl}(a_{cl}) n(a_{cl})}{k_{cl}(r) + \cdot 2k_{bf}} \cdot da_{cl}}{(1-\phi) + 3\phi \int_0^{\infty} \frac{k_{bf}(a_{cl}) n \cdot (a_{cl})}{k_{cl}(a_{cl}) + 2 \cdot k_{bf}} \cdot da_{cl}} \tag{1.12}$$

where $n(a_{cl})$ is the radius distribution function.

Xuan *et al.* introduced to the model of Maxwell the Brownian motion of the suspended nanoparticles and clusters. Through this, the authors state that the effective thermal conductivity dependency on the temperature could be predicted. The model is given by (XUAN et al., 2003):

$$k_{eff} = \frac{k_p + 2k_{bf} + 2(k_p - k_{bf}) \cdot \phi}{k_p + 2k_{bf} - (k_p - k_{bf}) \cdot \phi} \cdot k_{bf} + \frac{\rho_p \cdot \phi \cdot c_{v,p}}{2} \cdot \sqrt{\frac{k_B \cdot T}{3\pi \cdot a_{cl} \cdot \mu_{bf}}} \tag{1.13}$$

The author claims that the model predictions provide a good agreement with the experimental results. However, the model may be wrong, since the second term of the equation has incorrect units.

Yu *et al.* proposed a modification to the model of Maxwell, assuming that the base fluid molecules nearly to the solid surface of the nanoparticles form solid-like layered structures. Hence, the nano-

layer works as a thermal bridge or thermal barrier between a solid nanoparticle and a bulk liquid. The expression resulted was (YU et al., 2003):

$$k_{eff}=\frac{k_{pe}+2k_{bf}+2\left(k_p-k_{bf}\right)\cdot(1+\varrho)^3\cdot\phi}{k_{pe}+2k_{bf}-\left(k_p-k_{bf}\right)\cdot(1+\varrho)^3\cdot\phi}\cdot k_{bf} \quad 1.14$$

where $k_{pe}$ can be expressed as:

$$k_{pe}=\frac{[2(1-\gamma)+(1+\varrho)^3\cdot(1+2\gamma)]\cdot\gamma}{-(1-\gamma)+(1+\varrho)^3\cdot(1+2\gamma)}\cdot k_p \quad 1.15$$

where $\gamma=k_{layer}/k_p$, and $\varrho=\delta/a_p$.

The thickness of the nano-layer at the nanoparticle/liquid interface can be calculated according to Hashimoto *et al.* (HASHIMOTO et al., 1974):

$$\delta=\sqrt{2\pi}\cdot\sigma_{TB} \quad 1.16$$

where $\sigma_{TB}\approx 0.2\sim 0.8\ nm$, is the thermal boundary layer diffusiveness.

Jang *et al.* modelled the conductivity considering four modes of energy transfer, the thermal diffusion in the base fluid and nanoparticles, the collision between nanoparticles due to Brownian motion, and the nanoscale convection caused by the same random motion of the nanoparticles (JANG et al., 2004). They concluded that the contribution of the collisions between nanoparticles is negligible when compared to the contribution of the remaining modes. The resulting expression was:

$$k_{eff}=k_{bf}\cdot(1-\phi)+k_p\cdot\phi+3c_p\frac{d_{bf}}{d_p}\cdot k_{bf}\cdot Re_p^2\cdot P_r\cdot\phi \quad 1.17$$

where $d_{bf}$ is the diameter of the base fluid molecules.

Another model based on the nanoscale convection of the nanoparticles was proposed by Kumar *et al.* (KUMAR et al., 2004). The model is given by:

$$k_{eff}=\left(1+C\cdot\left(\frac{2k_B\cdot T}{\pi\cdot\mu\cdot d_p^2}\right)\cdot\frac{\phi\cdot a_{bf}}{k_{bf}\cdot(1-\phi)\cdot a_p}\right)\cdot k_{bf} \quad 1.18$$

where $C$ is a constant of adjustment.

Furthermore, also Koo *et al.* postulated that the enhancement of the thermal conductivity is mainly due to Brownian motion. They introduced to the EMT of Maxwell this mechanism, obtaining a model expressed as (KOO et al., 2004):

$$k_{eff}=\frac{k_p+2k_{bf}+2(k_p-k_{bf})\cdot\phi}{k_p+2k_{bf}-(k_p-k_{bf})\cdot\phi}\cdot k_{bf}+\left[\left(5\times10^4\right)\cdot\varpi\cdot\phi\cdot\rho_p\cdot c_{v,p}\cdot\sqrt{\frac{k_B\cdot T}{\rho_p\cdot d_p}}\cdot f(T,\phi,\ldots)\right] \quad 1.19$$

where $\varpi$ is the fraction of the base fluid volume that moves with the particle, and $f(T,\phi,\ldots)$ is a fraction function that can only be determined from experimental data, *i.e*. through experimental data fitting.

Xie *et al.* developed another analytical expression considering the nano-layer structure at the interface with linear thermal conductivity distribution. This model takes into account the effects of nano-layer thickness, nanoparticles size, volume fraction, and thermal conductivities of both nanoparticles and base fluid (XIE et al., 2005):

$$k_{eff}=\left(1+3\vartheta\cdot(1-\phi)+\frac{3\vartheta^2\cdot\phi^2}{1-\vartheta\cdot\phi}\right)\cdot k_{bf} \quad 1.20$$

where $\vartheta$ is a relation function between the thermal conductivity of both nanoparticles and nanofluid (XIE et al., 2005). They found that the obtained theoretical results were in agreement with only some of the experimental data, suggesting that nano-layer formation may not be the only mechanism responsible for the thermal conductivity enhancement.

Later, Yajie *et al.* upgraded the model of Xie *et al.* (XIE et al., 2005), introducing the effect of the Brownian motion on the thermal conductivity. The model is given by (YAJIE et al., 2005):

$$k_{eff}=\left(1+f(Pe)+3\vartheta\cdot(1-\phi)+\frac{3\vartheta^2\cdot\phi^2}{1-\vartheta\cdot\phi}\right)\cdot k_{bf} \quad 1.21$$

where $f(Pe)$ is an empirical function that reflects the nanoscale convention of the particles during their Brownian diffusion.

Prasher *et al.* suggested that the effective thermal conductivity enhancement originates from the Brownian motion of the nanoparticles. Though an order-of-magnitude analysis, they deduced that the nanoscale convection is more active than the Brownian collision. From these study, they proposed the following model (PRASHER et al., 2005):

$$k_{eff}=\frac{k_p+2k_{bf}+2\phi\left(k_p-k_{bf}\right)}{k_p+2k_{bf}-\phi\left(k_p-k_{bf}\right)}\cdot k_{bf}+A\cdot Re^{m}\cdot Pr^{0.333}\cdot\phi \qquad 1.22$$

where *A* and *m* are empirical constants determined through experimental data. For larger particles, *Re* becomes *0* and the model is reduced to the EMT of Maxwell.

One year later, Prasher *et al.* considered the nanoparticle aggregation as a governing factor for the thermal conductivity enhancement. The nanoparticles aggregates are considered as a new particle composed by primary particles with an equivalent radius $a_{cl}$ that enhances the heat conduction through the percolation structure. They reformulated their model as follows (PRASHER et al., 2006):

$$k_{eff}=\frac{k_{cl}+2\cdot k_{bf}+2\phi_{cl}\left(k_{cl}-k_{bf}\right)}{k_{cl}+2\cdot k_{bf}-\phi_{cl}\left(k_{cl}-k_{bf}\right)}\cdot k_{bf}+A\cdot Re^{m}\cdot Pr^{0.333}\cdot\phi \qquad 1.23$$

Another model based on the nano-layer structure at the interface solid particle-liquid was developed by Murshed *et al.* (MURSHED et al., 2008). This model can be expressed as:

$$k_{eff}=\frac{\left(k_p-k_{layer}\right)\cdot\phi\cdot k_{layer}\cdot\left[\psi_1^3-\psi^3+1\right]+\left(k_p+k_{layer}\right)\cdot\psi_1^3\cdot\left[\phi\cdot\psi^{\cdot 3}\left(k_{layer}-k_{bf}\right)+k_{bf}\right]}{\psi_1^3\cdot\left(k_p+k_{layer}\right)-\left(k_p-k_{layer}\right)\cdot\phi\cdot\left[\psi_1^3+\psi^3-1\right]} \qquad 1.24$$

where $\psi=1+\gamma$ and $\psi_1=1+\gamma/2$.

Later, Murshed *et al.* introduced to its model the effect of the Brownian motion of the particle, particle surface chemistry, and interaction potential (MURSHED et al., 2009). The updated model can be expressed as:

$$k_{eff}=\left[\frac{\phi\cdot\omega\cdot\left(k_p-\omega\cdot k_{bf}\right)\cdot\left[2\psi_1^3-\psi^3+1\right]+\left(k_p+2\omega\cdot k_{bf}\right)\cdot\psi_1^3\left[\phi\cdot\psi^{\cdot 3}(\omega-1)+1\right]}{\psi_1^3\cdot\left(k_p+2\omega\cdot k_{bf}\right)-\left(k_p-\omega\cdot k_{bf}\right)\cdot\phi\cdot\left[\psi_1^3+\psi^3-1\right]}\right]\cdot \mathrm{k_{bf}}$$

$$+\left[\phi^2\cdot\psi^6\cdot k_{bf}\cdot\left(3\cdot\Lambda^2+\frac{3\Lambda^2}{4}+\frac{9\Lambda^3}{16}\frac{k_{cl}+2k_{bf}}{2k_{cl}+3k_{bf}}+\frac{3\Lambda^4}{2^6}+\ldots\right)\right] \qquad 1.25$$

$$+\left[\frac{1}{2}\cdot\rho_{cl}\cdot c_{p_{cl}}\cdot L_s\left(\sqrt{\frac{3k_B\cdot T\left(1-1.5\psi^3\cdot\phi\right)}{2\pi\cdot\rho_{cp}\cdot\psi^3\cdot a_p^3}}+\frac{G_T}{6\pi\cdot\psi\cdot a_p\cdot L_s}\right)\right]$$

where $G_T$ is the total interparticle interaction, $\omega$ is an empirical parameter that depends on the orderliness of the fluid molecules in the interface and is given by:

$$\omega=\frac{k_{layer}}{k_{bf}} \tag{1.26}$$

and,

$$\Lambda=\frac{k_{cl}-k_{bf}}{k_{cl}+2k_{bf}} \tag{1.27}$$

$$k_{cl}=\frac{2\left(k_p-k_{layer}\right)+\psi^3\cdot(k_p+2k_{layer})}{\left(k_{layer}-k_p\right)+\psi^3\cdot(k_p-2k_{layer})}\cdot k_{layer} \tag{1.28}$$

Wei *et al.* developed another non-based EMT model, considering the effect of the nano-layer structure at the interface and the contribution of the Brownian motion of the particles (WEI et al., 2012). The model can be expressed as:

$$k_{eff}=k_{bf}+\frac{3\phi\cdot q\cdot P/P_0}{1-\phi\cdot q\cdot P/P_0} \tag{1.29}$$

where $q$ is a dipole factor, $P$ and $P_0$ are the total dipole moment of the spherical particles (WEI et al., 2012).

More recently, Xiao *et al.* proposed a predictive model based on dimensionless parameters. According to the authors, the models predict the effect of the Brownian motion of the particles and their respective interaction, and the nano-layer structure at the interfaces (XIAO et al., 2013). The model is given by:

$$k_{eff}=k_c+k_s \tag{1.30}$$

where $k_c$ is the thermal conductivity by heat convection caused by the Brownian motion of the particles, and $k_s$ is the thermal conductivity by stationary nanoparticles in the base fluid, which is identical to the Maxwell model (XIAO et al., 2013).

### Models for nanofluids of non-spherical or elongated particles

As seen, Fricke, and Hamilton and Crosser proved the influence of the particle geometry on the thermal conductivity enhancement of suspensions. Therefore, for suspensions of non-spherical nanoparticles, it is required alternative formulations to the previously presented. The most studied non-spherical nanoparticles are the CNTs. These have a tubular shape, usually depicted as cylindrical with high aspect ratio.

In 2003, Nan *et al.* proposed a predictive model, based on the multiple scattering theory and the EMT, for CNTs based composites (NAN et al., 2003). In this, the enhancement of the nanofluids thermal conductivity is considered to be only related to the ballistic thermal conductivity of the CNTs, and the model over predicted the experimental results available in the literature. One year later, Nan *et al.* updated the model, introducing the limitation on the thermal conductivity enhancement due to the interfacial resistance. The model, described as a more generalist EMT, can be expressed as (NAN et al., 2004):

$$k_{eff}=\frac{3+\phi\left(2\beta_{xx}\cdot(1-L_{xx})+\beta_{zz}\cdot(1-L_{zz})\right)}{3-\phi(2\beta_{xx}\cdot L_{xx}+\beta_{zz}\cdot L_{zz})}\cdot k_{bf} \quad 1.31$$

where

$$\beta_{xx}=\frac{k_{xx}^{eq}-k_{bf}}{k_{bf}+L_{xx}\cdot\left(k_{xx}^{eq}-k_{bf}\right)} \quad 1.32$$

$$\beta_{zz}=\frac{k_{zz}^{eq}-k_{bf}}{k_{bf}+L_{zz}\cdot\left(k_{zz}^{eq}-k_{bf}\right)} \quad 1.33$$

The parameters $k_{xx}^{eq}$ and $k_{zz}^{eq}$ are, respectively, the equivalent thermal conductivities along transverse $(xx')$ and longitudinal $\left(zz'\right)$ axes of a carbon nanotube coated with a thin interfacial thermal barrier layer (Kapitza resistance) and can be expressed as:

$$k_{xx}^{eq}=\frac{k_p}{1+\frac{2a_k}{d_p}\cdot\frac{k_p}{k_{bf}}} \quad 1.34$$

$$k_{zz}^{eq}=\frac{k_p}{1+\frac{2a_k}{l_p}\cdot\frac{k_p}{k_{bf}}} \quad 1.35$$

The parameters $L_{xx}$ and $L_{zz}$ are the depolarization factors of the particles that reacts as shape factor (LANDAU et al., 1984). According to Huxtable *et al.*, $R_k$ is $8\times10^{-8}$ K m$^2$/W, for CNTs dispersed in heavy water (HUXTABLE et al., 2003). The axis $(zz')$ represents the longitudinal axis of the CNTs, and axes $(xx')$ and $(yy')$ are the other two axes of the CNTs (NAN et al., 2004).

Xue developed a model that accounts for the effect of the stochastic space distribution of very elongated particles and the nano-layer structure at the particle-medium interface (XUE, 2003). Xue introduced to the effective medium theory of Largarkov *et al.* a complex nanoparticle composed by

a particle inside an elliptical shell with a different thermal conductivity and with a specific thickness (LAGARKOV et al., 1996). The model can be expressed as:

$$9\left(1-\frac{\phi}{\lambda}\right)\cdot\frac{k_{eff}-k_{bf}}{2k_{eff}-k_{bf}}+\frac{\phi}{\lambda}\cdot\left[\frac{k_{eff}-k_{c,z}}{k_{eff}+L_{zz}\cdot\left(k_{c,z}-k_{eff}\right)}+4\cdot\frac{k_{eff}-k_{c,x}}{2k_{eff}+(1-L_{zz})\cdot\left(k_{c,x}-k_{eff}\right)}\right]=0 \quad (1.36)$$

Where $\lambda$ is the volume fraction of the complex nanoparticles, and $k_{c,x}$ and $k_{c,z}$ are the effective dielectric constant along the axis.

Yu *et al.* extended Equation 1.14, a model for spherical particles that accounts with the nanoscale layer that improves the thermal conductivity, to non-spherical particles. In this model, the nano-layer is modulated as a confocal ellipsoid with a solid particle (YU et al., 2004). This model can be written as:

$$k_{eff}=\left(1+\frac{3\varphi^{-1.55}\cdot\phi_e\cdot YC}{1-\phi_e\cdot YC}\right)\cdot k_{bf} \quad (1.37)$$

where the parameter *YC* is defined as

$$YC=\frac{1}{3}\cdot\sum_{j=a,b,c}\frac{\left(k_{pj}-k_{bf}\right)}{k_{pj}+(m-1)\cdot k_{bf}} \quad (1.38)$$

And $\phi_e$ is the equivalent volume concentration of the complex ellipsoids, $k_{pj}$ is the equivalent thermal conductivities along the axes of the complex ellipsoid, and $m$ is a generalized empirical shape factor (YU et al., 2004).

In 2005, Xue presented another model for CNT based composites. Based on Maxwell model, Xue suggested that the model is capable to account the stochastic space distribution of the very large axial ratio of the CNT based composites (XUE, 2005). This model can be expressed as:

$$k_{eff}=\frac{1-\phi+2\phi\frac{k_p}{k_p-k_{bf}}\cdot ln\frac{k_p+k_{bf}}{2k_{bf}}}{1-\phi+2\phi\frac{k_{bf}}{k_p-k_{bf}}\cdot ln\frac{k_p+k_{bf}}{2k_{bf}}}\cdot k_{bf} \quad (1.39)$$

The difference between this model and the Hamilton and Crosser model is the consideration of the stochastic space distribution of the very elongated nanoparticles, as mentioned earlier. However, the model only predicts the increase of effective thermal conductivity with volume fraction

increment. Moreover, the relative dependence of effective thermal conductivity on the particles aspect ratio seems to be somehow neglected in this model.

In 2006, Gao *et al.* proposed an improvement, to the model of Nan *et al.* (NAN et al., 2003), through the principle of Bruggeman for higher volumes (GAO et al., 2006). In this model, the effect of the Kapitza resistance is considered through the adjustment of the anisotropic thermal conductivity of the particles. Later, Ordóñez-Miranda *et al.* proposed a similar model, with the same premises, for coated particles (ORDÓÑEZ-MIRANDA et al., 2010).

In 2007, Sabbaghzadeh *et al.* proposed a model for non-spherical particles that include the effect of the Brownian motion of the particles, the nano-layer structure at the interface, and agglomeration formation. The model is given by (SABBAGHZADEH et al., 2007):

$$k_{eff}=k_{bf}\cdot\left(1-\phi\cdot(1+t_{nl})\right)+\phi\cdot\left(k_p+k_{layer}\cdot t_{nl}\right)+\frac{\phi\cdot(1+t_{nl})\cdot d_{bf}}{P_r\cdot d_{cl}}\cdot\left(0.35+0.56\cdot Re^{0.52}\right)\cdot P_r^{0.3}\cdot k_{bf} \qquad 1.40$$

where $t_{nl}$ is a parameter that represent the thickness of the nano-layer structure, and $d_{cl}$ is the equivalent diameter of the cluster.

In line with the Equation 1.24, Murshed *et al.* proposed a model for the effective thermal conductivity of nanofluids of cylindrical nanoparticles through the considering the effect of the nanoscale layer at the solid particle/liquid interface (MURSHED et al., 2008). The model can be expressed as:

$$k_{eff}=\frac{\left(k_p-k_{layer}\right)\cdot\phi k_{layer}\cdot\left[\psi_1^2-\psi^2+1\right]+\left(k_p+k_{layer}\right)\cdot\psi_1^2\cdot\left[\phi\cdot\psi^2\left(k_{layer}-k_{bf}\right)+k_{bf}\right]}{\psi_1^2\cdot\left(k_p+k_{layer}\right)-\left(k_p-k_{layer}\right)\cdot\phi\cdot\left[\psi_1^2+\psi^2-1\right]} \qquad 1.41$$

Sastry *et al.* proposed a predictive model, non-based on the EMT, for the effective thermal conductivity of CNTs based nanofluids. The model considers that the Brownian motion causes a random orientation on the well dispersed CNTs and is formed a chain where the heat could also be transferred by the solid phase and, therefore, by the corresponding thermal resistance network, as can be depicted from Figure 1.3 (SASTRY et al., 2008).

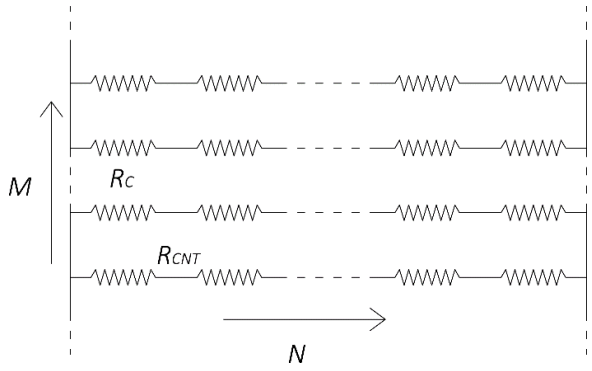


Figure 1.3: Adapted thermal resistance network idealized by Sastry *et al.* (SASTRY et al., 2008).

A CNTs suspension inside of a control volume $L_{cell}^3$ with cross section $A_{cell}$ is considered, and the effective thermal conductivity is expressed as:

$$k_{eff}=\frac{L_{cell}}{R_{net}\cdot A_{cell}} \tag{1.42}$$

where $R_{net}$ is the resistance network of the suspension and is expressed as:

$$R_{net}=\sum_{i=1}^{n}\left[\frac{\frac{R_{CNT\,i,P}+2R_C}{M}\cdot R_{F\,i,P}}{\frac{R_{CNT\,i,P}+2R_C}{M}+R_{F\,i,P}}\right] \tag{1.43}$$

$M$ represents the total number of parallel chains (Figure 1.3) and can be calculated as:

$$M=\frac{4\phi\cdot L_{cell}^3}{\pi\cdot d_p^2\cdot l_p\cdot B} \tag{1.44}$$

and $B$ represents the number of carbon nanotubes connections in a chain, which is 1 in the Sastry *et al.* model.

$R_{CNT}$ is the individual resistance of the CNT, $R_C$ is the resistance between the CNTs and the interfacial liquid between two CNTs (Kapitza resistance), and $R_{FP}$ is the resistance in the parallel liquid path:

$$R_{CNT\,i,P}=\frac{l_{i,P}}{k_p\cdot A_{cs}} \tag{1.45}$$

$$R_C=\frac{1}{G\cdot d_p{}^2} \tag{1.46}$$

$$R_{Fi,P}=\frac{l_{i,P}\cdot sin\varphi_i\cdot cos\vartheta_i}{k_{bf}\cdot A_{cell}} \tag{1.47}$$

where $A_{cs}$ is the CNTs cross section, the $\varphi$ and $\vartheta$ are the azimuth and colatitude angles, respectively, of the CNT *i*.

In Sastry *et al.* model, the percolation was implemented by considering one collision per CNT, which may not be true, since the probability of interparticle collisions, increases with the rise in volume fraction and aspect ratio. Koo *et al.* improved the work of Sastry *et al.* by considering an empirical factor that describes the number of collision per CNT, based on the *excluded volume theory* (Appendix A):

$$B = 2\phi \cdot \left(\frac{l_p}{d_p}\right) \qquad 1.48$$

With this consideration, the authors claim that the non-linear variation of the effective thermal conductivity with CNTs volume fraction could be predicted. This empirical factor is applied for calculating the number of random variables that have to be derived for each CNT in the chain, in order to calculate the maximum length between two contact points on a CNT. Then, the overall solid path length will be reduced with volume fraction and/or aspect ratio rising (KOO et al., 2008).

Deng *et al.* presented a simple analytical model for CNTs based composites that include the influence of volume fraction, anisotropic thermal conductivities, aspect ratio, non-straightness, thermally interparticle interaction, and Kapitza resistance of the CNTs (DENG et al., 2007). They considered that the high thermal anisotropy phenomenon of CNTs induces nearly perfect one-dimensional thermal cables with negligibly small thermal flux losses during long distance thermal conduction (HONE, 2002). This could be described as:

$$\frac{k_{xx}^{eq}}{k_{zz}^{eq}} \ll 1 \qquad 1.49$$

The Deng et al. model could be expressed as:

$$k_{eff} = k_{bf} \cdot \left(1 + \frac{\eta \cdot \emptyset}{\frac{3k_{bf}}{\eta \cdot k_{zz}^{eq}} + \frac{3H \cdot \eta \cdot l_p}{d_p}}\right) \qquad 1.50$$

where *H* is a parameter that the influence of the aspect ratio of the CNTs:

$$H=\frac{1}{\left(\frac{l_p}{d_p}\right)^2-1}\cdot\left[\frac{\frac{l_p}{d_p}}{\sqrt{\left(\frac{l_p}{d_p}\right)^2-1}}\cdot ln\left(\frac{l_p}{d_p}+\sqrt{\left(\frac{l_p}{d_p}\right)^2-1}\right)-1\right] \quad 1.51$$

and $\eta$ represents the influence of the non-straightness of the CNTs:

$$\eta=\frac{l_p^{ce}}{l_p} \quad 1.52$$

where $l_p^{ce}$ is the distance between the two ends of the non-straight CNTs.

The Deng *et al.* model suggests that using CNTs with higher aspect ratio and straightness ratios was an efficient means to get much better thermal conductivity enhancements. Furthermore, they state that the non-linear behaviour on the enhancements versus CNTs volume fraction can be attributed to the interaction effect among CNTs (DENG et al., 2009).

In 2009, Gensheng *et al*. used the model of Jang *et al.* (Equation 1.17), developed for spherical nanoparticles, to predict the thermal conductivity of CNTs based nanofluids. The Jang *et al.* model, which considers the contribution of the nano-layer structure at the interface, was updated to account for the nanoparticle shape, through the introduction of an equivalent thermal conductivity for the non-spherical particle, given by (GENSHENG et al., 2009):

$$k_p^{eq}=k_p\cdot\frac{\frac{0.75\cdot d_p}{l_p}}{\frac{0.75\cdot d_p}{l_p}+1} \quad 1.53$$

Ordónez-Miranda *et al.* proposed a model that introduces the effect of the energy carriers to the model of the Nan *et al.*, (ORDONEZ-MIRANDA et al., 2012b, 2011). The authors attempted to develop a generic model, considering particles with complex thermal conductivities, according to the kinetic theory. However, the behaviour of these energy carriers across the interface still is a theoretical challenge, being necessary various empirical parameters to be adjusted. Despite that, the authors, proposed an generalized EMT model trough the introduction of the principle of Bruggeman (ORDONEZ-MIRANDA et al., 2012a). The latter can be expressed as:

$$\left(\frac{k_{eff}/k_{bf}^{com}-\alpha}{1-\alpha}\right)\cdot\left(\frac{k_{bf}^{com}}{k_{eff}}\right)^{\frac{1}{2}}=(1-\phi) \quad 1.54$$

where $k_{bf}^{com}$ is the complex thermal conductivity of the base fluid, which take in consideration the effect of the energy carriers, and $\alpha$ is a function of $k_{bf}^{com}$ and the complex thermal conductivity of the particles, energy carriers and particle radius (ORDONEZ-MIRANDA et al., 2012a).

### Thermal conductivity models summary

During the conducted survey, it was found many theories developed to explain the effective thermal conductivity enhancement of nanofluids. In addition to those provided by the classical theories, the authors highlighted the Brownian motion of the particles, diffusion and nanoscale convention, the nano-layer structure at the solid-liquid interface and the nanoparticles agglomeration. In the Table 1.6 it is summarized the derived predictive models and their respective mechanisms that underlie.

Table 1.6: Summary of the effective thermal conductivity models and respective proposed mechanisms.

| Authors | Thermal interaction | Nanoparticle shape | Kapitza Resistance | Brownian motion | Nano-layer structure | Agglomeration |
|---|---|---|---|---|---|---|
| (MAXWELL, 1873) | | | | | | |
| (FRICKE, 1925) | | X | | | | |
| (BRUGGEMAN, 1935) | X | | | | | |
| (HAMILTON et al., 1962) | | X | | | | |
| (HASHIN et al., 1962) | | | | | | |
| (HASSELMAN et al., 1987) | | X | X | | | |
| (WANG et al., 2003a) | | | | | | X |
| (YU et al., 2003) | | | | | X | |
| (XUAN et al., 2003) | | | | | X | |
| (XUE, 2003) | X | X | | | X | |
| (JANG et al., 2004) | | | | X | | |
| (KUMAR et al., 2004) | | | X | | | |
| (KOO et al., 2004) | | | | X | | |
| (NAN et al., 2004) | | X | X | | | |

| Authors | Thermal interaction | Nanoparticle shape | Kapitza Resistance | Brownian motion | Nano-layer structure | Agglomeration |
|---|---|---|---|---|---|---|
| (YU et al., 2004) | | X | | | X | |
| (XIE et al., 2005) | | | | | X | |
| (XUE, 2005) | X | | | | | |
| (YAJIE et al., 2005) | | | | X | X | |
| (PRASHER et al., 2005) | | | | X | | |
| (PRASHER et al., 2006) | | | | X | | X |
| (GAO et al., 2006) | X | X | | | | |
| (SABBAGHZADEH et al., 2007) | | X | | X | X | X |
| (MURSHED et al., 2008) | | X | | | X | |
| (SASTRY et al., 2008) | | X | X | | | X |
| (KOO et al., 2008) | | X | X | | | X |
| (MURSHED et al., 2009) | | | X | X | X | X |
| (DENG et al., 2009) | | | X | | | X |
| (GENSHENG et al., 2009) | | X | | | X | |
| (ORDÓÑEZ-MIRANDA et al., 2010) | X | X | | | | |
| (ORDONEZ-MIRANDA et al., 2012a) | X | X | X | | X | |
| (WEI et al., 2012) | | | | X | X | |
| (XIAO et al., 2013) | | | | X | X | X |

## 1.6 THESIS CONTRIBUTION

The increasing demand for sustainable energy systems and the constant miniaturization of electronic devices has introduced new challenges in the development for cooling systems with enhanced effectiveness. Several efforts have been developed for the enhancement of heat exchanger devices. However, the low capacity for heat conduction of conventional fluids still is a limiting factor. In past few years, it has been claimed that it is possible to produce fluids with improved thermo-physical properties, through the suspension of specific nanoparticles. Such next-generation thermal fluids have been designated as nanofluids.

Several authors reported anomalous thermal conductivity enhancements in nanofluids, as these cannot be described by the classical physical theories. As expected, the search for possible theoretical explanations for these improvements led to a growing scientific interest in nanofluids (see Section 1.5.3.3). However, divergences on proposed theories resulted in the publication of several predictive models with different premises, causing unrelated effects and an unacceptable level of discrepancy.

Possible reasons behind these differences might be the aggregation of the nanoparticles that usually is uncontrolled and not characterized in both experimental and numerical studies, and the unknown nanoparticles size distribution, since the researchers rarely report on the size distribution of the nanoparticles (or aggregates) and rely upon the manufacturer, even after processing this. Furthermore, these announced discrepancies might be induced through the different methods for the nanofluids preparation that form distinct morphological structures, which may provide inaccuracy to the cross-comparison among the reported observations (SIDDIQUE et al., 2010). In general, the particles geometry and phase distribution were not full characterized in most nanofluids experiments, discouraging the cross-comparison among the several authors, and respective validation of the theoretical predictive models. It has been found out that the type of nanoparticle and its geometry, as well as the method of synthesis and particle dispersion, induces distinct effects on the heat conduction capacity improvements of the mixture (GE et al., 2006, KHANAFER et al., 2011, NASEH et al., 2010). In addition, in order to ensure successful application of nanofluids, their respective thermo-physical properties may stand for long periods, and this is definitely related to their colloidal stability.

The conducted bibliography survey revealed that it is broadly accepted that MWCNTs are the most promising nanoparticle for thermal conductivity enhancement. Such behaviour may be explained by their reported thermal conductivity and spatial distribution induced by their elongated geometry, making them the most promising for industrial applications since its volume fraction could be slighter, as it can be depicted from Figure 1.4. This is a fundamental feature to avoid an undesired increase of the fluid viscosity as well as to decrease, their production cost.

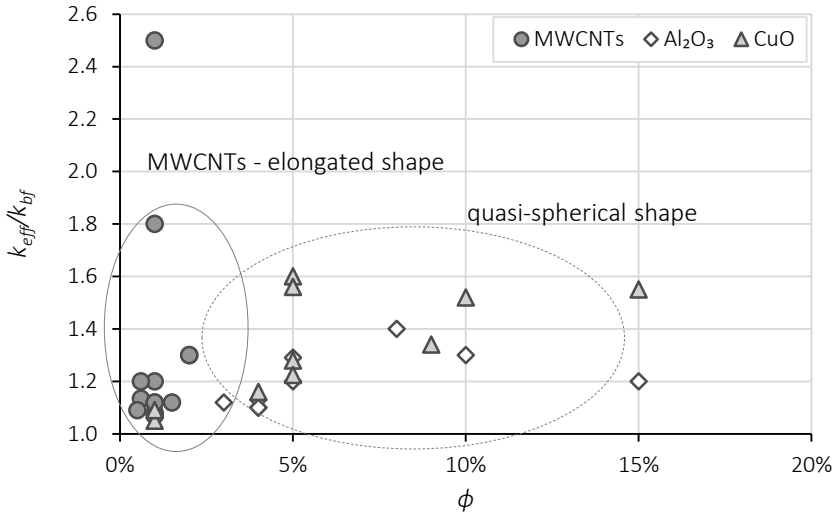


Figure 1.4: Summary of the experimental data available on the open literature for nanofluids.

In addition, measuring the thermal conductivity of liquids is a very difficult task, since it is necessary to ensure a set of conditions that prevent overestimated readings. This problem is even more serious when dealing with dispersions, since the degree of homogeneity among them may cause a high degree of uncertainty. As such, it is necessary to define the morphological conditions of the nanofluids and ensure that these are constant for all the samples subjected to the experimental measurements, enabling, therefore, their cross-comparison.

Therefore, this research aims to contribute to the nanofluids research, by the experimental and theoretical characterization of the thermal conductivity of long-term MWCNTs based nanofluids that meet the stability requirements towards industrial application as next-generation thermal fluids. To this end, long-term thermal nanofluids are defined in detail and samples are properly characterized, enabling a better and more coherent reading of the inherent thermo-physical mechanisms governing the heat conduction in nanofluids. A physical predictive model for the thermal conductivity is also developed and experimentally validated. It is expected that the acquired experimental and theoretical results contribute to present scientific knowledge as well as a support for future work, both at fundamental and engineering level.

## 1.7 THESIS ORGANIZATION

In Chapter 1 the objectives and contribution of the thesis are postulated. Additionally, and supporting the later, a comprehensive literature review on the synthesis and heat transport properties of nanofluids, including experimental data and theoretical models, is presented. In Chapter 2, the classical mechanisms responsible for the enhancement of the thermal conductivity

of dispersion are revised in detail, and based on these, a novel physical predictive model is proposed.

Chapter 3 presents a methodology for the production of long-term nanofluids based on well-established theories. In addition, this Chapter also deals with the methods and materials that were used to prepare and characterize stability of the nanofluid samples. In Chapter 4 it is discussed the obtained experimental thermal conductivity results and the predictive model is experimentally validated. Finally, Chapter 5 summarizes the major results obtained and some recommendations for future research are provided.

## 1.8 CHAPTER CONCLUSIONS

The conducted literature survey revealed that the dispersion of specific nanoparticles in conventional fluids results in a thermal conductivity enhancement of the base fluid, usually described as anomalously high. This is a result of the apparently unpredictable effect of the nanoparticles on the nanofluid heat conduction enhancement, namely through the classical theory, *i.e*. the *effective medium theory*. Still, some researchers found that the thermal conductivity of these nanofluids may lie within the bounds of the *effective medium theory*. Such lack of agreement between the experimental observations suggests the need of a well-designed experimental parametric study to identify the intrinsic mechanisms affecting the heat transfer rate in these fluids. Moreover, it is important to redefine the term nanofluid at least for thermal energy transport, and ensure constant measurement conditions in an attempt to improve the cross-comparison conditions and respective results. A huge variety of theories were proposed to predict the effective thermal conductivity of nanofluids, apparently without success regarding their generalization.

# 2 MODELLING THERMAL CONDUCTIVITY OF DISPERSIONS

## 2.1 CHAPTER SYNTHESIS

In this Chapter, the classical mathematical formulation to predict the effective thermal conductivity of perfectly stable dispersions is verified. The various morphological structures that such dispersions could present, namely *diluted structure*, *non-diluted structure*, and *percolation-like structure* are described. The formation of these morphological structures depends on the dispersed particle geometry and volume fraction. The transition through these arrangements provides strongly impact on the effective thermal conductivity of the mixture, as suggested by the classical predictive models. Based on these classical theories, a predictive model for the thermal conductivity of interactive elongated nanoparticles is proposed. The latter, designated as *extended differential effective medium theory*, takes into consideration the particle geometry and spatial distribution, Kapitza resistance, and interparticle thermal interaction.

## 2.2 THERMAL CONDUCTIVITY OF DISPERSIONS

It should be noted the difference between the term *solution* and *dispersion*. The term *solution* is referred in the colloid science to thermodynamically stable mixtures, *i.e.* mixtures produced spontaneously when the solute and the solvent are brought together. The addition of energy to a solution will accelerate the mixture process. Without chemical or temperature changes, a solution is stable indefinitely. Conversely, *dispersions* are kinetically stable, requiring energy input to be produced and, if allowed to stand long enough, the reverse process occurs spontaneously. As envisaged in thermodynamics, these spontaneous processes occur in the direction of decreasing Gibbs free energy $\Delta G$ (HIEMENZ, 1977). Therefore, it is seems evident that a mixture of solid particles in a base fluid may be considered as a dispersion.

It is distinguishable that the effective thermal conductivity of dispersions strongly depend upon the thermo-physical properties and spatial distribution of both phases from which are composed. The spatial distribution (the general arrangement of all the phases with respect to each other) can present three distinct geometric morphologies depending on their volume fraction, and on the geometry of the dispersed phase, as described by the *excluded volume theory* (EVT), defined in detail in the Appendix A. The three geometrical morphologies are the *diluted structure*, *non-diluted structure*, and *percolation-like structure*, as showed in Figure 2.1.

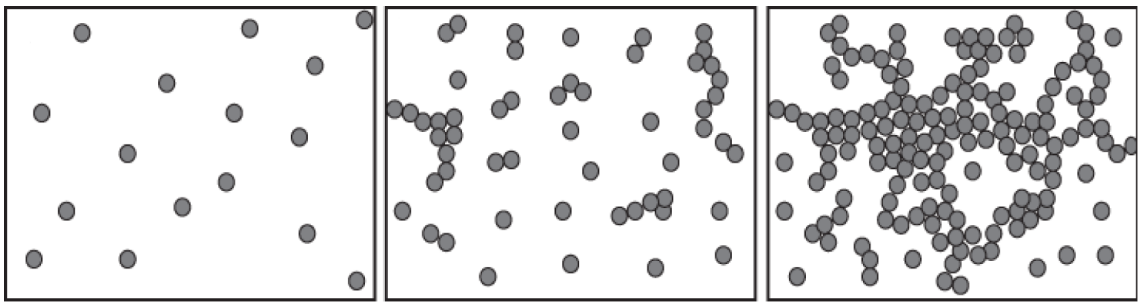

Figure 2.1: Schematic microstructure evolution of spherical particles dispersions: a) *diluted structure*; b) *non-diluted structure*; c) *percolation-like structure*.

From the analysis of the previous Figure, it becomes clear that the evolution through the arrangements modifies the effective thermal conductivity of the mixture observed at the macro scale in distinct ways, especially for the *non-diluted structure* and *percolation-like structure* where the interparticle interaction cannot be neglected since, as it will be seen in the Section 2.3, they may provide an higher enhancement on this property.

Percolation theory describes the degree of connectivity of chaotic systems, like dispersions. Suppose $p$ is a variable that defines the average degree of connectivity between particles. For $p$=0, all the particles inside of a control volume are totally isolated from each other's. In contrast, for $p$=1, all the particles are connected to some maximum number of neighbouring particles. The percolation threshold is the critical $p$, or $p_c$, that describes the minimum degree of interparticle connections that forms a spanning cluster that connects both sides of the representative control volume (STAUFFER, 1979). The volume fraction at the percolation threshold is generally represented as $\phi_c$, and determines the transition from *non-diluted structure* to *percolation-like structure*.

Balberg *et al.* found that the EVT is particularly efficient to ascertain the transition to the *percolation-like structure*, especially in systems where the dispersed particles are elongated with high aspect ratio (BALBERG et al., 1984a). The excluded volume of a particle is the volume around an object which the centre of another similar is not allowed to enter if overlapping of the two objects is to be avoided (EVT described in detail in Appendix A). According to the EVT, $\phi_c$ decreases when the geometry of the dispersed phase changes from spherical to elongate. In Figure 2.2 is illustrated the efficiently spatial distribution of elongated particles when compared to dispersion of spherical particles, for the same volume fraction.

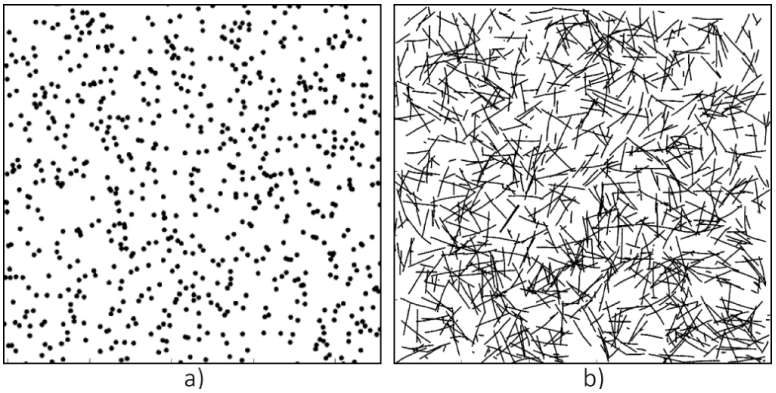


Figure 2.2: Illustration of the spatial distribution for a fixed volume fraction of spherical particles a), and elongated particle b).

The classical predictive models for the thermal conductivity of dispersions are based on the *effective medium theory* (EMT). The EMT is a set of physical models that meant to describe the macroscopic properties of composites, based on the individual properties of the materials that constitute them. These models are commonly used for the prediction of several properties, such as optical, magnetic, diffusion, electrical and thermal conductivity, among others (CHOY, 1999).

As verified in the literature review, the thermal conductivity predictive models of dispersions can be catalogued by the geometry of the dispersion phase. Of these, the simplest models are those that simplify the model through the consideration that the mixture is composed by spherical particles.

## 2.3 THERMAL CONDUCTIVITY OF SPHERICAL DISPERSIONS

Maxwell was a pioneer in the development of an EMT model for the conductivity of composites. The original expression was derived for the electrical conductivity and later was extended to the thermal conductivity, since both are governed by similar equations (MAXWELL, 1873). There is considerable experimental evidence on the validity of the Maxwell model for thermal conductivities for non-nanoscale particles suspension, at very small volume fractions that yield a *diluted structure* (see Figure 2.1). Moreover, the Brownian diffusion of the particles is neglected, *i.e.* it is assumed that the system is homogeneous and static, or motionless.

### 2.3.1 EFFECTIVE MEDIUM THEORY OF MAXWELL

To derive the Maxwell's effective thermal conductivity model for nanofluids, it is considered that a sphere of diameter $d_p$ is immersed in an infinite base fluid subjected to a uniform heat flux, as shown in Figure 2.3.

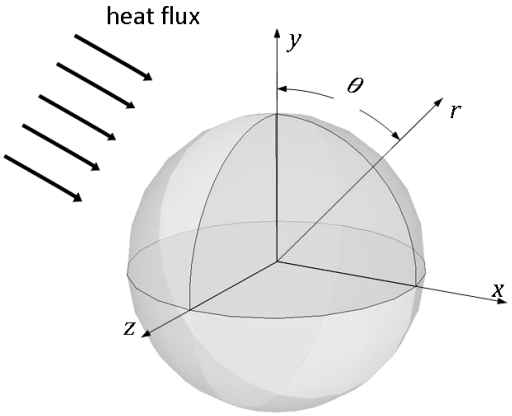


Figure 2.3: Spherical particle dispersed in an infinite base fluid and subjected to a uniform heat flux.

The temperature-field distribution inside the particle $T_p$ and in the infinite medium $T_{bf}$ can be expressed as (HASSELMAN et al., 1987):

$$T_p = A \cdot r \cdot \cos\vartheta \tag{2.1}$$

$$T_{bf} = (\nabla T) \cdot r \cdot \cos\vartheta + \frac{B}{r^2} \cdot \cos\vartheta \tag{2.2}$$

where $\nabla T$ is the temperature gradient at large distances away from the sphere, $r$ and $\vartheta$ are the usual spherical coordinates, and $A$ and $B$ are constants to be solved. The second term of the Equation 2.2 represents the thermal disturbance, or thermal interaction, induced by the presence of the particle, which is vanished as $r \to +\infty$.

To find the solution for the unknowns $A$ and $B$, Equation 2.1 and 2.2 are subjected to the following boundary conditions at the surface of the sphere, *i.e.* $r = d_p/2$:

1) $$T_p = T_{bf} \tag{2.3}$$

2) $$k_p \cdot \frac{\partial T_p}{\partial r} = k_{bf} \cdot \frac{\partial T_{bf}}{\partial r} \tag{2.4}$$

That is, the temperature of the fluid and particle are equal at the surface. It should be noted that this implies a perfect interface, *i.e.* the absence of an interfacial resistance. In line, the second boundary conditions imply that the heat flux is constant at the surface. Solving for the boundary conditions, $A$ and $B$ are solved to:

$$A = \frac{3(\nabla T) k_{bf}}{k_p + 2k_{bf}} \tag{2.5}$$

$$B=\frac{(\nabla T)d_p{}^3\left(k_{bf}-k_p\right)}{8\left(k_p+2k_{bf}\right)} \qquad 2.6$$

Introducing Equation 2.6 into Equation 2.2, the temperature of the base fluid at any point outside the particle is:

$$T_{bf}=(\nabla T)r\cdot cos\vartheta\left(1+\frac{d_p{}^3\left(k_{bf}-k_p\right)}{8r^3\left(k_p+2\cdot k_{bf}\right)}\right) \qquad 2.7$$

Through the same perspective, the temperature at any point inside the particle is:

$$T_p=\frac{3(\nabla T)k_{bf}}{k_p+2k_{bf}}\cdot r\cdot cos\vartheta \qquad 2.8$$

Considering a monodispersion of *N* spherical particles with an average interparticle distance long enough to ensure no thermal interaction, the temperature of the base fluid (Equation 2.7) becomes:

$$T_{bf}=\sum_{i=1}^{N}(\nabla T)r_i\cdot cos\vartheta\left(1+\frac{N\cdot d_p{}^3\left(k_{bf}-k_p\right)}{8\cdot r_i^3\left(k_p+2k_{bf}\right)}\right) \qquad 2.9$$

Assuming that the same *N* particles are equivalent to one large imaginary sphere of diameter $d_{eff}$, that exhibit an effective thermal conductivity $k_{eff}$, the temperature outside the sphere will be similar to the Equation 2.9, and is given by:

$$T_{bf}=(\nabla T)r\cdot cos\vartheta\left(1+\frac{d_{eff}^3\left(k_{bf}-k_{eff}\right)}{8r^3\left(k_{eff}+2k_{bf}\right)}\right) \qquad 2.10$$

Solving the equality of Equation 2.9 and 2.10, and considering $\phi=N\cdot d_p{}^3/d_{bf}^3$, the *effective medium theory* of Maxwell is obtained. This is expressed in the Equation 1.3.

$$k_{eff}=\frac{k_p+2k_{bf}+2\phi(k_p-k_{bf})}{k_p+2k_{bf}-\phi(k_p-k_{bf})}\cdot k_{bf} \qquad \text{(Equation 1.3)}$$

In Figure 2.4 is a comparison of effective thermal conductivity enhancement ratio $k_{eff}/k_{bf}$, predicted through the EMT of Maxwell. As expected, the effective thermal conductivity enhancement ratio increases with the rise on volume fraction and ratio of thermal conductivity of the particles and base fluid.

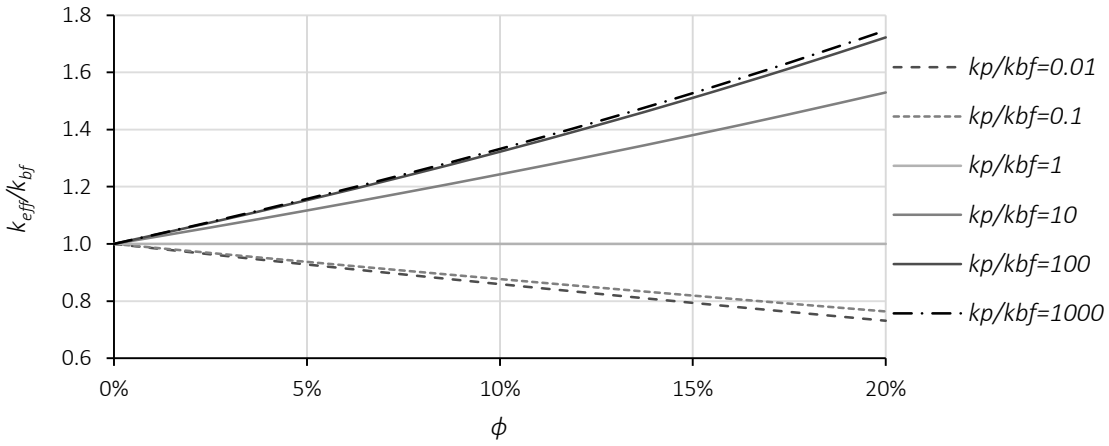


Figure 2.4: Effective thermal conductivity enhancement ratio predicted through the EMT of Maxwell.

Nevertheless, the previous Figure suggested that the effective thermal conductivity enhancement as an upper and lower saturation for $k_p/k_{bf}$. Therefore, in Figure 2.5, it is represented the effective thermal conductivity enhancement ratio with $k_p/k_{bf}$, for a volume fraction of 10%. The latter suggest a lower and an upper saturation point near 0.1 and 100, respectively.

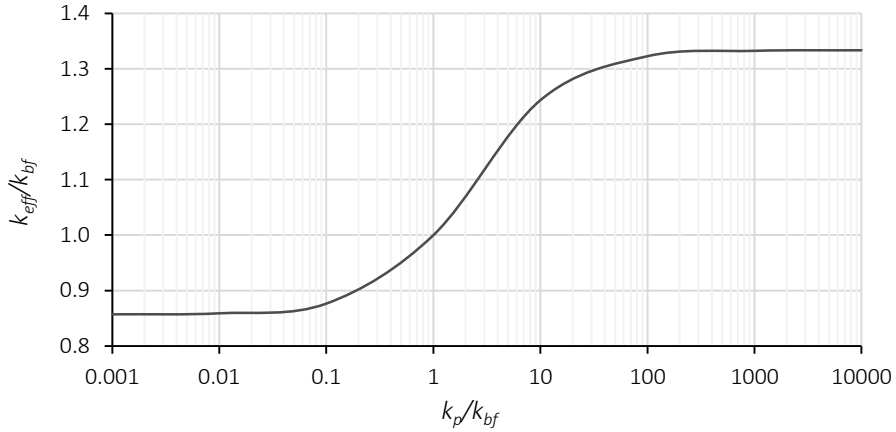


Figure 2.5: Effective thermal conductivity enhancement ratio for a dispersion of particles with $\phi$=10% predicted through the EMT of Maxwell, for different $k_p/k_{bf}$.

### 2.3.2 Differential effective medium theory of Bruggeman

Nevertheless, for a given volume fraction, far below the percolation threshold, the particles become to be affected by the disturbance of the temperature field induced by the conducting neighbouring particles. Such behaviour is noticed from the transition to *non-diluted structure* arrangements. In these arrangements, the interparticle distance is dramatically reduced, inducing a thermal disturbance on the medium, due to their distinct thermal conductivity to the base fluid. It is distinguishable that this disturbance may interact with the surrounding particles. In Figure 2.6, is represented the temperature gradient of a medium with two dispersed particles with higher

thermal conductivity. As it can be depicted, through the decrease of the interparticle distance, the temperature gradient is increased. That is, the temperature felt by the particle at right is higher with decreasing the interparticle distance, causing higher temperatures over longer distances. This mechanism is herein designated as *thermal interparticle interaction*.

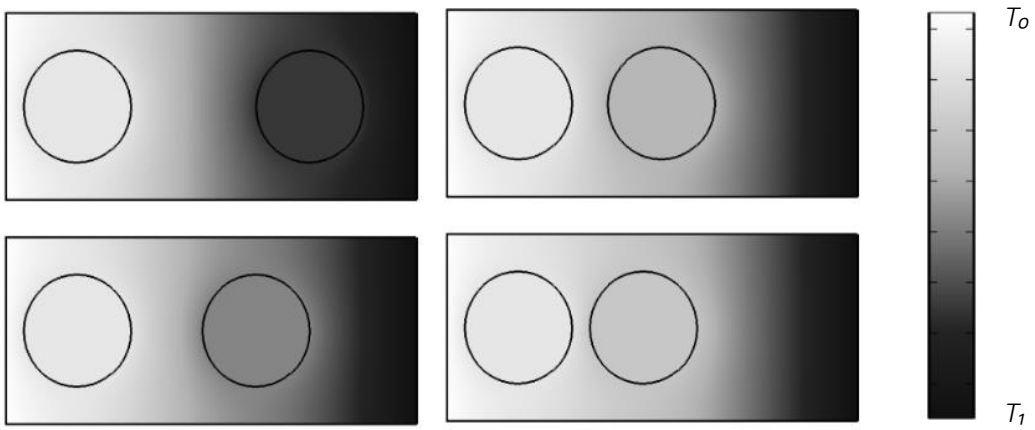


Figure 2.6: Schematic representation of a thermal interparticle interaction of two neighbouring particles ($T_0>T_1$).

To meet the limitation of the EMT of Maxwell, Bruggeman proposed an iterative principle, known as *differential effective medium theory* (DEMT) (BRUGGEMAN, 1935, MINKOWYCZ et al., 2012, TORQUATO, 2002). Through this, it is possible to estimate the effective thermal conductivity of a two-component mixture at higher particle volume fraction that meet both *non-diluted* and *percolation-like structure*.

According to Bruggeman, the effective thermal conductivity of a dispersion may be given by:

$$k_{eff}(\phi)=k_{bf}\cdot\left[1+f_1\left(k_{bf},k_p,P\right)\cdot\phi+f_2\left(k_{bf},k_p,P\right)\cdot\phi^2+\ldots\right] \qquad 2.11$$

where $f_1$ and $f_2$ are dimensionless functions of both thermal conductivity of the base fluid and the particles, and other properties $P$, like particle size, shape, orientation, and others. The dimensionless function $f_1$ determines the behaviour of the effective thermal conductivity in the dilute limit, and $f_2$ takes into account the first-order correction to the dilute limit and the contribution of interparticle interactions. Furthermore, higher-order coefficients of $\phi$ represent strongly related interparticle interactions (BRUGGEMAN, 1935, TORQUATO, 2002).

Through an integration-embedding principle, $k_{eff}(\phi+\Delta\phi)$, the thermal effect of particles added before is taken into account at the next iteration step. That is, in every iterative step, it is considered that the thermal conductivity of the base fluid is equal to the effective thermal

conductivity of a dispersion with less particle volume fraction of the previous step, *i.e.* for $\phi=0 \longrightarrow k_{eff}=k_{bf}$ and for $\phi+\Delta\phi \longrightarrow k_{eff}+\Delta k_{eff}$, as schematically represented in the Figure 2.7. Through this, the Bruggeman approach considers a *dilute dispersion* and, therefore, the coefficient of order $\phi^2$ and above are neglected.

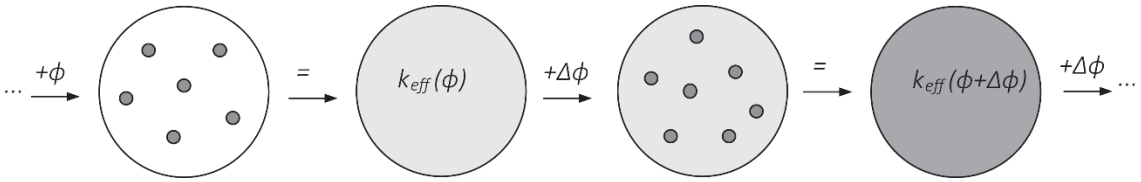


Figure 2.7: Schematic view of the integration-embedding principle of Bruggeman.

Under such conditions, low increment $\Delta k_{eff}$ of the DEMT of Bruggeman is be expressed as:

$$\Delta k_{eff}=\frac{k\cdot f_1\left(k_{bf},k_p,P\right)}{(1-\phi)}\cdot\Delta\phi \qquad 2.12$$

Integrating Equation 2.12 for the limits $k_{bf}$ and $k_{eff}$, and for the limits 0 and $\phi$, the Equation is reduced to:

$$\int_{k_{bf}}^{k_{eff}}\frac{dk}{k\cdot f_1\left(k_{bf},k_p,P\right)}=\int_0^{\phi}\frac{d\phi}{1-\phi} \qquad 2.13$$

From these assumptions, it is established that the effective thermal conductivity of dispersions with arbitrary volume fractions can be derived from their *diluted structure*. Therefore, a prediction model valid for low volume fractions may be used to generate a new formula for high volume fractions.

Simplifying the EMT of Maxwell (Equation 1.3) to:

$$k_{eff}=k_{bf}\cdot\left[1+\frac{3\left(k_p-k_{bf}\right)}{k_p+2k_{bf}-\phi\left(k_p-k_{bf}\right)}\cdot\phi\right] \qquad 2.14$$

the dimensional function $f_1$ of first order of $\phi$, become:

$$f_1\left(k_{bf},k_p,P\right)=\frac{3\left(k_p-k_{bf}\right)}{k_p+2k_{bf}} \qquad 2.15$$

Replacing Equation 2.15 into Equation 2.13, and substituting $k_{bf}$ for $k$, the integration process is reduced to:

$$\left[\frac{1}{3}ln(k) - ln\left(k_p - k\right)\right]\Big|_{k_{bf}}^{k_{eff}} = -ln(1-\phi) \qquad 2.16$$

From this, the Bruggeman model for dispersion of spherical particles, with negligible Kapitza resistance can be simplified to Equation 1.4:

$$\left(\frac{k_p - k_{eff}}{k_p - k_{bf}}\right) \cdot \left(\frac{k_{bf}}{k_{eff}}\right)^{\frac{1}{3}} = (1-\phi) \qquad \text{(Equation 1.4)}$$

According to the Bruggeman approach, thermal interparticle interaction affects the effective thermal conductivity enhancement of dispersions of spherical particles, at volume fractions above ~15%, as can be depicted from Figure 2.8. Above this volume fraction, the thermal conductivity presents an exponential-like enhancement. Moreover, the thermal conductivity enhancements ratio for volume fractions below ~15% match with the ones calculated through the Maxwell model (BRUGGEMAN, 1935).

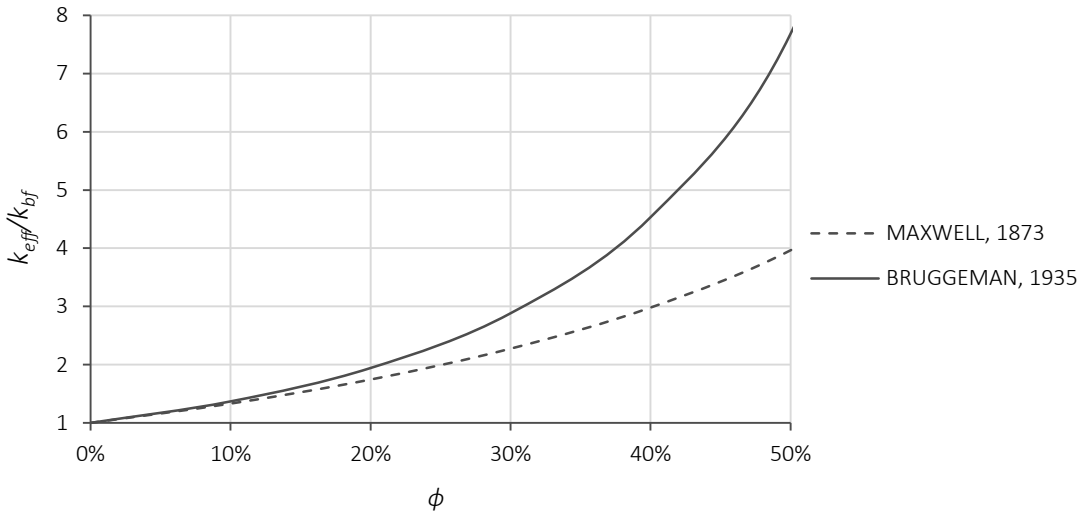


Figure 2.8: Predicted thermal conductivity enhancement ratio through the Maxwell and Bruggeman model, for $k_p/k_{bf}=100$.

It is expected a dependence of the effective thermal conductivity, predicted by the DEMT of Bruggeman, with the volume fraction and ratio of the thermal conductivity of particles and base fluid. In line with the results presented in Figure 2.4, such dependence is represented in Figure 2.9. In addition, It is noticed a convergence of the results with those predicted by the EMT of Maxwell for the volume fractions below 15%.

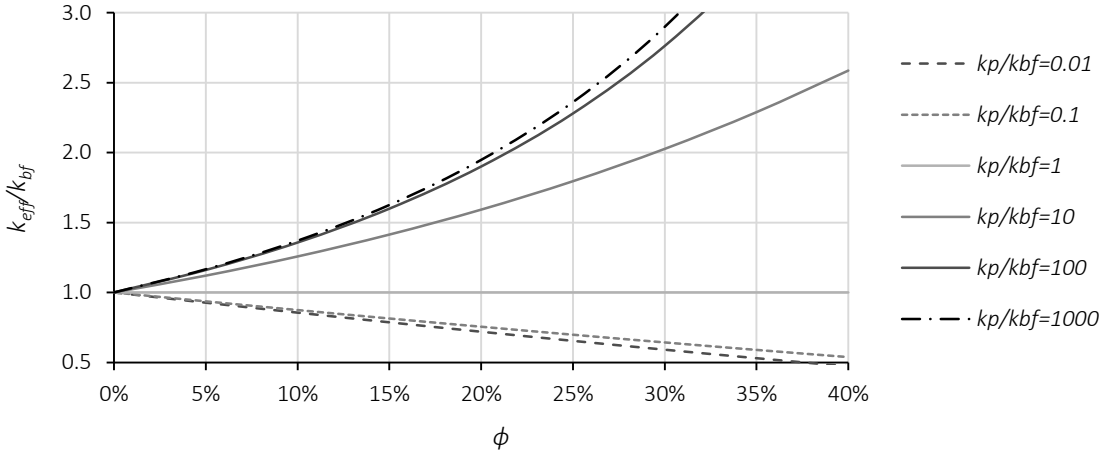


Figure 2.9: Effective thermal conductivity enhancement ratio predicted through the DEMT of Bruggeman.

As seen in the Maxwell model, the Bruggeman model presents a lower and upper limit saturation dependence with $k_p/k_{bf}$, of 0.1 and 100, respectively. Such behaviour can be depicted in Figure 2.10.

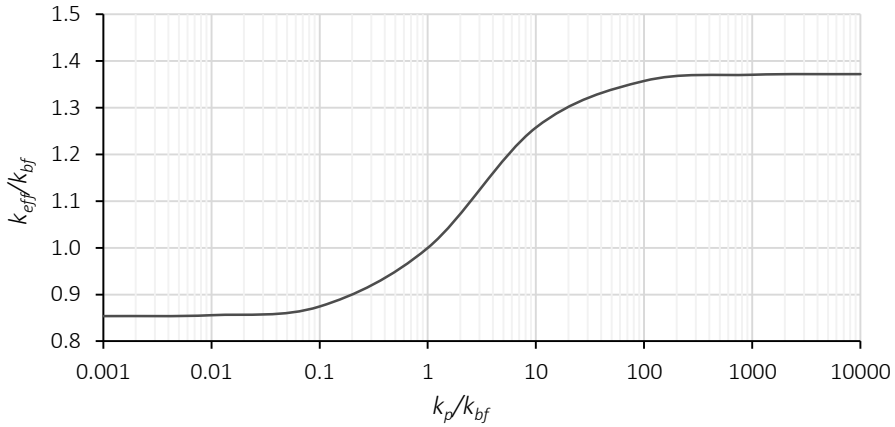


Figure 2.10: Effective thermal conductivity enhancement ratio for a dispersion of particles with $\phi$=10% predicted through the DEMT of Bruggeman, for different $k_p/k_{bf}$.

The results shown so far suggests that the thermal interparticle interaction only contribute for the effective thermal conductivity enhancement at higher particles volume fractions (>15%). In fact, regarding thermal nanofluids, such concentrations may be undesired due to a higher probability of unstable dispersions and/or greater effective viscosity. Nevertheless, as previously verified in Figure 2.2, it is expected a higher degree of interparticle interaction, even at very low volume fractions, for the MWCNTs based nanofluids due to the elongated aspect of the nanoparticles.

## 2.4 THERMAL CONDUCTIVITY ACROSS THE INTERFACE PARTICLE-MEDIUM

As mentioned, *percolation theory* suggests the existence of a critical volume fraction $\phi_c$, also known as percolation threshold, from which the dispersed phase forms a spanning cluster that connects both sides of the control volume (STAUFFER, 1979). This critical volume fraction points out the transition to the *percolation-like structure* arrangement, represented in Figure 2.1.

The transition to *percolation-like structure* suggests a dramatic change in the conductivity properties of the dispersion, especially when the conductivity ratio between the two phases is high. For instance, regarding nanocomposites, Biercuk *et al.* found experimentally that the MWCNTs have an extremely low percolation threshold, due to their elongated geometry (BIERCUK et al., 2002). They measure the electrical conductivity of MWCNTs in epoxy composites at various volume fractions. The results revealed a suddenly jump (discontinuity), in the order of $10^4$, for volume fractions above 0.1%. These results were attributed to the transition to the *percolation-like structure*, from where the conduction of electricity is more effectively. Nevertheless, the same samples were subjected to the measurement of the effective thermal conductivity, and the results showed a continuous enhancement, *i.e.* without the percolation transition effect. These observations were attributed to a thermal discontinuity at the interface of the particles, also known as Kapitza resistance.

The Kapitza resistance is a well-known thermal resistance at the interface of two materials. According to Kapitza, the temperature at the particle-medium interface undergoes a change proportional to the normal component of the heat flux through the interface $q_{interface}$, as follows (CHERKASOVA, 2009, KAPITZA, 1941):

$$T_p - T_{medium} = -R_K \cdot q_{interface} \qquad 2.17$$

Due to the relatively good contact between liquid and solid materials, the Kapitza resistance is rather low compared to the resistance of solid-solid interfaces. This resistance is associated with the differences in electronic and phonon spectra of the two materials. Therefore, this exists even at atomically perfect interfaces and differs from contact resistance (KAPITZA, 1941, SWARTZ et al., 1989).

In solids, thermal energy can be carried by electrons and lattice vibrations (phonons). In metals, the thermal energy is dominantly carried through electrons while non-metals is dominantly through phonons (CAHILL et al., 2003, CAHILL et al., 2001, HOPKINS, 2013, HOPKINS et al., 2011). Given the

interruption of the crystalline lattice at the interface solid-medium, a thermal resistance is produced. The phonons traverse a certain distance before scattering and losing their thermal energy, establishing a temperature gradient, the mean free path. At room temperature, the mean free path may range from 1 to 100 nm (CAHILL et al., 2003). For nanoparticles of same order of the mean free path, it seems that additional scattering events arise and the phonon thermal conductivity is greatly reduced. Therefore, in nano-systems the thermal transport across the interface may dictate the overall thermal conductivity. The thermal conductance across the interface is, therefore, intimately related to the characteristics of the interface in addition to the fundamental atomistic properties of the materials comprising the interface itself (HOPKINS et al., 2011). However, the fundamental mechanisms driving these electron and phonon interaction at this scale are still a challengeable subject and are not clear yet.

Another interesting theory to describe the heat transfer across the interface is the molecular-level layering concept. This states that the molecules from a liquid near a solid surface (such as a nanoparticle surface) become more organized than the remaining, forming a solid-like layer structure (not crystalized) (SNOOK et al., 1978). As revealed in the previous Chapter, several authors suggested that these ordered structures provide a thermal bridge effect that enhances the heat conduction in nanofluids, due to phonon effects on these solid structures. Somehow, this theory may contradict the effect of Kapitza resistance, since it is expect that the one provides and enhancement and the other a penalty in the heat conduction phenomena.

In fact, many metals exhibit no penalty in their thermal conductivity upon melting. Despite the transition from crystalline to the non-crystalline suggests no effect on the thermal conductivity, a significant contribution to the heat transport in metals (both crystalline and molten metals) is due to electrons rather than phonons (POIRIER et al., 1994). In contrast, the thermal conductivity of liquid water, at the melting point, is almost 4 times smaller than that of the ice (LIDE, 2004). This suggests that, for non-metal materials, the crystalline ordering may have a significant effect on the thermal conductivity since, as seen, the contribution of electrons to the heat transport is not the dominant one.

This behaviour was verified, through non-equilibrium molecular dynamic simulations, by several authors (EVANS et al., 2007, XUE et al., 2004). The results suggested, that in liquid water, the thermal conductivity present a significant enhancement only for crystalline ordered structures. For water molecules near a solid surface, it was verified the formation of the ordered structures,

however, with imperfections that provide scattering sites for the heat carrying phonons. Moreover, such imperfections can also be observed for hydrophilic surfaces, since only very high electrical fields diminished these. Likewise, the dynamic behaviour of the particles, caused by the incessant Brownian motion may also contribute to a higher formation of the mentioned imperfections that scatter the heat transfer at the interface.

Therefore, it seems quite evident that the Kapitza resistance may be the dominant heat transfer mechanism at the interfaces. Even so, the fundamental mechanisms driving the Kapitza resistance are still a challengeable subject and are not clear yet. Due to the requirement of a more detailed understanding of heat conduction at these interfaces, than that achievable through the Fourier' law, many theoretical models were developed to quantitatively analyse the Kapitza resistance based on the statistical mechanics equation of Boltzmann. However, it should be reminded that in these equations the electrons and phonons are treated as particles, suggesting the requirement for different theoretical approaches.

For the moment, the theoretical models developed include the acoustic and diffusive mismatch models, (AMM) and (DMM) respectively (KHALATNIKOV et al., 1973, SWARTZ et al., 1989), lattice dynamics models (CHEN, 1998, STONER et al., 1993, YOUNG et al., 1989, ZHAO et al., 2002) and, more recently, molecular dynamics models (CHOI et al., 2004, SHENOGIN et al., 2004a, SHENOGIN et al., 2004b, SHENOGINA et al., 2005, XUE et al., 2003, ZHONG et al., 2006). Nevertheless, the models underestimate the few experimental data available, except for extremely low temperatures. This may be explained by other dominant mechanisms for thermal energy exchange across the interface, such as surface wettability, inclusions, energy carrier scattering with interfaces, among others (BAYRLE et al., 1989, HUXTABLE et al., 2003, KIM et al., 2008a, POLLACK, 1969, SHENOGIN et al., 2004b).

The effective thermal conductivity enhancement limitation, as a result of the Kapitza resistance, becomes even more important for nano-systems due to the high density of interfaces and nanoparticles sizes order. At the nanoscale, the surface-to-volume ratio is higher than that at microscale, increasing the density of interfaces. Therefore, the effective thermal conductivity of nanofluids may have to be modelled at molecular level theories, which would establish a significant breakthrough in the perception of the actual heat transfer mechanisms across the interface. Nevertheless, given the lack of fundamental theories to describe the nature of the heat transfer

across the interface solid-medium at the nanoscale, the available models should be improved and adjusted meanwhile.

Cahill's research group measured the transient changes in the optical absorption of MWCNTs suspensions in heavy water stabilized with sodium dodecyl-sulphate surfactant. These transient changes are a result of the temperature change in the MWCNTs. Using the time constant associated with the optical absorption decay and the heat capacity of the CNTs, they computed the Kapitza resistance to $\approx 8\times10^{-8}$ K m$^2$/W (HUXTABLE et al., 2003). Later, through molecular dynamics simulations, they predicted this Kapitza resistance as $\approx 4\times10^{-8}$ K m$^2$/W, an half of the experimental measurements. They speculated that a possible reason for the discrepancy is the fact that in their molecular dynamics simulations all phonons are excited at all temperatures, while in the experiments a significant portion of the modes is not excited due to quantum effects (SHENOGIN et al., 2004b).

Furthermore, they reported that the magnitude of $R_K$ may range from $0.8\times10^{-8}$ K m$^2$/W to $2\times10^{-7}$ K m$^2$/W for nano-systems (CAHILL et al., 2001, WILSON et al., 2002), depending on both thermo-physical properties of the phases and degree of interaction (interface bonding). Through molecular dynamic simulation, they found that hydrophilic interfaces presents 2-3 times lower Kapitza resistance than hydrophobic interfaces (GE et al., 2006). Lee suggests that the hydrophilic compounds, generally oxides groups, attract and bind the counter ions with opposite polarity of the liquid. Since the ions of the hydrophilic groups are often hydrated, they will associate with the water molecules at the interface, forming liquid columns that reduce the Kapitza resistance (LEE, 2007). Perhaps, this liquid columns can be regarded as a nano-layer ordering, with less imperfections than that formed near a hydrophobic surface, reducing, therefore, the magnitude of the Kapitza resistance.

The nanoparticles are also typically wetted by the base fluid resulting in not direct contact between them. Also, the small contact area will result in a large solid-solid contact resistance. Zhong *et al.* found that the interfacial thermal resistance at the solid-solid contact could be increased in a factor of order 4 with an intimate contact (ZHONG et al., 2006). In contrast, Cahill's research group suggested that this resistance at the solid-solid contact is increased by a factor of 2 (HUXTABLE et al., 2003).

Another usual form to characterize the Kapitza resistance is through the Kapitza length, $a_K$ (Equation 1.11, in section 1.5.3.4). According to the Fourier's law, this represents the equivalent thickness of the medium, with the same thermal conductivity, over which is caused the equivalent temperature drop at the interface. In general, for $a_K$ smaller than the particle size, the effective thermal conductivity increases with the rise on volume fraction. Conversely, when $a_K$ is large than the particle size, the effective thermal conductivity decreases with the rise on volume fraction.

As previously seen, both Maxwell and Bruggeman models assume perfect temperature continuity at the solid-liquid interface, which contradicts the Kapitza theory. For this reason, Benveniste *et al.* (BENVENISTE, 1987, BENVENISTE et al., 1986) modified the Maxwell and Bruggeman models, replacing $k_p$ by an equivalent thermal conductivity of a complex particle with an interfacial layer $k^{eq}$:

$$k^{eq} = \frac{k_p}{1 + \frac{2R_K \cdot k_p}{d_p}} \qquad 2.18$$

It is expected that the thermal interparticle interaction strongly depend on the magnitude of $R_K$, since this lower the heat conduction of each dispersed particle. In Figure 2.11 is plotted the effective thermal conductivity enhancement predicted through the models of Maxwell and Bruggeman, modified by the principle of Benveniste *et al.*. In this, it was considered a spherical nanoparticle with 100 nm diameter and a thermal conductivity ratio of 500. As expected, a system with a Kapitza resistance equal to the lower bound of the Cahill's research group (~$1\times10^{-8}$ K m$^2$/W) presents a further enhancement induced by the thermal interparticle interaction. Moreover, for this magnitude, the Bruggeman model predicts thermal interparticle interaction above ~10% volume fractions, in contrast to the ~15% for the perfect interface. However, in contrast with the lower bound, for the Kapitza resistance of $1\times10^{7}$ K m$^2$/W it is observed a degradation of the effect induced by the thermal interparticle interaction, a undesired effect in what heat exchange enhancement concerns. Even so, it should be reminded that the Cahill's research group suggested a Kapitza resistance of ≈$8\times10^{-8}$ K m$^2$/W for MWCNTs dispersions. Furthermore, in this, it is expected a higher degree of interparticle interaction at lower volume fraction.

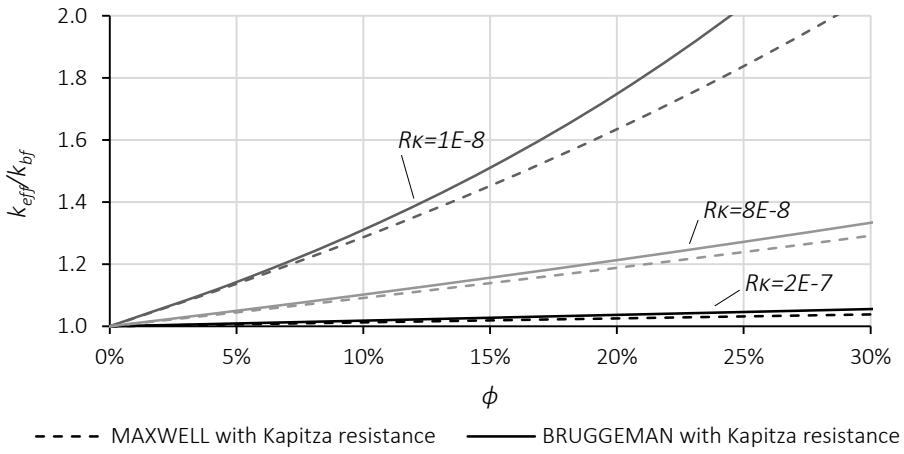


Figure 2.11: Effect of the Kapitza resistance on thermal conductivity enhancement ratio, predicted through modified Maxwell and Bruggeman models for $k_p/k_{bf}$ =500 (modified to take into account the Kapitza resistance).

## 2.5 THERMAL CONDUCTIVITY OF NON-SPHERICAL DISPERSIONS

As earlier verified by Fricke, and Hamilton and Crosser, the shape of the particles is also a key factor for the magnitude of the effective thermal conductivity of dispersions (FRICKE, 1925, HAMILTON et al., 1962). Recently, Nan *et al.* proposed an interesting model, based on the multiple scattering theory, that could be regarded as an upgrade to the Maxwell model for non-spherical particles dispersions (NAN et al., 2003).

### 2.5.1 EFFECTIVE MEDIUM APPROACH OF NAN *ET AL.*

The effective medium approach of Nan *et al.* considers a statistically homogeneous dispersion of randomly oriented ellipsoidal particles. Since the model presents a greater degree of spatial inhomogeneity to the problem, they used the Green function, a solving function for inhomogeneous differential equations, to compute the heat conduction through the effective medium (NAN et al., 2003, NAN, 1993, NAN et al., 1997).

The boundary conditions for the model derivation were similar to that of Maxwell's effective medium approach (Equation 2.3 and 2.4). With this, the interfacial resistance is neglected, simplifying the derivation of the model. Despite considering the spatial distribution of the elongated particles, the model neglects the thermal interparticle interaction. This allowed obtaining a simpler model, only valid for *diluted structures*, schematically represented in Figure 2.12, in a similar way to the represented in Figure 2.1 for spherical particles dispersions.

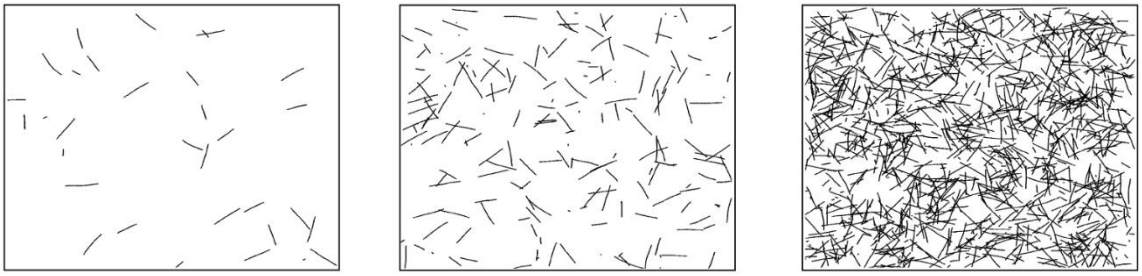

a) b) c)

Figure 2.12: Schematic microstructure evolution of elongated particles dispersions: a) *diluted structure*; b) *non-diluted structure*; c) *percolation-like structure*.

The computed Nan *et al.* model, for a dilute suspension of randomly oriented spheroidal particles with perfect interfacial surface and thermal interaction negligible is given by Equation 1.31. Moreover, the model also enables to predict the effective thermal conductivity of cylindrical or elongated particles dispersions, through the approximation of this to a very elongated spheroidal particle.

$$k_{eff}=\frac{3+\phi\left(2\beta_{xx}(1-L_{xx})+\beta_{zz}(1-L_{zz})\right)}{3-\phi(2\beta_{xx}\cdot L_{xx}+\beta_{zz}\cdot L_{zz})}\cdot k_{bf} \qquad \text{(Equation 1.31)}$$

where $L_{xx}$ and $L_{zz}$ are depolarization factors and,

$$\beta_{xx}=\frac{k_{xx}-k_{bf}}{k_{bf}+L_{xx}\left(k_{xx}-k_{bf}\right)} \qquad \text{(Equation 1.32)}$$

$$\beta_{zz}=\frac{k_{zz}-k_{bf}}{k_{bf}+L_{zz}\left(k_{zz}-k_{bf}\right)} \qquad \text{(Equation 1.33)}$$

As mentioned before, the model was, at first, derived assuming a perfect interface particles-medium. Later, Nan *et al.* introduced the effect of the Kapitza resistance through the consideration of equivalent resistance that substitute the parameters $k_{xx}$, and $k_{zz}$, as previously suggested by Benveniste *et al.* (NAN et al., 2004).

Considering suspension of cylindrical or elongated particles with diameter $d_p$ and length $l_p$, the $k_{xx}^{eq}$, and $k_{zz}^{eq}$ can be derived through the mixture rule for a simple series of resistance, *i.e.* the equivalent resistance method, as can be depicted in the Figure 2.13.

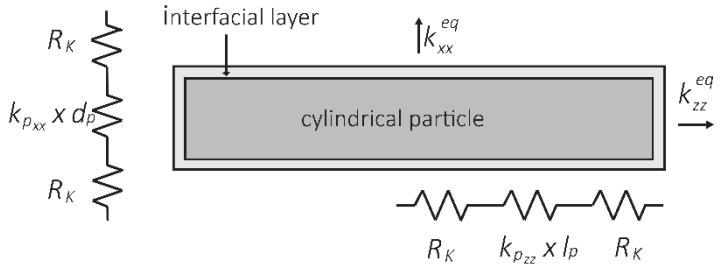


Figure 2.13: Schematic illustration of the equivalent thermal resistance along the 33 axis, of a cylindrical or elongated particle with an interfacial thermal resistance.

The equivalent thermal resistance can be derived trough the following equations (INCROPERA et al., 2006):

($xx'$)

$$R_{eq_{xx}} = \frac{d_p}{k_{xx}^{eq}} = R_K + \frac{d_p}{k_{p_{xx}}} + R_K \tag{2.19}$$

$$\Longrightarrow k_{xx}^{eq} = \frac{1}{\frac{1}{k_{p_{xx}}} + \frac{2R_K}{d_p}} = \frac{k_{p_{xx}}}{1 + \frac{2a_k}{d_p} \cdot \frac{k_{p_{xx}}}{k_{bf}}} \tag{2.20}$$

and,

($zz'$)

$$R_{eq_{zz}} = \frac{l_p}{k_{zz}^{eq}} = R_K + \frac{l_p}{k_{p_{zz}}} + R_K \tag{2.21}$$

$$\Longrightarrow k_{zz}^{eq} = \frac{1}{\frac{1}{k_{p_{zz}}} + \frac{2R_K}{l_p}} = \frac{k_{p_{zz}}}{1 + \frac{2a_k}{l_p} \cdot \frac{k_{p_{zz}}}{k_{bf}}} \tag{2.22}$$

where $a_k = R_K \cdot k_{bf}$ as stated in Equation 1.11.

The depolarization factors, $L_{xx}$ and $L_{yy}$ from Equation 1.32 and 1.33, are functions of the shape and degree of homogenization of the particles (LANDAU et al., 1984). They describe the influence of the geometrical shape and orientation on the temperature gradient or disturbance in the medium. These can be obtained by the following expressions:

$$L_{xx} = L_{yy} = \begin{cases} \frac{(l_p/d_p)^2}{2\left((l_p/d_p)^2 - 1\right)} - \frac{(l_p/d_p)}{2\left((l_p/d_p)^2 - 1\right)^{3/2}} \cdot \cosh^{-1}(l_p/d_p), & (l_p/d_p) > 1 \\ \frac{(l_p/d_p)^2}{2\left((l_p/d_p)^2 - 1\right)} + \frac{(l_p/d_p)}{2\left((l_p/d_p)^2 - 1\right)^{3/2}} \cdot \cos^{-1}(l_p/d_p), & (l_p/d_p) < 1 \end{cases} \tag{2.23}$$

$$L_{zz}=1-L_{xx}-L_{yy}=1-2L_{xx} \quad (2.24)$$

Nevertheless, in the case of very elongated particles ($l_p/d_p$>10), they can be simplified to $L_{xx}=1/2$ and $L_{zz}=0$ (LANDAU et al., 1984). This behaviour can be depicted from Figure 2.14, in which is represented the depolarization factor *Lxx* varying with the nanoparticle aspect ratio $(l_p/d_p)$.

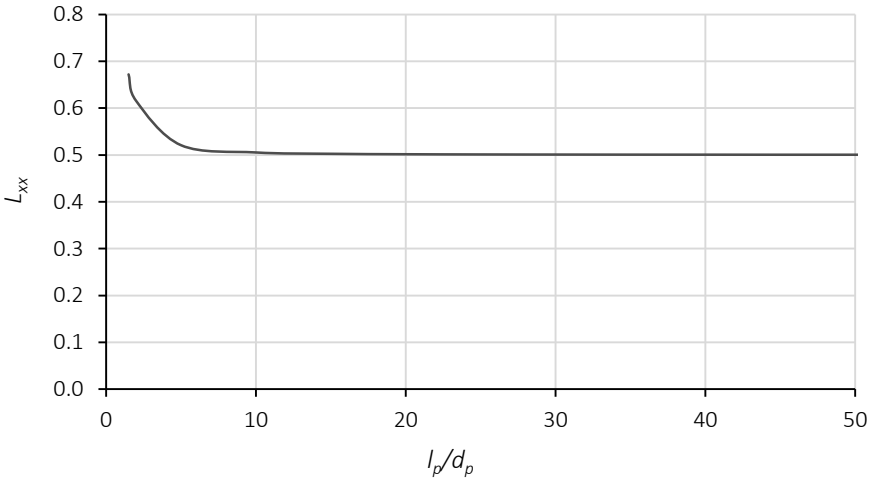


Figure 2.14: Depolarization factor *Lxx* of elongated nanoparticles of different aspect ratio $(l_p/d_p)$.

Through this, the effective medium approach of Nan *et al.* for suspensions of very elongated particles could be reduced to (NAN et al., 2004):

$$k_{eff}=\frac{3+\phi\cdot\left(\frac{2\left(k_{xx}^{eq}-k_{bf}\right)}{k_{xx}^{eq}+k_{bf}}+\frac{k_{zz}^{eq}}{k_{bf}}-1\right)}{3-\phi\cdot\frac{2\left(k_{xx}^{eq}-k_{bf}\right)}{k_{xx}^{eq}+k_{bf}}}\cdot k_{bf} \quad (2.25)$$

The effective medium approach of Nan *et al.* is considered the more generalist of the EMT. This is based on the same heat conduction mechanism and boundary conditions devised by Maxwell, with the addition of the effect of the Kapitza resistance and the particle shape. For spherical particles, all the depolarization factors are equal to 1/3, and the model coincides with the Maxwell equation (Equation 1.3). However, it should be reminded that this model neglects the thermal interparticle interaction.

In Figure 2.15, it is performed an assessment between the calculated thermal conductivity enhancement ratio for dispersions of spherical particles, $(l_p/d_p)$=1, and isotropic elongated particles with an aspect ratio of 100, $(l_p/d_p)$=100. In this Figure, it was considered a perfect interparticle

interface, *i.e.* $R_K$=0 K m$^2$/W. As can be seen, for dispersion of large aspect ratio particles, the predicted thermal conductivity enhancement ratio can dramatically exceed that of spherical particles.

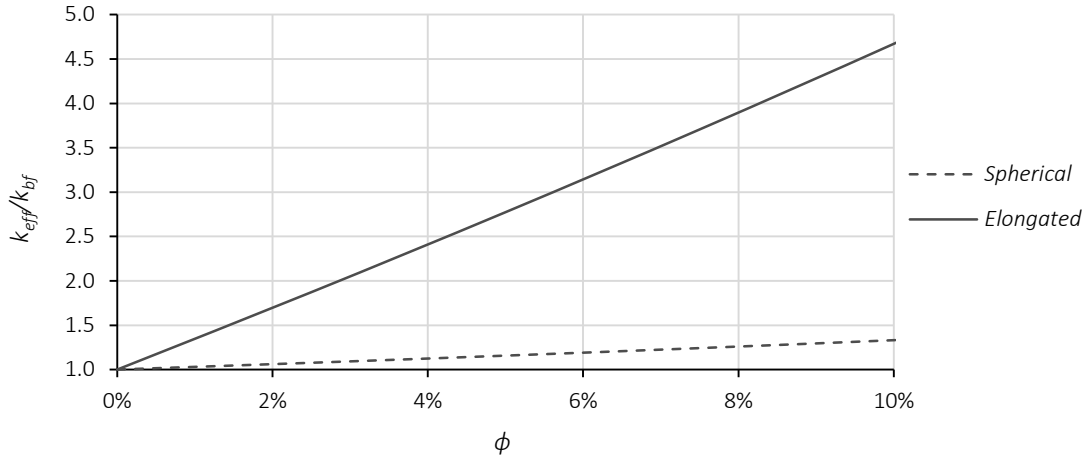


Figure 2.15: Comparison of the predicted thermal conductivity enhancement ratio for spherical particles and very elongated particles ($l_p/d_p$)=100, for $k_p/k_{bf}$ =50 and $R_K$=0.

Moreover, the model suggests that the effective thermal conductivity present distinct saturation behaviour with the ratio of the thermal conductivities of both materials, $k_p/k_{bf}$, with the variation of the aspect ratio, as can be observed in Figure 2.16. It should however be noted, that in this Figure was considered the lower bound of the Kapitza resistance suggested by Cahill's research group.

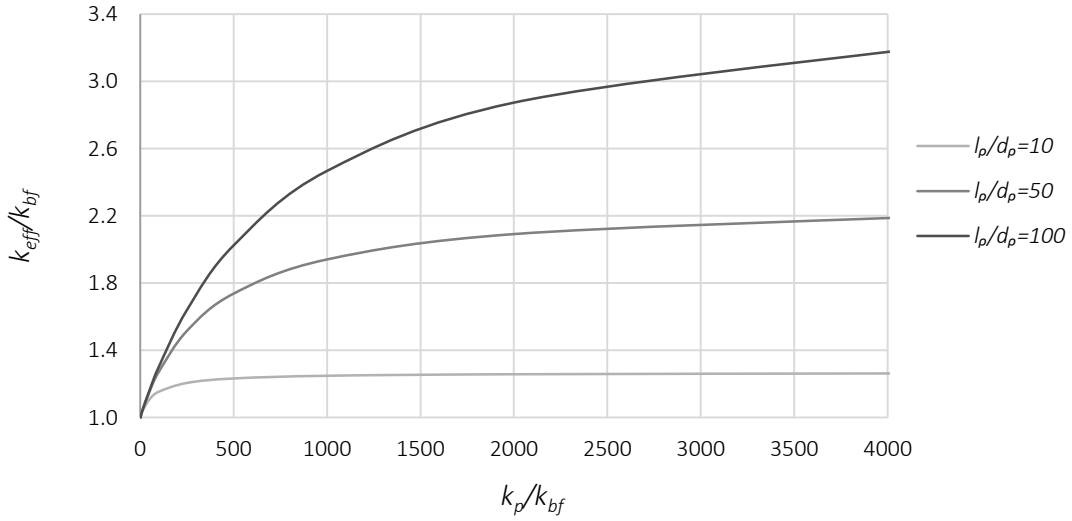


Figure 2.16: Effect of $k_p/k_{bf}$ on the calculated thermal conductivity enhancement for elongated particles with $R_K$=$10^{-8}$ K m$^2$/W and $\phi$=1%.

It is expected a variation of the magnitude of the variables, with the variation of the Kapitza. As was verified by Cahill's research group, the Kapitza resistance may range from $0.8\times10^{-8}$ K m$^2$/W to $2\times10^{-7}$ K m$^2$/W, for nanoparticles dispersed in conventional fluids. In Figure 2.17 is shown the effect of the Kapitza resistance on the enhancement of the effective thermal conductivity for various $k_p/k_{bf}$. As expected, the Kapitza resistance presents a strong impact, diminishing the ratio of the $k_p/k_{bf}$, for their upper bound.

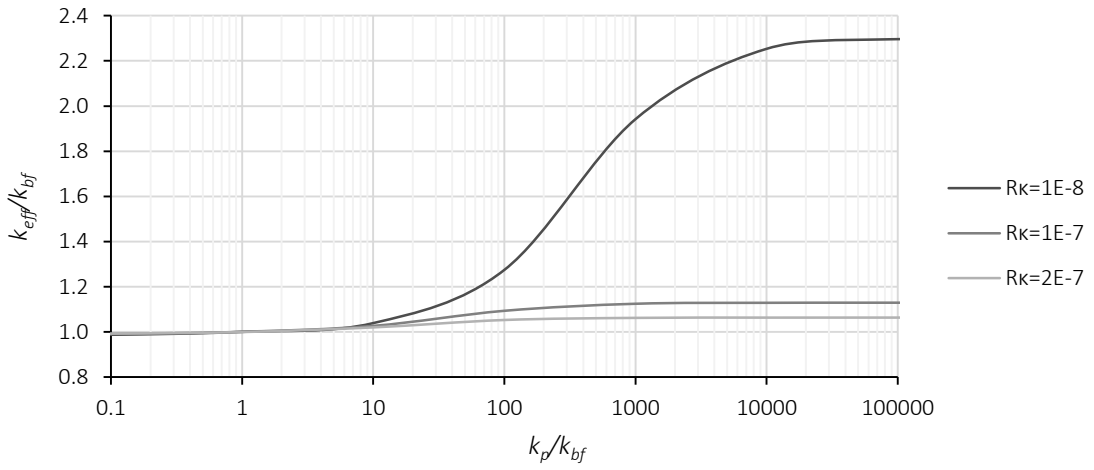


Figure 2.17: Effective thermal conductivity enhancement ratio for a dispersion of particles with $\phi$=1% and $l_p/d_p$=50, predicted through the model of Nan *et al.*, for different $k_p/k_{bf}$, in the range of Kapitza resistances of the Cahill's group.

Figure 2.18 presents an evaluation of the Kapitza resistance effect of dispersions of different aspect ratio elongated particles, when $k_p/k_{bf}$=500. The results clearly show that the increase of the nanoparticle aspect ratio induces a higher enhancement in the effective thermal conductivity; however, this is strongly limited with the increase of the Kapitza resistance.

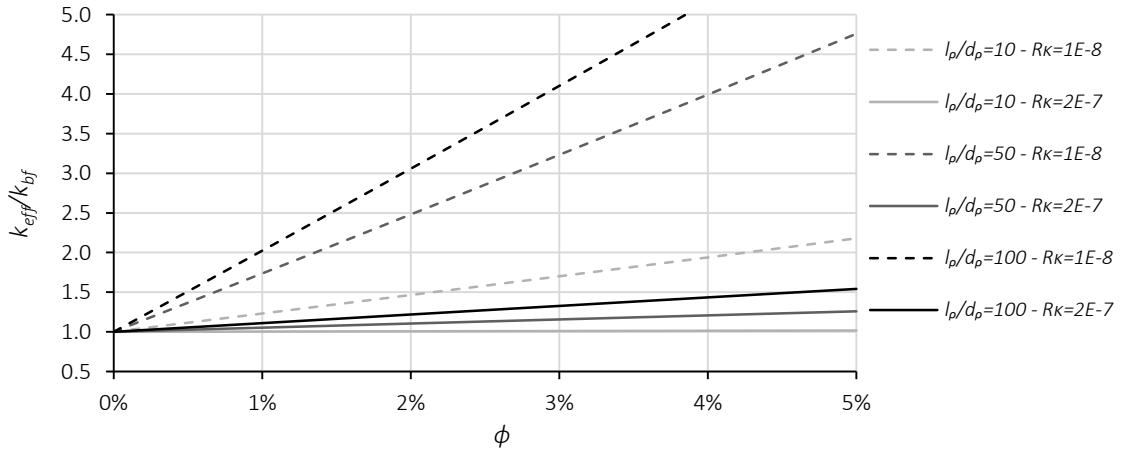


Figure 2.18: Effect of the Kapitza resistance on the calculated thermal conductivity enhancement ratio for elongated particles of different aspect ratio ($k_p/k_{bf}$ =500).

### 2.5.2 AN EXTENDED DIFFERENTIAL EFFECTIVE MEDIUM THEORY – THE PROPOSED MODEL

As verified, Nan *et al.* model suggests that the transition from spherical to non-spherical particles induces a strong enhancement on the effective thermal conductivity of dispersions (Figure 2.15). Nevertheless, the model was developed considering that the dispersed nanoparticles present a spatial distribution classified as a *diluted structure*, with negligible thermal interparticle interaction. Although, as verified by Biercuk *et al.*, MWCNTs have the ability to easily interact, even at low volume fractions (BIERCUK et al., 2002).

Since the thermal interparticle interaction is observed at concentrations below the percolation threshold, it is expected that this become more pronounced in suspensions of MWCNTs, as they are very elongated nanoparticles. Despite the limitation due to the high Kapitza resistance announced by Cahill's research group (CAHILL et al., 2001, WILSON et al., 2002), Nan *et al.* model can be improved to take into account the interparticle interaction. Therefore, in this study it is proposed a variation of the *differential effective medium theory* (DEMT) based on Nan *et al.* model to predict the effective thermal conductivity of elongated particles at any volume fraction. This proposed model was designated as *extended differential effective medium theory* (EDEMT) model.

For this purpose, the model of Nan *et al.*, represented in Equation 1.31, was rearranged in order to meet the Equation 2.11 of Bruggeman. The resulting expression was:

$$k_{eff}=k_{bf}\cdot\left[1+\frac{\phi\cdot(2\beta_{xx}+\beta_{zz})}{3-\phi\cdot(2\beta_{xx}\cdot L_{xx}+\beta_{zz}\cdot L_{zz})}\right] \qquad 2.26$$

From Equation 2.26, it comes that the first order dimensionless coefficient $f_1(k_{bf},k_p,P)$ can be expressed as:

$$f_1(k_{bf},k_p,P)=\frac{2\beta_{xx}+\beta_{zz}}{3} \qquad 2.27$$

Through the substitution of $\beta_{xx}$ and $\beta_{zz}$ for Equation 1.32 and 1.33, respectively, $f_1(k_{bf},k_p,P)$ becomes:

$$f_1(k_{bf},k_p,P)=\frac{2(k_{xx}-k_{bf})\cdot\left(k_{bf}+L_{zz}\cdot(k_{zz}-k_{bf})\right)+(k_{zz}-k_{bf})\cdot\left(k_{bf}+L_{xx}\cdot(k_{xx}-k_{bf})\right)}{3\left(k_{bf}+L_{zz}\cdot(k_{zz}-k_{bf})\right)\left(k_{bf}+L_{xx}\cdot(k_{xx}-k_{bf})\right)} \qquad 2.28$$

Nevertheless, given the complexity of the obtained function, and since it is intended to integrate the function in order to $k_{bf}$, $f_1(k_{bf},k_p,P)$ was simplified through the incorporation of constant

variables for the remaining parameters. The resulting simplified dimensionless function of first order, of the integration-embedding principle of Bruggeman, can be expressed as:

$$f_1\left(k_{bf},k_p,P\right)=\frac{k_{bf}^{\ 2}\cdot C_1+k_{bf}\cdot C_2+C_3}{3\left(k_{bf}^{\ 2}\cdot C_4+k_{bf}\cdot C_5+C_6\right)} \quad 2.29$$

where,

$$C_1=L_{xx}+2L_{zz}-3 \quad 2.30$$

$$C_2=k_{xx}^{eq}\cdot(2-L_{xx}-2\cdot L_{zz})+k_{zz}^{eq}\cdot(1-L_{xx}-2L_{zz}) \quad 2.31$$

$$C_3=k_{xx}^{eq}\cdot k_{zz}^{eq}\cdot(L_{xx}+2L_{zz}) \quad 2.32$$

$$C_4=-L_{xx}-L_{zz}+L_{xx}\cdot L_{zz}+1 \quad 2.33$$

$$C_5=(k_{xx}^{eq}+k_{zz}^{eq})\cdot(L_{xx}-L_{xx}\cdot L_{zz}) \quad 2.34$$

$$C_6=k_{xx}^{eq}\cdot L_{xx}\cdot k_{zz}^{eq}\cdot L_{zz} \quad 2.35$$

and $L_{xx}$ and $L_{zz}$ for elongated particles are given by Equation 2.23 and 2.24, respectively.

Replacing Equation 2.29 into Equation 2.13, and substituting $k_{bf}$ for $k$, the integration process is reduced to:

$$\left[ln\left(k^{E_1}\right)+ln\left((2C_1\cdot k+A+C_2)^{E_2}\right)+ln\left((-2C_1\cdot k+A-C_2)^{E_3}\right)\right]\Big|_{k_{bf}}^{k_{eff}}=-ln(1-\phi) \quad 2.36$$

From this, the proposed DEMT for dispersions of non-spherical particles is derived:

$$\left(\frac{k_{eff}}{k_{bf}}\right)^{E_1}\cdot\left(\frac{2C_1\cdot k_{eff}+A+C_2}{2C_1\cdot k_{bf}+A+C_2}\right)^{E_2}\cdot\left(\frac{2C_1\cdot k_{eff}-A+C_2}{2C_1\cdot k_{bf}-A+C_2}\right)^{E_3}=(1-\phi) \quad 2.37$$

where,

$$A=\sqrt{C_2^{\ 2}-4\cdot C_1\cdot C_3} \quad 2.38$$

$$B=6C_4\cdot C_2^{\ 2}+6C_1(2C_6\cdot C_1-2C_4\cdot C_3-C_5\cdot C_2) \quad 2.39$$

$$E_1=-\frac{3C_6}{C_3} \quad 2.40$$

$$E_2=\frac{-6C_4\cdot C_2\cdot A+6C_5\cdot C_1\cdot A-B}{2A\cdot C_1\cdot(A+C_2)} \quad 2.41$$

$$E_3=\frac{6C_4\cdot C_2\cdot A-6C_5\cdot C_1\cdot A-B}{2A\cdot C_1\cdot(A-C_2)} \quad 2.42$$

According to the theory, it is expected that the proposed model enable to predict the effective thermal conductivity of elongated particles dispersions, independently of the structural arrangement or degree of spatial distribution of the dispersed phase. The impact of the shape of the particles is reflected through the depolarization factors (Equation 2.23 and 2.24) and in the anisotropic equivalent thermal conductivities (Equation 2.20 and 2.22) of the particles, which depends on their average diameter and length distribution.

Nevertheless, for very elongated particles ($l_p/d_p$>10), the depolarization factors $L_{xx}$ and $L_{yy}$ converge to 0.5, and $L_{zz}$ to 0. This convergence was previously represented in the Figure 2.14. Assuming this, it is possible to simply the proposed model for very elongated cylinders. The simplified constant variables of the model $C_i$, for very elongated cylinders can be expressed as:

$$C_1 = {}^{-5}/_{2} \quad (2.43)$$

$$C_2 = \frac{(3k_{xx}^{eq} + k_{zz}^{eq})}{2} \quad (2.44)$$

$$C_3 = \frac{k_{xx}^{eq}\, k_{zz}^{eq}}{2} \quad (2.45)$$

$$C_4 = {}^{1}/_{2} \quad (2.46)$$

$$C_5 = \frac{k_{xx}^{eq}}{2} \quad (2.47)$$

$$C_6 = 0 \quad (2.48)$$

In addition, the model also enables to be reduced to spherical particles through the consideration of $L_{xx}=L_{yy}=L_{zz}= 1/3$. In such case, the model is reduced to the DEMT of Bruggeman, with imperfect interface as suggested by Benveniste *et al.*, and the constant variables of the model, $C_i$ become:

$$C_1 = -2 \quad (2.49)$$

$$C_2 = k_{xx}^{eq} = k_p \quad (2.50)$$

$$C_3 = k_{xx}^{eq} \cdot k_{zz}^{eq} = k_p{}^2 \quad (2.51)$$

$$C_4 = {}^{4}/_{9} \quad (2.52)$$

$$C_5 = \frac{2(k_{xx}^{eq} + k_{zz}^{eq})}{9} = \frac{4k_p}{9} \quad (2.53)$$

$$C_6 = \frac{k_{xx}^{eq} \cdot k_{zz}^{eq}}{9} = \frac{k_p{}^2}{9} \quad (2.54)$$

In summary, the novel proposed model accounts for the geometry of the dispersed particles, their volume fraction, Kapitza resistance and interparticle interaction. In Figure 2.19, it is shown the

effect of the Kapitza resistance on the enhancement of the effective thermal conductivity for various $k_p/k_{bf}$. As expected, the Kapitza resistance presents a strong impact, diminishing the ratio of the $k_p/k_{bf}$, for their upper bound.

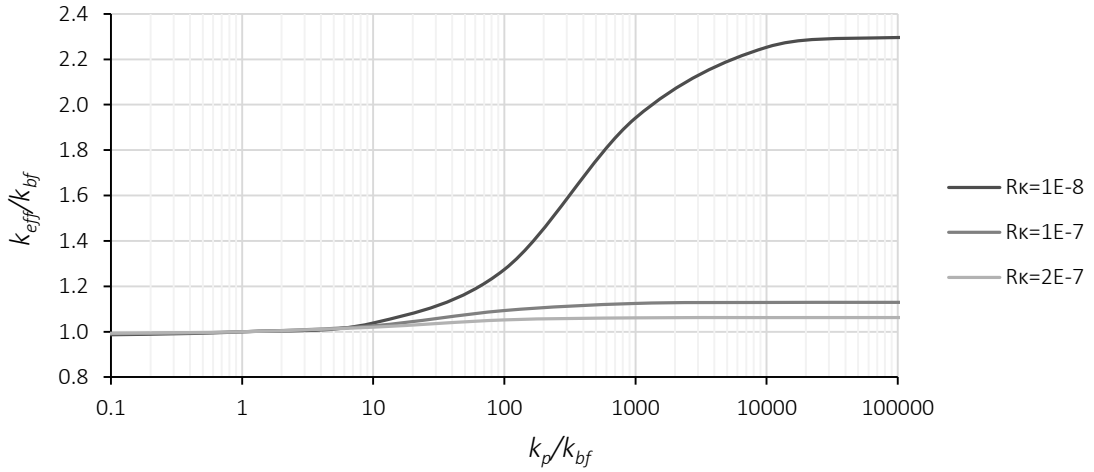


Figure 2.19: Effective thermal conductivity enhancement ratio for a dispersion of particles with $\phi$=1% and $l_p/d_p$=50, predicted through the proposed model, for different $k_p/k_{bf}$, in the range of Kapitza resistances of the Cahill's group.

Figure 2.20, presents the predicted ratio of thermal conductivity enhancement through the Nan *et al.* model and through the proposed EDEMT model. In this analysis, it was considered that the dispersed particles have an aspect ratio $(l_p/d_p)$ of 100, and a particle-base fluid thermal conductivity ratio $(k_p/k_{bf})$ of 3000. As expected, the predicted thermal conductivity strongly depends on the Kapitza resistance magnitude. In addition, it is observed that the effect of the interparticle interaction is more intense for lower Kapitza resistance. The saturation point seems to be nearly $2\times10^{-7}$ K m$^2$/W.

Moreover, it should be noted that Cahill's research group (HUXTABLE et al., 2003) experimentally measured the Kapitza resistance of MWCNTs dispersed in heavy water, reporting $8\times10^{-8}$ K m$^2$/W. As can be depicted in Figure 2.20, the proposed model suggest an enhancement on the effective thermal conductivity caused by the thermal interparticle interaction for this Kapitza resistance value.

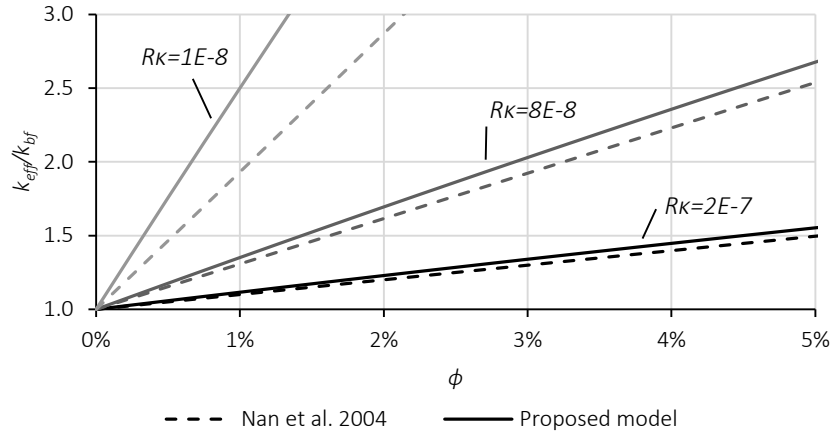


Figure 2.20: Predicted thermal conductivity enhancement ratio through the Nan *et al.* and the proposed model, for $k_p/k_{bf}$=3000, and $l_p/d_p$=100.

The effect of the nanoparticle aspect ratio on the effective thermal conductivity ratio enhancement is represented In Figure 2.21. As can be depicted, it is expected a higher thermal interparticle interaction effect on the observed conductivity, for the typical Kapitza resistance observed at the nanoscale.

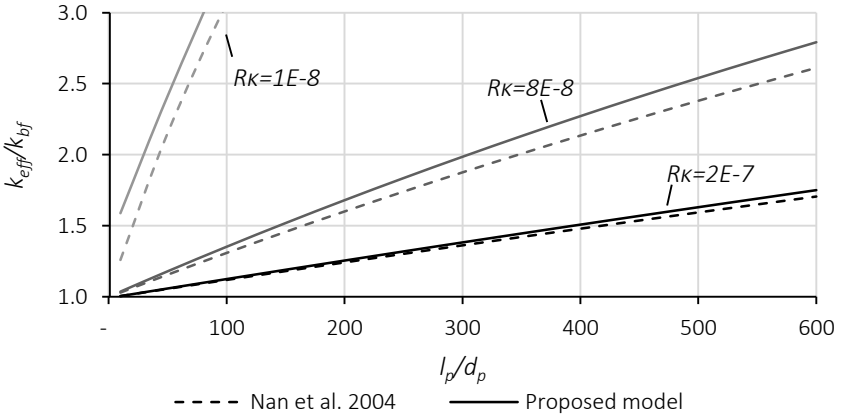


Figure 2.21: Effect of the particles aspect ratio on the thermal conductivity enhancement predicted by the Nan *et al.* and the proposed model ($k_p/k_{bf}$ of 3000 and $\phi$=1%).

It is important to note that the proposed EDEMT model is valid for statistically homogeneous dispersion, with negligible nanoparticles sedimentation and agglomeration.

## 2.6 CHAPTER CONCLUSIONS

It was verified that the dispersion of non-agglomerated particles in a medium can present distinct microstructural arrangements, depending upon the geometry of the particle and respective volume fraction. These arrangements can be categorized as *diluted structure*, *non-diluted structure*,

and *percolation-like structure*. The transition through these arrangements provides strong impact on the effectiveness of heat conduction of the mixture. Taking these morphological arrangements into consideration, it was presented an overview on the classical predictive model for the effective thermal conductivity. The conventional understanding of the thermal conductivity of mixtures originates from the *effective medium theory* (EMT) of Maxwell, which reflects on very dilute suspensions of non-thermally interacting spherical particles. Later, Bruggeman proposed the *differential effective medium theory* (DEMT), enabling to reflect on the interparticle thermal interaction, observed for higher volume fractions. It was also verified that the mathematical formulation of Nan *et al.*, in line with the EMT of Maxwell, is valid for very dilute suspensions of non-thermally interacting, yet for non-spherical particles. Given the lack of predictive models for non-spherical particles dispersions that could interact thermally, it is proposed a predictive model (EDEMT), through a similar differential principle of Bruggeman, but including the shape of the particle, and the Kapitza resistance (interfacial thermal resistance).

# 3 LONG-TERM MWCNTS BASED NANOFLUIDS ENGINEERING

## 3.1 CHAPTER SYNTHESIS

In this Chapter, it is defined in detail the term *nanofluid*, according to their final applicability. Since nanofluids are dispersion of nanoparticles in conventional fluids, they can present several forms of instabilities, such as aggregation, sedimentation, and/or disintegration of their solid particle structure (*e.g.* reduction of the size distribution with variation of the temperature). Therefore, the proposed nanofluids to be developed must prevent these instability phenomena. To address these conditions, a methodology for the preparation of the defined long-term nanofluids is proposed. It is also presented the experimental and numerical apparatus to verify the morphological structure, or spatial distribution, and assess the defined stability conditions. The sizes' distribution of the dispersed MWCNTs is preformed through intensive analysis to SEM images. Thermo-gravimetric analysis revealed that may exist slight structural damages on the functionalized MWCNTs, nevertheless, negligible for the test temperatures. The Zeta potential measurements and analytical centrifuge revealed negligible probability of agglomeration, thus phase separation rate is hindered and shows high resistance to centrifugal force fields. It is also proposed a numerical model that enables to assess the dynamical interparticle interaction of stable dispersion of CNTs.

## 3.2 LONG-TERM NANOFLUIDS ENGINEERING

Thermal nanofluids are dispersions of solid nanoparticles in conventional liquids, with the purpose to improve the thermal conductivity of the mixture. Nanofluids can be considered as colloids, since the dispersed phase is composed of individual particles with dimensions ranging from $10^{-10}$ m to $10^{-6}$ m. Conventionally, the liquid and the particles are respectively designated as *continuous* phase and *dispersed* phase. Sometimes, colloids have the appearance of solutions since their dispersed phase is difficult to identify.

The literature abounds with studies on several nanoparticles to be used on nanofluids engineering. Among those, MWCNTs are continuously, both experimentally and theoretically, referred to as the most promising nanoparticle as to thermal properties are concerned. This might be explained by their increased thermal conductivity and high elongated shape. The latter enables a higher degree of spatial distribution that improves the effective thermal conductivity enhancement, as suggested by the classical models described in detail in Chapter 2.

It appear, therefore, that MWCNTs are the best suited nanoparticle for thermal nanofluids engineering. As elucidated in the Chapter 1, in this study it is intended the development and thermal characterization of MWCNTs based nanofluids, for the heat exchange intensification of energy systems. Nevertheless, for a proper preparation of nanofluids, it is of utmost importance to define the nanofluids final purpose and applicability, to better understand what the thermo-physical characteristics desired for that are.

As previously envisaged, the production of thermal nanofluids with improved thermo-physical properties, will enable the design of smaller and lighter heat exchangers, and improve the energy efficiency in industrial processes and systems. In order to ensure that nanofluids become the next-generation heat transfer fluids for these systems, it is of utmost importance that their engineered thermo-physical properties remain constant, or with negligible variation, over time. Therefore, the term *stability* must describe the quality of the effective thermo-physical properties being free from change or variation, which strongly depends on the behaviour and spatial distribution of both phases over a desired period.

More importantly, it is imperative that the produced nanofluids present good stability, in order to reduce eventual noise factors, ensuring repeatability of the results and, therefore, a better inference on the experimental results that will be taken. This is also assumed as imperative for the development and validation of the reliable predictive model for the effective thermal conductivity of nanofluids. It is strongly necessary to ensure constant morphological arrangements (described in the Chapter 2), homogeneity, during the several experimental measurements, in order to be possible for their cross-comparison.

### 3.2.1 STABILITY OF DISPERSIONS

The manners and rate through which the two-phase separation occurs in a dispersion during a desired period, leads to the typical assignment of *unstable* or *stable* dispersion. Therefore, these terms may be meaningless unless the process to which they are applied has been clearly defined. For instance, a protein molecule may undergo hydrolysis to alter the size, shape, and the solubility of the molecule. Despite being stable with respect to phase separation, the mixture is unstable with respect to chemical change (HIEMENZ, 1977).

Regarding nanofluids, typical forms of instability usually reported are the aggregation and phase separation (or sedimentation). It is quite possible for a nanofluid to be unstable with respect to

sedimentation and stable with respect to aggregation, and vice-versa. Nevertheless, as it will be proposed ahead, another form of instability may be the degradation of the size distribution of the nanoparticles over time. The latter, as previously envisaged in Chapter 2, may strongly affect the spatial distribution degree of the nanoparticles in the medium.

#### *3.2.1.1 AGGREGATION*

Particles in dispersion may adhere together and form aggregates of increased size. The rate of aggregation is in general determined by the frequency of interparticle collisions and the probability of cohesion. The frequency of interparticle collisions depend on the intensity of the random walk of the solid particles and, according to the *excluded volume theory* (EVT), on their size, shape and concentration (HIEMENZ, 1977, RUSSEL et al., 1989).

The random walk of the particles is the stochastic Brownian motion, caused by the impact of the base fluid molecules on the surface of the particles. This was discovered by Robert Brown in 1828, and physically described in 1956, by Einstein. According to the kinetic theory of matter, the random walk of each individual particle is independent and eternal, being composed of translation and rotation movement. Brownian motion is more active in liquids with lower viscosity, for higher temperatures, and for the smaller dispersed particle (BROWN, 1828, EINSTEIN et al., 1956, PERRIN, 2005).

Despite the interactions, unless there is some attraction between the particles, the Brownian interparticle collisions could never occur and/or lead to aggregation. Derjaguin, Verway, Landau and Overbeek (DVLO) developed a theory suggesting that aggregation is determined by the sum of the van der Waals attractive and repulsive forces between the approaching Brownian particles. According to DLVO theory, if the attractive forces are larger than the repulsive forces, the particles will collide and aggregate (DERJAGUIN et al., 1993, VERWEY et al., 1999). On the other hand, if the attractive forces are lower than the repulsive forces, the particles may collide (or not), but without a permanently fixed contact.

The aggregated particles generate new structures, with increased sizes and mass, and different shapes that move as single units. Such dispersion can also be categorized as polydispersion. However, it should be noted that the term monodispersion is an ideal case, since it is extremely difficult to obtain a dispersion of particles with strictly equal size and shape (HIEMENZ, 1977).

Nevertheless, for simplicity, the term monodispersion is herein attributed to an aggregation-free dispersion.

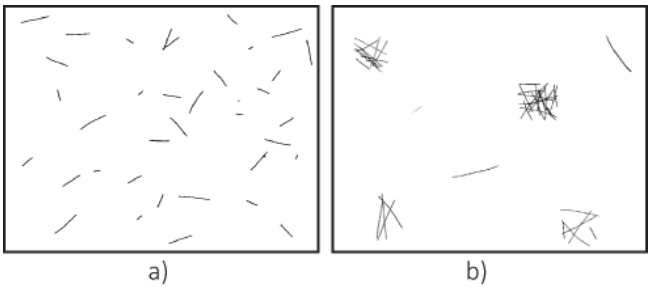


Figure 3.1: Schematic representation of a) a monodispersion and b) a polydispersion, for a given concentration of MWCNTs.

In Figure 3.1 is shown a monodispersion and a polydispersion, for a given concentration of MWCNTs. It is distinguishable that a polydispersion of MWCNTs may be classified as *unstable*, since the degree of aggregation is difficult to control. The aggregates may present a significant distribution of mass and shapes, leading to phase separation at different rates due to gravity or other centrifugal forces. In addition, even without phase separation, the final properties of the dispersion may be unsteady and even stratified or with local gradients, if the dispersion is allowed to stand long enough to occur aggregation. For instance, in the case of thermal nanofluids, the thermo-physical properties can change significantly with the degree of aggregation (PRASHER et al., 2006).

Therefore, it seems obvious that if the particles present higher repulsion than attractive forces, the dispersion will have an improved stability, and higher probability of homogeneous thermo-physical properties. The interparticle repulsions may be categorized as electrostatic and steric repulsion. Electrostatic repulsions may be achieved by charging the particles surface, *e.g.* through the accumulation or depletion of electrons at the surface of the particles, and the dissociation of surface charged species (VERWEY et al., 1999). In the nanofluids research, these electrostatic repulsions are usually applied through intense ultrasonication, ball milling or high speed shearing (DAS et al., 2003a, DAS et al., 2003b, EASTMAN et al., 1997, XUAN et al., 2000).

Even so, perhaps the most effective way for reducing the degree of aggregation is through steric repulsions. Such repulsive forces may be achieved through the particle adsorption of polymers or active species. The steric effect of polymer dispersants, or surfactants, is significantly determined by their concentration at the solid-medium interface. This is an economic method to enhance the

wettability of the particles. Surfactants consists of a hydrophobic tail portion, usually a long-chain hydrocarbon, and a hydrophilic polar head group than increases the continuity of the two phases. The hydrophilic polar head enables the solubility of the particles in polar solvents, such as distilled water or ethylene glycol.

Nevertheless, equivalent active species can be enduringly bonded to the particles surface through covalent functionalization. Covalent functionalization presents some advantages over surfactants for the production of thermal nanofluids. It is recognized that surfactants may influence negatively the effective thermo-physical properties of nanofluids as it forms an interfacial layer between the two phases. Moreover, the heat and cooling routine processes may lead to the degradation of the surfactants and the formation of foams (NASIRI et al., 2011). Nguyen *et al.* found that the effective viscosity of nanofluids may have hysteresis behaviour, possibly by the surfactant degradation which culminates in the agglomeration of the nanoparticles (NGUYEN et al., 2007). Moreover, surfactants can be separated from their action zone during the pumping continuous routine of the thermal fluid. During these, the fluid is subjected to centrifugal forces that impose the separation of the surfactant, since this is not physically/covalently attached to the surfaces of the particles.

To ensure that there is no aggregation of particles, the repulsive forces must extent over distances, at least, equal to the range of the van der Waals attraction forces. This range of interaction of the repulsive forces is referred herein as *action layer*. When two Brownian particles approach, the distance of separation between the particles decreases during the aggregation process, and the action layers begin to overlap as can be depicted in the Figure 3.2. The approaching particles experience an increase of the $\Delta G$ that prevents the aggregation of the particles, due to a repulsion induced by the equal polarity of the charged surfaces. This mechanism is designated as *steric stabilization* (HIEMENZ, 1977, RUSSEL et al., 1989).

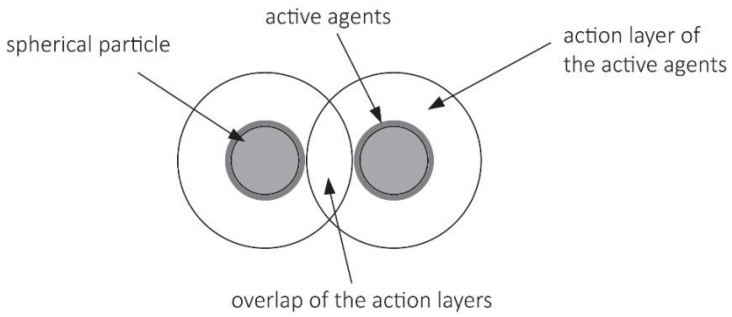


Figure 3.2: Overlap of the action layer of the active agents of two dispersed particles.

#### 3.2.1.2 PHASE SEPARATION

Phase separation, or the typically called sedimentation, is perhaps the best indicator of instability of a nanofluid, since it can be usually detected at the naked eye. For that reason, the sedimentation was the method most applied to the date, to assess the colloidal stability of nanofluids. Sedimentation represents the rate of separation of the two phases that occurs through the influence of gravity or centrifuge force field. Furthermore, sedimentation may also be a reflection of aggregation. As seen, aggregation produces structures of larger volume and mass, which cause a more rapid phase separation.

A key relationship in understating the phase separation rate is the hydrodynamic Stokes' law. In 1850, Stokes derived an analytical formula (Equation 3.1) for the settling velocity of a single sphere suspended in a Newtonian fluid, under the influence of gravity (STOKES, 1850). This model takes into account the gravitational, buoyancy, and drag forces to which the particle is subjected. However, this model has limitations since, in most practical cases, the suspensions have more than one particle.

$$v_s = \frac{g \cdot \left(\rho_p - \rho_{bf}\right) \cdot d_p^2}{18 \cdot \mu_{bf}} \qquad 3.1$$

During phase separation, the particle produces the displacement of fluid in the opposite direction, as shown in the Figure 3.3. The velocity of the moving fluid has a gradient variation from layer to layer near the surface of the sphere. At a certain distance, the fluid velocity influenced by the settling particle equals zero, and starts to behave as if the particle were not present.

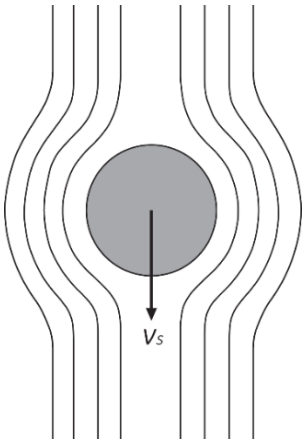


Figure 3.3: Distortion of flow streamlines around a settling particle.

Therefore, for two neighbouring particles, the settling velocity may be lower than that predicted by Equation 3.1. This phenomenon is explained by the mentioned fluid displacement on the opposite direction to the movement of the particles, that disturbs the motion of the surrounding one. This effect was experimentally verified by Batchelor (BATCHELOR, 1972). Batchelor found that a suspension containing 3% volume fraction of spheres has an average settling velocity 20% lower than predicted by Stokes due to these hydrodynamics interactions.

The shape of the particle may also play an important role on the sedimentation rate of the suspensions. For instance, in suspensions of elongated particles, these hydrodynamics interactions and physical interparticle interactions become more appreciable even for lower concentrations. For a given concentration the average distance between particles is reduced for elongated particles, increasing the influence produced by the displacement of the fluid. In such a suspension, the phase separation rate depends on the orientation of the particles, due to a variation of their drag coefficient. Moreover, the orientation of the particles is always changing due to fluctuations of the fluid viscosity resulting from the settling of the surrounding particles (HIEMENZ, 1977, KUMAR et al., 1991, TURNEY et al., 1995, VERWEY et al., 1999). Other factors may also reduce the settling velocity, namely hydrodynamics interparticle interactions and collisions. Sedimentation that has these in significant magnitudes is designated as hindered settling (BEISER et al., 2004, FEIST et al., 2007, HERZHAFT et al., 1999, RICHARDSON et al., 1954).

The interaction between elongated particles is significantly higher than for equivalent spherical ones. Therefore, if a suspension of elongated particles (or MWCNTs) presents stability regarding aggregation, i.e. the repulsive forces between the particles are higher than the attractive ones, the sedimentation rate may be decreased. However, in the opposite situation, the agglomeration of particles is enhanced due to a higher particles contact, as predicted by the EVT, and the rate of sedimentation is higher.

Nevertheless, there is a factor operating that prevents the complete sedimentation of small particles, namely, particles diffusion. According to Fick's law, diffusion may be seen as the opposite process of sedimentation, since this has the tendency to keep things dispersed. Nevertheless, particles diffusion depends on the shape and size of the particles, and may be negligible for larger particles (FICK, 1855). Particles diffusion is the result of the random walk of the particles, i.e. their Brownian motion. As previously seen, this motion is caused by the random collisions of the medium molecules on the surface of the suspended particles. These collisions are a consequence

of the constant thermal motion of the medium molecules, also known as molecular diffusion (BROWN, 1828, EINSTEIN et al., 1956).

Once the sedimentation becomes equal or less that the diffusion rate of the dispersed particles, the system is at equilibrium, presenting no macroscopic changes, *i.e.* the dispersion is stable regarding sedimentation.

### 3.2.2 Definition of MWCNTs based nanofluids for thermal purposes – Stability conditions

To ensure a long-term stability to the MWCNTs based nanofluids, it was identified the possible mechanism that may directly contribute to the degradation of their thermal conductivity, according to the classical theories. These are the structural integrity of the nanoparticles, agglomeration and sedimentation, since all are main factors that contribute to the spatial distribution of the nanofluids over space and time.

Assuming that the thermal conductivity of nanofluids depend on the spatial distribution of the nanoparticles in the medium, as suggested by the classical theories provided in Chapter 2, it is essential that the geometrical properties of the particles remain constant, at all the operative temperatures. The degradation of the initial tubular structure of the MWCNTs will reduce their degree of spatial distribution and probability of interaction that may contribute to the effective thermal conductivity enhancement. Moreover, such thermal degradation does not occur through a controlled way, causing the transition from monodispersion to polydispersion.

It is also of utmost importance that the MWCNTs present low probability of agglomeration. Despite some authors argue that agglomeration of nanoparticles may contribute to a higher effective thermal conductivity enhancement (see Section 1.5.3.3), this is herein considered as a form of instability (PRASHER et al., 2006). Given the practical difficulty in controlling the formation of the aggregates, it becomes clear that the enhancement of the thermal conductivity will become stratified or only locally observed (see Figure 3.1). This is an undesired behaviour during the operation of a thermal fluid, since the local average thermal conductivity in the heat exchanger may be always changing. Furthermore, the nanoparticles aggregation may lead to an increased effective viscosity, another undesired effect (KEBLINSKI et al., 2008). The aggregation of nanoparticles produces structures with increased size and shape that settle more rapidly, inducing the separation of the phases, clogging of the flow channel and/or abrasion of the heat exchange surface. Regarding the experimental measurement of the effective thermal conductivity, the

stratification of the samples will clearly be a noise factor, due to the uncontrolled rate of aggregation and sedimentation during the experimental observations. It is of utmost importance to ensure the homogeneity within the sample during the readings.

However, due to a hydrophobic surface, pristine MWCNTs seems to spontaneously agglomerate in polar solvents, such as water and ethylene glycol. Moreover, due to their high surface-to-volume ratio, their van der Waals attraction forces are more intense. In the Figure 3.4 is schematically represented a pristine CNT. In order to improve the solubility of pristine CNTs in a polar solvent, it is necessary that their lateral surface became hydrophilic to enhance the interaction with the solvent and increase the van der Waals repulsive forces (CAO, 2004, MEYYAPPAN, 2004). As previously seen, MWCNTs can become hydrophilic through specific covalent functionalization.

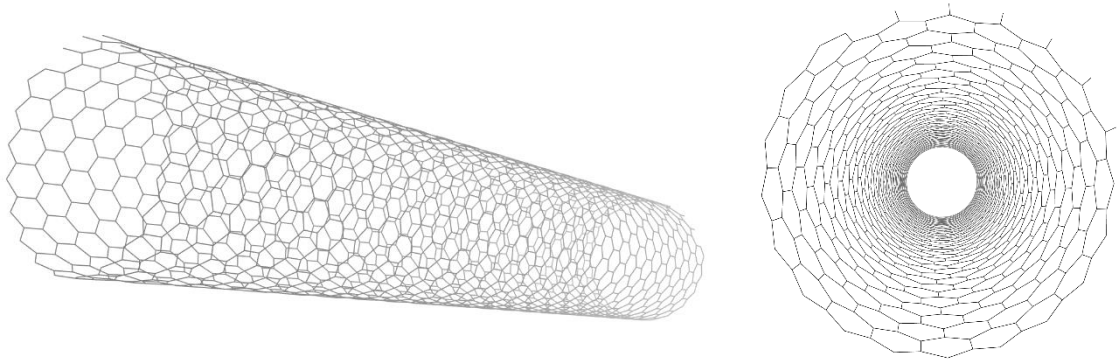

Figure 3.4: Schematic representation of a pristine CNT.

The most common covalent functionalization techniques are the oxidative treatments which are capable of attach oxygenated functional groups, such as carboxylic (-COOH) and alcohol groups (-OH). This can be achieved through chemical treatment, such as boiling nitric and/or sulphuric acid (ESUMI et al., 1996, NASEH et al., 2010, XIE et al., 2011, XIE et al., 2003).

The carboxylic groups behave as weak acids and possess ion-exchange properties, having both hydrogen acceptors and hydrogen donors (SHIM et al., 2001). This will improve the MWCNTs wettability, due to a more hydrophilic surface structure, and reduce agglomeration by increasing the repulsions van der Waals that counter-balances with the attractive ones. Additionally, both carboxyl and alcohol groups have polar properties, contributing for their solubility in polar solvents. In the Figure 3.5 is schematically illustrated a CNT functionalized with carboxylic groups in the lateral surface.

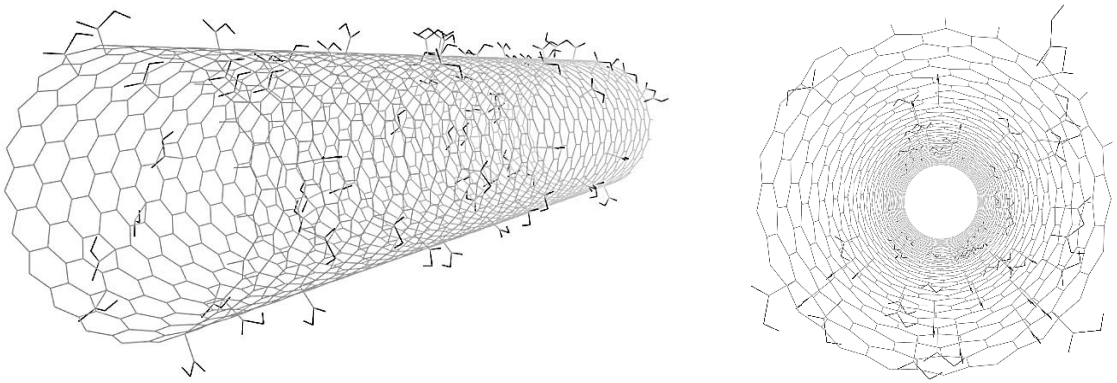

Figure 3.5: Schematic representation of a functionalized CNT.

On the other hand, chemical treatment also causes the shortening of the MWCNTs, reducing their ability to enhance the spatial distribution (BANERJEE et al., 2005, NASEH et al., 2010, YUDIANTI et al., 2011). The distribution length reduction of the MWCNTs depends on the extent and intensity of the reaction. Yet, given the lack of specific approaches to measure the sizes distribution of elongated nanoparticles, the new distribution has to be determined by scanning electron microscope (SEM) or transmission electron microscopy (TEM).

Moreover, pristine MWCNTs present a very high thermal conductivity, nearly 3000 W/mK, usually described as ballistic (HONE, 2002). Through molecular dynamics simulations, Shenogin et al. verified that the degree of covalent functionalization causes a drop on the thermal conductivity of the MWCNTs. Even so, the thermal conductivity of covalently functionalized MWCNTs converge to 1700 W/mK for the highest degree of functionalization (SHENOGIN et al., 2004a). Furthermore, as verified in Chapter 2, hydrophilic surfaces contribute to the decrease of the Kapitza resistance, an interface thermal resistance that strongly reduces the effective thermal conductivity enhancement of suspensions.

Even assuming that the functionalized MWCNTs have very low probability of agglomeration, they are permanently subjected to gravitational and other centrifugal force fields, which will induce the separation of the phases. Nevertheless, the elongated shape of the MWCNTs enables a higher degree of hydrodynamics and interparticle interaction that hindered the separation process.

In summary, the proposed next-generation MWCNTs based nanofluids for heat exchange intensification should present negligible agglomeration and statistically homogeneous spatial distribution of the nanoparticles in the base fluid and over time. Nanofluids that fulfil these conditions of stability may ensure long-term homogeneous thermal properties that are essential

for their assessment through the common available measurement techniques (see Section 1.5.3.1). Moreover, such nanofluids enable the elimination of experimental noise factors, due to a higher probability of repeatability, contributing to a better inference over the experimental measurements.

That is, the stability conditions desired for the long-term nanofluids are:

1. Agglomeration free
2. Phase separation free
3. Constant geometrical structure of the nanoparticle.

## 3.3 DESIGN OF EXPERIMENTS

As postulated in Section 1.6, it is intended to contribute with a well-established parametric study on the effective thermal conductivity of nanofluids, enabling to demystify the intriguing behaviour reported in the open literature. To this end, an appropriate *design of experiments* (DOE) is developed to verify the mechanisms proposed in the open literature.

The conducted survey presented in the Chapter 1 suggested that the anomalous effective thermal conductivity may be explained through the Brownian motion of the nanoparticles, the nano-layer ordering structure, and the aggregation and percolation of the heat through the nanoparticles. In contrast, the classical theories state that suspensions can be regarded as statistically motionless and homogeneous, and the effective thermal conductivity depends upon the spatial distribution of the nanoparticles and, depending on the geometry and volume fraction of the particles, in thermal interparticle interactions.

Four main control factors that may influence the final overall thermo-physical properties were identified. These are the (1) MWCNTs geometry (sizes distribution), their (2) volume fraction, the (3) base fluid and the (4) temperature. It should be noted that a control factor of an experiment is a controlled independent variable. In the Table 3.1, it is presented a summary of the expected relation between the identified control factors and the mechanisms proposed for the enhancement of the effective thermal conductivity of nanofluids. As noticeable, the effect of the aggregation and percolation of heat through the particles was neglected, since this was identified as a form of instability. Therefore, the aggregation of the nanoparticles will be treated separately, as explained ahead in the Section 3.8.

Table 3.1: Expected relation of the control factors on the mechanisms governing the effective thermal conductivity.

| | Open literature | | Classical theories/proposed | |
|---|---|---|---|---|
| | Brownian motion | Nano-layer structure | Spatial distribution | Interparticle interaction |
| Nanoparticle geometry | X | X | X | X |
| Volume fraction | X | X | X | X |
| Base fluid | X | X | | |
| Temperature | X | | | |

As previously seen, the Brownian motion of the particles depends upon the base fluid viscosity and temperature, on the geometry of the nanoparticle, since this affect their size, mass and drag coefficient, and on the volume fraction. The latter, increase the interparticle interaction that may hinder their motion. The nano-layer ordering structure of the base fluid molecules near a solid surface may be affected by the nanoparticle geometry, due to distinct surface-to-volume ratios, by the volume fraction, which enhances the density of solid surfaces on the medium, and by the base fluid thermo-physical properties that may produce distinct ordering nano-layer thickness. Furthermore, the spatial distribution and dynamic interparticle interaction may depend on the MWCNTs geometry and structural flexibility, volume fraction, and Brownian motion. Therefore, these are characterized through the dynamic numerical model provided in Section 3.6.

From the previous Table, it appears that the MWCNTs geometries may present the most intriguing impact on the effective thermal conductivity, due to the impact on all the mechanisms proposed. Therefore, six different MWCNTs were selected for the present study. The manufacture and geometric properties of the selected MWCNTs are described in Table 3.2.

Table 3.2: Nanoparticles designation and their geometric properties.

| MWCNTs designation | Nanoparticle manufacture | Ash [wt.%] | Purity [wt.%] | $\rho_{CNT}$ [kg/m³] | $l_p/d_p$ |
|---|---|---|---|---|---|
| *d*50-80 *l*10-20 | Cheaptubes Inc. | <1.5 | >95 | 2160 | 231 |
| *d*60-100 *l*5-15 | Shenzhen NanoTech Port Co., Ltd. | <3.0 | >97 | 2160 | 125 |
| *d*60-100 *l*1-2 | Shenzhen NanoTech Port Co., Ltd. | <3.0 | >97 | 2160 | 19 |
| *d*20-40 *l*10-30 | Cheaptubes Inc. | <1.5 | >95 | 2160 | 667 |
| *d*20-40 *l*5-15 | Shenzhen NanoTech Port Co., Ltd. | <3.0 | >97 | 2160 | 333 |
| *d*20-40 *l*1-2 | Shenzhen NanoTech Port Co., Ltd. | <3.0 | >97 | 2160 | 50 |

These particles description may be summarized by two diameters distributions, $d_p$<50 and $d_p$>50. These are full crossed with three length distributions, $l_p$1-2, $lp$=5-15 and $l_p$>15. The diameter and length distributions are used for the designation of each MWCNTs type in a quite obvious way. In addition, the nanoparticle sizes were chosen in order to cover a broad interval both in what

concerns diameter as well as length, to enable appropriate data interpolation and further analysis. Although the particles were achieved through different manufacturers, all the carbon nanotubes were produced by catalysed chemical vapour deposition (CCVD), inferring identical structural and thermo-physical properties.

In line with the MWCNTs geometry, the nanoparticles volume fraction was identified also as an important control factor. It should be reminded the intriguing linearity or non-linearity behaviour suggested by the researcher community, cited in Section 1.5.3.2. Therefore, five volume fractions were selected, ranging from 0.25 to 1.5%vol., namely 0.25, 0.50, 0.75, 1.00, and 1.50%vol. It is known that the viscosity increases considerably with the nanoparticles loading (KANAGARAJ et al., 2008, PONMOZHI, 2009, PONMOZHI et al., 2009). Since the viscosity is an important parameter in practical heat transfer processes, the 1.50%vol. was selected as the upper limit in the present studied. Furthermore, higher volume fractions will require more MWCNTs, which are yet expensive in the worldwide market. It is expected that five volume fractions enable to assess the possible non-linearity of this control factor.

The base fluid produce changes in the thermo-physical properties of the medium, which may perform a statistically significant difference in the results. In the eventual case of Brownian motion producing some effect on the results, it should be important to verify this through the variation of the viscosity of the medium. Therefore, two distinct base fluids are selected, specifically aqueous solution of ethylene glycol at 30% and 60% (DW+30%EG and DW+60%EG, respectively). Aqueous solutions of ethylene glycol are common in heat transfer applications due to its antifreeze, low corrosive and lubricant properties. Furthermore, the measurement of the thermal conductivity of fluids is not easy, and the accuracy of the results may be improved for fluids with higher viscosity than water. Nevertheless, it is herein recognized that the base fluid may induce some impact on the magnitude of the Kapitza resistance. Given the lack of fundamentals mechanisms to describe this resistance, the selection of only two base fluids allows the reduction of the *degrees of freedom* that could be induced by the Kapitza resistance, preventing for lack of inference on the results. In Appendix B, it is presented the thermo-physical properties of the aqueous solutions of ethylene glycol.

As pointed out, quite a few researchers suggest a strong dependence of the effective thermal conductivity on the temperature. It is known that the increase of the temperature speed up the Brownian motion and, perhaps, the dynamical interparticle interaction. Hence, six temperatures

were selected, ranging from 283.15 K to 323.15 K. The upper limit temperature 323.15 K represents the limit to ensure the accuracy of the thermal conductivity measurements, as stated in Section 4.2.

In Table 3.3, it is summarized the control factors selected for the study and their respective *degrees of freedom*.

Table 3.3: Control factors and their range of settings for the experiment.

| Control factor | MWCNT | Base fluid | $\phi$ [%] | Temperature [K] |
|---|---|---|---|---|
| | *A* | *B* | *C* | *D* |
| Level 1 | *d*50-80 /10-20 | DW+30%EG | 0.25 | 283.15 |
| Level 2 | *d*60-100 /5-15 | DW+60%EG | 0.50 | 293.15 |
| Level 3 | *d*60-100 /1-2 | - | 0.75 | 298.15 |
| Level 4 | *d*20-40 /10-30 | - | 1.00 | 303.15 |
| Level 5 | *d*20-40 /5-15 | - | 1.50 | 313.15 |
| Level 6 | *d*20-40 /1-2 | - | - | 323.15 |
| *degrees of freedom* | 5 | 1 | 2 | 5 |

It is distinguishable that the experiments have a factorial design. In order to decrease the cost and time of experimental measurements, it can be applied a fractional factorial design. However, from the literature review conducted in the Chapter 1, it was verified that a lack of systematically and identical nanofluids production and characterization may have contributed to noise factors and development of controversy theories. Therefore, a full factorial design of experiments was selected in this research, to ensure a higher degree of inference over the experimental results. In this, all levels of each factor are combined with those of other factors. Therefore, the problem results in 360 experimental data points $\left(6^2 \cdot 2^1 \cdot 5^1 = 360\right)$, *i.e. ABCD* accordingly to the identification provided in Table 3.3.

The three basic principles of design of experiments are *randomization*, *blocking*, and *replication*. By randomly distribute the experimental events, it is possible to average the effects of extraneous factors that may be present. Blocking allows to increase the precision when randomization is impossible or undesired. Therefore, the design is blocked by the factor temperature, virtually decreasing the number of experimental runs to 60, the total number of nanofluids (*ABC*). Through this procedure, it is reduced the time for the experimental measurements, since it is preventing the selection of temperature in each run, enabling to programme this as a routine, as described in detail in Chapter 4.

Replication of experimental measurements can identify the source of experimental variance and uncertainties. If the number replication is too low, the experiment will lack the precision on the results, and if is too high, time and resources will be wasted for minimal gain. Therefore, the calculation of the sample size is crucial for an efficient design of experiments. This is described in Section 4.2.

## 3.4 MWCNTs FUNCTIONALIZATION METHODOLOGY

The base fluids used for the preparation of the nanofluids are aqueous solutions of ethylene glycol that are polar solvents. Therefore, it is necessary to transform the hydrophobic surfaces of the pristine MWCNTs on hydrophilic surfaces. As previously seen, the best available approach to create a hydrophilic surface on the MWCNTs is through a covalent functionalization. The most common covalent functionalization techniques are the oxidative treatments which are capable of attach oxygenated functional groups on the tubes such as carboxylic and alcohol groups. These techniques present advantages over the use of surfactants for thermal transport nanofluids.

Therefore, in the present research, the pristine MWCNTs were covalently functionalized through the methodology proposed by Esumi *et al.* (ESUMI et al., 1996). Other technique, non-chemical and dry, can be used for the carboxyl functionalization of the MWCNTs surface, namely dielectric barrier charge (DBD) plasma. However, there are evidences that this technique produces less functional groups on the MWCNTs surface and, far more important, have an prohibitive cost of applications when compared to the chemical methodology (BANERJEE et al., 2005, CHEN et al., 2011, NASEH et al., 2010, WANG et al., 2006).

It was prepared 50 ml of each MWCNTs based nanofluid. The volume fraction of the nanofluids was obtained through the following expression:

$$\phi = \frac{m_{CNT} \cdot \rho_{CNT}}{m_{CNT} \cdot \rho_{CNT} + V_{bf}} \cdot 100 \qquad 3.2$$

The previously expression suggested the measurement of distinct volume of base fluid $V_{bf}$, depending on the volume fraction of the nanofluid. Additionally, this volume may be difficult to measure due to the magnitude of the graduated cylinder, since they can become decimal or centesimal, inducing noise errors to the system. Therefore, the $V_{bf}$ ($V_{DW} + V_{EG}$) was fixed to 50 ml, and the total volume of the nanofluid will be nearly 50 ml, depending on the volume fraction of the

nanoparticles. In Appendix D, Equation D.2 provides the mathematical formulation for the experimental volume fraction error.

In Table 3.4, it is presented the amount of nanoparticles needed to produce the samples that were tested, for each of the MWCNTs geometries selected. The total amount of MWCNTs calculated is majored in 50% to avoid for some badly dispersion achievement (unstable), which must be repeated. Furthermore, according to Esumi *et al.*, it is also expected nearly 35 to 40% mass loss of the initial pristine MWCNTs, during the chemical treatment. Therefore, a total of 20 g (≈19 g) of MWCNTs, for each of the geometries selected, were functionalized.

Table 3.4: Materials and quantities required for preparation of the samples.

| Base fluid | $\phi$ | $V_{DW}$ [ml] | $V_{EG}$ [ml] | $m_{CNT}$ [g] | $\Delta\phi$ |
|---|---|---|---|---|---|
| DW+30%EG | 0.25% | 35 | 15 | 0.271 | 0.01% |
| | 0.50% | 35 | 15 | 0.543 | 0.02% |
| | 0.75% | 35 | 15 | 0.816 | 0.03% |
| | 1.00% | 35 | 15 | 1.091 | 0.04% |
| | 1.50% | 35 | 15 | 1.645 | 0.06% |
| DW+60%EG | 0.25% | 20 | 30 | 0.271 | 0.01% |
| | 0.50% | 20 | 30 | 0.543 | 0.02% |
| | 0.75% | 20 | 30 | 0.816 | 0.03% |
| | 1.00% | 20 | 30 | 1.091 | 0.04% |
| | 1.50% | 20 | 30 | 1.645 | 0.06% |
| Total | - | - | - | 8.730 | |

The following steps describe the chemical treatment process for each MWCNTs geometry (ESUMI et al., 1996):

1. Inside the hood, it was measured 20 g of pristine MWCNTs and transferred to a 5 litre beaker;
2. Then, these were mixed with 200 ml of nitric acid ($HNO_3$) and 600 ml of sulphuric acid ($H_2SO_4$), a 1:3 volume ratio. This performs 40 ml of acids per gram of MWCNTs, as suggested by several authors (CHEN et al., 2004, ESUMI et al., 1996, KANAGARAJ et al., 2008, PONMOZHI et al., 2009, VEINGNON et al., 2011, XIE et al., 2011, XIE et al., 2003, ZHOU et al., 2008);
3. The mixture was boiled for 30 minutes at 413.25 K on a hot plate with a magnetic stirrer;
4. After the end of the chemical reaction, the mixture was cooled naturally for 24 hours and diluted with distilled water;

5. The particles were intensely washed with distilled water until the supernatant show no signs of acidity. When necessary, the particles are washed with a centrifuge (Heraeus Multifuge 1L). At this step, the carboxylic groups are already bonded to the surface of the MWCNTs, being impossible to reach the pH of the distilled water (≈7) (SHIM et al., 2001, XIE et al., 2003).
6. The cleaned MWCNTs were collected and dried at 373.15 K in an oven, becoming a hard pellet.
7. Finally, the dried nanoparticles pellets were powdered with an analytical miller.
8. The functionalized MWCNTs were stored in a desiccator. Through this, it was avoided the gain of moisture, which change the effective density of the nanoparticles that contributes to noise factors.

Other authors used this method for the MWCNTs functionalization and reported good dispersion results (CHEN et al., 2004, ESUMI et al., 1996, KANAGARAJ et al., 2008, PONMOZHI et al., 2009, VEINGNON et al., 2011, XIE et al., 2011, XIE et al., 2003, ZHOU et al., 2008).

In Figure 3.6, it can be depicted SEM images of pristine MWCNTs and covalently functionalized MWCNTs. In this, it is perceptible that the pristine MWCNTs are highly entangled and, in contrast, the covalently functionalized MWCNTs are disentangled. Furthermore, it seems that the tubular structure integrity was maintained after the chemical treatment. Nevertheless, it should be noted that this does not indicate that the size distribution of the final MWCNTs dispersed in the base fluids is equal to that of the pristine MWCNTs, and announced by the manufacturers.

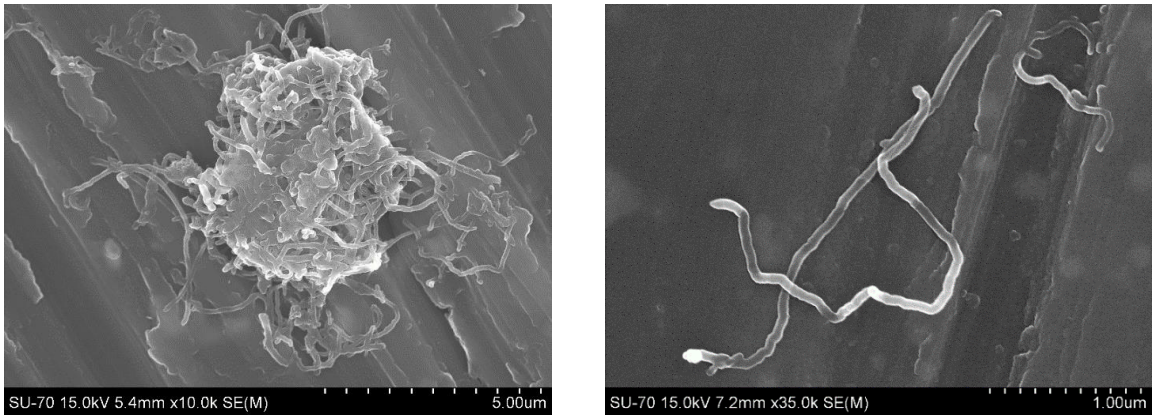


a) b)

Figure 3.6: SEM image of a) pristine MWCNTs and b) covalently functionalized MWCNTs.

## 3.5 QUALITY OF THE FUNCTIONALIZED MWCNTS

As seen, in order to produce the long-term nanofluids projected, it was necessary the functionalization of the pristine MWCNTs. In this Section, it is provided an experimental characterization and assessment to the quality of the functionalized MWCNTs.

### 3.5.1 IDENTIFICATION TO THE FUNCTIONAL GROUPS PRODUCED

Fourier transform infrared spectroscopy (FTIR) was performed in pristine and functionalized MWCNTs, in order to identify the functional groups attached to the MWCNT surface after functionalization.

The FTIR analysis method uses infrared light to scan the samples and observe chemical compounds. During the analysis, an absorbance spectrum of the sample is registered, providing information about the chemical bonds and molecular structure of the material under test. It should be reminded that, to reduce the probability of agglomeration, the MWCNTs were covalently functionalized with carboxylic groups (-COOH), which increased interparticle van der Waals repulsive forces. Thus, it is intended herein to verify the formation of such compounds on the MWCNTs.

The FTIR measurements were performed in a *Brucker Tensor-27* spectrometer in the range of 400 to 4000 $cm^{-1}$. The final spectrum is the mean of 3 measurements replications with a resolution of 4 $cm^{-1}$. Each spectrum was collected over 256 scans. Since the MWCNT detains high absorbance, they were mixed with KBr, and pellets were prepared.

In Figure 3.7, it is illustrated the FTIR spectra of the pristine and functionalized MWCNTs. The spectra are vertically shifted for better visualization purposes.

As it can be depicted, all functionalized MWCNTs exhibit a peak nearby 1630 $cm^{-1}$, which represents the carbon skeleton (C=C) (RAHIMPOUR et al., 2012), suggesting that the integrity of the MWCNTs was not affected by the chemical treatment. The peak ranging from 1150 $cm^{-1}$ to 1210 $cm^{-1}$ is associated with C-O stretching of phenolic and carboxylic groups, the peak near 1150 $cm^{-1}$ identifies the O-H, and the peak close to 1710 $cm^{-1}$ corresponds to C=O stretching of the same groups (KIM et al., 2008b, PENG et al., 2003, RAHIMPOUR et al., 2012, SHAFFER et al., 1998, XIE et al., 2003, ZHANG et al., 2003). These results reveal the quality of the functionalization procedure.

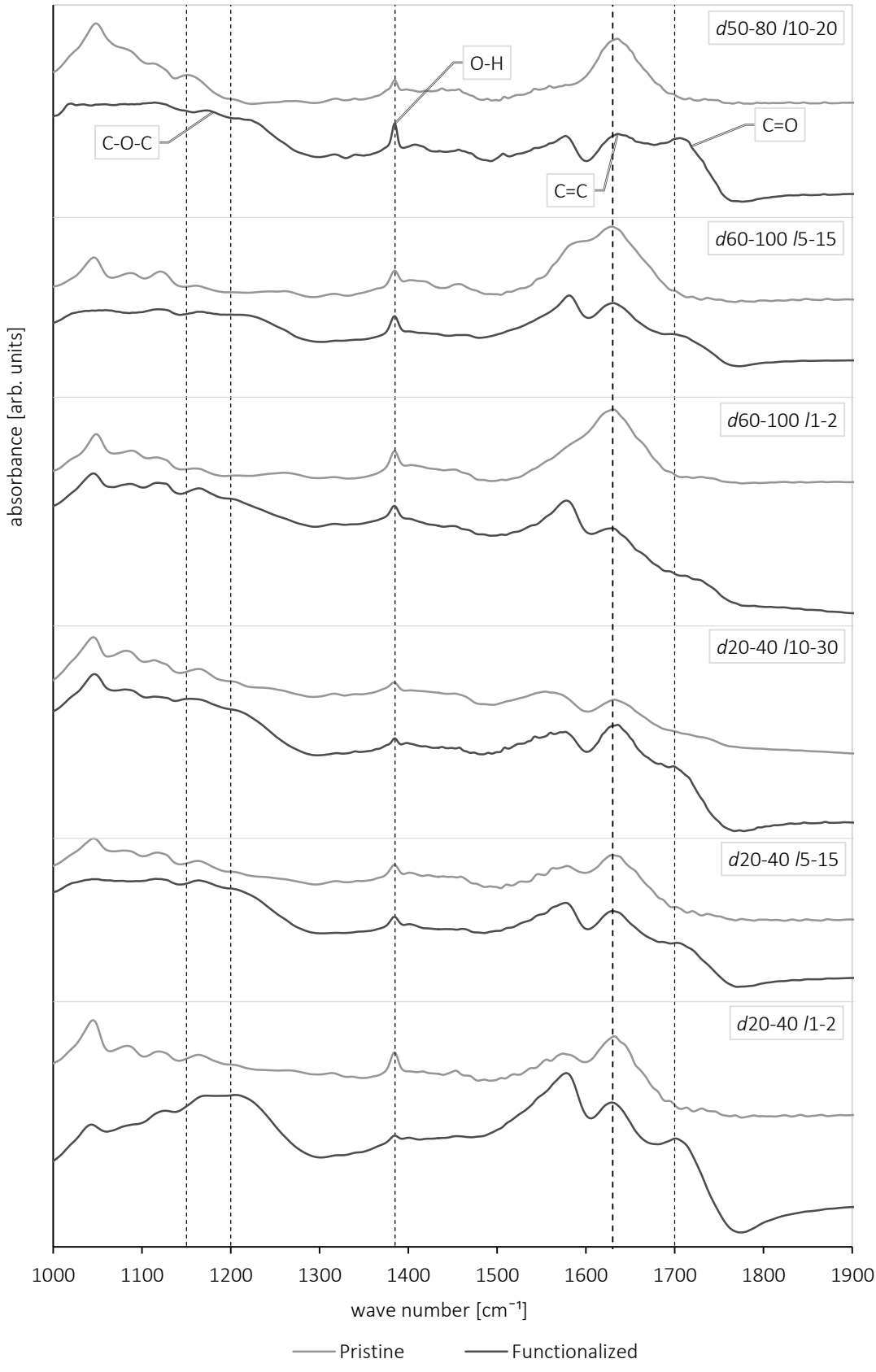


Figure 3.7: FTIR spectra of studied pristine and functionalized MWCNTs.

### 3.5.2 FUNCTIONALIZED MWCNTS STRUCTURAL DAMAGES AND INTEGRITY ASSESSMENT

It was already seen that the structure of the dispersed MWCNTs is achieved through the analysis of the SEM images. Nevertheless, thermo-gravimetric analysis (TGA) was used to evaluate the thermal behaviour, and stability of the functionalized MWCNTs at higher temperatures and, far more important, to assess possible structural damage induced by the functionalization methodology, which may decompose the MWCNTs when the temperature of test is changed. A negligible structural degradation of the MWCNTs at the distinct measuring temperature ensures constant test conditions regarding structural morphology and spatial distribution of the samples during the measurements, appraising possible noise factors at the higher temperatures.

TGA measure the mass-loss of the sample as a function of the temperature, indicating the decomposition rate of the samples. Therefore, the mass-loss curve of the functionalized MWCNTs is compared to that of the corresponding pristine MWCNTs.

The measurements were conducted in *a SETSYS Setaram DSC-TG.* This apparatus measure the mass-loss at heating rate ranging from 0.1 to 100 K per minute, with a resolution of 0.002 µg, within a temperature range from 293.15 K to 2673.15 K (SETARAM, 2013). Even so, the mass-loss of the samples were preformed from 293.15 K to 1023.15 K with a heating rate of 10 K/min under an atmosphere of nitrogen.

It is known that the heating rate influence the temperature of decomposition of the sample, i.e. for a higher heating rate, the temperature of decomposition may also be slightly enhanced. Nevertheless, the trend line of the mass-loss are similar and since it is not intended to specifically identify the temperature of degradation, but possible structural degradation and/or damage, this typical medium-slow heating rate (10 K/min) was selected (HSIEH et al., 2010, TALAEI et al., 2011).

Furthermore, TGA measurements are also strongly influenced by the atmosphere. The nitrogen ensures an inert atmosphere, providing a more reliable measurement of the structural degradation of the nanoparticles with the temperature rather than an oxidative atmosphere, since it is intended to predict the thermal behaviour and possible structural damage of the functionalized MWCNTs dispersed in a fluidic medium. For instance, an oxygen atmosphere will certainly react faster with the functional groups and oxidize the MWCNTs, decomposing them faster. Therefore, an inert atmosphere enables to asses such structural damage, which degrades the MWCNTs with the temperature, rather than through chemical reactions.

In Figure 3.8, it can be depicted the mass change of both pristine and functionalized *d*50-80 /10-20 MWCNTs as a function of the temperature. This results suggests that the pristine MWCNTs have perfect stability, since no mass change was detected for temperature ranging from 293.15 to 1023.15 K. In contrast, the functionalized MWCNTs present a slight linear degradation of the original mass, yet, without an evident temperature set point of decomposition, *i.e.* a pronounced decay of mass to 0%. Nevertheless, the trend line reveals that, at least, 90% of the mass do not decompose and evaporate. This may indicate the presence of some impurities or some MWCNTs fragments that were not washed during the functionalization treatment, which might easily degrade at higher temperatures, evaporating, and perhaps the decomposition of the functional group attached to the side walls of the MWCNTs. Similar results were obtained for the remaining MWCNTs analysed and are reported in the Appendix E.

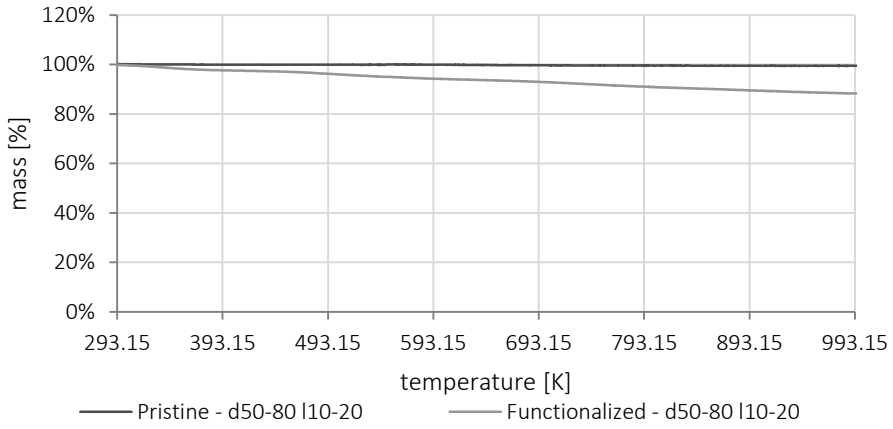


Figure 3.8: TGA of functionalized and pristine MWCNTs (*d*50-80 /10-20).

In Table 3.5, it is summarized the mass-loss % for two different temperatures, 323.15 K and for 1023.15 K. As it can be depicted, for 323.15 K, the functionalized MWCNTs present, in general, negligible mass-loss, indicating an acceptable thermal stability for the tested conditions. These results are of greatest importance to ensure that the samples may present similar morphological and structural conditions at several experimental conditions, thereby reducing noise factors.

Table 3.5: Mass-loss achieved in the TGA test at 323.15 and 1023.15 K, for all the functionalized MWCNTs.

| Nanoparticle | mass-loss @ 323.15 K | mass-loss @ 1023.15 K |
|---|---|---|
| *d*50-80 /10-20 | -0.8% | -12.0% |
| *d*60-100 /5-15 | -1.2% | -16.9% |
| *d*60-100 /1-2 | -0.4% | -5.8% |
| *d*20-40 /10-30 | -0.9% | -9.7% |
| *d*20-40 /5-15 | -1.3% | -15.6% |
| *d*20-40 /1-2 | -0.7% | -10.7% |

### 3.5.3 FUNCTIONALIZED MWCNTS SIZE DISTRIBUTIONS ANALYSIS

Although the dispersion method enables the production of non-agglomerated dispersions of MWCNTs in polar solvents, it is recognized that the covalent functionalization cause degradation of the geometry of the nanoparticle, namely length reduction (HILDING et al., 2003). Therefore, the size distribution of the functionalized nanoparticles differs from the announced by the manufacturer (Table 3.2) and cannot be applied in the predictive models.

The literature highlights a few novel techniques to assess the size distribution of particles at the nanoscale, such as laser diffraction, dynamic light scattering, sieving, sedimentation, microscopy, among others. However, for a complete description of the nanoparticle, it is required two parameters: length, and diameter. The majority of the sizing techniques mentioned, which generally have prohibitive costs, assume that the particles are spherical, describing these through an equivalent diameter, of a sphere with the same mass, volume, surface area, or sedimentation rate, among others (ALLEN, 1996).

As it can be depicted from Section 1.5.3.4 and 2.5, to describe the effective thermal conductivity of MWCNTs based nanofluids, it may be required the respective diameter and length distribution of the dispersed MWCNTs. The assumption of a spherical shape of the nanotubes will lead to the underestimation of the effective conductivity, as suggested in Figure 2.15. Therefore, it is of utmost importance the selection of the appropriate methodology to assess the two-dimensional size distributions of the dispersed MWCNTs.

In this research, the size distributions of the MWCNTs were achieved through microscopy, namely *scanning electron microscope* (SEM), and image analysis. SEM scans the surface of the sample through a high energy electron beam, and the back scattering from the electrons forms an image. These images enable to observe the structure and dimensions of the MWCNTs. Moreover, the manufacturers were contacted and these revealed that the provide sizes distribution of pristine MWCNTs were also achieved by similar technique.

The diameter and length distribution of the functionalized-MWCNTs was determined in a *Hitachi SU-70.* It should be noted that this microscopic technique must work in a vacuum being, therefore, required dried nanoparticles. The functionalized MWCNTs, of each selected geometry, were dispersed in ethanol in very low concentration. Drops of these dispersions are then deposited over

the surface of the samples' holder and it is allowed to dry. Then it is performed a sputter coating of carbon to ensure that the samples are electron conductive.

Several images are taken from each sample for analysis and measurement. Ideally, the images should be processed by specific image analysis software. However, these would require MWCNTs completely isolated from each other and, preferably, stretched. The combination of these factors induces noise factors in the automatic image analysis, requiring constant monitoring and co-processing/validation during the analysis. Recognizing the possibility of human error, the measurement of the sizes distribution of the dispersed MWCNTs was performed manually, using a free CAD software, DraftSight from *Dassult Systemes* (DASSAULT-SYSTEMES, 2013).

To minimize the associated error, a large number of images and measurements were taken, and it is assumed that the latter have a normal distribution, enabling to estimate their respective confidence interval and statistical error. However, as it will be seen, the functionalized MWCNTs present a high length reduction that produced asymmetric normal distributions that also predict negative lengths, a physical impossibility. Therefore, the lengths' normal distributions were truncated in the interval $]0 ; +\infty[$. The truncated normal distribution is a probability distribution from a normal distribution, were the values have, at least, one bound (LAWLESS, 2006). In Appendix D, is provided the mathematical formulation of both distributions, as well as the methodologies to test the *goodness-of-fit* of the distributions over the observed results, which reveals satisfactory adherence. Therefore, the mean (and truncated mean) and standard deviation (and truncated standard deviation) can be used to describe the sizes distribution of the functionalized MWCNTs.

As mentioned, the size distributions of the dispersed MWCNTs were measured through an intensive SEM image analysis, as schematically represented in Figure 3.9. Nonetheless, it should be noted that the performed measurements are executed in projected images, which induces a certain unknown degree of inaccuracy, mainly in what concerns length estimation due to the three-dimensional nature of the analysed structures. Even so, this methodology enables the assessment of the two-dimensional size distributions at the nanoscale.

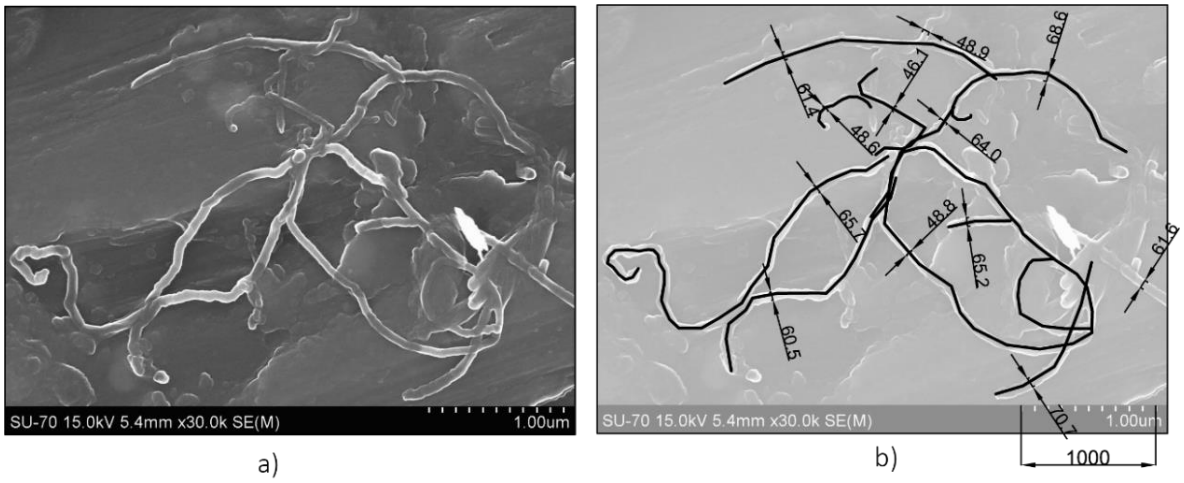


Figure 3.9: a) illustration of a given SEM image of dispersed MWCNTs and b) schematic representation of the measurement procedure used.

It is known that the samples have dispersed nanoparticles with different sizes, which are characterized by the obtained sizes distribution. Nevertheless, the mean (and truncated mean) of these sizes distribution is used to characterize the experimental observed results. This technique also enabled to verify the structural integrity of the dispersed functionalized-MWCNTs, *i.e.*, their tubular shape (Figure 3.6).

For each of the studied MWCNTs, it was analysed a large number of SEM images, to obtain higher samples size and, therefore, decrease the standard deviation error of the measured size distributions. In Table 3.6, is provided samples size obtained from the SEM analysis, for each of the MWCNTs tested. The larger number of diameters observed when compared to the number of considered lengths results from the fact that some SEM images do not permit a truthful measurement of the MWCNTs length. In such cases, only the diameter was measured.

Table 3.6: Samples size obtained from the SEM images analysis.

| MWCNT designation | $N_{d_p}$ | $N_{l_p}$ |
|---|---|---|
| *d*50-80 /10-20 | 263 | 70 |
| *d*60-100 /5-15 | 131 | 111 |
| *d*60-100 /1-2 | 189 | 171 |
| *d*20-40 /10-30 | 401 | 130 |
| *d*20-40 /5-15 | 175 | 106 |
| *d*20-40 /1-2 | 189 | 122 |
| *average* | *225* | *118* |

In Figure 3.10, it is illustrated the measured diameters and lengths distributions of the functionalized MWCNTs *d*50-80 /10-20. It should be noted that, in this Figure, the measured sizes

are rounded to perform the histogram graph, which is only used to visualize the distributions. Moreover, all the results from this analysis outcomes from the original measured values. Similar results were obtained for the remaining MWCNTs analysed and are reported in the Appendix E. As it can be observed, the functionalized MWCNTs physical dimensions (diameter and length), exhibit a normal distribution. From this, it was obtained the mean diameter and length and respective confidence interval of 95%, for all the studied MWCNTs. The mathematical formulation to estimate the 95% confidence range of the mean for the considered samples is expressed in Appendix D.

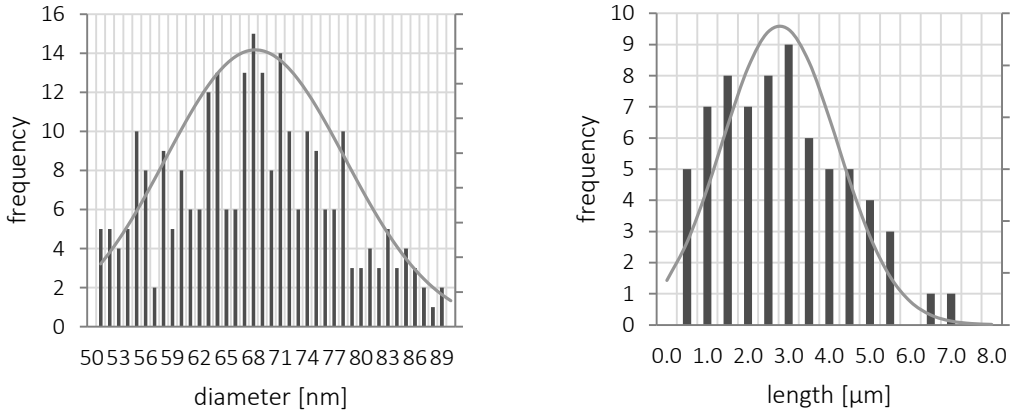


Figure 3.10: Diameter and length distribution of the dispersed MWCNTs *d*50-80 /10-20.

In the Appendix E similar Figures of the statistical convergence for the remaining studied nanoparticles are provided.

As mentioned, since the diameters and lengths comply within the normal and truncated normal distributions, the mean (and truncated mean) and standard deviation (and truncated standard deviation) of the measurements can be used to describe the sizes distribution of the functionalized MWCNTs.

The results obtained for the studied MWCNTs are summarized in Table 3.7. These are the results for a mean sample size of 218 measured diameters and 118 measured lengths, as shown in Table 3.6. The uncertainty interval of the mean diameter and mean length for a 95% confidence level were calculated through Equation D.7 and D.9, respectively, presented in the Appendix D.

Table 3.7: Diameter and length distribution assessment, after functionalization (uncertainty and 95% confidence interval C.I. according to Appendix D).

| | diameter | | | length | | |
|---|---|---|---|---|---|---|
| MWCNTs designation | $\overline{d_p}$ [nm] | $\Delta\overline{d_p}$ [nm] | 95% C.I. | $\overline{l_{p_{tru}}}$ [nm] | $\Delta\overline{l_{p_{tru}}}$ [nm] | 95% C.I. |
| *d*50-80 /10-20 | 68 | ± 1.194 (1.8%) | [49;88] | 2865 | ± 342 (11.9%) | [246;5485] |
| *d*60-100 /5-15 | 62 | ± 1.985 (3.2%) | [37;86] | 2012 | ± 181 (9%) | ]0;4050] |
| *d*60-100 /1-2 | 58 | ± 1.927 (3.3%) | [36;84] | 1702 | ± 181 (10.6%) | ]0;3516] |
| *d*20-40 /10-30 | 50 | ± 0.766 (1.5%) | [34;65] | 1799 | ± 149 (8.3%) | [179;3420] |
| *d*20-40 /5-15 | 50 | ± 1.331 (2.7%) | [32;68] | 1590 | ± 189 (11.9%) | ]0;3232] |
| *d*20-40 /1-2 | 42 | ± 1.133 (2.7%) | [27;58] | 1052 | ± 151 (14.4%) | ]0;2174] |

As expected, the MWCNTs lengths are the parameter most affected by the functionalization process, assuming as valid the initial size distribution announced by the manufacturers. The average aspect ratio reduction, for all the studied MWCNTs, was of -56%.

Table 3.8 summarizes the geometrical properties of the dispersed MWCNTs under study that may be relevant to the experimental results' assessment.

Table 3.8: Geometrical properties of the dispersed MWCNTs under study.

| MWCNTs designation | $\overline{d_p}$ [nm] | $\overline{l_{p_{tru}}}$ [nm] | $\overline{l_{p_{tru}}}/d_p$ | V [nm³] | S/V [nm$^{-1}$] | S [nm²] |
|---|---|---|---|---|---|---|
| *d*50-80 /10-20 | 68 | 2865 | 42 | 10406208 | 0.059 | 612130 |
| *d*60-100 /5-15 | 62 | 2012 | 32 | 6073070 | 0.065 | 391811 |
| *d*60-100 /1-2 | 58 | 1702 | 29 | 4497895 | 0.069 | 310200 |
| *d*20-40 /10-30 | 50 | 1799 | 36 | 3532834 | 0.080 | 282627 |
| *d*20-40 /5-15 | 50 | 1590 | 32 | 3122603 | 0.080 | 249808 |
| *d*20-40 /1-2 | 42 | 1052 | 25 | 1457167 | 0.095 | 138778 |

Assuming that the final geometry of the nanoparticles caused by the dimensional degradation induced by the functionalization process depends of the initial dimensional properties of the MWCNTs (provided by the manufacturer), it is possible to develop a statistical predictive model, based on multivariate linear regression technique. In Equation 3.3 it is presented a multivariate linear regression to predict both magnitude of the diameter and length of the MWCNTs after the dispersion process, based on the original dimensional data disclosed by the manufacturers (Table 3.2).

$$X=a_1+\frac{d_p}{a_2}+\frac{a_3}{l_p}+\frac{a_4}{l_p^{\,2}}+\frac{a_5}{l_p^{\,3}} \qquad 3.3$$

where *X* is the variable to be predicted, *i.e.* the functionalized diameter or length in m, and $a_{1...5}$ are the model adjustment factors shown in the Table 3.9.

Table 3.9: Values of the adjustment factors for the multivariate linear regression for both diameter and length prediction.

| Variable | diameter | length |
|---|---|---|
| $a_1$ | -4.2742E-08 | -6.104E-06 |
| $a_2$ | 2.8000E-01 | 1.070E+01 |
| $a_3$ | 2.6684E-12 | 2.420E-10 |
| $a_4$ | -2.0912E-17 | -1.925E-15 |
| $a_5$ | 2.5625E-23 | 2.366E-21 |

In Figure 3.11, it is shown the scatter chart of the proposed multivariate linear regression. As this is a multivariable problem, the graph is represented in terms of *output* versus *target*, where, *output* is the statistical results shown in Table 3.7, and *target* the results achieved through the model, as schematically defined in Table 3.10. As it can be seen, the regression model presents an acceptable correlation with the statistical results ($r^2$>0.99), suggesting that this can be used to predict the final geometry properties of MWCNTs functionalized through the methodology described in the Section 3.4. In Table 3.11 is a comparison of between the mean diameter and mean truncated length achieved by the normal distributions with the predicted through Equation 3.3.

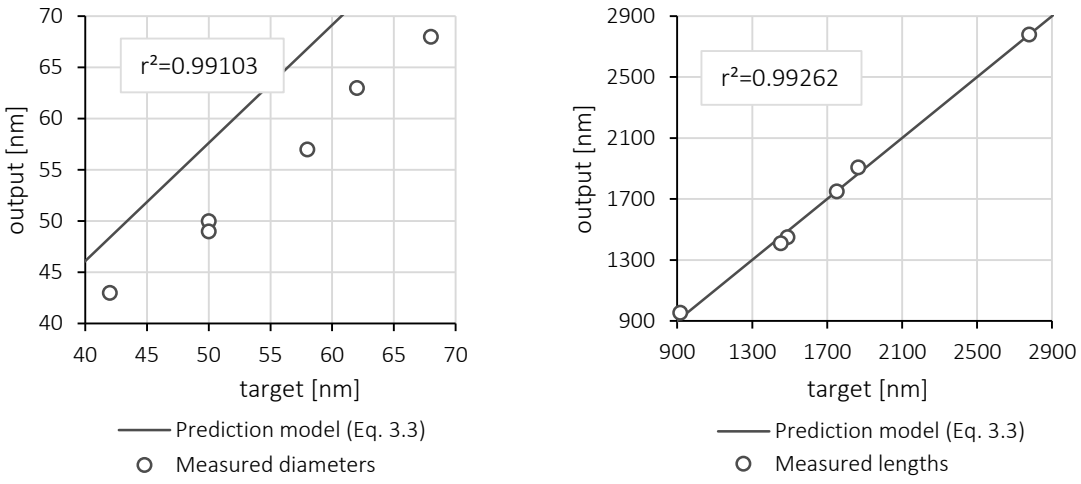


Figure 3.11: Multivariable regression for the achieved diameters and lengths of the functionalized MWCNTs.

Table 3.10: Schematic defined of the terms target and output, used in Figure 3.11.

| | Predictive model | Measured experimentally values |
|---|---|---|
| target (x) | predicted | measured |
| output (y) | predicted | predicted |

Table 3.11: Comparison of between the mean diameter and mean truncated length achieved by the normal distributions with the predicted through Equation 3.3.

| MWCNTs designation | $\bar{d}_p$ [nm] | $\overline{l_{p_{tru}}}$ [nm] | $\bar{d}_p$ predicted [nm] | $\bar{l}_p$ predicted [nm] |
|---|---|---|---|---|
| *d*50-80 /10-20 | 68 | 2 865 | 68 | 2 870 |
| *d*60-100 /5-15 | 62 | 2 012 | 63 | 2 067 |
| *d*60-100 /1-2 | 58 | 1 702 | 57 | 1 642 |
| *d*20-40 /10-30 | 50 | 1 799 | 50 | 1 800 |
| *d*20-40 /5-15 | 50 | 1 590 | 49 | 1 532 |
| *d*20-40 /1-2 | 42 | 1 052 | 43 | 1 107 |

### 3.5.4 BRIEF DISCUSSION

So far, it was verified that the functionalization technique attached the desired carboxyl groups to the sidewall of the pristine MWCNTs. Through this, it is expected the creation of the hydrophilic surface on the MWCNTs. The TGA revealed that the chemical treatment produced some structural damages. Nevertheless, this is only noticeable for very high temperatures (~1000 K). For the projected temperatures for thermal conductivity assessment, the functionalized nanoparticles present satisfactory thermal stability, since the damage caused by the chemical treatment seems to be unnoticeable for this temperature range.

Even so, the major drawback of the functionalization methodology used is the MWCNTs length distribution reduction. The latter clearly provide a higher thermal conductivity enhancement for the same volume fractions. Though, it should be noted that it is not desired to obtain the maximum thermal conductivity enhancement in a nanofluid. A thermal nanofluid should present long-term effective thermo-physical properties, even if these present an initial penalty.

## 3.6 NUMERICAL MODELLING OF NANOPARTICLES INSIDE A FLUIDIC MEDIUM

As verified in Section 1.5.3.4, the predictive models for non-spherical particles (expect for Deng *et al.*) simplify « the flexible geometry of the MWCNTs to rigid cylinders. Such assumption defines that the flexible structure of the tubular nanoparticle has no impact on the degree of spatial distribution and, therefore, does not contribute to the effective thermal conductivity. This structural flexibility maybe even more pronounced in the results due to the molecular dynamic behaviour of dispersions. Furthermore, one of the controversial theories to describe the anomalous thermal behaviour of nanofluids is the Brownian motion of the particles.

Therefore, in the next Section is formulated a numerical analysis that enables to assess the Brownian behaviour of dispersed CNTs in conventional fluids. The numerical model, based on

continuum mechanics, allows measuring the dynamic interparticle interaction, and respective spatial distribution, of flexible and rigid CNTs, at different volume fractions and geometrical properties.

Since the classical predictive models for the effective thermal conductivity of nanofluids are based on static mechanism, *i.e.* motionless mixture, it is expected to verify if the dynamics behaviour of the nanoparticles can be considered as statistically motionless or static. Among the various dynamics behaviour of the particles is their spatial distribution and interparticle interactions that, due to the natural motion of the particles, are constantly modifying.

### 3.6.1 DYNAMIC NUMERICAL MODELS

The Brownian motion explains the random movement among the particles through a fluid, at any time step, caused by the impact of the base fluid molecules. Owning to the high aspect ratio of CNTs, it is expected a high degree of spatial distribution, which will contribute to higher effective heat conduction. However, CNTs are flexible which could affect the spatial distribution and respective transition through the microstructural arrangements shown in Figure 2.12.

Therefore, two continuum numerical models are proposed to assess the dynamic interparticle interaction of (1) *flexible* and (2) *rigid* CNTs. In these, the influence of the Brownian field intensity, CNTs geometry, and volume fraction are dynamically studied in detail. It is expected that the numerical models confirm that the dynamical behaviour of the particles can be treated as statistically motionless and, thereby, corroborate the proposed models for the effective thermal conductivity. It should be noted that the latter was based on static physical mechanisms.

In both numerical models it is assumed that the nanoparticles are suspended in a base fluid, inside a cubic control volume, and comply with continuum mechanics theory. The variation in the particle rigidity will be used to understand if the interparticle interaction and respective spatial distribution inside the control volume are influenced by the structural flexibility of CNTs. A higher number of random collisions indicate a superior interaction between the particles and, as a consequence, a higher degree of spatial distribution. Furthermore, the number of interparticle interaction enables to identify the existence of thermal interparticle interaction, since the latter is observed even after the contact of the particles, as seen in Figure 2.6.

#### 3.6.1.1 STRUCTURAL FLEXIBILITY OF CARBON NANOTUBES

The dynamics of a CNT suspended in a stationary base fluid are dominated by Brownian forces, which tend to curve them, and elastic forces, which oppose this bend. Fakhri *et al.* studied the Brownian bending dynamics of an individual SWCNT in water. Their results suggested that the SWCNT had no static curvature, since the measured mean amplitude of the bending angle was essentially zero (FAKHRI et al., 2009). Moreover, the results suggested that the Brownian field is unable of permanently bend the CNTs.

The angle between the axis of the deformed CNTs and the initial straight axis is defined as the bending-angle $\alpha$. The critical bending buckling, for critical bending angle $\alpha_c$, is expressed by Equation 3.4:

$$\kappa_c = \frac{\alpha_c}{l_p} \qquad 3.4$$

The critical bending buckling represents the curvature limits that a CNT can be bent without a permanent deformation (see Figure 3.12). Experimental and theoretical studies show that carbon nanotubes are remarkably flexible (FAKHRI et al., 2009, IIJIMA et al., 1996, YAKOBSON et al., 1996). Dividing the nanotube in two rigid sections with equal length $l_p/2$, the bending angle is represented in Figure 3.12:

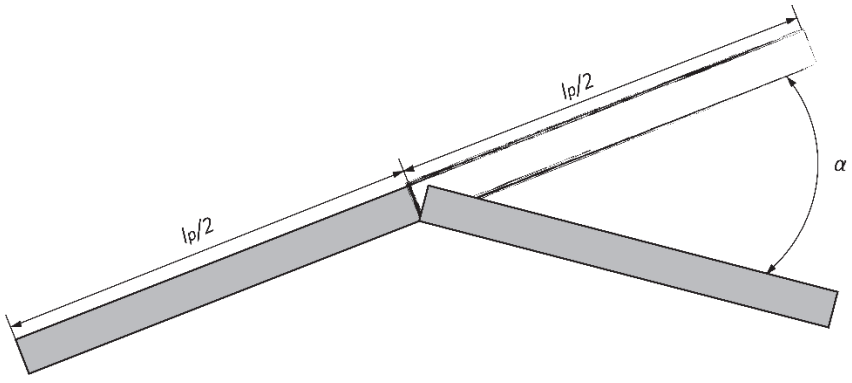


Figure 3.12: Curvature of a CNT divided in two rigid sections.

Iijima *et al.* found that the critical angle strongly depends on the SWCNTs diameter (IIJIMA et al., 1996):

$$\kappa_c = \frac{1.49}{(10d_p)^2} \cdot \left[1 + \frac{9.89}{(10d_p)^5} \cdot 10^3 \cdot \cos\left(\frac{\pi}{6}\right)\right] \qquad 3.5$$

In addition, Yakobson *et al.* also studied the nonlinear mechanical behaviour of SWCNTs by molecular dynamics simulation, proposing an alternative expression for the critical curvature (YAKOBSON et al., 1996):

$$\kappa_c = \frac{0.155}{(d_p)^2} \qquad 3.6$$

A simple evaluation of the two correlations presented (Equation 3.5 and 3.6) is made in the Figure 3.13. As can be seen, the two correlations fit perfectly.

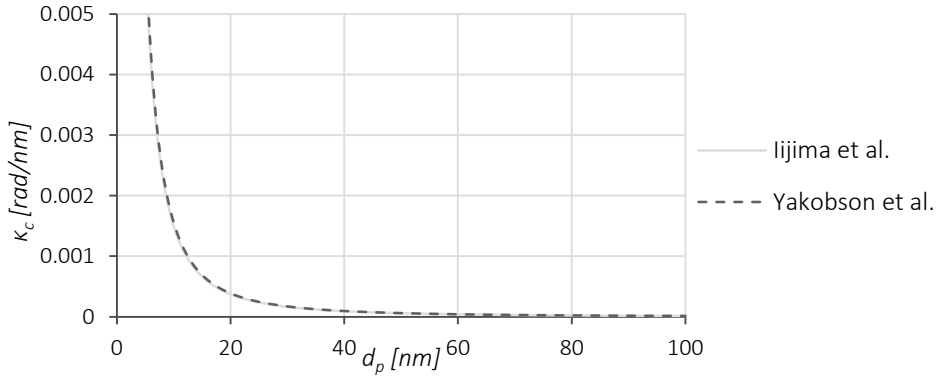


Figure 3.13: Comparison of the two correlations for bending angle calculation.

The above correlations were achieved for SWCNTs, being expected a significant difference in the bending behaviour of MWCNTs due to the presence of the inner tubes (see Figure 1.2). However, correlations for bending buckling for MWCNTs do not seem to be available in the literature so far. Even so, it is expected that the MWCNTs present lower bending buckling than SWCNTs being, therefore, assess the worst-case scenario.

For the proposed *flexible* model, the structural flexibility of the CNTs meet the bending buckling of Yakobson *et al.* due to its simplicity.

#### *3.6.1.2 BROWNIAN MOTION*

When a sufficiently small particle is suspended in a fluid, it will exhibit a stochastic motion. This natural phenomenon is the so-called *Brownian motion*, described by Robert Brown in 1828 (BROWN, 1828). Experimental and theoretical work, supported by the kinetic theory of matter, postulates that (PERRIN, 2005):

- Particle motion is composed of translational and rotational movement;

- Particles move independently;
- Particle motion is more active for smaller particles;
- Particle motion is more active for less viscous fluid;
- Particle motion is more active the higher the temperature;
- Particle motion never ceases.

The theory of Brownian motion began with Albert Einstein, when he derived the diffusion equation (Equation 3.9) for a sphere of diameter $d_p$ immersed in a fluid of viscosity $\mu_{bf}$, supported by the Stokes law for friction force. According to the molecular-kinetic theory of heat, Einstein has shown that solid bodies can perform movements when suspended in liquids (EINSTEIN et al., 1956). Later, Langevin derives an equation for spherical bodies based on the Newton law of motion (REIF, 1965):

$$m\frac{d^2\vec{\xi}}{dt^2}=-\beta\cdot\frac{d\vec{\xi}}{dt}+\overrightarrow{F_s}(t) \qquad 3.7$$

where $\xi$ is the displacement of the particle at the time $t$, $F_s$ is a stochastic force and $m$ is the mass. The dynamical friction constant $\beta$ is governed by the Stokes' law and comes from the surrounding medium and geometry of the small particle:

$$\beta=3\pi\cdot\mu_{bf}\cdot d_p \qquad 3.8$$

By assuming the diffusion coefficient $D$ given by Stokes-Einstein (Equation 3.9) and the stochastic force (Equation 3.10), it was possible to derive the mean displacement for a long time (Equation 3.11).

$$D=\frac{k_B\cdot T}{\beta} \qquad 3.9$$

where $k_B$ is the Boltzmann constant ( $1.38\times10^{-23}$J/K ) and $T$ is the absolute temperature.

$$\overrightarrow{F_s}(t)=G_{rand}\cdot\sqrt{\frac{2k_B\cdot T\cdot\beta}{\Delta t}} \qquad 3.10$$

where $G_{rand}$ is a zero mean Gaussian random number.

The mean displacement was shown to be in agreement with the Einstein result for a long time interval $(\Delta t\gg\beta^{-1})$, and can be expressed as (EINSTEIN et al., 1956, REIF, 1965):

$$\left|\vec{\xi}\right|=\sqrt{2D\cdot\Delta t} \qquad 3.11$$

As it can be noticed, the shape of CNTs does not seem to fit into this theory. An adaptation is needed in order to simulate this dynamical behaviour of suspended solid bodies in a base fluid. For that, individual CNTs will be assumed to be inside of a surrounding sphere, which will describe the random movement at each time step, as represented in Figure 3.14. The considered surrounding sphere should have an equivalent diameter $d_{eq}$ that equals the drag coefficient of the CNT, based on the cross-sectional area.

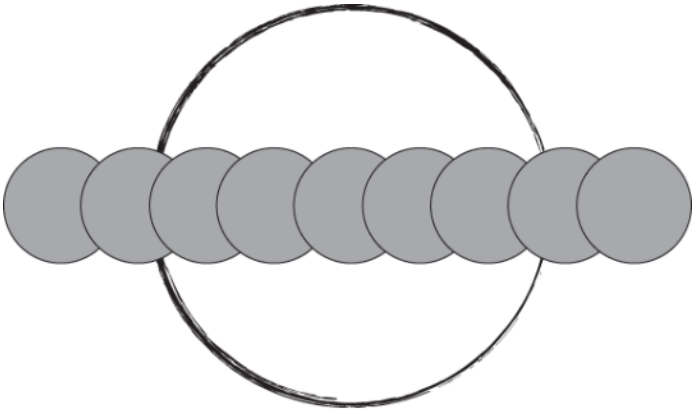

Figure 3.14: Schematics of the surrounding sphere on a CNT made of spheres.

The drag coefficient of a body immersed in a fluid in motion can be described by the following expression (WHITE, 1998):

$$C_d = \frac{2F_d}{\rho_{bf} \cdot v^2 \cdot A_{cs}} \tag{3.12}$$

where $F_d$ is the drag force, $\rho_{bf}$ is the mass density of the fluid, $v$ is the relative velocity and $A_{cs}$ is the cross-sectional area of the CNT. For the surrounding sphere, the equivalent cross-sectional area is defined as:

$$A_{cs_{eq}} = \frac{\pi}{4} \cdot d_{eq}^{\,2} \tag{3.13}$$

However, the cross-sectional area of the CNT strongly depends on the CNT orientation in relation to the movement performed. The minimum cross-sectional area that accounts for less resistance against the movement occurs when the CNT is fully stretched and with the tube axis parallel to the movement, shown in Figure 3.15 (a). The maximum resistance against the movement occurs when the CNT is stretched, and the tube axis is perpendicular to the movement, represented in Figure 3.15 (b).

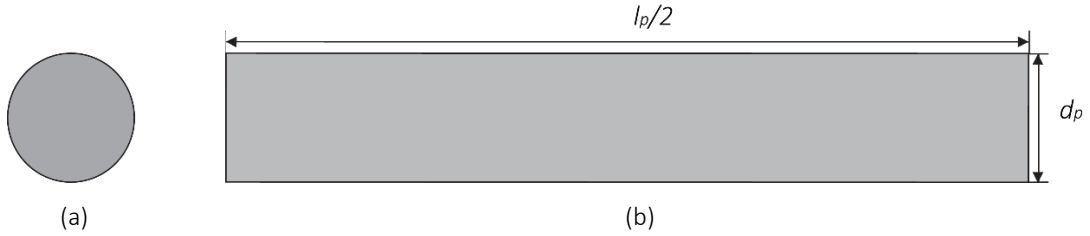


Figure 3.15: Illustration of the minimum (a) and maximum (b) cross section of the CNT.

Knowing the direction of the movement it is, therefore, possible to estimate the $A_{cs_{eq}}$ of the CNT based on its relative angle to the movement. Nevertheless, the surrounding sphere, used to estimate the Brownian movement, will have an equivalent diameter within:

$$d_{eq} \in \left[ d_p; \sqrt{\frac{l_p \cdot d_p}{2\pi}} \right] \qquad 3.14$$

For simplicity, the equivalent diameter of each CNT is assumed to be in the medium of this interval (Equation 3.15) and applied in the Equation 3.8 in order to compute the mean displacement that this must perform.

$$d_{eq} = \frac{\sqrt{{d_p}^2 + \frac{l_p \cdot d_p}{2\pi}}}{2} \qquad 3.15$$

In addition, the estimated mean displacement per time step of each CNT is recorded, and an estimation of the average Brownian velocity of the CNTs inside the control volume is derived. The latter is used to verify the sedimentation stability of the nanofluids.

#### *3.6.1.3 CARBON NANOTUBE SUSPENSION DYNAMICS*

Through considering that each CNT is composed of $n_{sec}$ connected and perfectly solid spheres, whose diameter is the same of the CNT, shown in Figure 3.14, it is expected to include a model which favours the calculation of collision rate. The number of spheres $n_{sec}$ (or sections) required to describe each CNT is a function of the nanotube length and model discretization, *i.e.*, sphere diameter, and is given by:

$$n_{sec} = \frac{l_p}{d_p} \qquad 3.16$$

Each CNT is be plotted by the aggregation of each direction vector with norm $d_p$. For the direction vectors construction, $n_{sec}+1$, points need to be defined for each CNT, as represented in Figure 3.16.

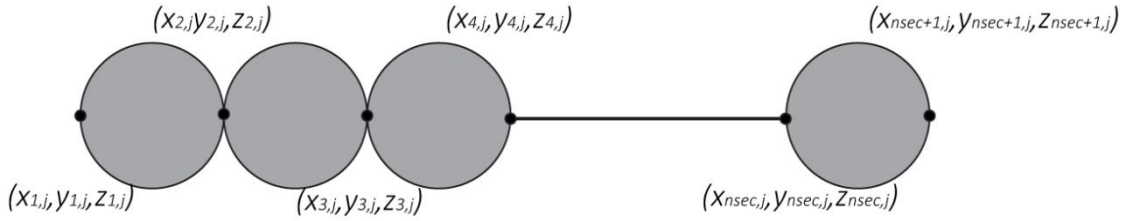


Figure 3.16: Schematic representation of points used for the direction vectors definition.

Each CNT ($j$) starts the simulation (at $t$=0) in a random position inside of a control volume. This random position can be achieved by:

$$x_{1,j}=rand\cdot l_{cv} \tag{3.17}$$

$$y_{1,j}=rand\cdot l_{cv} \tag{3.18}$$

$$z_{1,j}=rand\cdot l_{cv} \tag{3.19}$$

where *rand* is a random number $\in [0,1]$ and $l_{cv}$ is the characteristic length of the control volume.

As mentioned before, the colloid is at rest with no flow or external force field application. Thus, the orientation of each carbon nanotube is arbitrary. This random orientation can be achieved by the orientation of the first direction vector, which can be expressed by the second point:

$$x_{2,j}=x_{1,j}+l_p\cdot sin\varphi_{1,j}\cdot cos\vartheta_{1,j} \tag{3.20}$$

$$y_{2,j}=y_{1,j}+l_p\cdot sin\varphi_{1,j}\cdot sin\vartheta_{1,j} \tag{3.21}$$

$$z_{2,j}=z_{1,j}+l_p\cdot cos\varphi_{1,j} \tag{3.22}$$

where $\varphi$ and $\vartheta$ is the azimuth and colatitude angles respectively, and defined as:

$$\varphi_{1,j}=rand\cdot 2\pi \tag{3.23}$$

$$\vartheta_{1,j}=rand\cdot \pi \tag{3.24}$$

The next points, which define the remains direction vectors, can be achieved by:

$$x_{i,j}=x_{i-1,j}+l_p\cdot sin\varphi_{i-1,j}\cdot cos\vartheta_{i-1,j} \tag{3.25}$$

$$y_{i,j}=y_{i-1,j}+l_p\cdot sin\varphi_{i-1,j}\cdot sin\vartheta_{i-1,j} \tag{3.26}$$

$$z_{i,j}=z_{i-1,j}+l_p\cdot cos\varphi_{i-1,j} \quad 3.27$$

for $i \in [3,n_{sec}+1]$.

These points define the structural flexibility of the carbon nanotubes. In order to assure the rigidity and flexibility of each model, the following angles derivation is needed.

### Flexible model

By this model, each pair of spheres can bend at a maximum angle equal to $\alpha_c$, expressed in Section 3.6.1.1. Thus, it was assumed that the stochastic force is not enough to bend the CNTs to reach the deformation point.

$$\varphi_{s,j}=\varphi_{s-1,j}+G_{rand}\cdot\alpha_c \quad 3.28$$

$$\vartheta_{s,j}=\vartheta_{s-1,j}+G_{rand}\cdot\alpha_c \quad 3.29$$

for $s \in [2,n_{sec}]$

This model can be depicted in Figure 3.17 (a).

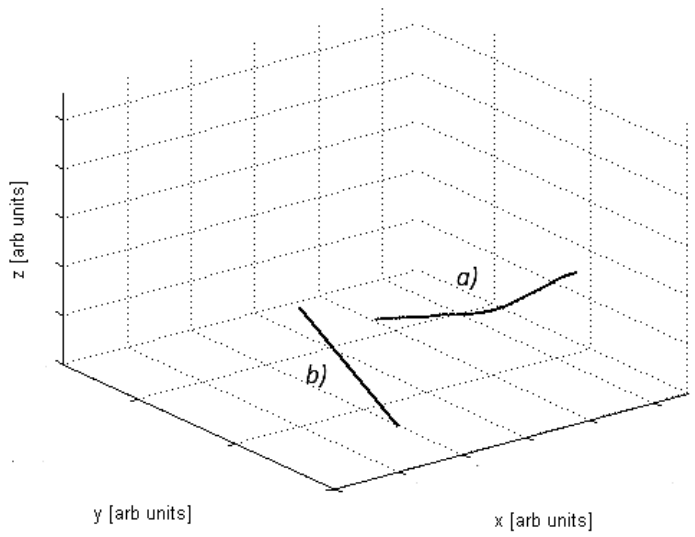


Figure 3.17: Representation of a) *flexible* and b) *rigid* carbon nanotube inside of the control volume.

Rigid model

Since the CNTs in this model cannot be bent, the azimuth and colatitude angle will be constant for all points, as following:

$$\varphi_{s,j}=\varphi_{s-1,j} \quad 3.30$$

$$\vartheta_{s,j}=\vartheta_{s-1,j} \quad 3.31$$

for $s \in [2,n_{sec}]$

This model can be depicted in Figure 3.17 (b).

### 3.6.1.4 PARTICLE DISPOSITION EVOLUTION

The previous mathematical models place the nanoparticles randomly within the volume control for the first initial moment ($t$=0). In addition to the deformation and reorientation of the CNTs, the Brownian motion will cause a random displacement of the nanoparticle within the overall control volume (for $t$>0). In order to adjust this random movement, the CNTs were considered to behave like an equivalent sphere (see Section 3.6.1.2), which will be subjected to the mentioned stochastic force.

At each equivalent sphere, the mean square displacement will be calculated for each time step. This displacement is incremented in the first direction vector and is then reflected in the others.

For the *rigid* model, where the deformation is neglected, the rotation will be limited by the first direction vector, since the direction angles who define the remaining spheres will be constant. In the improbable event, where all the constituting vectors of the CNT bend to the same direction, the maximum global azimuth and colatitude angle can be described by:

$$\varphi_{s,j}=\varphi_{s-1,j}+G_{rand}\cdot\alpha_c\cdot n_{sec} \quad 3.32$$

$$\vartheta_{s,j}=\vartheta_{s-1,j}+G_{rand}\cdot\alpha_c\cdot n_{sec} \quad 3.33$$

For the *flexible* model, the azimuth and colatitude angle will randomly vary each time step, with a maximum variation between each pair of spheres, equal to the critical bending angle. With this assumption, it is possible to verify the effect of the structural flexibility of CNTs on the average interparticle interaction and spatial distribution.

### 3.6.1.5 *DYNAMIC INTERPARTICLE INTERACTIONS MEASUREMENT*

Through counting all the collisions achieved between the CNTs inside the control volume, it is possible to characterize the interparticle interactions. These are directly proportional to the degree of spatial distribution.

Nevertheless, it should be noted the meaning of the term collision. Given the stability desired for the thermal nanofluids, stated in the Section 3.2.2, it is assumed in both numerical models, no fixed contact after a collision, *i.e.* each CNT encounters the others in its vicinity, thus forming a dynamic percolation chains in the suspension, without aggregation or fixed contacts.

For the collisions detection, at the end of all time steps, the distance (*dist*) between the centre point of each sphere (representing an individual CNT) and all the centre point of the remaining spheres will be calculated through Equation 3.34. When the distance between two spheres is equal or less than the diameter of the CNT, one collision is counted. Moreover, the collisions' count model rejects more than one contact for the same particle (usually defined as a short circuit). For instance, two contacts may be representative of only one interparticle collision/bond, as shown in the Figure 3.18.

$$dist=\sqrt{\left(x_{i,j}-x_{i,j+n}\right)^2+\left(y_{i,j}-y_{i,j+n}\right)^2+\left(z_{i,j}-z_{i,j+n}\right)^2} \qquad 3.34$$

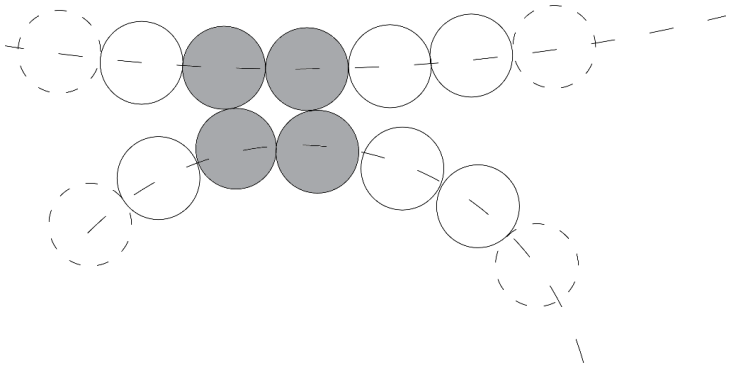

Figure 3.18: Schematic representation of a bond created by two spherical contacts.

### 3.6.1.6 *NUMERICAL MODEL CALIBRATION*

Due to the small dimensions of the CNTs, it is expected that they are strongly affected by the Brownian force field. In addition, these particles are structurally flexible, yielding a dispersion of particles with variable shape. It is expected that both factors may contribute to their interparticle

interaction. Currently, the interparticle interaction is usually predicted through the *excluded volume theory* (EVT). As mentioned, the excluded volume of a particle is defined as the volume around an object which the centre of another similar particle is not allowed to enter if overlapping of the two objects is to be avoided. A detailed description of this theory can be found in Appendix A.

The EVT enables to predict the number of interparticle contacts, or bonds $B$, of a motionless and homogenous dispersion of rigid particles. Moreover, the EVT states that in the percolation threshold of very long rigid cylinders, the particles present nearly 1.4 particles bonded per particle $B_c$. In order to verify that the numerical models developed comply with the continuum mechanics of the EVT, the *rigid* model was used to verify the number of particles bonded per particle inside the control volume, at the critical volume fraction.

Since in both numerical models it is imposed that the CNTs are generated strictly within the control volume, it is expected that the interparticle interaction become affected for very low characteristic length $l_{cv}$, since the particles can be strangled and placed all at the centre. However, if selected a very higher $l_{cv}$, the required computational resources to solve the model will be also very higher. As such, the optimal $l_{cv}$ was predicted through a convergence of the rigid model with the EVT.

Therefore, it was selected a rigid elongated CNT with an aspect ratio of 100 ($d_p$=100 *nm* and $l_p$=10 *μm*), without Brownian motion, *i.e.* the CNTs are only dispersed randomly for a time step $t$=0. According to the EVT, this CNT geometry present a percolation threshold nearly 0.7% (Equation A.1).

In the Figure 3.19 is represented the average $B_c$ of the rigid model for various $l_{cv}$ to $l_p$ ratios, and its respective convergence with the EVT, $B_c$≈1.4 of the selected CNT geometry. The simulations where repeated 10 times for each of $l_{cv}$ to $l_p$ ratio, enabling to measure the standard deviation that is represent by the error bar. As can be depicted, the convergence of the model happens for at $l_{cv}$=10$l_p$.

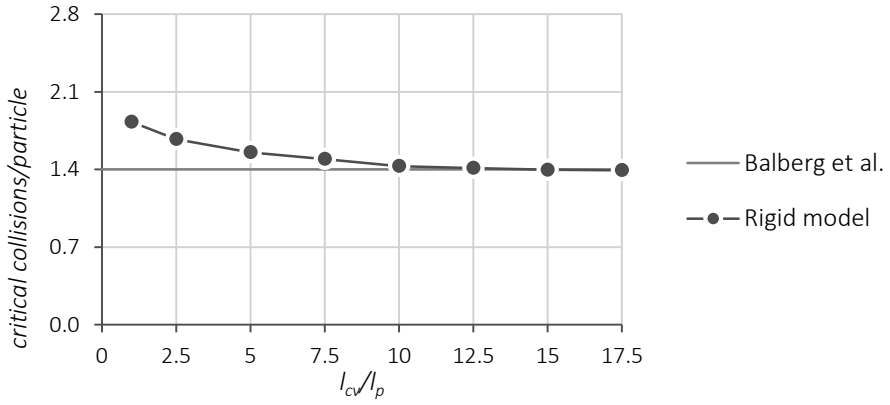


Figure 3.19: Critical collisions per particle inside a control volume with a length $l_{cv}$ dependent on the CNT length $l_p$.

From these results, it is possible to assert that the mathematical model is in agreement with the literature. Moreover, in order to reduce the calculation time, the length of the control volume is defined as 10 times greater than the CNTs length.

### 3.6.2 NUMERICAL STUDY OF THE DYNAMIC BEHAVIOUR OF LONG-TERM NANOFLUIDS

The conducted survey, presented in Chapter 1, suggested that the anomalous enhancement of the effective thermal conductivity of MWCNTs based nanofluids may be explained by the Brownian motion of the nanoparticles. Therefore, correspondent samples to that obtained from the DOE presented in Section 3.2 are numerical studied through the dynamic numerical model proposed.

In this numerical study, it is used the obtained particles mean size from the SEM analysis (Section 3.5.1), ensuring closely boundary conditions to that of the experimental. The influence of the Brownian motion intensity in the results was also evaluated. For that purpose, the nanoparticles were assumed to be suspended on their correspondent base fluid at two different temperatures, namely 283.15 and 323.15 K. The proposed numerical model shows that the variation of the base fluid temperature and dynamical viscosity induces a variation in the intensity of the Brownian motion.

In all numerical simulations, it was considered a total of 100 time steps of 1 second each. The number of interparticle interaction, *i.e.* collisions without permanent contact, was counted in each time step. The standard deviation of the number of interactions for each sample is used to verify the influence of the Brownian motion of the spatial distribution of the nanoparticles.

Moreover, the Brownian mean displacement of each nanoparticle inside the control volume is registered at each time step, and the overall mean Brownian velocity of the sample is calculated.

These enable to compare with the phase separation rate experimental achieved, and described in detail in the next Sections. This overall mean Brownian rate also enables to compare the Brownian diffusion with the thermal diffusion of the base fluid and, therefore, verify the significance of the nanoscale convection induced by the Brownian motion.

The proposed predictive model for the effective thermal conductivity of MWCNTs based nanofluids assumes that the nanoparticles can be treated as rigid cylinders, *i.e.* rod-like particles. Nevertheless, as verified in the Section 3.6.1.1, the MWCNTs have a structural flexibility that may influence the average spatial distribution of the particles in the medium. Indeed, the only predictive model for such nanofluids that accounts for the structural flexibility of the MWCNTs was proposed by Deng *et al.* (DENG et al., 2007, DENG et al., 2009).

In Figure 3.20, is represented the average interparticle collisions per MWCNT, of the studied nanoparticles dispersed in DW+30%EG at 283.15 K. In this, it can be seen that the average interparticle collisions are equal for the *flexible* and *rigid* numerical models, suggesting a negligible influence of the nanoparticle structural flexibility on the interparticle interaction and spatial distribution in the medium. The error bar in the Figure is the standard deviation of the 100 time steps numerically achieved. As can be seen, the standard deviation is rather low, suggesting an almost constant interparticle interaction in time.

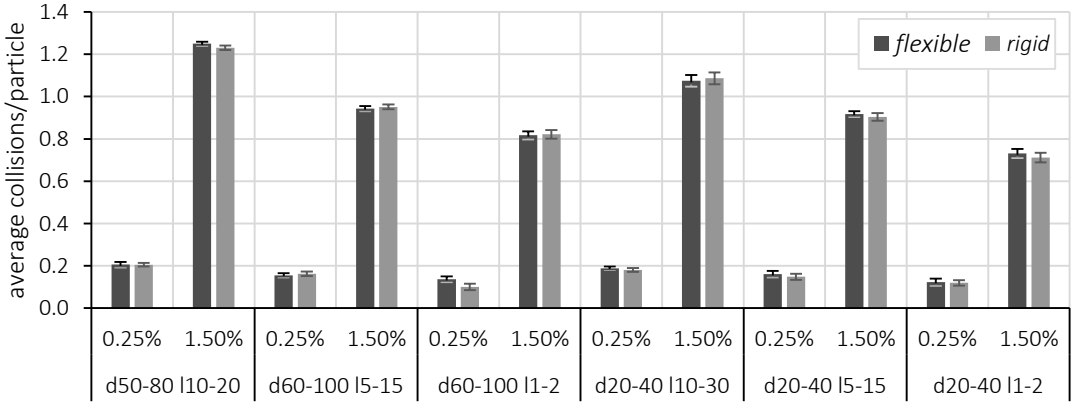


Figure 3.20: Influence of the structural flexibility of the MWCNTs on the spatial distribution in the medium.

These results enable to corroborate the assumed rod-like geometry of the nanoparticles, by the majority of the predictive model available in the open literature, and by proposed model in Section 2.5.2, since the spatial distribution of flexible and rigid MWCNTs is slightly equivalent. The influence of the Brownian motion intensity in the spatial distribution and interparticle interaction was also evaluated, and the results are plotted in the Figure 3.21.

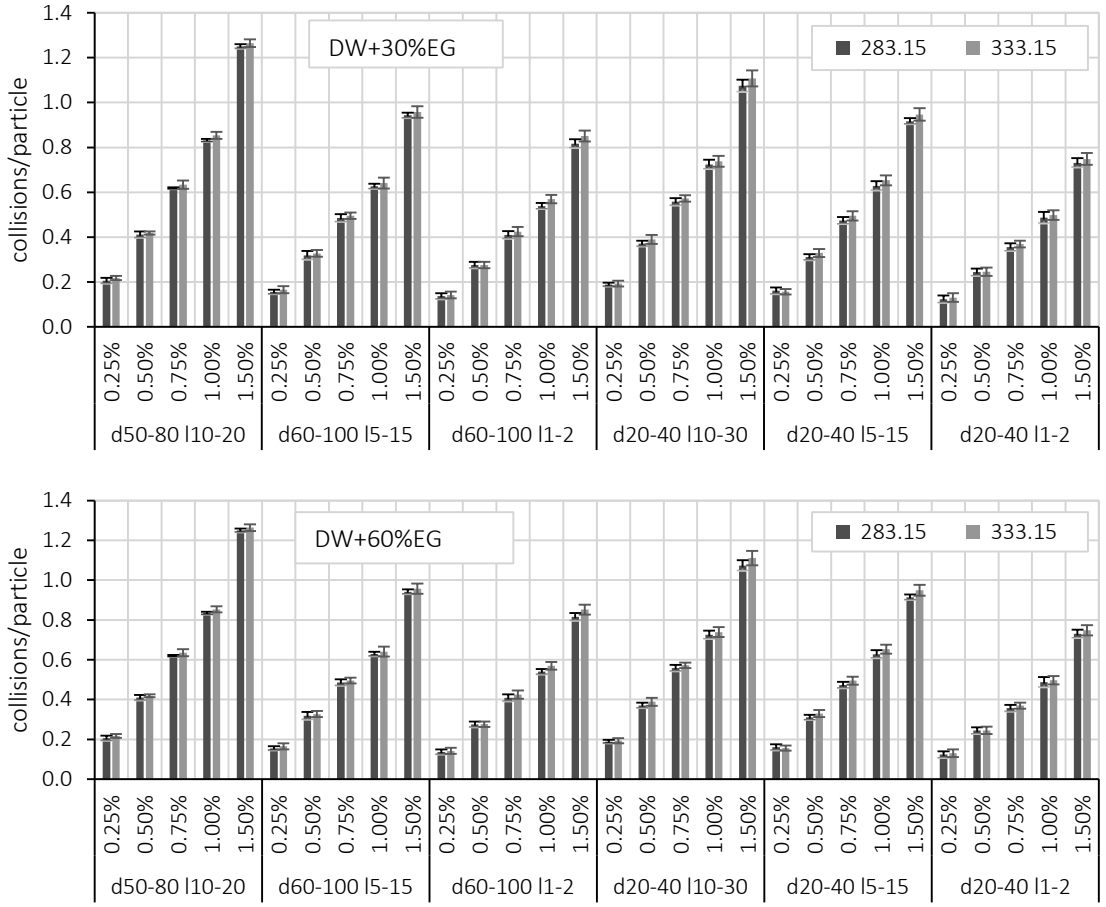


Figure 3.21: Influence of the Brownian motion intensity on the average collision per particle.

As it can be seen, the numerical results suggest that the Brownian motion intensity has a probably negligible impact on the interparticle collisions, since the average collisions and standard deviation seems to be independent of the base fluid viscosity and temperature. In addition, the results suggest that the interparticle interaction and spatial distribution depend on the aspect ratio and volume fraction of the nanoparticles. This behaviour was previously verified by the *excluded volume theory* (EVT), discussed in the Appendix A. The EVT states that the number of interparticle collisions per particle, inside a control volume, is given by:

$$B \approx 2\phi \cdot \left(\frac{l_p}{d_p}\right) \qquad 3.35$$

In Figure 3.22, is the scatter chart of the results obtained and shown in the Figure 3.21. As it can be seen, the results lies within the previously equation of the EVT.

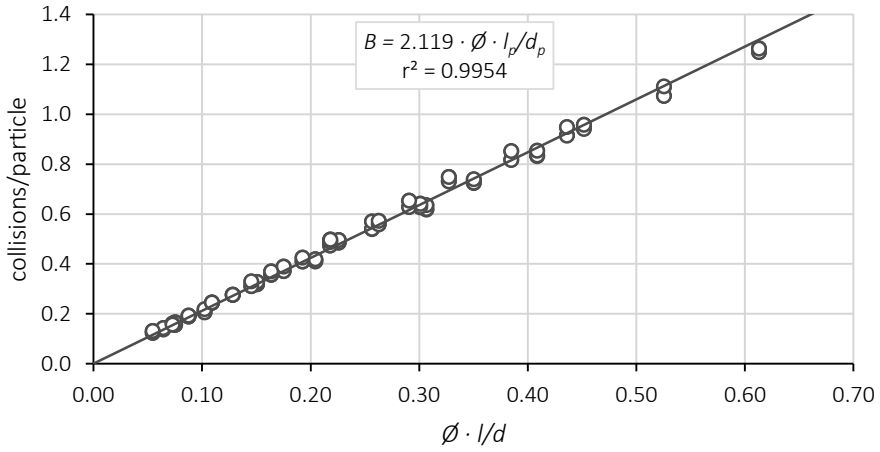


Figure 3.22: Average collisions per MWCNTs obtained from Figure 3.21.

According to this theory (EVT), the *percolation-like structure threshold* is observed for nearly ($B\approx$) 1.4 collisions per particle. Due to the high reduction on the length distribution of the nanoparticles, caused by the dispersion approach, it seems that this morphological microstructure has very low probability to be achieved in any of the prepared nanofluids. Even so, it is known that thermal interparticle interaction occurs far below percolation threshold, and it was verified the high degree of interparticle interaction induced by the elongated aspect ratio of the MWCNTs.

Some authors suggested that due to the nanoscale size of the dispersed nanoparticles, the temperature dependence may be explained by the higher Brownian diffusion of the nanoparticles $D_{BM}$ than that of the thermal diffusion of the base fluid $D_T$. Considering the equivalent diameter of Equation 3.14, and introducing these into Equation 3.9, it can be estimated the average $D_{BM}$ of the studied samples. In contrast, the $D_T$ can be estimated through the following expression:

$$D_T = \frac{k_{bf}}{c_{p_{bf}} \cdot \rho_{bf}} \qquad 3.36$$

In Figure 3.23, it can be depicted the average thermal diffusion to Brownian diffusion ratio estimated through the numerical model. The results reveal that the $D_T$ is always higher than $D_{BM}$, in order of $10^4$, suggesting that the thermal diffusion is much faster that Brownian diffusion for heat transport mechanisms. That is, the heat is diffused through the base fluid at a higher rate than the Brownian diffusion of the nanoparticles and, therefore, the probability of heat transfer through interparticle collisions and micro-convection is very low. Similar conclusions for spherical nanoparticles suspensions where analytically proposed by Keblinski *et al.* (KEBLINSKI et al., 2002).

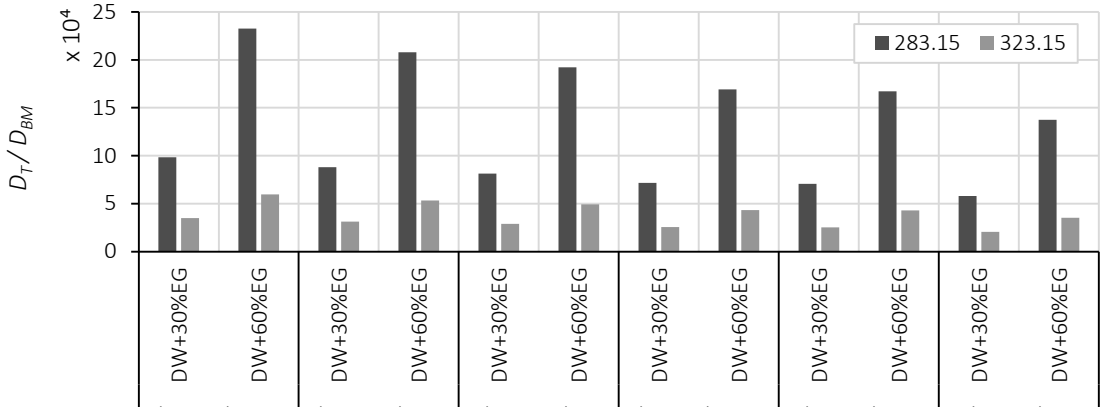


Figure 3.23: Estimation of the average thermal diffusion to Brownian diffusion ratio of the samples studied.

In conclusion, the results achieved through this numerical analysis highlight that the structural flexibility of the nanotubes has a negligible impact on the spatial distribution and interparticle interaction of the studied nanofluids, as it can also be depicted from Figure 3.24. It was also verified that the two forms of Brownian mechanisms, that may contribute to the effective thermal conductivity enhancement, suggested by some authors, may also present negligible impact in the studied samples. It should be noted that these results comply within the proposed EDEMT model for the effective thermal conductivity of nanofluids based on elongated particles.

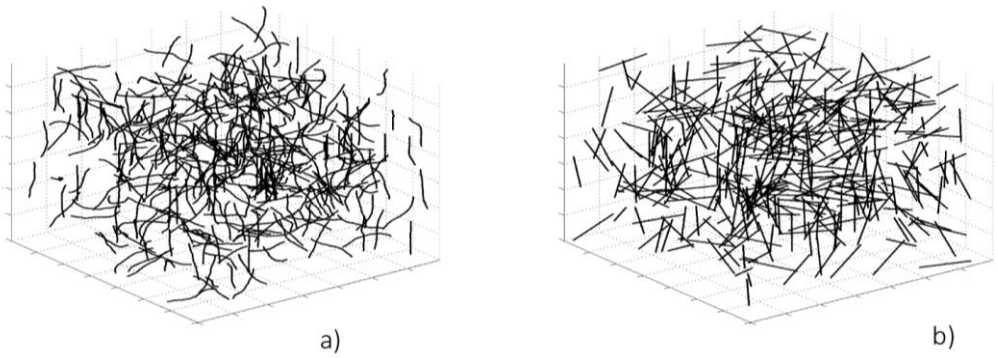


Figure 3.24: Illustration of the spatial distribution for the a) *flexible* and b) *rigid* MWCNTs (0.15% *d*50-80 /10-20). Note: for higher volume fractions, the Figure becomes very dense due to 3D effect.

The results obtained by the numerical models enable to understand the effect of the MWCNTs geometry and structural flexibility in the spatial distribution and morphology, such degree of interparticle interactions. Nevertheless, these results require an experimental validation. This may be possible through proper imaging on these systems through epi-fluorescence microscopy. The latter, enable to visualize nanoscale wetted systems, like nanofluids. However, there have prohibitive costs associated with the process.

## 3.7 NANOFLUIDS DISPERSION METHODOLOGY

In this Section, it is provided the methodology for the dispersion of the functionalized MWCNTs in the base fluids, to form the so-called nanofluid. In Table 3.4 it was provided the materials quantities for the preparation of each of the 60 nanofluids that will be tested. The following steps describe the final process for the production of the long-term MWCNTs based nanofluids:

1. With a high-precision balance ($\Delta m$=0.001 g), it was measured the total amount of nanoparticles dispersed (Table 3.4);
2. With a graduated cylinder ($\Delta V$=0.5 ml), it was measured each base fluid (Table 3.4);
3. The solution was homogenised at naked eye with a magnetic stirrer for a short period;
4. In a magnetic stirrer, it was applied ultrasonication energy of 60 kJ in the Bioblock Scientific Vibra-Cell 75043 sonicator with 20kHz±50Hz at 21% amplitude and with a low intensity of cavitation probe (630-0210) enabling the release of energy over a greater area (SONICS & MATERIALS, 2013). In contrast, probes with high intensity of cavitation release the energy in a narrower area, increasing the probability of the MWCNTs suffering higher degradation;
5. The dispersion was cooled naturally during 10 minutes;
6. The steps 4 and 5 where repeated more three times, until the ultrasonication energy performs 240 kJ, *i.e.* 4.8 kJ/ml. These energy is equivalent to the reported by previous researchers (KANAGARAJ et al., 2008, PONMOZHI et al., 2009).

The above steps were carefully repeated for all the 60 nanofluids produced. Furthermore, it should be noted that it was always attempted the reduction of noise factors. As noticeable, the ultrasonication contribute to the electrostatic stabilization of the nanoparticles.

## 3.8 ASSESSMENT TO THE LONG-TERM COLLOIDAL STABILITY

As stated in the Section 3.2.2, the term *stability* must imply the ability to preserve the projected thermo-physical properties with negligible variation. Therefore, it is intended that the long-term MWCNTs based nanofluids must present stability regarding:

- Structural integrity of the dispersed nanoparticles over the test temperatures conditions;
- Negligible agglomeration of the nanoparticles
- Negligible phase separation of the nanoparticles

It should be reminded that the first condition mentioned was verified and granted in Section 3.5.2.

### 3.8.1 PROBABILITY OF AGGLOMERATION

Despite the presence of functional groups, identified by the FTIR analysis in Section 3.5.1, the probability of agglomeration may not be as negligible, as desired. Therefore, the repulsion forces of the functionalized MWCNTs were assessed through the measurement of their zeta potential.

According to the DVLO theory (Section 3.2.1), if the van der Waals interparticle repulsive forces are higher than the attractive, the probability to occur agglomeration during a Brownian collision is low. The zeta potential of the particles is regarded as an index of the magnitude of the interparticle interaction (DERJAGUIN et al., 1993, VERWEY et al., 1999).

In general, dispersions with an absolute zeta potential less than 25 mV are considered unstable regarding agglomeration. In contrast, an absolute zeta potential higher than 25 mV indicates satisfactory stability. Nevertheless, for zeta potentials above 60 mV it can be considered a negligible agglomeration probability, *i.e.* excellent stability regarding agglomeration Following is a Table summarizing the index of stability according to several authors (DERJAGUIN et al., 1993, GHADIMI et al., 2011b, LI et al., 2007, RUSSEL et al., 1989, VERWEY et al., 1999):

Table 3.12: Zeta potential and associated dispersion stability.

| Absolute zeta potential range [mV] | Stability |
|---|---|
| 0 to 10 | Little or no stability |
| 10 to 25 | Some stability but slight |
| 25 to 40 | Moderate stability |
| 40 to 60 | Good stability |
| >60 | Excellent stability |

The zeta potential is not measureable, but can be estimated through theoretical models, generally provided by the software of the experimental instrument. In this research, the zeta potential measurements were conducted in a *Malvern ZS Nano S* analyser at 293.15 K. In this, it is applied an electric field to the dispersion, allowing to the particles travel, with a given velocity, in the direction of the electrode. This velocity is measured through light scattering, enabling to calculate the electrophoretic mobility and, from this, the zeta potential of the sample is estimated through the equation of Smoluchowski.

Since zeta potential measures the velocity of the particles through light scattering, it is required diluted samples. Therefore, diluted samples of the functionalized MWCNTs at 0.02% volume fraction, dispersed in the two studied base fluids were prepared. This diluted nanofluids are

prepared with the same base fluid of the original nanofluids that will be studied, ensuring similar interfacial equilibrium of the nanoparticles with the medium, i.e. the dilution is not performed with a different solvent. Furthermore, the nanofluids have low nanoparticles loadings (maximum of 1.5% volume fraction). Therefore, the zeta potential may be similar and extrapolated for the studied volume fractions (DERJAGUIN et al., 1993, VERWEY et al., 1999). This similarity is verified by the reduced phase separation (or sedimentation) for the higher volume fractions, indicating that these are hindered and, therefore, present low probability of agglomeration. This behaviour is verified in the following Section.

It should be noted that it was performed 5 runs for each sample, enabling to verify the repeatability of the measurements and estimate the mean value and respective experimental uncertainty, as described in Appendix D.

The dielectric constant of the DW+30%EG and DW+60%EG, considered in the experiments, are 69.73 and 59.00, respectively, and the refractive index is 1.36 and 1.39, respectively, as provided in the Table 3.13 (KUMBHARKHANE et al., 1992, REFRACTOMETER, 2011). Furthermore, the viscosity was the provided in Table B.1 and B.2.

Table 3.13: Dielectric constant of aqueous solutions of ethylene glycol, for room temperature.

| $\phi$ DW | $\phi$ EG | Dielectric constant | Refractive index |
|---|---|---|---|
| 0% | 100% | 40.89 | 1.44 |
| 10% | 90% | 46.43 | - |
| 20% | 80% | 52.06 | - |
| 30% | 70% | 56.00 | - |
| *40%* | *60%* | *59.00* | *1.39* |
| 50% | 50% | 64.36 | 1.39 |
| 60% | 40% | 64.65 | 1.37 |
| *70%* | *30%* | *69.73* | *1.36* |
| 80% | 20% | 73.00 | 1.35 |
| 90% | 10% | 75.60 | 1.34 |
| 100% | 0% | 80.1 | 1.33 |

As it can be observed in Figure 3.25, the measured samples presented an absolute zeta potential ranging from 40 to 60mV, suggesting a good to excellent stability regarding agglomeration, *i.e.* low probability of agglomeration (Table 3.12). Furthermore, since the interface nanoparticle-base fluid is constant, for a given base fluid, it can be considered that the samples with higher volume fraction present equal absolute zeta potential (DERJAGUIN et al., 1993, LI et al., 2007, RUSSEL et

al., 1989, VERWEY et al., 1999). The uncertainties provided in the Figure 3.25 where calculated through the methodology suggested in Appendix D.

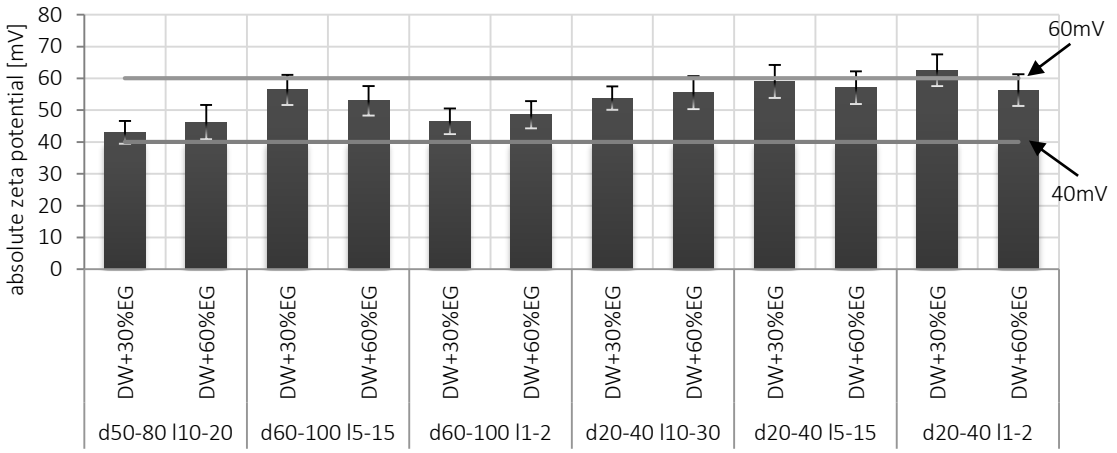


Figure 3.25: Zeta potential of the studied samples, estimated through the model of Smoluchowski.

In addition, the previous Figure suggests no relation between the absolute zeta potential and the base fluid type. Far more important, regarding agglomeration, it can be considered that all the tested nanofluids meet the statistical agglomeration conditions idealized in the Section 3.2.

### 3.8.2 PHASE SEPARATION RATE

As seen in Section 1.5.2.2, UV-visible spectrophotometry and sedimentation photograph are commonly used for evaluate the phase separation in nanofluids. These methods identify the concentration of the nanoparticle dispersed, at each time step. It is recognized the technical impossibility to determine the sedimentation or flotation velocity of nanofluids using these approaches, since it will take a large amount of time for a full sedimentation or flotation to occur.

In contrast, analytical centrifuge is an effortless and undemanding method that allows for estimating the phase separation of the suspensions (LERCHE, 2002). In this, a centrifuge field accelerates the phase separation phenomenon, evaluating the change in concentration by detecting the transmission profiles along the entire height of the sample. Through the measurement of the separation rate for high centrifugal force fields, it is possible to extrapolate this to the gravitational field.

The phase separation rate of the engineered MWCNTs based nanofluids were achieved through the *Stability Analyser LUMiSizer 6120* kindly provided by Dias de Sousa SA (LERCHE, 2002). Accordingly to this methodology, fluid samples are subjected to different centrifugal fields

(RCF=centrifugal acceleration/earth acceleration) that accelerate the particle settling process, and a calibrated NIR light beam intensity is continuously measured by a CCD sensor after intersecting the fluid sample. In each time step, a light transmission profile through the sample is registered in a gradient colour picture. The phase separation behaviour along with the entire height of the samples is registered, and it can be easily observed from Figure 3.26. Furthermore, the light transmission profiles change with time, enable the calculation of the phase separation velocity for each RCF. If the deposition/particle decay velocity is proportional to the RCF, the phase separation for gravity conditions (RCF=1) could be extrapolated, and the shelf life regarding sedimentation of each sample predicted. This analytical centrifuge allows the measurement of samples without the need for dilution. It is a great advantage compared to conventional methods, since the distance between nanoparticles is unchanged, ensuring all original interparticle interactions that hinder the phase separation.

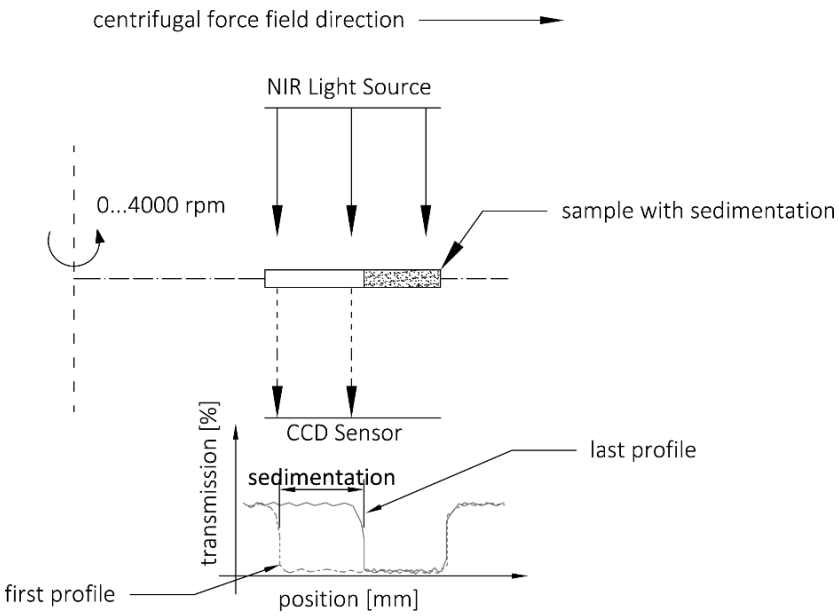


Figure 3.26: Schematic illustration of the measuring principle of the Stability Analyser.

For cost reduction and problem simplification, the DOE developed for the effective thermal conductivity assessment, and presented in the Section 3.3, is reduced for the volume fractions of 0.25%, 0.50%, and 1.50%. It is, therefore, considered that the remaining samples are within the range of the observed values.

The samples are tested at a controlled temperature of 298±1 K, at 3 proportional centrifugal force fields, described in detail in Table 3.14. The particle decay/deposition phenomenon is measured by a near infrared (NIR) light (865 nm wavelengths). As it will be seen, the particle decay/deposition

rate is proportional to the RCF, proving that the selection of these does not affect the final results. The mean experimental uncertainty of the phase separation is described in Appendix D.

Table 3.14: Stability Analyser measuring conditions for each sample.

| Test Nr. | rpm | RCF [G] | Time step [s] | Total time [h] | Nr. profiles |
|---|---|---|---|---|---|
| 1 | 1990 | 500 | 200 | 14 | 255 |
| 2 | 2800 | 1000 | 100 | 7 | 255 |
| 3 | 4000 | 2000 | 50 | 3.5 | 255 |

In Figure 3.27, it is shown the a transmission profile portion, to improve the readability, of the sample 0.25%vol. *d*50-80 /10-20 in DW+30%EG, when subjected to an RCF of 2000 G. The complete transmission profiles, as well for the remaining RCF are proportional to the presented and are reported in Appendix G, Figure G.1.

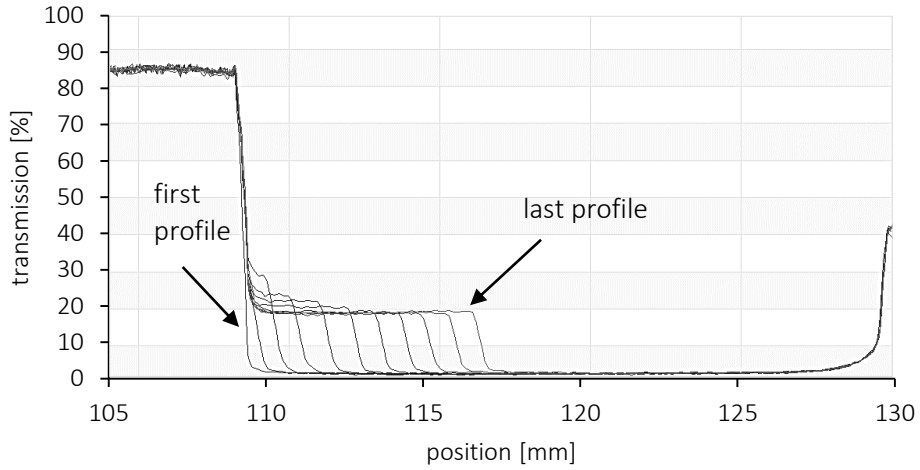


Figure 3.27: Evolution of transmission profiles of sample 0.25%vol. *d*50-80 /10-20 in DW+30%EG at 2000 G.

In Figure 3.27, the profiles are spaced at about 20 min, revealing a phase separation rate constant over time. In addition, as the shape of the transmission profiles is constant, equally spaced and quasi-vertical, it indicates that the suspension is composed by monodispersed particles that moves at the same velocity (LERCHE, 2002). This an important requirement to ensure thermal conductivity homogeneity (LEE et al., 2010). This behaviour may indicate that the functionalization process and the application of the ultrasonication for the MWCNTs dispersion in the base fluid broke the MWCNTs aggregates, as previously stated from Figure 3.6. Nevertheless, it should be noted that this does not indicate that the size distribution of the final MWCNTs dispersed in the base fluids is equal to that of the pristine MWCNTs, and as previously verified in Section 3.5.3. The behaviour

described here for the sample 0.25%vol. *d*50-80 *l*10-20 in DW+30%EG was observed for all the remaining tested samples.

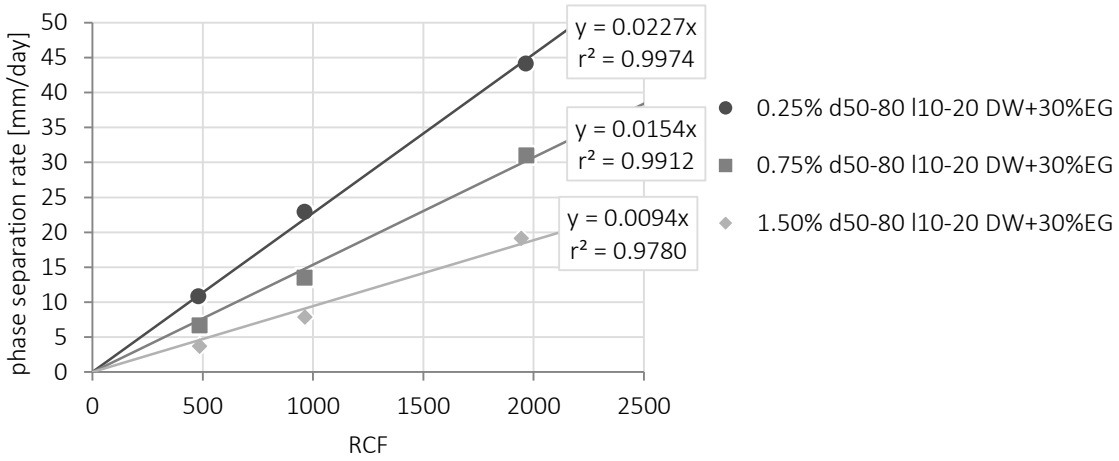


Figure 3.28: Representation of the linear regression of the phase separation rate obtained for some of the samples.

Through linear regressions, as represented in Figure 3.28, it was found the constant of proportionality between the RCF and phase separation rate for each sample. In these regressions, it was considered a null ordinate at the origin ($y=m_c \cdot x$), since it is assumed that no sedimentation occurs if the force field is null. In Appendix G, Table G.1 and Table G.2 summarizes the result of the previous linear regression, and the extrapolation of settling velocity subjected to the gravitational field (RCF=1) of all the samples. The constant of proportionality of each sample enables the extrapolation of the results to the rest conditions, *i.e.* to the gravitational force field (RCF=1). The results are shown in Figure 3.29. The mean experimental uncertainty of the phase separation is described in Appendix D.

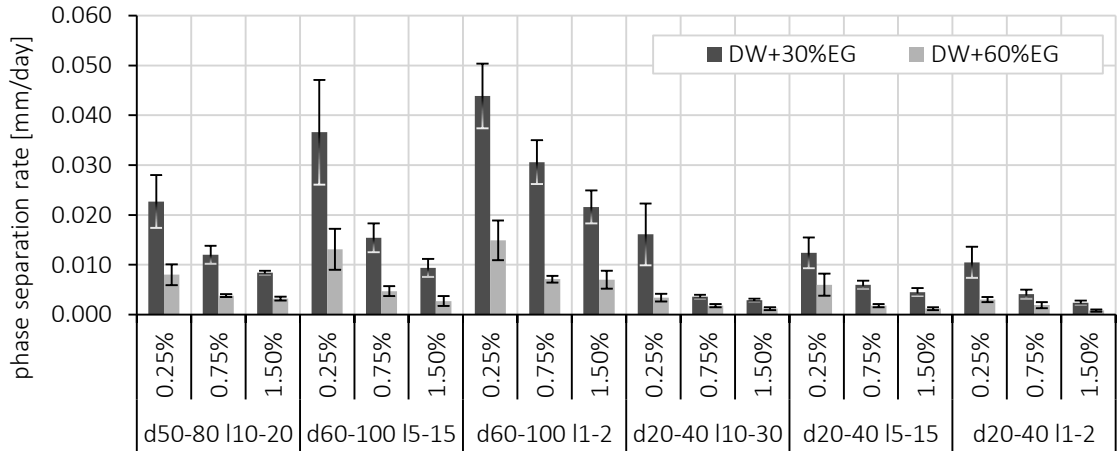


Figure 3.29: Phase separation rate at gravity field (RCF = 1) for the studied samples.

The results obtained suggest that it is possible to produce nanofluids with long shelf life. Moreover, for the analysed concentration, MWCNTs based nanofluids are characterized by hindered settling. The latter corresponds to a significant decrease in the phase separation rate of the immersed particles, with increasing hydrodynamic interparticle interactions.

From Figure 2.12 it was possible to visualize the transition of the microstructure on these nanofluids through the increase of the nanoparticles volume fraction. The transition through the various stages of microstructure enhances the number of interparticle collision and electrostatic repulsions, reducing significantly the settling velocity and phase separation. Furthermore, during phase separation, the particles displace liquid in the opposite direction to their movement, which affects the motion of the surrounding ones.

In addition, according to the *excluded volume theory*, and by the results achieved by the numerical model in Section 3.6.2, the interparticle interactions increase with increasing nanoparticles aspect ratios (BALBERG et al., 1984a). In general, this behaviour is also observed in the present results, where the nanoparticles with greater lengths show a lower average phase separation rate. This hindered behaviour was anticipated in Section 3.2.1.2.

However, the MWCNTs that show lower phase separation (*d*20-40 *l*1-2) are the shortest, suggesting that other mechanisms may also play an important role. Perhaps, due to their small size, these nanoparticles begin to behave as molecules of the fluid itself. Furthermore, it appears that the phase separation rate decreases with increasing base fluid viscosity, as expected.

Nevertheless, during these centrifugal accelerations, the Brownian rate of the MWCNTs becomes negligible due to the imposed centrifugal force field. Therefore, it is assumed that the extrapolated phase separation rate for rest of the conditions does not account for the Brownian effect. As previously noted, if this random motion is more intense than the sedimentation rate, the sample can be considered free of phase separation. As such, the phase separation rate measured is compared with the Brownian rate achieved through the numerical model and reported in Section 3.6.2.

However, the numerical Brownian model does not account for the hindered effect caused by the MWCNTs physical and hydrodynamic interactions. Therefore, the sedimentation rate, $v_s$, of a MWCNT is calculated using an equivalent formulation of Stokes (STOKES, 1850) (Equation 3.37), and the hindered rate  is therefore estimated and applied to the Brownian rate.

$$v_{s_{eq}} = \frac{g \cdot \Delta\rho \cdot d_{eq}^{\,2}}{18 \cdot \mu_{bf}} \tag{3.37}$$

where $d_{eq}$ is the equivalent diameter of a sphere that equals the drag coefficient of the MWCNTs, based on its cross-sectional area, expressed in Equation 3.15.

Considering that the hydrodynamics and physical interactions of the MWCNTs are independent from the movement direction, it can be stated that the Brownian motion is reduced through an equal factor. It is known that this is not entirely true, since in an accelerated phase separation, all the particles move in the same direction. Even so, applying the same hindered rate to the Brownian movement of the particles, the hindered Brownian rate ($H_{BM}$) is underestimated. Therefore, it is analysed the worst-case scenario. The hindered rate $H_{ratio}$ can be defined as:

$$H_{ratio} = \frac{phase\ separation\ rate}{v_{s_{eq}}} \tag{3.38}$$

From this, hindered Brownian motion ($H_{BM}$) of the MWCNTs is a reduction of the Brownian rate, or Brownian diffusion ($D_{BM}$), achieved in the numerical study presented in Section 3.6.2, such as:

$$H_{BM} = H_{ratio} \cdot D_{BM} \tag{3.39}$$

For a given RCF threshold ($RCF_{threshold}$), the phase separation rate equals the ratio of the hindered Brownian rate ($H_{BM}$). These thresholds delimitates the transition to the stability of the nanofluids regarding phase separation, *i.e.* when the phase separation for given centrifugal force field become less intense than the constantly diffusion homogeneity induced by the Brownian motion. This formulation is evidenced in the following expression:

$$H_{BM} = phase\ separation = m_c \cdot RCF_{threshod} \tag{3.40}$$

where $m_c$ is the constant of proportionality between RCF and the phase separation rate (Figure 3.28 and Table G.2).

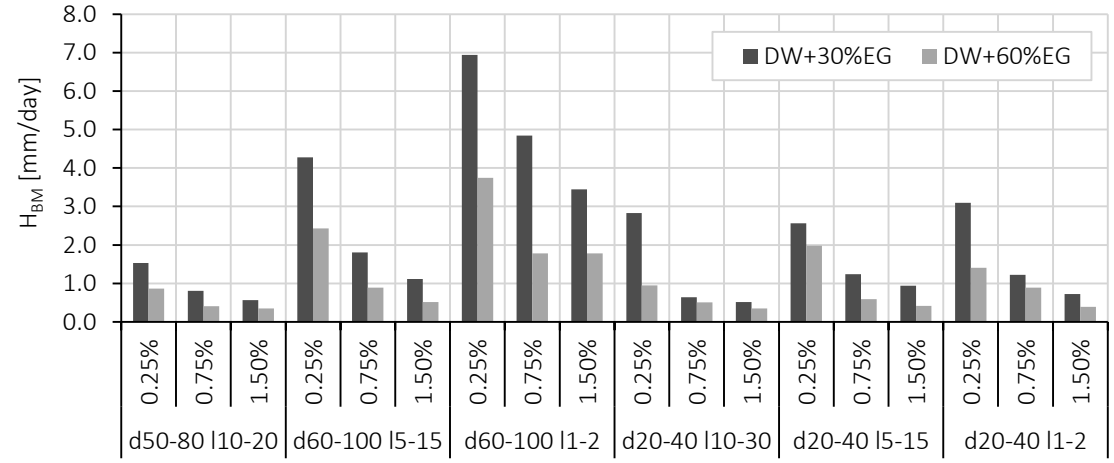


Figure 3.30: Estimated Brownian rate reduced through the application of the estimated hindered rate.

The hindered Brownian rates are shown in Figure 3.30. As it can be verified, the estimated Brownian rates are much higher than the experimental phase separation rate shown in Figure 3.29. Furthermore, the results suggest that the Brownian motion is, in average, 244 times higher than these phase separation rate. The ratio of Brownian motion and phase separation rate ($RCF_{threshold}$) range from 70 to 550 (expressed in the Figure 3.31), *i.e.* the Brownian rate is always higher than the phase separation rate. These were expected results, since they are below the RCF selected for the phase separation rate assessment. It should be noted that during this, it was observed sedimentation, as revealed by the transmission profile represent in Figure 3.27.

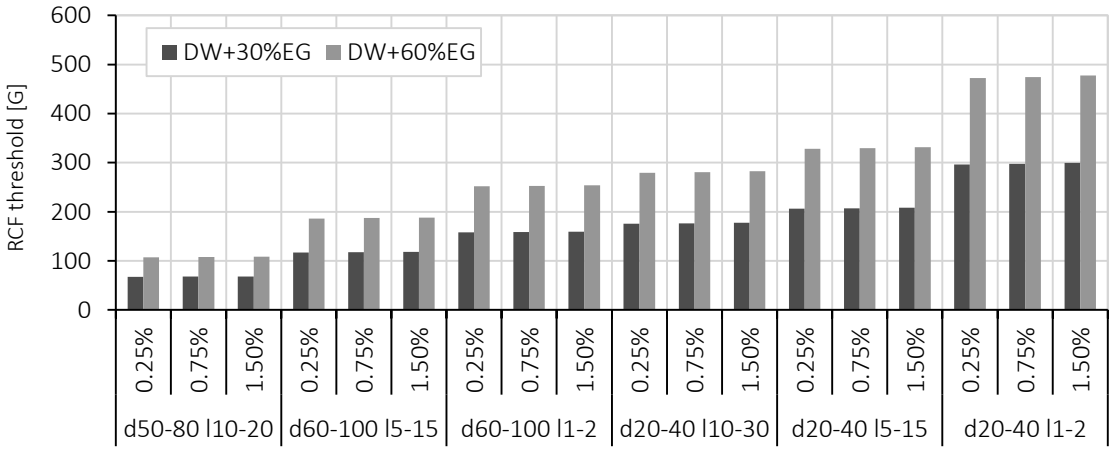


Figure 3.31: RCF thresholds of the studied samples.

Therefore, since the Brownian motion is considerably more intense than the phase separation rate, it can be stated that all the nanofluids tested are stable regarding phase separation at the rest condition. Nevertheless, during the application of the nanofluids, these are constantly subjected to

centrifugal forces in the heat exchange/transfer circuit of the energy system. In the Figure 3.31, it is provided the ratio of the centrifugal and earth accelerations' threshold of the studied samples, which reveals the maximum centrifugal force fields that each sample could suffer until become instable regarding phase separation.

When tailoring a nanofluid for a specific sustainable energy system, it should be predicted the centrifugal acceleration at which the nanoparticles will be subjected in the heat transfer circuit, in order to select the appropriate nanofluid that meet the stability requirements and thermo-physical properties to ensure a long-term applicability of these.

### 3.8.3 BRIEF DISCUSSION

So far, it was verified that the nanofluids produced present negligible probability of agglomeration and phase separation. In addition, despite the high reduction in the length distribution of the MWCNTs due to the dispersion methodology used, the nanoparticle seems to present low damaged structure and acceptable thermal stability. Therefore, combining all these stability conditions, it can be stated that these nanofluids accomplish the conditions for the measurement of their thermal conductivity, and for their industrial application. This feature is of utmost importance, since the measurement of the thermal conductivity, for the various temperatures, takes several hours per nanofluid. Thus, it is ensured that the samples are homogeneous during the measurement periods, reducing, therefore, noise factors.

## 3.9 CHAPTER CONCLUSIONS

Through the overview of the instability mechanisms that dispersions may suffer, it is proposed, in detail, the minimum stability requirements for nanofluids, namely long-term agglomeration-free, phase separation free, and constant structural integrity of the nanoparticles. Only respecting these stability conditions it is ensured the correct measurement of their thermo-physical properties (similar morphological structures in all the samples) and, as well, its implementation at the industrial scale. Knowing the desired morphological conditions for the nanofluids, it is developed a *design of experiments* that estimated the production of 60 nanofluids that will be tested at 6 distinct temperatures, resulting in 360 experimental observations. To achieve the desired long-term stability projected, the MWCNTs are covalently functionalized through acid chemical treatment and dispersed in the base fluids with ultrasonication. Since it is expected the degradation of the geometry of the MWCNTs, the size distribution of these was achieved through SEM image analysis. It was verified that the dispersion methodology caused a high degree of aspect

ratio destruction, in an average of -56% in relation to the provided by the manufacturer. The stability is assessed through zeta potential, to verify the probability of agglomeration, phase separation rate, and thermo-gravimetric analysis, to verify the structural integrity at all the measuring temperatures. It should be noted that these assessments also enable to predict the morphological distribution of the nanoparticles within the medium, reducing noise factors during the experimental data analysis. The spatial distribution of the nanoparticles was verified through a numerical model, which suggested that the functionalized MWCNTs easily interact, being expected thermal interaction as a mechanism for thermal conductivity enhancement.

# 4 EXPERIMENTAL ASSESSMENT OF NANOFLUIDS THERMAL CONDUCTIVITY PROPERTIES

## 4.1 CHAPTER SYNTHESIS

An experimental assessment to the effective thermal conductivity of the MWCNTs based nanofluids is performed. To this end, it is shown the experimental apparatus for assertively measure the effective thermal conductivity of the developed long-term nanofluids. The latter presents experimental repeatability for the base fluids measurements, with a maximum 1.8% deviation from the theoretical values. The experimental thermal conductivity assessment reveal an enhancement up to 18.5%, for the test conditions. Given the high number of experimental observations, a statistical analysis is delineated in an attempt to easily verify the existence of some of the recent theories suggested to explain the observed anomalous behaviour. The statistical analysis implemented to the experimental thermal conductivity revealed non-anomalous behaviour, predictable by the EDEMT model with a maximum fraction error of 4.5%.

## 4.2 NANOFLUIDS THERMAL CONDUCTIVITY MEASUREMENT

As seen through the conducted survey, presented in the Section 1.5.3.1, the one of the most used technique to assess the thermal conductivity of liquid samples is the transient hot-wire, given their inexpensive and accuracy. Therefore, the effective thermal conductivity of the produced samples was measured through coated transient hot-wire technique, namely through *Decagon KD2 Pro (DECAGONDEVICES, 2013)*. Since the measuring probe of the *Decagon KD2 Pro* is coated, it is ensured that the influence of the eventual electrical conductivity of the nanoparticles do not influence the readings (Section 1.5.3.1). The different temperatures referred to in the DOE (Section 3.2) were guaranteed through a thermal bath (*Polyscience Model 1187P*). The overall experimental setup is schematically represented in Figure 4.1. It should be noted that this technique assumes that the measured properties are isotropic.

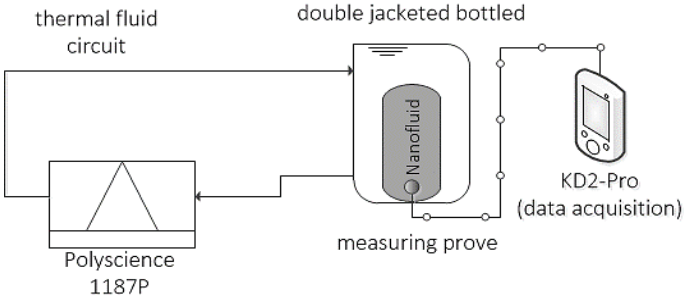


Figure 4.1: Schematic representation of the experimental apparatus for measurement of thermal conductivity.

As it can be seen, the temperature of the sample was ensured by circulating thermal bath in the double jacketed bottled (schematically illustrated in Figure H.1, Appendix H), fitted in a block cavity of a rigid polyurethane foam, to decrease the vibrations provided by the laboratory environment. Furthermore, the flow rate of the thermal bath was set to the minimum flow so that it does not produce any significant results, also due to vibrations. The double jacketed bottled requires nearly 10 ml of nanofluid to ensure the full fill of the container and the respective full immersion of the sensing probe. The coated sensing probe, KS-1, has 1.3 mm diameter and 60 mm long, with an accuracy of 5% from 0.2 to 2 W/mK and less than ±0.001 W/mK. Nevertheless, in order to avoid free convection near the sensing probe, the manufacturer suggests 323.15 K as the maximum temperature for measurements of aqueous solutions.

As the *KD2 Pro* enables data acquisition, each nanofluid was measured in ascending temperature order, remaining in each temperature set-point for 5 h, where the measurements are taken at each 15 min (performing 20 readings per temperature). It should be noted that the data acquisition registers the accuracy of each reading, and values with error higher than 0.01 should be rejected, as suggested by *Decagon* (DECAGONDEVICES, 2013). Therefore, if at least 10 readings do not present satisfactory accuracy, the measurement of the sample is repeated for that specific condition/temperature.

One of the recommendations for the use of this device is performing the readings with the probe needle in the vertical, fully immersed into the base fluid (to reduce free convection and other phenomena) (DECAGONDEVICES, 2013). Thus, the readings were performed with the probe needle vertically inserted from the bottom of the sample, ensuring a more efficiently immersion. Given the high measuring time required for each sample (at least 40 h), it is imperative to consider that the agglomeration and sedimentation of nanoparticles are negligible over time. As seen, the agglomerates behave as a single particle of increased size and mass that settles more rapidly. This sedimentation will cause a gradient in the nanoparticles volume fraction, with largest magnitude in the region where the measurement is performed, as represented in Figure 4.2. Nevertheless, as previously verified in Chapter 3, the probability of this issue was reduced through the colloidal stability observed for the prepared nanofluids.

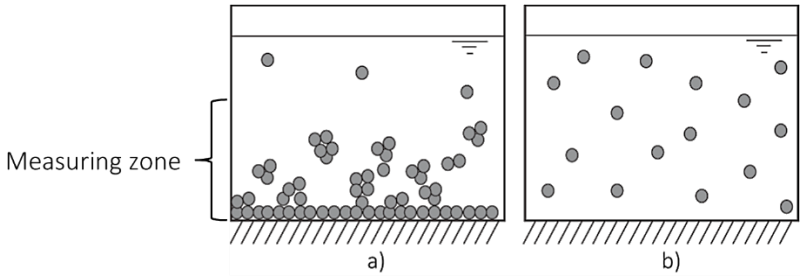


Figure 4.2: Schematic representation of samples with a) inhomogeneous and b) homogeneous effective thermal conductivity.

It is expected that a polydispersion nanofluid present a superior thermal conductivity at the bottom, where the particle concentration is higher. Therefore, if the thermal conductivity measurement is performed vertically, as in the typical steady-state and the transient hot-wire methods (where the needle is placed vertically from the bottom), the readings may be overestimated.

The experimental apparatus was calibrated with both base fluids, with a maximum variation of 1.8% from the theoretical values, despite the declared 5% of accuracy of the *KD2 Pro*. The results are illustrated in Figure 4.3 and summarized in Table 4.1. In Appendix D, Equation D.21 provides the mathematical formulation for the experimental thermal conductivity uncertainty, for a confidence interval of 95%.

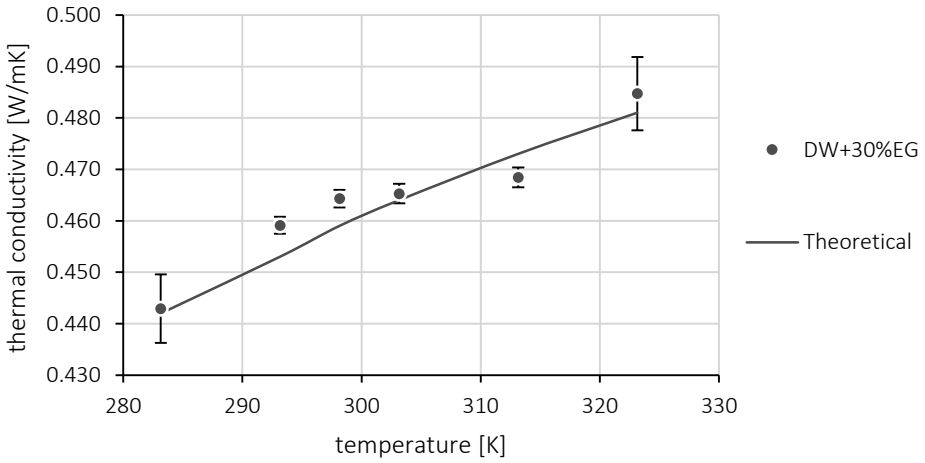

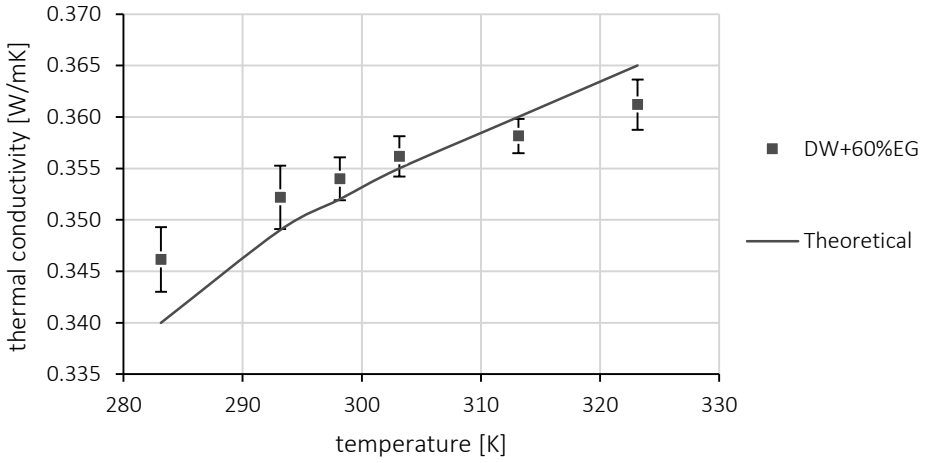


Figure 4.3: Thermal conductivity experimental apparatus calibration curve.

Table 4.1: Theoretical versus experimental thermal conductivity achieved in the experimental apparatus (ASHRAE, 2005).

| Base fluid | DW+30%EG | | | | | |
|---|---|---|---|---|---|---|
| Temperature [K] | 283.15 | 293.15 | 298.15 | 303.15 | 313.15 | 323.15 |
| $k_{theoretical}$[W/mK] | 0.442 | 0.453 | 0.459 | 0.464 | 0.473 | 0.481 |
| $\bar{k}$ [W/mK] | 0.443 | 0.459 | 0.464 | 0.465 | 0.468 | 0.485 |
| $\Delta\bar{k}$ [W/mK] | 0.007 | 0.002 | 0.002 | 0.002 | 0.002 | 0.007 |
| variation [%] | 0.2% | 1.4% | 1.2% | 0.3% | 1.0% | 0.8% |

| Base fluid | DW+60%EG | | | | | |
|---|---|---|---|---|---|---|
| Temperature [K] | 283.15 | 293.15 | 298.15 | 303.15 | 313.15 | 323.15 |
| $k_{theoretical}$[W/mK] | 0.340 | 0.349 | 0.352 | 0.355 | 0.360 | 0.365 |
| $\bar{k}$ [W/mK] | 0.346 | 0.352 | 0.354 | 0.356 | 0.358 | 0.361 |
| $\Delta\bar{k}$ [W/mK] | 0.003 | 0.003 | 0.002 | 0.002 | 0.002 | 0.002 |
| variation [%] | 1.8% | 0.9% | 0.6% | 0.3% | 0.5% | 1.0% |

## 4.3 NANOFLUIDS EFFECTIVE THERMAL CONDUCTIVITY

### 4.3.1 MULTIVARIABLE STATISTICAL ANALYSIS METHODOLOGY

Given the large amount of experimental data (360 experimental observation), in these Section it is provided the statistical analysis used for the analysis of the experimental results that are exposed in detail in the Appendix H, in the form of thermodynamic Tables and Figures. In these, the uncertainties are the confidence interval of 95% of the experimental mean, as provided in detail in the Appendix D.

The statistical analysis is performed to ascertain how and how much the control factors (identified in the DOE, Section 3.3), produces significant impact on the results. Moreover, through the

interaction among control factors assessment, it is possible to find out if the mechanisms proposed to the effective properties are valid.

A control factor interaction occurs if one factor affects the results differently depending on a second, or even a third control factor. In Table 4.2 is summarized the control factor interactions identified that may enable to assess the proposed mechanism that govern the effective thermal conductivity. It should be stated that the main effect of each individual control factors is also assessed.

Table 4.2: Identified possible control factors interactions.

| Id. Control factor (Table 3.3) | Brownian motion | Nano-layer structure | Spatial distribution | Interparticle interaction |
|---|---|---|---|---|
| *AB* | | | X | X |
| *AC* | X | X | | |
| *AD* | X | | | |
| *BD* | X | | | |
| *ABC* | | X | X | X |
| *ABD* | X | | | |

Legend:

- *AB* – MWCNTs geometry x Volume fraction
- *AC* – MWCNTs geometry x Base fluid
- *AD* – MWCNTs geometry x Temperature
- *BD* – Volume fraction x Temperature
- *ABC* – MWCNTs geometry x Volume fraction x Base fluid
- *ABD* – MWCNTs geometry x Volume fraction x Temperature

The statistical contribution of each control factor and control factor interaction is assessed through a *main effect* analysis. The latter, enables a graphical representation to better interpretation. A *main effect* can be described as the difference between the factor level average and the overall mean, representing the effect of an independent variable on the dependent variable, ignoring the effects of all the others independent variables. Then main effect can be expressed as (JACCARD, 1998):

$$main\ effect = \overline{X_{c_n}} - \overline{X} \tag{4.1}$$

where $\bar{X}$ is the overall mean, or grand mean, of the experimental results under analysis, and $\overline{X_{c_n}}$ is the mean of the experimental result under analysis, when the control factor (or control factor interaction) *c* is at the level *n*.

Therefore, a *main effect* occurs when the mean difference between the levels of a control factor is statistically significant to the overall mean. As will be seen, this is a rather quick and efficient way to visualize the effect of each parameter.

An *analysis of variance* (ANOVA) is also performed in order to verify which control factor have the greatest impact on the experimental thermal conductivity. Since it is a factorial design of experiments, it is assumed that the null hypothesis $H_{0,c}$ is that the means between the levels (*n*) of each parameter *c* are equal. That is, the mean of each level of the parameter is constant and does not significantly affect the experimental results. In contrast, the alternative hypothesis $H_{1,c}$ assumes that at least one of the levels means is different and therefore, the control factor has a significant impact on the experimental results. The null and alternative hypothesis can be expressed as:

$$H_{0,c}: \overline{X_{c_1}} = \overline{X_{c_2}} = \ldots = \overline{X_{c_n}} \quad 4.2$$

$$H_{1,c}: \overline{X_{c_1}} \neq \overline{X_{c_2}} \neq \ldots \neq \overline{X_{c_n}} \quad 4.3$$

Furthermore, regarding the effective thermal conductivity analysis, and since the base fluids selected present distinct thermal conductivities, the statistical analysis were performed to the effective thermal conductivity enhancement ratio, *i.e.* $X = k_{eff}/k_{bf}$. Through this methodology it is identified the enhancement produced in the thermal properties by the incorporation of the nanoparticles, independently on the magnitude of the thermal conductivity of the base fluids. This interpretation is also in line with the majority of the predictive models.

### 4.3.2 Analysis to the experimental thermal conductivity

So far, it was verified that the nanofluids produced satisfies the stability condition defined (Chapter 3). It should be noted that this ensures the reduction of noise factors and, therefore, improves the statistical inference from the results. The effective thermal conductivity of the samples was measured and, as expected, the results show an increase on the effective thermal conductivity with MWCNTs loadings. The experimental temperature presented a standard deviation, for each

experimental run, ranging from 0.1 K to 0.6 K, with an average standard deviation error for all the runs of 0.1 K.

The experimental results are exposed in detail in the Appendix H, in the form of thermodynamic Tables and Figures. In these, the uncertainties are those for a confidence interval of 95% of the experimental mean, as provided in detail in the Appendix D.

As mentioned in Section 4.2, the upper temperature limit of the KD2-Pro, the transient hot-wire used for thermal conductivity assessment, is 323.15 K. At this limit, the samples under test may suffer free convection near the testing needle, providing overestimated effective thermal conductivity. This issue is even more pronounced for less viscous fluid, or more diluted samples. For some of the samples, given to laboratory uncontrolled vibrations (HVAC system, other users, among others.) this issue was noticeable, especially for the lowest volume fractions, contributing to a slight main effect increase. Even so, as it will be noticeable, this issue is statistically negligible, as easily seen in the following Sections, and especially in Section 4.3.2.6.

Table 4.3 shows the experimental average and maximum results in thermal conductivity obtained, for each of the MWCNTs studied. It is important to notice that the maximum enhancement of 18.5% for the MWCNTs *d*50-80 *l*10-20. In addition, it is noticeable the low increment on thermal conductivity of the MWCNTs *d*20-40 *l*1-2, the nanoparticle with lower geometrical properties, i.e. aspect ratio, volume, surface to volume ratio, among others (Table 3.8).

Table 4.3: Average and maximum results obtained experimentally for each MWCNT geometry.

| | *average* | | *maximum* | |
|---|---|---|---|---|
| MWCNTs | $k_{eff}$-$k_{bf}$ | $k_{eff}/k_{bf}$ | $k_{eff}$-$k_{bf}$ | $k_{eff}/k_{bf}$ |
| *d*50-80 *l*10-20 | 0.030 | 1.072 | 0.082 | 1.185 |
| *d*60-100 *l*5-15 | 0.015 | 1.038 | 0.051 | 1.109 |
| *d*60-100 *l*1-2 | 0.014 | 1.033 | 0.037 | 1.107 |
| *d*20-40 *l*10-30 | 0.014 | 1.033 | 0.043 | 1.097 |
| *d*20-40 *l*5-15 | 0.016 | 1.038 | 0.037 | 1.102 |
| *d*20-40 *l*1-2 | 0.003 | 1.006 | 0.015 | 1.034 |

As mentioned in Section 4.3.1, the statistical analysis was performed over the thermal conductivity enhancement ratio, i.e. $k_{eff}/k_{bf}$. Through this approach the effect of the magnitude of the intrinsic thermal conductivity of the base fluid is diminished in the analysis. In addition, this approach lies within the majority of the predictive models proposed in the open literature, where $k_{bf}$ is in evidence in the majority of the equations, as it can be seen in Section 1.5.3.4.

An analysis of variance (ANOVA) was performed in order to verify which control factors have the greatest impact on the experimental thermal conductivity. The *F-distribution*, or Fisher-Snedecor distribution, was used to determine which of the hypotheses is likely to be true. The *F-distribution* is a continuous probability distribution used to validate the null hypothesis, through the comparison of the *F-distribution* with the tabulated *F-critical* (TAGUCHI, 1987). That is, *F-statistical* < *F-critical*, the null hypothesis is true, and when *F-statistical* > *F-critical*, the alternative hypotheses is true.

In Table 4.4 it is presented the ANOVA of the experimental results. As it can be depicted, the nanoparticles geometry, and volume fraction present an *F-statistical* higher than the *F-critical*. Therefore, for these control factors, it can be stated that the alternate hypothesis is true, i.e. their variation significantly affects the experimental results, an expected results since these are the control factors responsible for the spatial distribution of the nanoparticles in the medium. Also expected, the temperature and base fluid presents the lowest contribution to the experimental results.

Table 4.4: Multi-factor analysis of variance to the experimental thermal conductivity.

| | Sum of Squares | *dof* | Variance | F-statistical | F-critical | contribution |
|---|---|---|---|---|---|---|
| MWCNTs geometry | 0.132 | 5 | 0.026 | 91.0 | 2.2 | 24.1% |
| Volume fraction | 0.312 | 4 | 0.078 | 268.0 | 2.4 | 56.8% |
| Base fluid | 0.002 | 1 | 0.002 | 8.3 | 3.9 | 0.4% |
| Temperature | 0.003 | 5 | 0.001 | 1.9 | 2.2 | 0.5% |
| *Residual* | 0.100 | 344 | 0.000 | | | 18.2% |
| Total | 0.549 | 359 | | | | |

where contribution is the $Sum\ of\ Squares_c$ / $Sum\ of\ Squares_{Total}$, i.e. the respective contribution of the control factor to the total sum of squares.

The ANOVA allowed to recognise the control factors (or input parameters), that gave the greatest impact on the effective thermal conductivity. Nevertheless, it is also intended in this study, to evaluate the main effect of each control factor and of control factors interaction on the results. The definition of main effect was provided in the Section 4.3.1. This statistical analysis provides further inference to ascertain the mechanisms governing this thermal property.

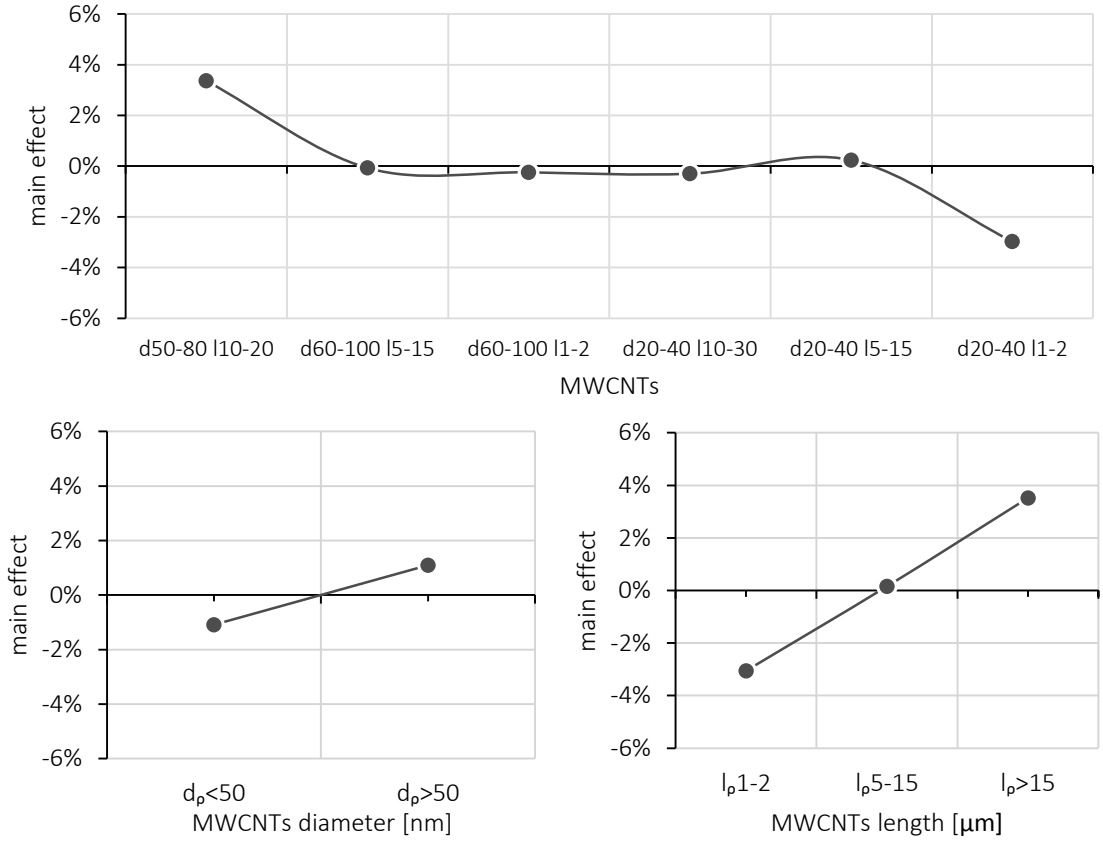


Figure 4.4: Main effect of the MWCNTs geometry in the experimental thermal conductivity.

As verified, the MWCNTs geometry seems to be one of the main control factors governing the effective thermal conductivity of nanofluids, evidencing that the nanoparticles should not be simplified as quasi-spherical ones. In Figure 4.4, it is shown the main effect of the MWCNTs geometry on the experimental thermal conductivity. As it can be seen, it appears that the MWCNTs *d*60-100 *l*5-15, *d*60-100 *l*1-2, *d*20-40 *l*10-30, and *d*20-40 *l*5-15 produce the same contribution to the overall mean of the experimental results. This may be explained by the similar geometrical properties of the MWCNTs after the functionalization procedure, as revealed in Table 3.8. Nevertheless, it should be noted that this does not imply that the results are strictly equal for these MWCNTs, and the interaction with other control factors, such as volume fraction, may produce distinct results. Such behaviour is clear through the analysis of the main effect of the MWCNTs diameter and length distribution. In these, it seems that the lower the diameter distribution, and the higher the length distribution, the higher the experimental thermal conductivity. Such behaviour may correspond with the increase on the aspect ratio of the MWCNTs ($l_p/d_p$) that contributes to a higher degree of spatial distribution through the medium for a given volume fraction. This behaviour is easily depicted from Figure 3.21.

As envisaged in Chapters 1 and 2, the aspect ratio of the MWCNTs is considered as one of the most important parameter affecting the effective thermal conductivity. In Figure 4.5, it is shown the main effect of the MWCNTs aspect ratio on the experimental thermal conductivity, suggesting that a significant increase of the aspect ratio provides a higher enhancement on the effective thermal conductivity. However, as observed in Figure 2.15, the thermal conductivity enhancement is directly proportional to the diameter distribution of the MWCNTs, being therefore clear that, for a given lengths distribution, it can be observed a higher enhancement for a lower aspect ratio of the MWCNTs. This behaviour is also evidenced in Figure 4.5.

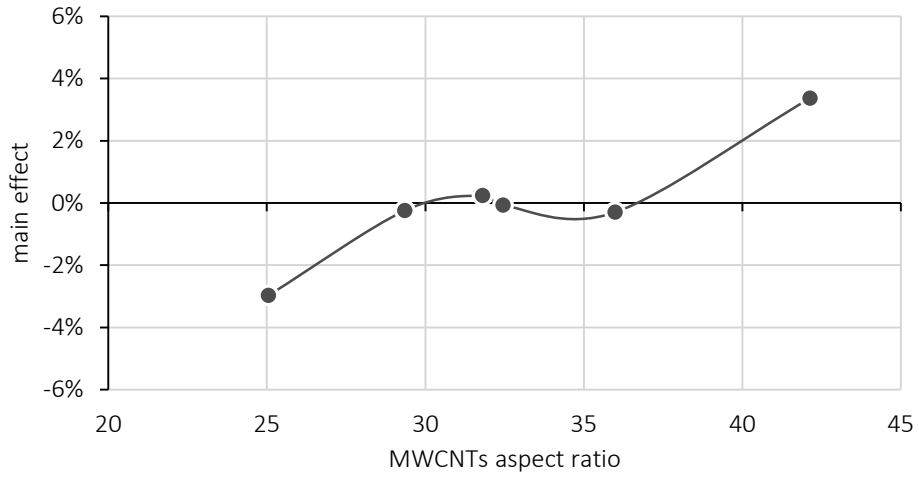


Figure 4.5: Main effect of the MWCNTs aspect ratio in the experimental thermal conductivity.

In Figure 4.6, it can be verified the main effect of the volume fraction on the experimental thermal conductivity. The latter suggest a slight non-linear relationship between the volume fraction and the effective thermal conductivity of the nanofluids. Importantly, several researchers reported similar observations (CHOI et al., 2001, DING et al., 2006, HARISH et al., 2012, LIU et al., 2005, WEITING et al., 2009, XIE et al., 2003, ZHANG et al., 2006). This was usually defined as an intriguing behaviour of nanofluids. Nevertheless, this was an expected results give the classical theories, and the non-linearity may suggest the thermal interparticle interaction due to the high degree of spatial distribution of the MWCNTs, even for the modest volume fractions studied.

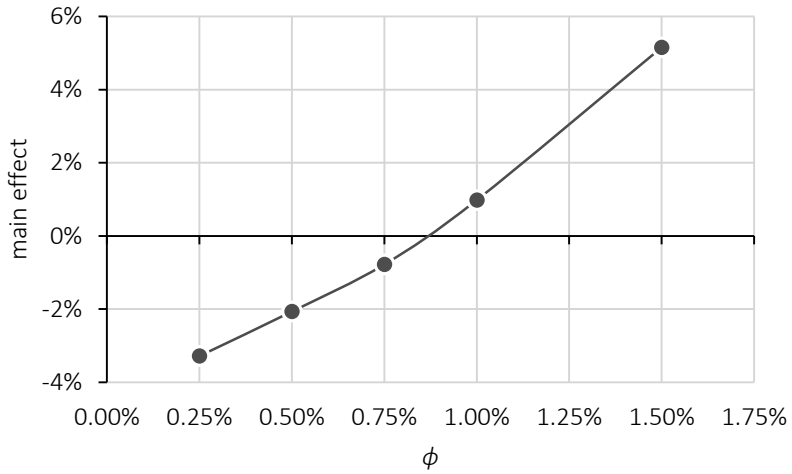


Figure 4.6: Main effect of the MWCNTs volume fraction in the experimental thermal conductivity.

In addition, the slight non-linear behaviour (poor significance) may indicate a high Kapitza resistance, as predicted in Figure 2.20. In this, it can be depicted that the increase on the Kapitza resistance decreases the contribution of the thermal interparticle interaction.

As previously identified by the ANOVA, and as can be seen in Figure 4.7, the base fluid presents negligible contribution to the effective thermal conductivity enhancement. It should be reminded that the main effects are calculated over the thermal conductivity enhancement ratio, diminishing the effect of the magnitude of the base fluid original thermal conductivity. The behaviour observed may suggest that the Brownian motion of the nanoparticles, higher for the less viscous base fluid, induces negligible impact on the experimental results. Furthermore, as noticed in Section 3.6.2, the dispersed MWCNTs are very interactive, even for the smallest volume fraction. These interparticle interactions reduce the random or Brownian motion of the MWCNTs. This theory is also revealed and established ahead. Nevertheless, the slight decrease in the thermal conductivity enhancement ratio for DW+60%EG may suggest an increased Kapitza resistance, due to a lower surface wettability of the nanoparticles and interface bonding for this more viscous base fluid. In a hypothetical scenario where the nanofluids are governed by nano-layer ordering liquid structures at the interface, it should be expected a higher thermal conductivity enhancement ratio for DW+60%EG, due to their higher viscosity and, hence, a higher probability of forming ordered structures at the hydrophilic interface.

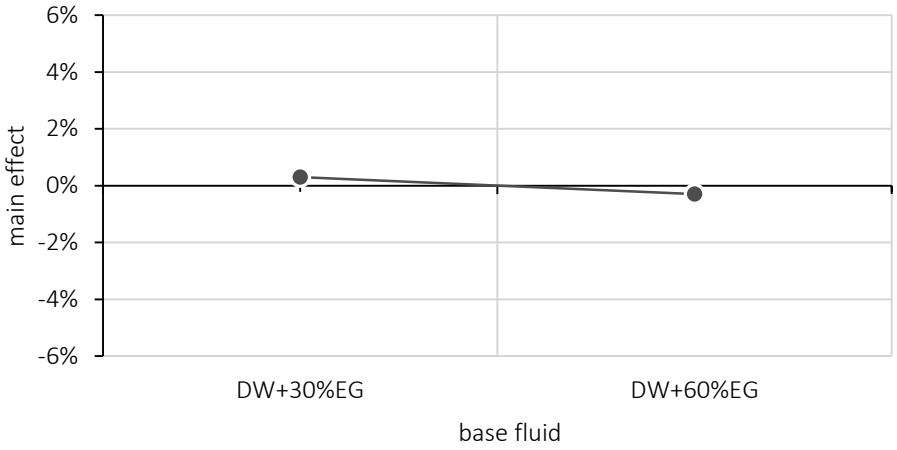


Figure 4.7: Main effect of the base fluid in the experimental thermal conductivity.

The temperature is another control factor with a negligible contribution on the experimental results, as can be seen in Figure 4.8. As also suggested by the analysis to the Figure 4.7, this behaviour may be related to a negligible impact of the Brownian motion of the nanoparticles. The increase on the effective thermal conductivity with the temperature seems to be related to the increase on that of the base fluid.

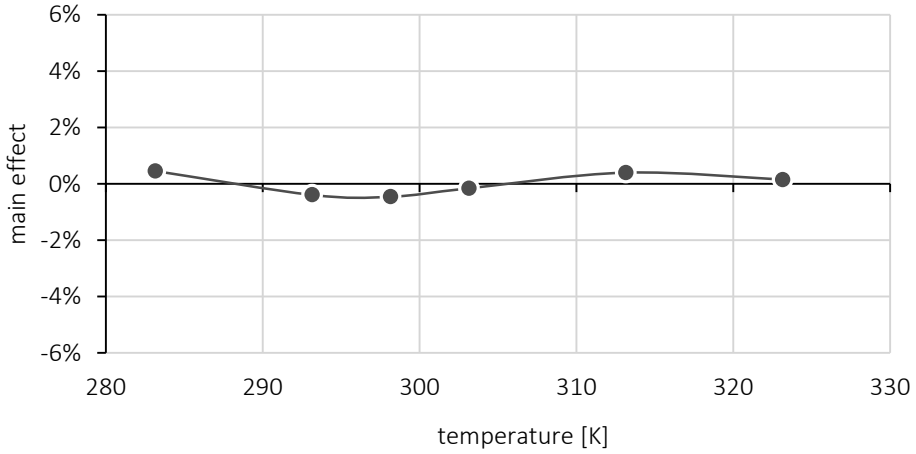


Figure 4.8 Main effect of the temperature in the experimental thermal conductivity.

In line with the ANOVA, the analysis to the main effect of the control factor revealed that the MWCNTs geometry and volume fraction are those that higher impact induces on the experimental thermal conductivity. In contrast, the base fluid and temperature seem to present lower effect on this thermal property. Nonetheless, despite their negligible impact, these may produce some interaction with the MWCNTs geometry and volume fraction. In the following subsections are presented an analysis to the control factors interactions, enabling to demystify the intriguing behaviour of the nanofluids based on the experimental observations.

#### 4.3.2.1 MWCNTs GEOMETRY VERSUS VOLUME FRACTION (AB)

The statistical interaction between the MWCNTs geometry and its volume fraction, shown in Figure 4.9, suggest that for the lowest volume fraction, 0.25%, the thermal conductivity enhancement ratio is independent of the MWCNTs geometry. For the remaining volume fractions, the statistical analysis revealed a non-linear enhancement proportional to the MWCNTs geometry. This behaviour may put in evidence the increase of the spatial distribution of the nanoparticles and the increase of the thermal interparticle interaction. According to Figure 3.21, the nanoparticle with the higher degree of spatial distribution and interparticle interaction is the MWCNTs *d*50-80 *l*10-20, being the opposite scenario attributed to the MWCNTs *d*20-40 *l*1-2. Moreover, for the remaining MWCNTs, the spatial distribution and interparticle interaction are very similar, as also observed for the thermal conductivity experimental results, as shown in Figure 4.9. This evidence is in accordance with the classical theories, described in Chapter 2, and are a heat conduction mechanisms of the proposed predictive model.

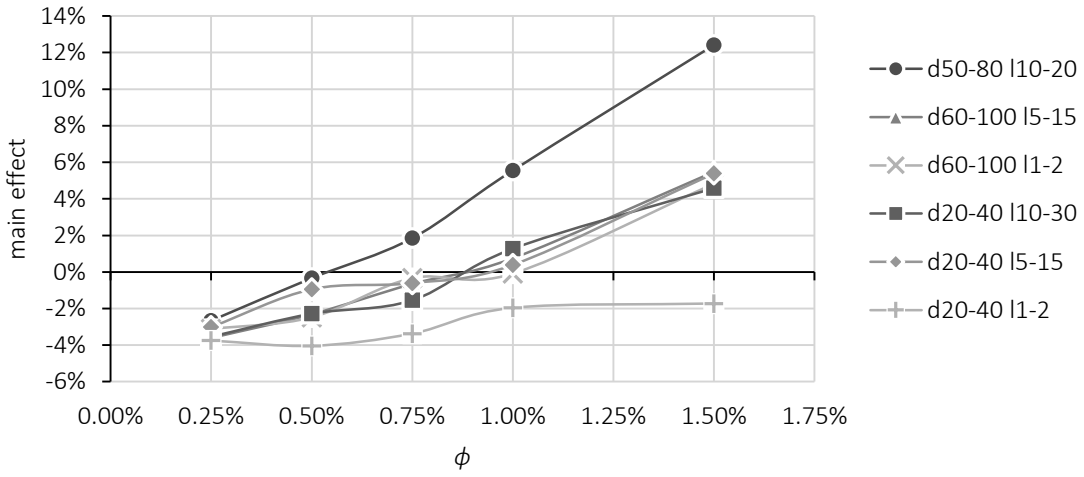


Figure 4.9: Main effect of the MWCNTs geometry and volume fraction interaction in the experimental thermal conductivity.

#### 4.3.2.2 MWCNTs GEOMETRY VERSUS BASE FLUID (AC)

Keblinski *et al.* (KEBLINSKI et al., 2002) verified analytically that the thermal diffusivity of the base fluid may be higher than the Brownian diffusion of the nanoparticles, even for the smaller nanoparticles. This result was also obtained for the elongated nanoparticles studied, MWCNTs, as suggested in the Section 3.6.2. Therefore, it is expected a non-proportional relation between the effective thermal conductivity and the viscosity of the base fluid.

However, as can be verified in the Figure 4.10, there is a slight interaction between the MWCNTs geometry and the base fluid, since the main effect on the thermal conductivity enhancement ratio is higher for the lowest viscous fluid, for all the MWCNTs geometries. It should be noted that the negligible main effect described in Figure 4.7, is also noticeable in this slight control factor interaction.

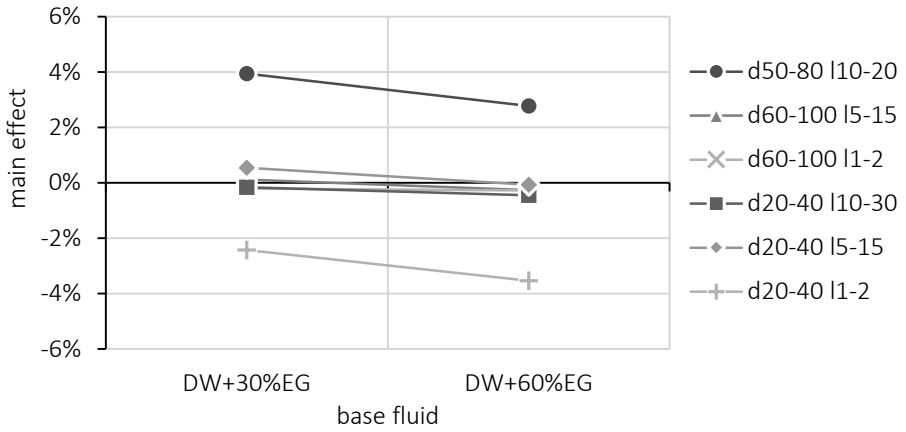


Figure 4.10: Main effect of the MWCNTs geometry and base fluid interaction in the experimental thermal conductivity.

With absence of information to attribute this behaviour to a Brownian mechanism, perhaps the results may be attributed to a higher thermal interface resistance, or Kapitza resistance, for the most viscous base fluid, contributing to the reduced thermal conductivity enhancement. Despite the lack of theoretical understanding on the Kapitza resistance at the nanoscale, it is recognized that this strongly depends on the MWCNTs surface wettability and interface bonding (see Section 2.4), which also depends on the thermo-physical properties of the base fluid.

#### *4.3.2.3 MWCNTs GEOMETRY VERSUS TEMPERATURE (AD)*

The control factors interaction between the MWCNTs geometry and temperature enables to verify the existence of the so announced Brownian contribution to the effective thermal conductivity. As depicted in Figure 4.11, for all the nanoparticles under study, there is no statistical evidence of thermal conductivity enhancement with the temperature rise, even for the smaller MWCNTs, *d*20-40 *l*1-2, which are expected to be most affected by the Brownian field. The main effects shown in the Figure, advocate negligible variation on the thermal conductivity enhancement ratio with the temperature rise, suggesting that this is little, if anything, influenced by the Brownian field. In a hypothetical scenario, where the results were affected by a Brownian mechanism, it should be expected an evident rise in the main effect of each MWCNTs geometry with the temperature rise.

It should be noted that the slightest variations in the Figure, in an imaginary main effect horizontal line for each MWCNTs geometry, are attributed to uncertainties of the experimental observations.

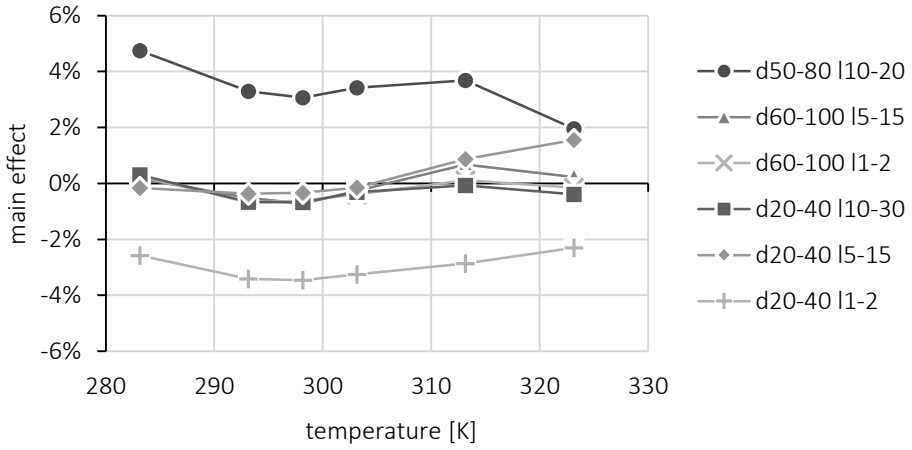


Figure 4.11: Main effect of the MWCNTs geometry and temperature interaction in the experimental thermal conductivity.

#### 4.3.2.4 *VOLUME FRACTION VERSUS TEMPERATURE (BD)*

In Figure 4.12, it is shown the main effects of the control factors interaction between the volume fraction and temperature. In this, it can also be depicted the absence of a Brownian mechanism in the thermal conductivity enhancement ratio, since this present the similar linear behaviour with that reported in the Figure 4.11.

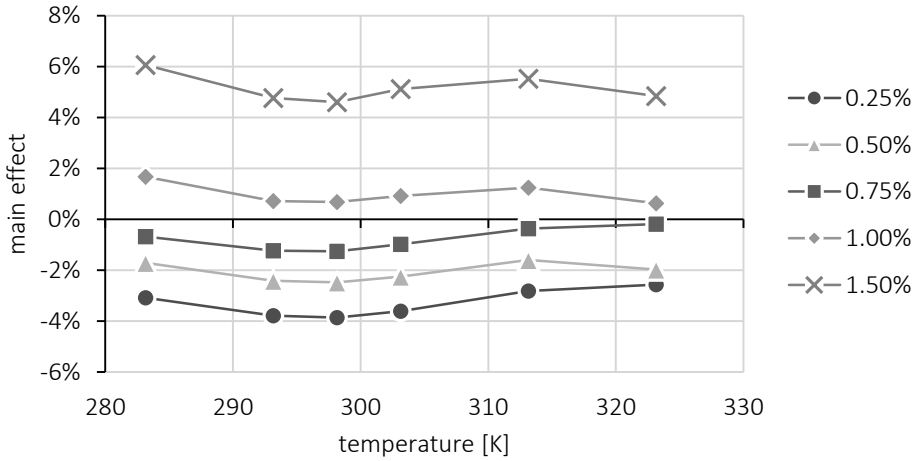


Figure 4.12: Main effect of the volume fraction and temperature interaction in the experimental thermal conductivity.

#### 4.3.2.5 *MWCNTS GEOMETRY VERSUS VOLUME FRACTION AND BASE FLUID (ABC)*

In Figure 4.13, it can be depicted the main effects of the interaction between the control factors MWCNTs geometry, volume fraction, and base fluid. In this, it can be seen that the experimental

results present a thermal conductivity enhancement ratio proportional to the MWCNTs geometry and volume fraction. In contrast, there is no evidence of a contribution of the base fluid on the experimental results. Such behaviour may indicate the inexistence of the so-called nano-layer structure, acting as a thermal bridge, and increasing the heat conduction through the medium.

In addition, the negligible impact of the nano-layer ordering structure was anticipated and explained in detail in Section 2.4. In the hypothetical scenario of the existence of such nano-layer structure at the interface, it is expected a thermal conductivity enhancement ratio proportional to both control factors under analysis. Nanoparticles with higher surface, at superior volume fraction, and more viscous fluids, will probably provide a higher density of nano-layers structures that increase the heat conduction.

Nevertheless, in line with the postulated previously, the results suggest that the nanoparticle spatial distribution and thermal particle interaction provide a non-linear thermal conductivity enhancement ratio, independently on the base fluid type.

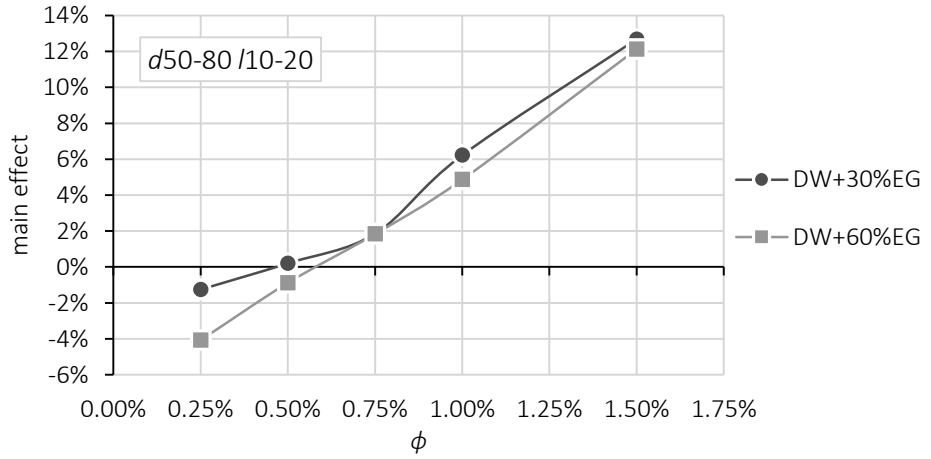


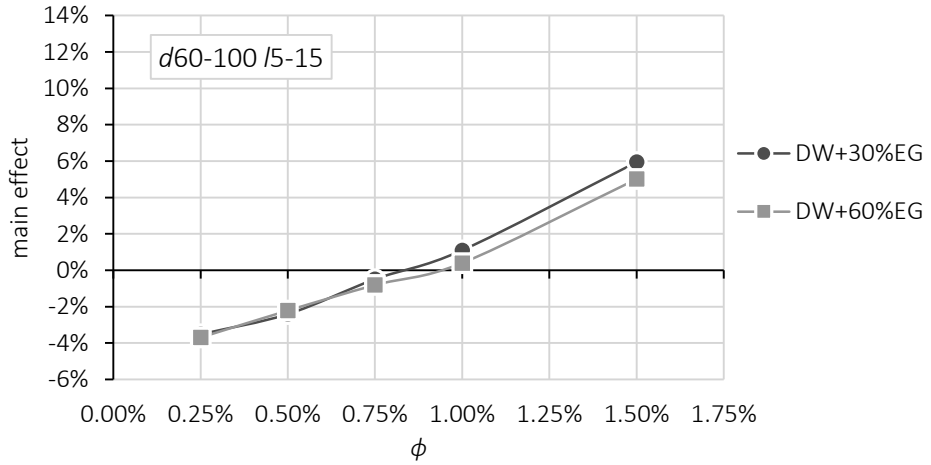

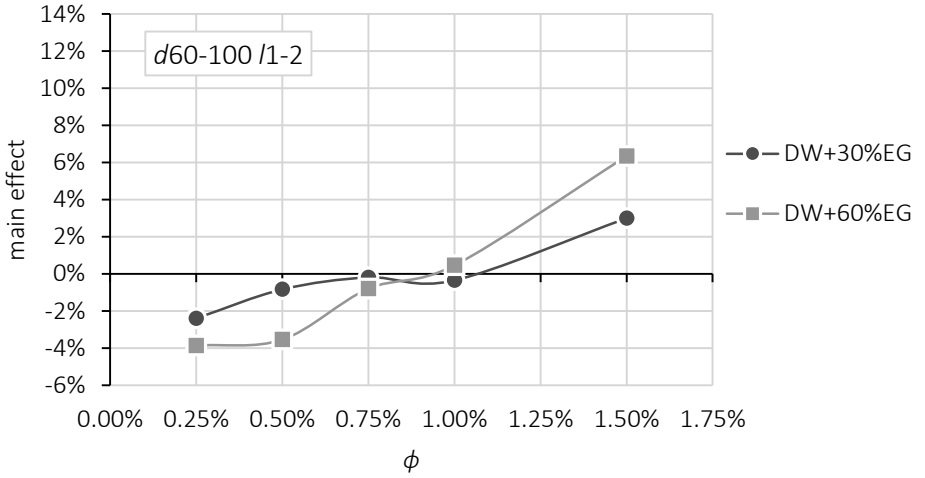
d60-100 /1-2
main effect
14%
12%
10%
8%
6%
4%
2%
0%
-2%
-4%
-6%
0.00% 0.25% 0.50% 0.75% 1.00% 1.25% 1.50% 1.75%
ϕ
DW+30%EG
DW+60%EG

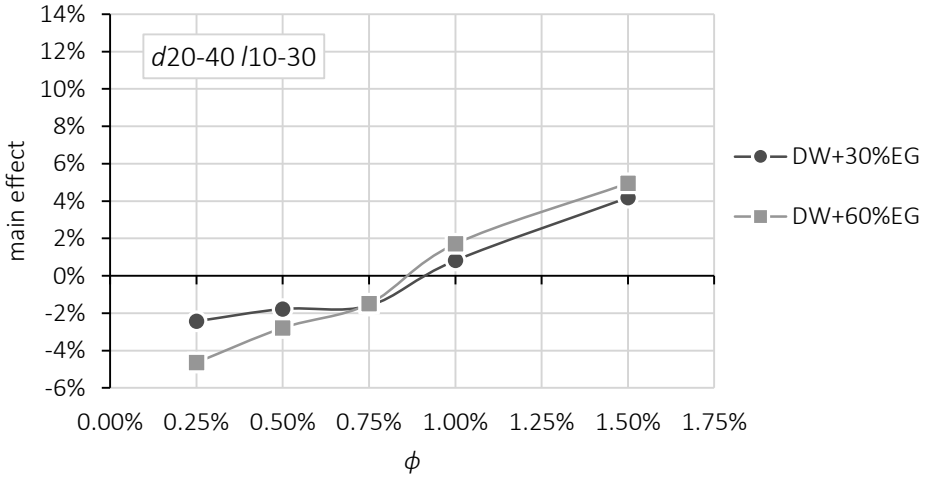
d20-40 /10-30
main effect
14%
12%
10%
8%
6%
4%
2%
0%
-2%
-4%
-6%
0.00% 0.25% 0.50% 0.75% 1.00% 1.25% 1.50% 1.75%
ϕ
DW+30%EG
DW+60%EG

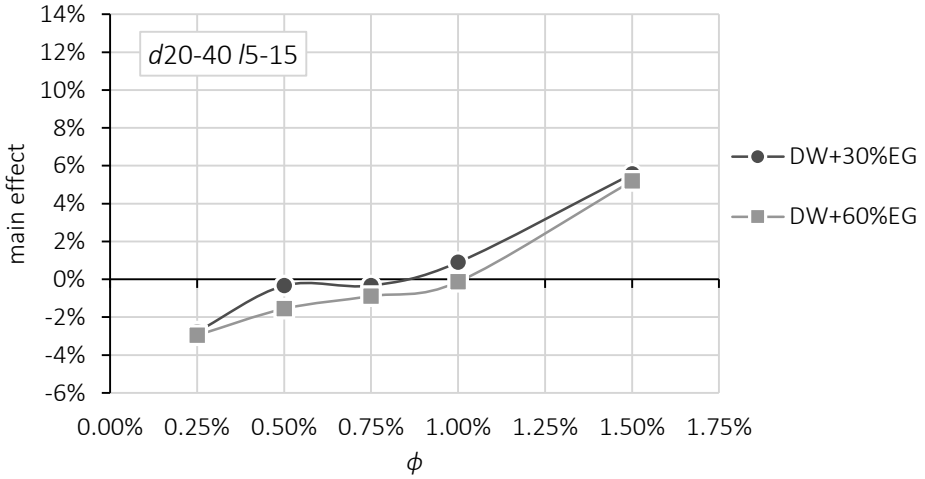
d20-40 /5-15
main effect
14%
12%
10%
8%
6%
4%
2%
0%
-2%
-4%
-6%
0.00% 0.25% 0.50% 0.75% 1.00% 1.25% 1.50% 1.75%
ϕ
DW+30%EG
DW+60%EG

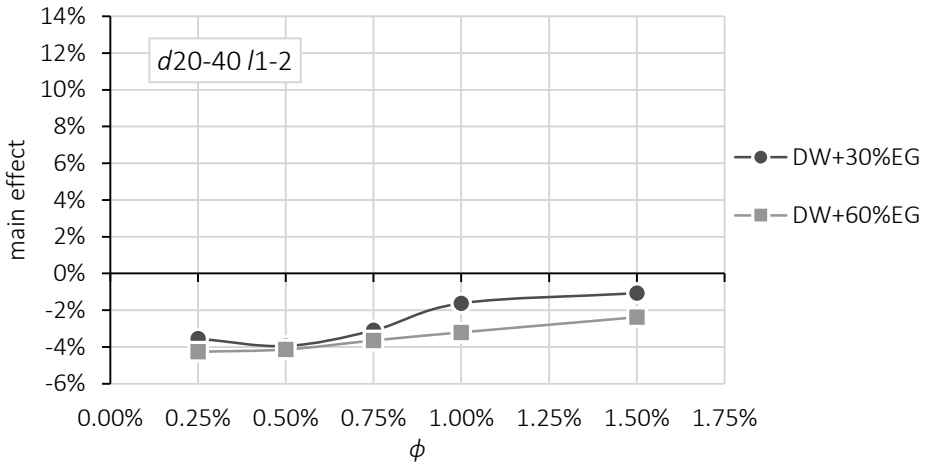


Figure 4.13: Main effect of the MWCNTs geometry, volume fraction and base fluid interaction in the experimental thermal conductivity.

#### 4.3.2.6 MWCNTs GEOMETRY VERSUS VOLUME FRACTION AND TEMPERATURE (ABD)

In line with the postulated in the Section 4.3.2.2, 4.3.2.3, and 4.3.2.4, Figure 4.14 revealed lack of evidence on Brownian mechanisms contributing to the thermal conductivity enhancement ratio.

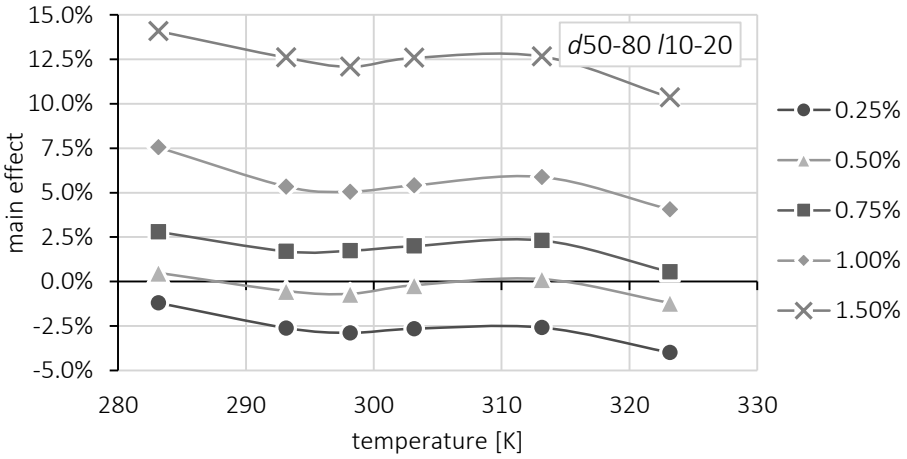


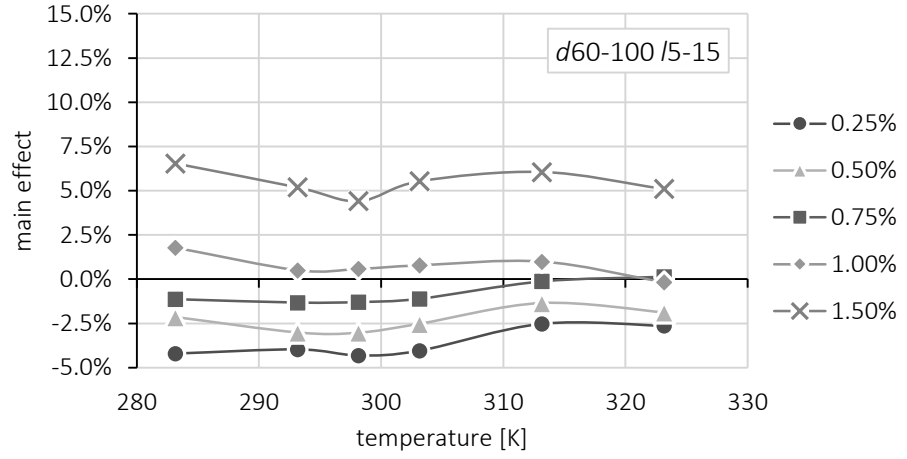

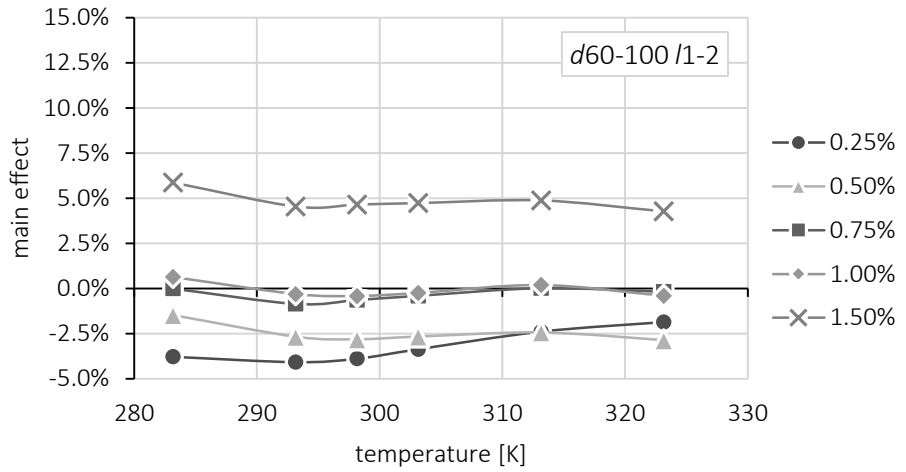
d60-100 l1-2
15.0%
12.5%
10.0%
7.5%
5.0%
2.5%
0.0%
-2.5%
-5.0%
main effect
280
290
300
310
320
330
temperature [K]
0.25%
0.50%
0.75%
1.00%
1.50%

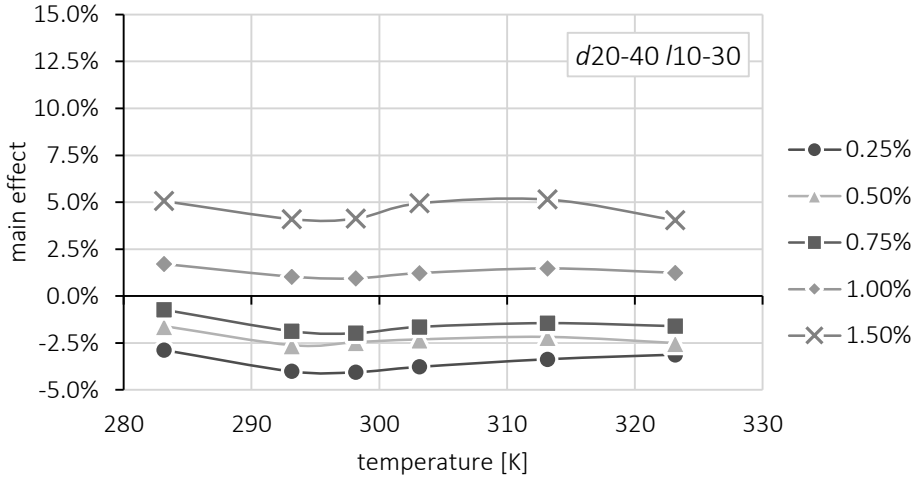
d20-40 l10-30
15.0%
12.5%
10.0%
7.5%
5.0%
2.5%
0.0%
-2.5%
-5.0%
main effect
280
290
300
310
320
330
temperature [K]
0.25%
0.50%
0.75%
1.00%
1.50%

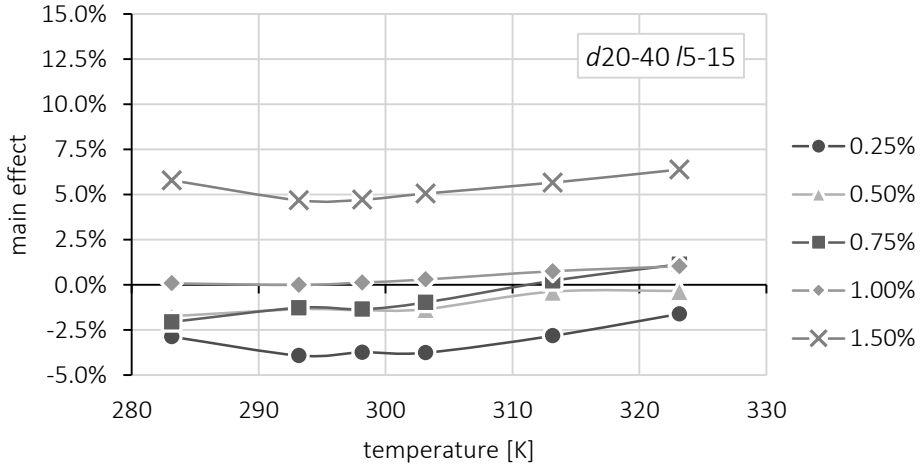
d20-40 l5-15
15.0%
12.5%
10.0%
7.5%
5.0%
2.5%
0.0%
-2.5%
-5.0%
main effect
280
290
300
310
320
330
temperature [K]
0.25%
0.50%
0.75%
1.00%
1.50%

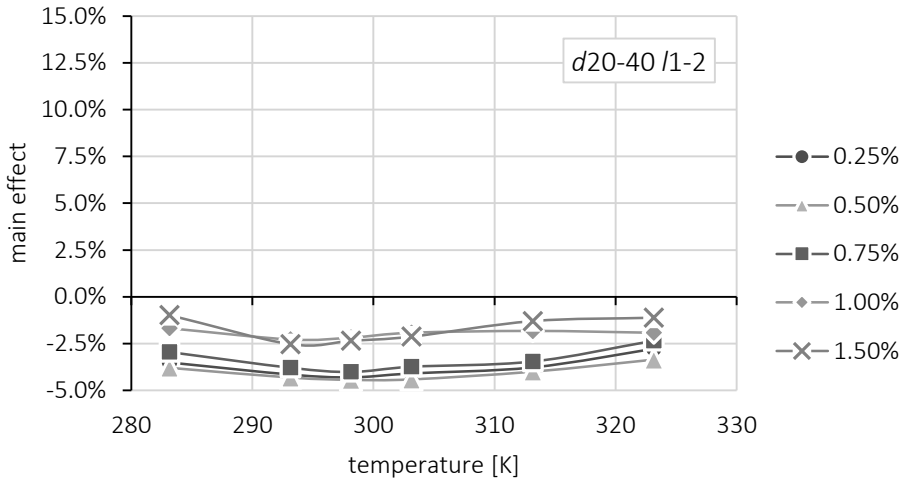


Figure 4.14: Main effect of the MWCNTs geometry, volume fraction and base fluid interaction in the experimental thermal conductivity.

It should be noted that for the MWCNTs *d*60-100 *l*5-15 and *d*20-40 *l*5-15 it was observed poorly/accuracy experimental results for some of the nanofluids with lowest volume fractions, at temperature 323.15 K. Such inaccurate results may induce in poor interpretation. Such uncertainties were anticipated in Section 4.2 and are related with the upper temperature limit of the *KD2 Pro*, the transient hot-wire used. At this limit, the samples under test may suffer free convection near the testing needle, providing overestimated effective thermal conductivity. Furthermore, this issue is amplified with uncontrolled laboratory vibrations (HVAC system, other users, among others.). Nevertheless, this behaviour did not show any pattern with the control factors under test, being certainly associated with poor measurements.

### 4.3.3 BRIEF DISCUSSION

The statistical analysis to the experimental results suggested that the effective thermal conductivity of MWCNTs based nanofluids strongly depends on the spatial distribution of the nanoparticles in the medium. Furthermore, there seems to be no evidence of some of the intriguing mechanisms suggested by some authors, namely Brownian motion, nano-layer structure of base fluid molecules at the interface, and nanoparticles agglomeration/percolation. The latter was excluded by the measurement of the Zeta potential of the samples, reported in the Section 3.8.1.

The molecular-level layering concept states that the molecules from a liquid near a solid surface (such as a nanoparticle surface) become more organized than the remaining, forming a solid-like layer (not crystalized) structure that acts as a thermal bridge. In Section 2.4, it was verified that in materials where heat conduction is governed by electrons, such metals, this might be true, since it

is not needed the formation of a crystalline structure (POIRIER et al., 1994). However, for materials with heat conduction dominated by phonons, a non-crystalline structure seems to present imperfections that scatter the heat conductive phonons (EVANS et al., 2007, XUE et al., 2004). These behaviour is easily established by the thermal conductivity of liquid water (~0.6 W/mK) and ice (~2.2 W/mK), at the melting temperature point (LIDE, 2004). Despite being known that a hydrophilic surface may enhance the formation of the solid-like layer, it is also known that, in order to these present a significant enhancement on the effective thermal conductivity, strong electric fields are required. Therefore, it seems unlikely to be formed by the hydrophilic surface itself (EVANS et al., 2007, XUE et al., 2004).

On the other hand, as suggested by several authors, the hydrophilic surface induces a lower magnitude on the Kapitza resistance (GE et al., 2006, LEE, 2007). Perhaps, this lowering of magnitude may be induced by a nano-layer ordered of the base fluid molecules, with fewer imperfections that scatter the heat conduction phonons, when compared to hydrophobic ones (LEE, 2007). As all the MWCNTs studied, have hydrophilic surface, it is likely to the nano-layer become an integrant part of the Kapitza resistance, i.e. a fundamental mechanism of the Kapitza resistance, if exists. Nevertheless, no statistical evidence from the experimental results for distinct base fluids was verified.

Furthermore, the negligible impact induced by the Brownian motion was also anticipated by the results achieved through the numerical model, and expressed in Section 3.6.2. In this, it was verified that the Brownian motion among the particles has a negligible impact on the dynamic interparticle interaction and, in theory, is slower than the base fluid thermal diffusion. To corroborate these numerical results, no experimental evidence was found, namely a strong enhancement of the experimental results with the temperature rise and viscosity of the base fluid.

## 4.4 PREDICTIVE MODEL VALIDATION

The analysis to the previous results, suggested that the experimental results may comply within the theory of predictive model proposed in the Chapter 2. For these reason, this model, for non-agglomerated and very elongated nanoparticles, randomly dispersed in the base fluids, at volume fractions where thermal interparticle interaction may occur, was also used to verify the fitness to the results. It should be reminded that this model complies with the structural morphology and stability conditions preconized for the nanofluids, and experimentally verified. Even so, the *extended differential effective medium* (EDEMT), *i.e*. the proposed model, has two unknown input

parameters, the thermal conductivity of MWCNTs and the Kapitza resistance. As mentioned in the Section 3.2.2, the thermal conductivity of the functionalized MWCNTs were considered to be 1700 W/mK, as suggested by Shenogin *et al.* (SHENOGIN et al., 2004a). Through molecular dynamics simulations, they found that the degree of functionalization causes a drop on the thermal conductivity of the MWCNTs. Nevertheless, they also observed that the results converged to 1700 W/mK, for the highest degrees of functionalization.

Therefore, this value was adopted since the nanofluids prepared in this study present low probability of agglomeration, and the FTIR analysis of Section 3.5.1, suggested a high degree of functionalization. Furthermore, as shown in the Section 2.5, the EDEMT model presents converging results for the thermal conductivity of the nanoparticles above 1000 W/mK (see Figure 2.19, for Kapitza resistance above $8\times10^{-8}$ $K\,m^2/W$), being, therefore, slow impact caused by these assumption.

Given the lack of uncertainties in the Kapitza resistance mechanisms and magnitude, reported in the Section 2.4, this was used to fit the EDEMT model to the experimental observations as a single value, since the conventional base fluids used are both aqueous solutions of ethylene glycol. Nonetheless, it should be remembered that the experimental results suggest a slight difference in the Kapitza resistance for the two base fluids (Section 4.3.2.2). It is expected that the proposed Kapitza resistance achieved through this adjustment enables to predict the effective thermal conductivity of nanofluids composed by the same family of these conventional base fluids.

Nevertheless, as it can be seen in the Table 4.4, MWCNTs geometry and volume fraction are the control factors most important for the system, since they present the highest sums of squares, variance, and *F-statistical*. Therefore, it can be stated that fitting the Kapitza resistance to the experimental results does not necessarily force the EDEMT model to predict the behaviour of the experimental data.

In Figure 4.15, it is shown the scatter chart of the EDEMT model with the experimental thermal conductivity, also in terms of effective thermal conductivity, $k_{eff}$. As this is a multivariable problem, the graph is represented by means of *output* versus *target*, where the *outputs* are the obtained results, both experimental and analytical and the *target* the analytical, as schematically defined in Table 4.5. Therefore, the experimental results are the dispersed points, and the EDEMT model is represented by a straight line of slope 1. The Pearson's correlation $r^2$ between the experimental and predicted data was calculated through the Equation J.1, in Appendix J.

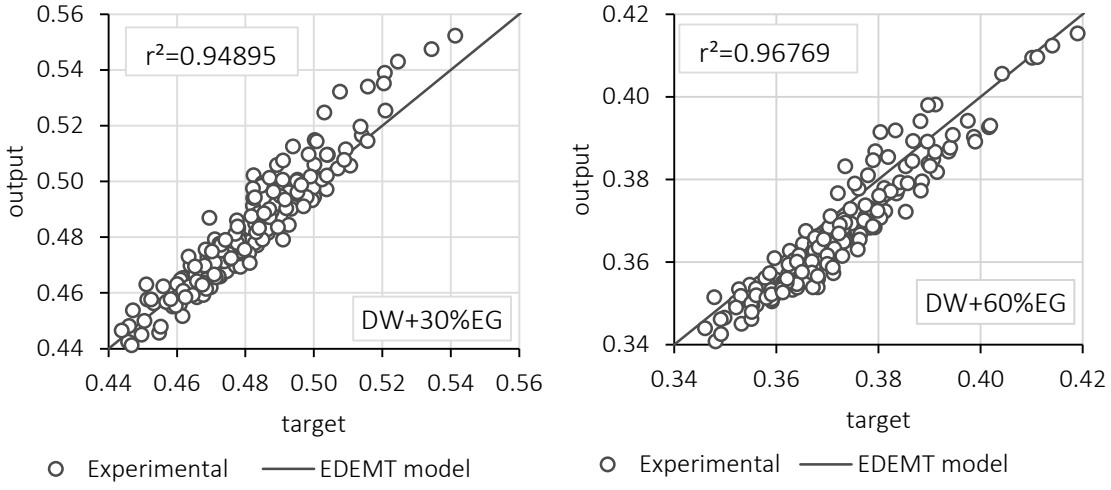


Figure 4.15: Scatter chart of the EDEMT model and experimental data (in terms of $k_{eff}$).

Table 4.5: Schematic defined of the terms target and output.

| | Predictive model | Experimental values |
|---|---|---|
| target (x) | predicted | measured |
| output (y) | predicted | predicted |

In this study, the Kapitza resistance that produced the best-fit, *i.e.* the best fitting parameters shown in Table 4.7, is $10.5\times10^{-8}$ K m$^2$/W. This value is close to that suggested by Huxtable *et al*. (HUXTABLE et al., 2003), $8\times10^{-8}$ K m$^2$/W for heavy water, an expected result since the nanofluids are both aqueous solutions of ethylene glycol. Furthermore, this Kapitza resistance magnitude is within the bonds reported by Cahill's research group (CAHILL et al., 2001, WILSON et al., 2002).

From the achieved Kapitza resistances, it is obtained an average Kapitza radius $a_K$ of 48 nm and 37 nm, respectively for DW+30%EG and DW+60%EG based nanofluids. These Kapitza radius is of the same order of magnitude of the diameter of the studied MWCNTs, an expected result. Nevertheless, for $a_K$ smaller than the particle size, the effective thermal conductivity increases with the rise on volume fraction. Conversely, when $a_K$ is larger than the particle size, the effective thermal conductivity decreases with the increase of the volume fraction.

Similar scatter charts for the predictive models available in the open literature (Section 1.5.3.4) are presented in the Appendix J. Through a simple visual comparison it can be verified that the EDEMT model has a better correlation with the experimental results, in relation to the other existing models in the open literature. This result corroborates that, nanofluids that comply with minimum stability conditions for thermal management, present heat conduction mechanisms proposed by

the classical theories, expressed in detail in the Chapter 2. Moreover, as can be seen from Figure J.3, the model of Nan *et al.* with a Kapitza resistance of $8\times10^{-8}$ K m$^2$/W (suggested by the authors) shows similar tendency in the distribution of the experimental results with the EDEMT model (NAN et al., 2004). This is an expected results since the EDEMT model is based on Nan *et al.* model, proving that adjusting the Kapitza resistance do not forcedly fit the results to the EDEMT model.

In Figure 4.16, it is shown the cumulative accuracy of the EDEMT model and Nan *et al.* model. In both models it was considered the best fitting Kapitza resistance, $R_K$=10.5×10$^{-8}$ K m$^2$/W. The curves represent all the 360 experimental thermal conductivities measured, and suggest that the EDEMT model is capable of predicting 80% of the results with a fractional error of less than 2% (in Appendix J.1, Equation J.2 provides the expression for the fraction error). Furthermore, all the data is predictable with less than 4.5% error. The standard deviation of the difference between the predicted and observed results is 0.9%, as expressed in Table 4.6. In this, the term *mse* represents the *mean square error* of each model (expressed in Equation J.4), an estimator of the accuracy of the predictive models. The smaller *mse*, the better the results fit to the model (JACCARD, 1998, TAGUCHI, 1987).

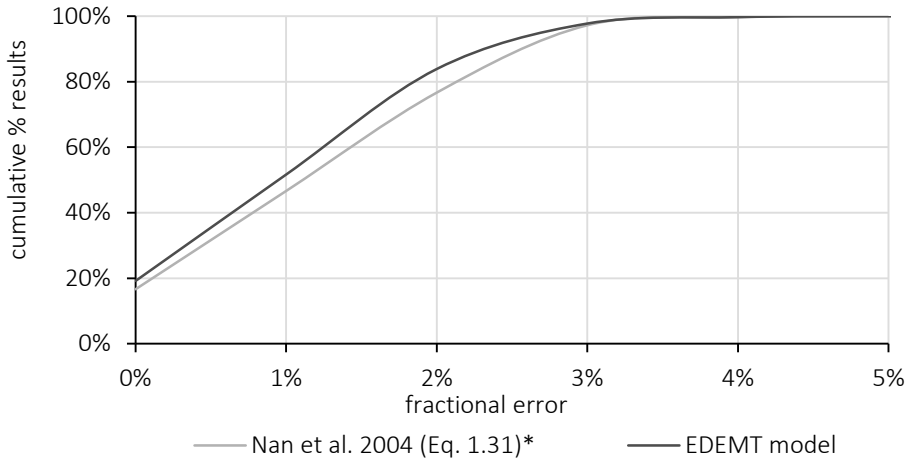


Figure 4.16: Cumulative percentage of experimental data predicted by the proposed EDEMT model within the fractional error ($R_K$=10.5×10$^{-8}$ K m$^2$/W).

Table 4.6: Fitness estimators of the models to the experimental results ($R_K$=10.5×10$^{-8}$ K m$^2$/W).

| Estimator | EDEMT model | Nan *et al.* 2004 (*Eq. 1.31**) |
|---|---|---|
| $r^2$ | 0.95832 | 0.93256 |
| *mse* | 0.00004 | 0.00005 |
| Maximum fractional error | 4.51% | 4.69% |
| Minimum fractional error | 0.01% | 0.00% |
| Average fractional error | 1.49% | 1.66% |
| Standard deviation of fractional error | 0.95% | 1.00% |

*this equation was actualized to the Kapitza resistance that best fit the EDEMT model ($R_K$=10.5×10$^{-8}$ K m$^2$/W).

More relevant, since the adjusted Kapitza resistance achieved is of order 10$^{-7}$ K m$^2$/W, the models are almost coincident, as expected since the thermal interparticle interaction becomes poorly significant to this order of Kapitza resistance as shown in Figure 2.20. Nevertheless, it is expected that the EDEMT model is more generalist since this is capable of predict the interparticle thermal interaction for higher MWCNTs lengths and volume fractions. Therefore, the EDEMT model may be used for nanofluids produced by nanoparticles with a lower degree of length destruction, a challenge for the future (see Figure 2.21). Such nanoparticle would allow for a higher increase in effective thermal conductivity of nanofluids. Furthermore, in an eventual case that, in the future, become possible to reduce the magnitude of the Kapitza resistance in these systems, the EDEMT model will be the more accurate.

In Figure 4.17, it is presented the cumulative percentage of experimental data predicted by the EDEMT model for Kapitza resistance ranging from 5×10$^{-8}$ K m$^2$/W to 20×10$^{-8}$ K m$^2$/W, suggested by the Cahill's research group (Section 2.4). As it can be depicted, the results suggest that for Kapitza resistances above 8×10$^{-8}$ K m$^2$/W, the value for MWCNTs suggested by the Cahill's research group, 80% of the experimental observations can be predicted with a maximum fractional error of ~7%. Moreover, for 15×10$^{-8}$ K m$^2$/W, the maximum fractional error achieved for the 100% experimental data is of ~9%. In contrast, for Kapitza resistance below 8×10$^{-8}$ K m$^2$/W, the divergence with the experimental data is higher, presenting a maximum fractional error of 16%, with 80% of the data below the 8% error.

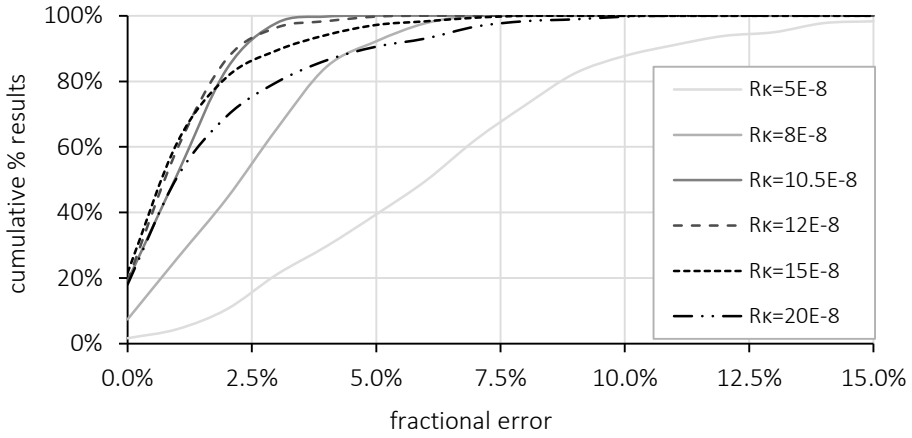


Figure 4.17: Cumulative percentage of experimental data predicted by the EDEMT model within the fractional error for different Kapitza resistance.

In Table 4.7 it is summarized the fitness estimators of the EDEMT model for different Kapitza resistance. In line with the results presented in the postulated previously, the results suggest that the best fit is achieved for $10.5\times10^{-8}$ K m$^2$/W. Moreover, a variation of 43% on the Kapitza magnitude can lead to a maximum fractional error of 4% achieved for the best fitting Kapitza resistance. In contrast, a variation of -52% on the Kapitza magnitude can produce a deviation of 11% on the results observed experimental, an undesired variation. Nevertheless, the results suggest that using a Kapitza resistance ranging from $8\times10^{-8}$ K m$^2$/W to $15\times10^{-8}$ K m$^2$/W, for these nanofluids family, provides satisfactory predictions of the thermal conductivity enhancement. It should be noted, however, that the nanofluids must meet the spatial distribution homogeneity described in Chapter 2, to be described for this predictive model.

Table 4.7: Fitness estimators of the EDEMT model to the experimental results for different Kapitza resistance.

| $R_K$ [K m$^2$/W] | $5\times10^{-8}$ | $8\times10^{-8}$ | $10.5\times10^{-8}$ | $12\times10^{-8}$ | $15\times10^{-8}$ | $20\times10^{-8}$ |
|---|---|---|---|---|---|---|
| $R_K$ variation | -52% | -24% | Ref. (0%) | 14% | 43% | 90% |
| r² | 0.93405 | 0.95872 | 0.95832 | 0.95192 | 0.92885 | 0.87513 |
| *mse* | 0.00085 | 0.00012 | 0.00004 | 0.00005 | 0.00010 | 0.00018 |
| Maximum fractional error | 17.23% | 6.95% | 4.51% | 5.68% | 8.42% | 11.32% |
| Minimum fractional error | 0.36% | 0.03% | 0.01% | 0.01% | 0.01% | 0.00% |
| Average fractional error | 6.64% | 2.81% | 1.49% | 1.41% | 1.57% | 2.19% |
| Standard deviation f.e. | 3.47% | 1.65% | 0.95% | 1.00% | 1.45% | 2.14% |

In general, it was shown that the EDEMT model is capable of predicting the thermal conductivity of long-term nanofluids. Furthermore, it was also shown that the structural morphology of the prepared nanofluids agrees with the physical mechanisms considered for development of the model. This is a characteristic that distinguishes this study from the remaining ones available in the

literature. Many of the predictive models available were developed and validated with modest experimental data, which are, in general, poorly characterized, regarding structural morphology, nanoparticles size distribution, and degree of stability. In addition, this study used a large amount of experimental data, with a special focus on the effect of the nanoparticle geometry and particle volume fraction. These were proved statistically as the parameters with the greatest impact on the effective thermal conductivity. Moreover, as envisaged in Figure 2.19, the consideration of the thermal conductivity of the MWCNTs as 1700 W/mK, did not affected the prediction values for the achieved Kapitza resistance magnitude.

Table 4.8: Fitness estimators of the models available in the literature to the experimental results (DENG et al., 2007, DENG et al., 2009, GENSHENG et al., 2009, KOO et al., 2008, MURSHED et al., 2008, NAN et al., 2004, SASTRY et al., 2008, XUE et al., 2003, XUE, 2005, YU et al., 2004).

| | $r^2$ | *mse* | maximum fractional error | minimum fractional error | average fractional error | standard deviation of f.e. |
|---|---|---|---|---|---|---|
| Xue 2003 (Eq. 1.36) | 0.80533 | 0.00005 | 12.30% | 0.80% | 2.77% | 1.94% |
| Nan *et al.* 2004 (Eq. 1.31) | 0.92956 | 0.00012 | 6.97% | 0.01% | 3.19% | 2.07% |
| Yu-Choi *et al.* 2004 (Eq. 1.37) | 0.78503 | 0.00019 | 14.16% | 0.80% | 3.07% | 2.37% |
| Xue 2005 (Eq. 1.39) | 0.81234 | 0.00124 | 18.83% | 0.44% | 7.40% | 3.65% |
| Murshed *et al.* 2008 (Eq. 1.41) | 0.75164 | 0.00013 | 15.48% | 0.80% | 3.42% | 2.73% |
| Sastry *et al.* 2008 (Eq. 1.42) | 0.80472 | 0.00024 | 14.47% | 0.82% | 3.35% | 2.52% |
| Koo *et al.* 2008 (Eq. 1.48) | 0.85799 | 0.00017 | 12.69% | 0.80% | 2.92% | 2.08% |
| Deng *et al.* 2009 (Eq. 1.50) | 0.79214 | 0.00024 | 14.69% | 0.82% | 3.40% | 2.64% |
| Gensheng *et al.* 2009 (Eq. 1.53) | 0.78006 | 0.00019 | 14.36% | 0.81% | 3.11% | 2.41% |
| *EDEMT model* | *0.95832* | *0.00004* | *4.51%* | *0.01%* | *1.49%* | *0.95%* |

In Table 4.8 and Figure 4.18, it is provided and compared the fitting parameters used, of the predictive models available in the open literature. These, in line with the scatter charts presented in the Appendix J, shows that the predictive models proposed by other researchers seems to worse represent the 360 experimental data of the MWCNTs based nanofluids. As such, the major contribution of this study was the development and calibration of a more generalist predictive model for the effective thermal conductivity of these next-generation thermal fluids. Moreover, this study reveals that the thermal conductivity of nanofluids is non-anomalously high, as announced by some researchers, and can be predicted by the *effective medium theory* (EMT).

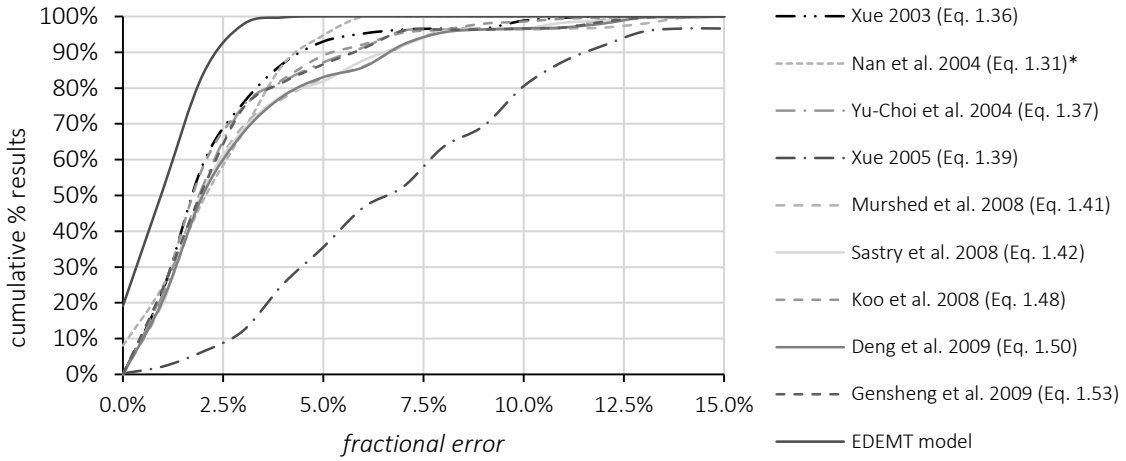


Figure 4.18: Cumulative percentage of experimental data predicted by the models within the fractional error (DENG et al., 2007, DENG et al., 2009, GENSHENG et al., 2009, KOO et al., 2008, MURSHED et al., 2008, NAN et al., 2004, SASTRY et al., 2008, XUE et al., 2003, XUE, 2005, YU et al., 2004).

## 4.5 CHAPTER CONCLUSIONS

In this Chapter, it was provided the experimental apparatus for the determination of nanofluids effective thermal conductivity. The effective thermal conductivity of the MWCNTs based nanofluids was achieved through transient hot-wire, namely *KD2 Pro* from *Decagon Devices*, which provided a maximum deviation of 1.8% from the theoretical values for the base fluids. The experimental results revealed a maximum enhancement of 18.5%, for the nanoparticles with highest length distribution and a volume fraction of 1.5%. A delineated control factor interaction provides the ability to verify the possible existence of the recent theories developed to explain the anomalous behaviour observed. It was found that MWCNTs based nanofluids present non-anomalous behaviour, predictable by the classical theories, *i.e.* the *effective medium theory*. The EDEMT model, based on these theories, seems to fit to the experimental results, with a maximum fractional error of 4.5%, for a Kapitza resistance of $10.5\times10^{-8}$ K m$^2$/W. In addition, the statistical analysis shows that the effective thermal conductivity strongly depends on the MWCNTs geometry and volume fraction, the control factors with high levels of inference.

# 5 CONCLUSIONS

## 5.1 CHAPTER SYNTHESIS

The main objective of this work was the development and characterization of carbon nanotubes based nanofluids, for thermal engineering applications. The available literature reports that the addition of highly conductive nanoparticles to conventional fluids produces a significant increase in their heat conduction characteristics. It was concluded that a long-term nanofluid, with negligible agglomeration and phase separation, will provide long-term thermo-physical properties over long periods, an essential feature towards their industrial application. It should however be mentioned how the dispersion methodology applied induced a certain penalty in what concerns the effective thermal conductivity of the samples associated with the reduction of the length distribution of the nanoparticles. The intrinsic mechanisms responsible for the heat conduction enhancement in these nanofluids were identified, and a predictive model for the effective thermal conductivity of these fluids was proposed and validated. The thermal characterization of the nanofluids was achieved through an experimental parametric analysis, revealing a strong dependence on the nanoparticles size distribution and volume fraction, with a maximum enhancement of 18.5% for the test conditions. Moreover, it was identified that a high Kapitza resistance at the interface of the nanoparticle is a limitation to the thermal conductivity enhancement, also decreasing the contribution of the thermal interparticle interaction.

## 5.2 CONCLUSIONS

This research focus on the development and characterization of nanofluids for heat exchange intensification. The conducted survey on the open literature, revealed that the addition of small amounts of nanoparticles to conventional fluids produces strong enhancements on the effective thermal conductivity of nanofluids. However, the latter also revealed an intriguing behaviour of nanofluids and a considerable lack of agreement between both experimental and theoretical studies.

Among the several thermo-physical properties of nanofluids, the thermal conductivity is still the most studied one. The latter was suggested to have an anomalous behaviour, since it seems to be unpredictable by the classical theories. Several nanoparticles were also studied worldwide, and these can be subdivided in quasi-spherical and non-spherical (or elongated) particles. From

experimental and theoretical results it is evident that elongated nanoparticles, such as multiwalled carbon nanotubes (MWCNTs) provide a higher thermal conductivity enhancement for a given volume fraction. Such results are of utmost importance for appropriate development of nanofluids with improved thermal conductivity but lower viscosities, to keep energy consumption to a minimum.

The classical theories for thermal conductivity enhancement in heterogeneous systems were developed by Maxwell, the *effective medium theory* (EMT), more than a century ago. In this, the particles are considered as spheres, homogeneously dispersed through the medium, at volume fractions so low that thermal interparticle interactions could be neglected. Later, Bruggeman proposed a *differential effective medium theory* (DEMT), enabling the prediction of this property for higher volume fractions. More recently, Nan *et al.* developed an extended EMT that accounts for the particle shape and interfacial thermal resistance, *i.e.* Kapitza resistance. However, this model is only valid for diluted mixtures, since the thermal interparticle interaction is neglected.

In an attempt to describe the anomalous behaviour of the thermal conductivity of nanofluids, a few theories were suggested in addition to the classical ones from which is highlighted the contribution of the (1) Brownian motion of the nanoparticles through collisions and micro-convection, (2) the probability for nanoparticles agglomeration and percolation of heat through the clusters, (3) and the formation of a solid-like layer of base fluid molecules near the interface of the nanoparticles. These theories have encouraged the development of several modern predictive models, with divergent premises.

The survey suggested that the controversial observations might have resulted from the lack of parametric studies, divergent techniques for sample preparation, uncontrolled nanoparticles aggregation and poor stability and unknown nanoparticles size distribution. To the date, the literature does not present a consensual and robust model capable of predicting the thermal conductivity of a generic nanofluid with an acceptable level of accuracy for engineering purposes.

Therefore, the study here presented contributes to the definition of long-term nanofluids and to the breaching of the mechanisms responsible for its effective thermal conductivity enhancement. The term nanofluid should represent a dispersion of nanoparticles in a base fluid (or a mixture of fluids) with structural stability at all operating temperatures, with negligible probability of agglomeration and phase separation. These requisites ensure a slightly constant morphological structure over time, mandatory to ensure persistent long-term thermo-physical properties and,

particularly important for the current research purposes, a correctly assessment to these properties. It should be reminded that, despite the fact that some researchers suggest that the nanoparticles agglomeration may contribute towards the effective thermal conductivity enhancement, this was assumed as a form of instability.

From a well-defined *design of experiments* (DOE), a total of sixty (60) different MWCNTs based nanofluids were estimated, and prepared through a methodology that ensures the preconized stability level. These 60 different fluids are the result of a full factorial arrangement of 6 MWCNTs geometries, dispersed in 2 distinct aqueous solutions of ethylene glycol at 5 volume fractions.

The MWCNTs were functionalized trough a chemical treatment that is capable of introducing carboxylic groups on the side-walls of the nanotubes, as confirmed by the Fourier transform infrared spectroscopy. However, the SEM images analysis revealed an intensive length distribution reduction, in relation to the announced by the manufacturer for the pristine MWCNTs. This is considered as the major drawback of the conducted research, since the results revealed that higher MWCNTs lengths produce higher thermal conductivity enhancement for the same volume fractions. Therefore, it is anticipated the requirement for the development of a similar functionalization technique, yet less destructive. In addition, thermo-gravimetric analysis revealed that the functionalized MWCNTs present a statistically negligible structural damage that contribute to the thermal stability at the test temperatures.

Through a numerical representation of a Brownian model analysis, the interparticle interaction of the functionalized MWCNTs, dispersed in a fluidic medium, were estimated. From this analysis, it was verified that the MWCNTs interact easily, even for the modest volume fractions. Additionally, the obtained numerical results supported that the structural flexibility of the dispersed nanofluids has a negligible impact on their spatial distribution and respective interparticle interaction. It was also verified that the Brownian diffusion of the functionalized MWCNTs is slower than the thermal diffusion of the base fluid, anticipating a negligible impact of the Brownian motion in the effective thermal conductivity enhancement. It should be noted that similar results were obtained by other researches for spherical nanoparticles.

The functionalized MWCNTs were dispersed in the base fluids through ultrasonication. In order to evaluate their long term stability, the produced nanofluids were subjected to a proper stability characterization. The Zeta potential and analytical centrifuge tests revealed that the samples have a low probability of nanoparticle agglomeration, and they may be subjected to high centrifugal

force fields without showing phase separation. Furthermore, these experimental and numerical analyses suggest that the prepared nanofluids present a structural morphology, or spatial distribution of the MWCNTs, as desired and postulated.

The effective thermal conductivity of the long-term MWCNTs based nanofluids were tested at 6 temperatures, performing 360 experimental observations. It was observed a maximum thermal conductivity enhancement of 18.5% for a volume fraction 1.5% of the nanoparticle with higher length distribution. The experimental results revealed that the effective thermal conductivity of the samples strongly depends upon the MWCNTs geometry (size distribution) and volume fraction, revealing that the spatial distribution of the nanoparticles is a key mechanism. Thus, it was shown that it is extremely important to identify the sizes distribution of the MWCNTs. More importantly, the experimental results suggested a non-anomalous behaviour, without revealing none of the recently theoretical mechanisms suggested (Brownian motion, nano-layer structure, and percolation through the agglomerates).

The contribution of the Brownian motion of the nanoparticles was negligible and anticipated by the numerical model, as mentioned. In addition, as verified by other researchers, the contribution of the nano-layer structure, for non-metal liquids is unlikely to occur. They suggest that the contribution of this ordering is only noticeable for crystalline structures due to imperfections that scatter the heat transfer phonon. The contribution of heat percolating though agglomerates, or clusters were avoided through the stability conditions achieved.

Given the lack of a classical predictive model for the thermal conductivity of mixtures of non-spherical nanoparticles with interfacial thermal resistance (or Kapitza resistance), that could interact thermally, it was proposed an extended DEMT. The latter rises from the application of the Bruggeman differential principal to the extended EMT of Nan *et al.,* for very dilute dispersions of spheroids. Therefore, this more generalist model takes into account both the thermal conductivity of the nanoparticle and of the medium, the nanoparticle geometry, the volume fraction and Kapitza resistance. It should be reminded that the EDEMT model also complies with the classical theories.

Nevertheless, due to the deficit of experimental and theoretical research on the magnitude of Kapitza resistance for the studied conditions (nanoscale), it was assumed as an adjustment parameter for the EDEMT model. Even so, it was verified that this adjustment did not force the results to fit the model. The experimental results present satisfactory fitness with the EDEMT

model, suggesting that the effective thermal conductivity of nanofluids may be predicted through the classical theories, after a proper upgrade, in order to account for particle geometry, thermal interparticle interactions and Kapitza resistance. However, it was verified that the magnitude of the Kapitza resistance is a limitation to the thermal conductivity enhancement, since it decreases the equivalent thermal conductivity of the nanoparticles. The 360 experimental observations were predicted with a maximum fractional error lower than 4.5%.

It can be concluded that the EDEMT model is valid and that it can be applied to homogeneous dispersions of MWCNTs, at any volume fraction. However, the model does not account for the nanoparticle agglomeration and, therefore, is unable to predict the thermal conductivity of unstable nanofluids, which is not a major limitation since those are not of a great value for engineering applications.

In addition, the Kapitza resistance magnitude reduces the contribution of the thermal interparticle interaction, and the experimental results can also be predicted through the extended EMT model of Nan *et al.*, yet with a slight divergence from the EDEMT model. Nevertheless, the EDEMT model is considered to be more generalist than this, opening the possibility for the research to decrease the magnitude of the Kapitza resistance.

In summary, this research provides evidences to answer the questions raised in the objectives of the thesis. Namely:

1. What are the stability conditions to achieve long-term CNT based nanofluids for thermal applications?

   The term stability for nanofluids must imply the ability to preserve the engineered thermo-physical properties of these, with negligible variation over the required duty cycle. Therefore, it is of utmost importance that the nanoparticles present low probability of agglomeration and phase separation, during a defined period. In addition, it is detrimental to ensure the geometrical integrity of the nanoparticle in the base fluid, at all operative temperatures. These stability requirements ensure a constant spatial distribution of the nanoparticles that, as seen, contribute for the effective thermal conductivity of the mixture.
2. What are the most important inherent physical mechanisms responsible for the effective thermal conductivity improvement presented by such CNT based nanofluids?

The experimental results have shown that the parameters that contribute for the thermal conductivity of these nanofluids are the size distribution, geometry and volume fraction of the nanoparticles. These, are associated to the degree of spatial distribution and to the contribution of the thermal interparticle interaction to the enhancement of these property. Furthermore, it was seen that the effective thermal conductivity of these mixtures is limited by the Kapitza resistance, which seem to decrease (yet without full elimination) the thermal interparticle interaction.

3. Is it possible to predict the thermal conductivity of CNT based nanofluids through a general physical-mathematical model?

   It was verified that these nanofluids, that respect the structural morphology and stability preconized, can be predicted through a generalized physical mathematical model. These, designated as *extended differential effective medium theory* (EDEMT), take into consideration both thermal conductivity of nanoparticle and medium, the nanoparticle geometry and volume fraction and Kapitza resistance. Given the lack of theoretical formalism for the Kapitza resistance, it was verified that this fits the experimental results for a magnitude of $10.5\times10^{-8}$ K m$^2$/W, predicting the thermal conductivity of nanofluids with a maximum fractional error of 4.5%. The mathematical formulation of the EDEMT model is described in detail in Section 2.5.2.

## 5.3 FUTURE RESEARCHES

The conducted research programme enabled to successfully answer to all the originally proposed research questions. Despite that, additional questions and research ideas were revealed as a natural result of the developed work.

For future work it is of the utmost importance to develop methodologies that allow the covalent functionalization of MWCNTs with carboxylic or equivalent groups, with a lower impact on their original length. Accordingly to the proposed predictive model, the incorporation of longer MWCNTs would produce a stronger enhancement on the effective thermal conductivity; unfortunately this effect was not experimentally verified due to the limitations associated to current functionalization methodologies.

In addition, it is important to deeply study the mechanisms associated with the Kapitza resistance, since this strongly limits the increase in thermal conductivity. From previous theoretical research, it becomes clear that this thermal resistance effect depends of the base fluid thermo-physical properties and surface properties of the nanoparticle. However, given the divergences reported from the experimental results, other mechanisms have to be identified and modelled. The development of a Kapitza resistance predictive model is also of maximum importance, in order to complete the presented study.

Finally, it is imperative a future validation of the EDEMT model, for the effective thermal conductivity of nanofluids based on quasi-spherical nanoparticles. However, it should be ensured that the nanofluids under test retain a structural morphology and stability similar to that proposed herein, in order to ensure the quality of the cross-validation procedure.

The present study revealed that it is possible to develop (quasi-) stable nanofluids, with improved thermal conductivity. However, in order to enable their industrial application, it is of utmost importance to characterize other thermo-physical properties, such as specific density, heat capacity, and viscosity.

# 6 REFERENCES

ALLEN, T. - Particle Size Measurement: Volume 1: Powder sampling and particle size measurement. Springer, 1996. ISBN 9780412729508.

AMROLLAHI, A.; HAMIDI, A. A.; RASHIDI, A. M. - The effects of temperature, volume fraction and vibration time on the thermo-physical properties of a carbon nanotube suspension (carbon nanofluid). Nanotechnology. ISSN 0957-4484. Vol. 19, n.º 31 (2008), p. 315701.

ASHRAE, AMERICAN SOCIETY OF HEATING, REFRIGERATING, AIR-CONDITIONING ENGINEERS - ASHRAE Handbook: Fundamentals. American Society of Heating, Refrigerating and Air-Conditioning Engineers, Inc., 2005. ISBN 1523-7230.

ASSAEL, M. J. [et al.] - Thermal conductivity enhancement in aqueous suspensions of carbon multi-walled and double-walled nanotubes in the presence of two different dispersants. International Journal of Thermophysics. ISSN 0195-928X. Vol. 26, n.º 3 (2005), p. 647-664.

BALASUBRAMANIAN, KANNAN; BURGHARD, MARKO - Chemically Functionalized Carbon Nanotubes. Small. ISSN 1613-6829. Vol. 1, n.º 2 (2005), p. 180-192.

BALBERG, I. [et al.] - Excluded volume and its relation to the onset of percolation. Physical Review B. Vol. 30, n.º 7 (1984a), p. 3933-3943.

BALBERG, I.; BINENBAUM, N.; WAGNER, N. - Percolation Thresholds in the Three-Dimensional Sticks System. Physical Review Letters. Vol. 52, n.º 17 (1984b), p. 1465-1468.

BANERJEE, S.; HEMRAJ-BENNY, T.; WONG, S. S - Covalent Surface Chemistry of Single-Walled Carbon Nanotubes. Advanced Materials. ISSN 1521-4095. Vol. 17, n.º 1 (2005), p. 17-29.

BATCHELOR, G. K. - Sedimentation in a dilute dispersion of spheres. Journal of Fluid Mechanics. ISSN 0022-1120. Vol. 52, n.º 02 (1972), p. 245-268.

BAYRLE, R.; WEIS, O. - Acoustic mismatch model and thermal phonon radiation across a tin/sapphire interface with radiation temperatures between 1.6 and 3.7 K. Journal of Low Temperature Physics. ISSN 0022-2291. Vol. 76, n.º 3-4 (1989), p. 129-141.

BEISER, M.; BICKERT, G.; SCHARFER, P. - Comparison of Sedimentation Behavior and Structure Analysis with Regard to Destabilization Processes in Suspensions. Chemical Engineering & Technology. ISSN 1521-4125. Vol. 27, n.º 10 (2004), p. 1084-1088.

BENVENISTE, Y. - Effective thermal conductivity of composites with a thermal contact resistance between the constituents: Nondilute case. Journal of Applied Physics. Vol. 61, n.º 8 (1987), p. 2840-2843.

BENVENISTE, Y.; MILOH, T. - The effective conductivity of composites with imperfect thermal contact at constituent interfaces. International Journal of Engineering Science. ISSN 0020-7225. Vol. 24, n.º 9 (1986), p. 1537-1552.

BEVINGTON, P.R.; ROBINSON, D.K. - Data reduction and error analysis for the physical sciences. McGraw-Hill, 2003. ISBN 9780072472271.

BIERCUK, M. J. [et al.] - Carbon nanotube composites for thermal management. Applied Physics Letters. ISSN 0003-6951. Vol. 80, n.º 15 (2002), p. 2767-2769.

BÖNNEMANN, H. [et al.] - Monodisperse copper- and silver-nanocolloids suitable for heat-conductive fluids. Applied Organometallic Chemistry. ISSN 1099-0739. Vol. 19, n.º 6 (2005), p. 768-773.

BOTHA, SUBELIA SENARA - Synthesis and characterization of nanofluids for cooling applications. University of the Western Cape, 2007.

BROWN, ROBERT - A brief account of microscopical observations made in the months of June, July and August 1827, on the particles contained in the pollen of plants; and on the general existence of active molecules in organic and inorganic bodies. Philosophical Magazine Series 2. ISSN 1941-5850. Vol. 4, n.º 21 (1828), p. 161 - 173.

BRUGGEMAN, D. A. G. - Calculation of various physical constants in heterogeneous substances. I. Dielectric constants and conductivity of composites from isotropc substances (German). Annalen der Physik. ISSN 1521-3889. Vol. 24, n.º 7 (1935), p. 636-679.

BUONGIORNO, JACOPO [et al.] - A benchmark study on the thermal conductivity of nanofluids. Journal of Applied Physics. Vol. 106, n.º 9 (2009), p. 094312.

CAHILL, DAVID G. [et al.] - Nanoscale thermal transport. Journal of Applied Physics. Vol. 93, n.º 2 (2003), p. 793-818.

CAHILL, DAVID G.; GOODSON, KENNETH; MAJUMDAR, ARUNAVA - Thermometry and Thermal Transport in Micro/Nanoscale Solid-State Devices and Structures. Journal of Heat Transfer. ISSN 0022-1481. Vol. 124, n.º 2 (2001), p. 223-241.

CAO, G. - Nanostructures & Nanomaterials: Synthesis, Properties & Applications. Imperial College Press, 2004. ISBN 9781860944802.

CASTRO, C. A. NIETO DE [et al.] - An apparatus to measure the thermal conductivity of liquids. Journal of Physics E: Scientific Instruments. ISSN 0022-3735. Vol. 9, n.º 12 (1976), p. 1073.

CHEN, G. - Thermal conductivity and ballistic-phonon transport in the cross-plane direction of superlattices. Physical Review B. Vol. 57, n.º 23 (1998), p. 14958-14973.

CHEN, LIFEI [et al.] - Nanofluids containing carbon nanotubes treated by mechanochemical reaction. Thermochimica Acta. ISSN 0040-6031. Vol. 477, n.º 1-2 (2008), p. 21-24.

CHEN, LIFEI; XIE, HUAQING; YU, WEI - Functionalization Methods of Carbon Nanotubes and Its Applications. InTech, Carbon Nanotubes Applications on Electron Devices. ISSN 978-953-307-496-2. (2011).

CHEN, QUAN [et al.] - Aggregation behavior of single-walled carbon nanotubes in dilute aqueous suspension. Journal of Colloid and Interface Science. ISSN 0021-9797. Vol. 280, n.º 1 (2004), p. 91-97.

CHERKASOVA, ANNA S. - Thermal conductivity enhancement in micro- and nano-particle suspensions. University of New Jersey, 2009.

CHOI, S. U.-S. - Nanofluid technology : current status and future research. 1998. ISBN ANL/ET/CP-97466; TRN: AH200128%%525 United StatesTRN: AH200128%%525Mon Feb 04 15:16:16 EST 2008OSTI as DE00011048ANL; EDB-01:070721English.

CHOI, S. U. S. [et al.] - Anomalous thermal conductivity enhancement in nanotube suspensions. Applied Physics Letters. Vol. 79, n.º 14 (2001), p. 2252-2254.

CHOI, SOON-HO [et al.] - Feasibility Study of a New Model for the Thermal Boundary Resistance at Thin Film Interfaces. Journal of the Korean Physical Society. Vol. 44, n.º 2 (2004), p. 317-325.

CHOI, STEPHEN; EASTMAN, JEFFREY- Enhancing thermal conductivity of fluids with nanoparticles**:** ASME International Mechanical Engineering Congress & Exposition. San Francisco, 1995.

CHOY, T.C. - Effective Medium Theory: Principles and Applications. Clarendon Press, 1999. ISBN 9780198518921.

CLANCY, THOMAS C.; GATES, THOMAS S. - Modeling of interfacial modification effects on thermal conductivity of carbon nanotube composites. Polymer. ISSN 0032-3861. Vol. 47, n.º 16 (2006), p. 5990-5996.

DAS, SARIT K. [et al.] - Nanofluids: Science and Technology. New Jersey: Wiley, 2008. ISBN 978-0-470-07473-2.

DAS, SARIT K.; PUTRA, NANDY; ROETZEL, WILFRIED - Pool boiling characteristics of nano-fluids. International Journal of Heat and Mass Transfer. ISSN 0017-9310. Vol. 46, n.º 5 (2003a), p. 851-862.

DAS, SARIT KUMAR [et al.] - Temperature Dependence of Thermal Conductivity Enhancement for Nanofluids. Journal of Heat Transfer. Vol. 25 (2003b), p. 3319-3322.

DASSAULT-SYSTEMES- DraftSight. 2013. Disponível em:<URL:http://www.3ds.com/products-services/draftsight/overview/>.

DAVIS, R. H. - The effective thermal conductivity of a composite material with spherical inclusions. International Journal of Thermophysics. ISSN 0195-928X. Vol. 7, n.º 3 (1986), p. 609-620.

DECAGONDEVICES - Decagon Devices, Thermal Properties Instruments [em linha]. [Consult. Disponível em:<URL:http://www.decagon.com/products/environmental-instruments/Thermal-Properties-Instruments/kd-2-pro/>.

DENG, FEI [et al.] - Effects of anisotropy, aspect ratio, and nonstraightness of carbon nanotubes on thermal conductivity of carbon nanotube composites. Applied Physics Letters. Vol. 90, n.º 2 (2007), p. 021914-3.

DENG, FEI; ZHENG, QUANSHUI - Interaction models for effective thermal and electric conductivities of carbon nanotube composites. Acta Mechanica Solida Sinica. ISSN 0894-9166. Vol. 22, n.º 1 (2009), p. 1-17.

DERJAGUIN, B.; LANDAU, L. - Theory of the stability of strongly charged lyophobic sols and of the adhesion of strongly charged particles in solutions of electrolytes. Progress in Surface Science. ISSN 0079-6816. Vol. 43, n.º 1–4 (1993), p. 30-59.

DING, YULONG [et al.] - Heat transfer of aqueous suspensions of carbon nanotubes (CNT nanofluids). International Journal of Heat and Mass Transfer. ISSN 0017-9310. Vol. 49, n.º 1-2 (2006), p. 240-250.

DING, YULONG [et al.] - Heat transfer intensification using nanofluids. KONA Powder and Particle. ISSN 0288-4534. Vol. 25, n.º 1-2 (2007), p. 23-28.

DUNCAN, MICHAEL A; ROUVRAY, DENNIS H - Microclusters. Scientific American. ISSN 0036-8733. Vol. v261, n.º n6 (1989), p. p110(6).

EAPEN, J.; LI, J.; YIP, S. - Beyond the Maxwell limit: Thermal conduction in nanofluids with percolating fluid structures. Physical Review E - Statistical, Nonlinear, and Soft Matter Physics. Vol. 76, n.º 6 (2007).

EAPEN, JACOB [et al.] - The Classical Nature of Thermal Conduction in Nanofluids. Journal of Heat Transfer. Vol. 132, n.º 10 (2010), p. 102402-14.

EASTMAN, J. A. [et al.] - Enhanced thermal conductivity through the development of nanofluids. Materials Research Society. (1997).

EASTMAN, J. A. [et al.] - Anomalously increased effective thermal conductivities of ethylene glycol-based nanofluids containing copper nanoparticles. Applied Physics Letters. Vol. 78, n.º 6 (2001), p. 718-720.

EASTMAN, J.A. [et al.] - Thermal Transport in Nanofluids. Annu. Rev. Mater. Res. Vol. 34 (2004).

EINSTEIN, A; FÜRTH, R - Investigations on the theory of the Brownian movement. Dover Publications, 1956. ISBN 9780486603049.

ESUMI, K. [et al.] - Chemical treatment of carbon nanotubes. Carbon. ISSN 0008-6223. Vol. 34, n.º 2 (1996), p. 279-281.

EVANS, WILLIAM; FISH, JACOB; KEBLINSKI, PAWEL - Thermal conductivity of ordered molecular water. The Journal of Chemical Physics. Vol. 126, n.º 15 (2007), p. 154504.

EVANS, WILLIAM [et al.] - Effect of aggregation and interfacial thermal resistance on thermal conductivity of nanocomposites and colloidal nanofluids. International Journal of Heat and Mass Transfer. ISSN 0017-9310. Vol. 51, n.º 5-6 (2008), p. 1431-1438.

FAKHRI, NIKTA [et al.]- Diameter-dependent bending dynamics of single-walled carbon nanotubes in liquids. National Academy of Sciences, 2009.

FEDELE, LAURA [et al.] - Experimental stability analysis of different water-based nanofluids. Nanoscale Research Letters. ISSN 1556-276X. Vol. 6, n.º 1 (2011), p. 300.

FEIST, M. [et al.] - Stokesian dynamics and the settling behaviour of particle–fibre-mixtures. The Canadian Journal of Chemical Engineering. ISSN 1939-019X. Vol. 89, n.º 4 (2007), p. 682-690.

FICK, ADOLF - Ueber Diffusion. Annalen der Physik. ISSN 1521-3889. Vol. 170, n.º 1 (1855), p. 59-86.

FRICKE, HUGO - A Mathematical Treatment of the Electric Conductivity and Capacity of Disperse Systems I. The Electric Conductivity of a Suspension of Homogeneous Spheroids. Physical Review. Vol. 24, n.º 5 (1924), p. 575-587.

FRICKE, HUGO - A Mathematical Treatment of the Electric Conductivity and Capacity of Disperse Systems ii. The Capacity of a Suspension of Conducting Spheroids Surrounded by a Non-Conducting Membrane for a Current of Low Frequency. Physical Review. Vol. 26, n.º 5 (1925), p. 678-681.

GAO, LEI; ZHOU, XIAO FENG - Differential effective medium theory for thermal conductivity in nanofluids. Physics Letters A. ISSN 0375-9601. Vol. 348, n.º 3–6 (2006), p. 355-360.

GARG, PARITOSH [et al.] - An experimental study on the effect of ultrasonication on viscosity and heat transfer performance of multi-wall carbon nanotube-based aqueous nanofluids. International Journal of Heat and Mass Transfer. ISSN 0017-9310. Vol. 52, n.º 21–22 (2009), p. 5090-5101.

GE, Z.; URBANA-CHAMPAIGN, UNIVERSITY OF ILLINOIS AT - Nanoscale Thermal Transport at Solid-liquid Interfaces. University of Illinois at Urbana-Champaign, 2006. ISBN 9780542988400.

GENSHENG, WU [et al.] - Thermal Conductivity Measurement for Carbon-Nanotube Suspensions with 3ω Method. Advanced Materials Research. Vol. 60-61 (2009), p. 394-398.

GHADIMI, A.; SAIDUR, R.; METSELAAR, H. S. C. - A review of nanofluid stability properties and characterization in stationary conditions. International Journal of Heat and Mass Transfer. ISSN 0017-9310. Vol. 54, n.º 17–18 (2011a), p. 4051-4068.

GHADIMI, A.; SAIDUR, R.; METSELAAR, H. S. C. - A review of nanofluid stability properties and characterization in stationary conditions. International Journal of Heat and Mass Transfer. ISSN 0017-9310. Vol. 54, n.º 17-18 (2011b), p. 4051-4068.

GOPALAKRISHNAN, J. - Chimie Douce Approaches to the Synthesis of Metastable Oxide Materials. Chemistry of Materials. ISSN 0897-4756. Vol. 7, n.º 7 (1995), p. 1265-1275.

HAAN, S. W.; ZWANZIG, R. - Series expansions in a continuum percolation problem. Journal of Physics A: Mathematical and General. ISSN 0305-4470. Vol. 10, n.º 9 (1977), p. 1547.

Electronic Components and Technology Conference, 2007. ECTC '07. Proceedings. 57th, 2007, Thermal Performance of Carbon Nanotube-Based Composites Investigated by Molecular Dynamics Simulation. City 2007. 269-272 p.

HAMILTON, R. L.; CROSSER, O. K. - Thermal conductivity of heterogeneous two-component systems. Industrial & Engineering Chemistry Fundamentals. ISSN 0196-4313. Vol. 1, n.º 3 (1962), p. 187-191.

HARISH, SIVASANKARAN [et al.] - Enhanced thermal conductivity of ethylene glycol with single-walled carbon nanotube inclusions. International Journal of Heat and Mass Transfer. ISSN 0017-9310. Vol. 55, n.º 13–14 (2012), p. 3885-3890.

HASHIMOTO, TAKEJI [et al.] - Domain-Boundary Structure of Styrene-Isoprene Block Copolymer Films Cast from Toluene Solutions. Macromolecules. ISSN 0024-9297. Vol. 7, n.º 3 (1974), p. 364-373.

HASHIN, Z.; SHTRIKMAN, S. - A Variational Approach to the Theory of the Effective Magnetic Permeability of Multiphase Materials. Journal of Applied Physics. Vol. 33, n.º 10 (1962), p. 3125-3131.

HASSELMAN, D.P.H.; JOHNSON, LLOYD F. - Effective Thermal Conductivity of Composites with Interfacial Thermal Barrier Resistance. Journal of Composite Materials. Vol. 21, n.º 6 (1987), p. 508-515.

HERNADI, K. [et al.] - Catalytic synthesis and purification of carbon nanotubes. Synthetic Metals. ISSN 0379-6779. Vol. 77, n.º 1–3 (1996), p. 31-34.

HERZHAFT, BENJAMIN [et al.] - Experimental study of the sedimentation of dilute and semi-dilute suspensions of fibres. Journal of Fluid Mechanics. ISSN 0022-1120. Vol. 384 (1999), p. 133-158.

HIEMENZ, P.C. - Principles of colloid and surface chemistry. Marcel Dekker Inc., 1977. ISBN 9780824765736.

HILDING, JENNY [et al.] - Dispersion of carbon nanotubes in liquids. Journal of Dispersion Science and Technology. ISSN 0193-2691. Vol. 24, n.º 1 (2003), p. 1-41.

HONE, J. - Carbon nanotubes: thermal properties. Marcel Dekker, Inc. (2002).

HONG, TAE-KEUN; YANG, HO-SOON; CHOI, C. J. - Study of the enhanced thermal conductivity of Fe nanofluids. Journal of Applied Physics. Vol. 97, n.º 6 (2005), p. 064311-4.

HOPKINS, PATRICK E. - Thermal Transport across Solid Interfaces with Nanoscale Imperfections: Effects of Roughness, Disorder, Dislocations, and Bonding on Thermal Boundary Conductance. ISRN Mechanical Engineering. Vol. 2013 (2013), p. 19.

HOPKINS, PATRICK E.; DUDA, JOHN C. - Introduction to Nanoscale Thermal Conduction [em linha]. Heat Transfer - Mathematical Modelling, Numerical Methods and Information Technology: InTech, 2011. [Consult. Disponível em:<URL:http://www.intechopen.com/books/heat-transfer-mathematical-modelling-numerical-methods-and-information-technology/introduction-to-nanoscale-thermal-conduction>. ISBN 978-953-307-550.

HSIEH, YU-CHEN [et al.] - Thermal Analysis of Multi-walled Carbon Nanotubes by Kissinger's Corrected Kinetic Equation Aerosol and Air Quality Research. ISSN: 1680-8584. Vol. 10 (2010), p. 212-218.

HSIN, Y. L. [et al.] - Production and in-situ Metal Filling of Carbon Nanotubes in Water. Advanced Materials. ISSN 1521-4095. Vol. 13, n.º 11 (2001), p. 830-833.

HUXTABLE, SCOTT T. [et al.] - Interfacial heat flow in carbon nanotube suspensions. Nature Mater. ISSN 1476-1122. Vol. 2, n.º 11 (2003), p. 731-734.

HWANG, Y. J. [et al.] - Investigation on characteristics of thermal conductivity enhancement of nanofluids. Current Applied Physics. ISSN 1567-1739. Vol. 6, n.º 6 (2006a), p. 1068-1071.

HWANG, Y. [et al.] - Stability and thermal conductivity characteristics of nanofluids. Thermochimica Acta. ISSN 0040-6031. Vol. 455, n.º 1-2 (2007), p. 70-74.

HWANG, Y. [et al.] - Thermal conductivity and lubrication characteristics of nanofluids. Current Applied Physics. Vol. 6 (2006b), p. e67-e71.

IIJIMA, SUMIO- Helical microtubules of graphitic carbon**:** Nature. 1991.

IIJIMA, SUMIO [et al.] - Structural flexibility of carbon nanotubes. The Journal of Chemical Physics. Vol. 104, n.º 5 (1996), p. 2089-2092.

INCROPERA, FRANK P. [et al.] - Fundamentals of Heat and Mass Transfer. 6. Wiley, 2006. ISBN 978-0-471-45728-2.

INGLE, JAMES D.; CROUCH, STANLEY R. - Spectrochemical analysis. Prentice Hall, 1988.

JACCARD, J. - Interaction Effects in Factorial Analysis of Variance. SAGE Publications, 1998. ISBN 9780761912217.

JANG, SEOK PIL; CHOI, STEPHEN U. S. - Role of Brownian motion in the enhanced thermal conductivity of nanofluids. Applied Physics Letters. Vol. 84, n.º 21 (2004), p. 4316-4318.

JEFFREY, D. J. - Conduction Through a Random Suspension of Spheres. Proceedings of the Royal Society of London. A. Mathematical and Physical Sciences. Vol. 335, n.º 1602 (1973), p. 355-367.

Photonics and Optoelectronics, 2009. SOPO 2009. Symposium on, 2009, Influence of pH on the Stability Characteristics of Nanofluids. City 2009. 1-4 p.

JOSE-YACAMAN, M. [et al.] - Catalytic growth of carbon microtubules with fullerene structure. Applied Physics Letters. Vol. 62, n.º 2 (1993), p. 202-204.

KANAGARAJ, S. [et al.]- Rheological study of nanofluids at different concentration of carbon nanotubes**:** Heat and Mass Transfer Conference. Department of Mechanical Engineering, University of Aveiro. 2008.

KAPITZA, P. L. - Zh. Eksp. Teor. Fiz, J. Phys. USSR. Vol. 4 (1941), p. 181.

KEBLINSKI, P. [et al.] - Mechanisms of heat flow in suspensions of nano-sized particles (nanofluids). International Journal of Heat and Mass Transfer. ISSN 0017-9310. Vol. 45, n.º 4 (2002), p. 855-863.

KEBLINSKI, PAWEL; PRASHER, RAVI; EAPEN, JACOB - Thermal conductance of nanofluids: is the controversy over? Journal of Nanoparticle Research. ISSN 1388-0764. Vol. 10, n.º 7 (2008), p. 1089-1097.

KEIDAR, M.; WAAS, A. M. - On the conditions of carbon nanotube growth in the arc discharge. Nanotechnology. ISSN 0957-4484. Vol. 15, n.º 11 (2004), p. 1571.

KESTIN, J.; WAKEHAM, W. A. - A contribution to the theory of the transient hot-wire technique for thermal conductivity measurements. Physica A: Statistical Mechanics and its Applications. ISSN 0378-4371. Vol. 92, n.º 1–2 (1978), p. 102-116.

KHALATNIKOV, I. M.; ADAMENKO, I.N. - Theory of the Kapitza temperature discontinuity at a solid body-liquid helium boundary. Soviet Physics JETP. Vol. 36 (1973).

KHAN, MESBAH G.; FARTAJ, AMIR - A review on microchannel heat exchangers and potential applications. International Journal of Energy Research. ISSN 1099-114X. Vol. 35, n.º 7 (2011), p. 553-582.

KHANAFER, KHALIL; VAFAI, KAMBIZ - A critical synthesis of thermophysical characteristics of nanofluids. International Journal of Heat and Mass Transfer. ISSN 0017-9310. Vol. 54, n.º 19–20 (2011), p. 4410-4428.

KIM, BO HUNG; BESKOK, ALI; CAGIN, TAHIR - Molecular dynamics simulations of thermal resistance at the liquid-solid interface. The Journal of Chemical Physics. Vol. 129, n.º 17 (2008a), p. 174701.

KIM, JUN YOUNG; HAN, SANG IL; HONG, SEUNGPYO - Effect of modified carbon nanotube on the properties of aromatic polyester nanocomposites. Polymer. ISSN 0032-3861. Vol. 49, n.º 15 (2008b), p. 3335-3345.

KOO, J.; KANG, Y.; KLEINSTREUER, C. - A nonlinear effective thermal conductivity model for carbon nanotube and nanofiber suspensions. Nanotechnology. ISSN 0957-4484. Vol. 19, n.º 37 (2008), p. 375705.

KOO, J.; KLEINSTREUER, C. - A new thermal conductivity model for nanofluids. Journal of Nanoparticle Research. Vol. 6, n.º 6 (2004), p. 577-588.

KOUSHKI, E.; MAJLES ARA, M. H.; AKHERAT DOOST, H. - Thermal conductivity in spherical nanocolloids. International Journal of Thermal Sciences. ISSN 1290-0729. Vol. 69, n.º 0 (2013), p. 14-20.

KUMAR, D. HEMANTH [et al.] - Model for Heat Conduction in Nanofluids. Physical Review Letters. Vol. 93, n.º Copyright (C) 2010 The American Physical Society (2004), p. 144301.

KUMAR, P.; RAMARAO, B. V. - Enhancement of the sedimentation rates of fibrous suspensions. Chemical Engineering Communications. ISSN 0098-6445. Vol. 108, n.º 1 (1991), p. 381-401.

KUMBHARKHANE, A. C.; PURANIK, S. M.; MEHROTRA, S. C. - Temperature dependent dielectric relaxation study of ethylene glycol-water mixtures. Journal of Solution Chemistry. ISSN 0095-9782. Vol. 21, n.º 2 (1992), p. 201-212.

KYRYLYUK, ANDRIY; VAN DER SCHOOT, PAUL - Continuum percolation of carbon nanotubes in polymeric and colloidal media. Proceedings of the National Academy of Sciences. Vol. 105, n.º 24 (2008), p. 8221-8226.

LAGARKOV, A. N.; SARYCHEV, A. K. - Electromagnetic properties of composites containing elongated conducting inclusions. Physical Review B. Vol. 53, n.º 10 (1996), p. 6318-6336.

LANDAU, L.D. [et al.] - Electrodynamics of continuous media. Pergamon, 1984. ISBN 9780080302751.

LAWLESS, J. F. - Truncated Distributions. In: Encyclopedia of Actuarial Science. John Wiley & Sons, Ltd, 2006. ISBN 9780470012505,

LEE, DONGGEUN - Thermophysical Properties of Interfacial Layer in Nanofluids. Langmuir. ISSN 0743-7463. Vol. 23, n.º 11 (2007), p. 6011-6018.

LEE, DONGGEUN; KIM, JAE-WON; KIM, BOG G. - A New Parameter to Control Heat Transport in Nanofluids: Surface Charge State of the Particle in Suspension. The Journal of Physical Chemistry B. ISSN 1520-6106. Vol. 110, n.º 9 (2006), p. 4323-4328.

LEE, J.-H. [et al.] - A Review of Thermal Conductivity Data, Mechanisms and Models for Nanofluids. International Journal of Micro-Nano Scale Transport. Vol. 1 (2010), p. 269-322.

LEE, JI-HWAN [et al.] - Effective viscosities and thermal conductivities of aqueous nanofluids containing low volume concentrations of Al2O3 nanoparticles. International Journal of Heat and Mass Transfer. ISSN 0017-9310. Vol. 51, n.º 11–12 (2008), p. 2651-2656.

LERCHE, D. - Dispersion Stability and Particle Characterization by Sedimentation Kinetics in a Centrifugal Field. Journal of Dispersion Science and Technology. ISSN 0193-2691. Vol. 23, n.º 5 (2002), p. 699 - 709.

LI, CALVIN H.; PETERSON, G. P. - Experimental investigation of temperature and volume fraction variations on the effective thermal conductivity of nanoparticle suspensions (nanofluids). Journal of Applied Physics. Vol. 99, n.º 8 (2006), p. 084314-8.

LI, XINFANG; ZHU, DONGSHENG; WANG, XIANJU - Evaluation on dispersion behavior of the aqueous copper nano-suspensions. Journal of Colloid and Interface Science. ISSN 0021-9797. Vol. 310, n.º 2 (2007), p. 456-463.

LI, YANJIAO [et al.] - A review on development of nanofluid preparation and characterization. Powder Technology. ISSN 0032-5910. Vol. 196, n.º 2 (2009), p. 89-101.

LIDE, D.R. - CRC Handbook of Chemistry and Physics, 85th Edition. Taylor & Francis, 2004. ISBN 9780849304859.

LISUNOVA, MILANA O. [et al.] - Stability of the aqueous suspensions of nanotubes in the presence of nonionic surfactant. Journal of Colloid and Interface Science. ISSN 0021-9797. Vol. 299, n.º 2 (2006), p. 740-746.

LIU, M.; LIN, M. C.; WANG, C. - Enhancements of thermal conductivities with Cu, CuO, and carbon nanotube nanofluids and application of MWNT/water nanofluid on a water chiller system. Nanoscale Research Letters. ISSN 1556276X. Vol. 6, n.º 1 (2011), p. 297.

LIU, MIN-SHENG [et al.] - Enhancement of thermal conductivity with carbon nanotube for nanofluids. International Communications in Heat and Mass Transfer. ISSN 0735-1933. Vol. 32, n.º 9 (2005), p. 1202-1210.

LIU, MIN-SHENG [et al.] - Enhancement of thermal conductivity with Cu for nanofluids using chemical reduction method. International Journal of Heat and Mass Transfer. ISSN 0017-9310. Vol. 49, n.º 17-18 (2006), p. 3028-3033.

LO, CHIH-HUNG [et al.] - Fabrication of copper oxide nanofluid using submerged arc nanoparticle synthesis system (SANSS). Journal of Nanoparticle Research. Vol. 7, n.º 2 (2005), p. 313-320.

MAXWELL, JAMES CLERK - A treatise on electricity and magnetism. 3. Oxford: Clarendon Press, 1873.

MEIBODI, MAJID EMAMI [et al.] - The role of different parameters on the stability and thermal conductivity of carbon nanotube/water nanofluids. International Communications in Heat and Mass Transfer. ISSN 0735-1933. Vol. 37, n.º 3 (2010), p. 319-323.

MERCHAN-MERCHAN, WILSON [et al.] - Combustion synthesis of carbon nanotubes and related nanostructures. Progress in Energy and Combustion Science. ISSN 0360-1285. Vol. 36, n.º 6 (2010), p. 696-727.

MEYYAPPAN, M. - Carbon Nanotubes: Science and Applications. Boca Raton: CRC Press, 2004. ISBN 0-8493-2748-2.

MINKOWYCZ, W.J.; SPARROW, E.M.; ABRAHAM, J.P. - Nanoparticle Heat Transfer and Fluid Flow. Taylor & Francis, 2012. ISBN 9781439861929.

MISSANA, TIZIANA; ADELL, ANDRÉS - On the Applicability of DLVO Theory to the Prediction of Clay Colloids Stability. Journal of Colloid and Interface Science. ISSN 0021-9797. Vol. 230, n.º 1 (2000), p. 150-156.

MOHAMMED, H. A. [et al.] - Heat transfer and fluid flow characteristics in microchannels heat exchanger using nanofluids: A review. Renewable and Sustainable Energy Reviews. ISSN 1364-0321. Vol. 15, n.º 3 (2011), p. 1502-1512.

MURSHED, S. M. S.; LEONG, K. C.; YANG, C. - A combined model for the effective thermal conductivity of nanofluids. Applied Thermal Engineering. ISSN 1359-4311. Vol. 29, n.º 11–12 (2009), p. 2477-2483.

MURSHED, S. M. S.; LEONG, K. C.; YANG, C. - Investigations of thermal conductivity and viscosity of nanofluids. International Journal of Thermal Sciences. ISSN 1290-0729. Vol. 47, n.º 5 (2008), p. 560-568.

NAGASAKA, Y.; NAGASHIMA, A. - Absolute measurement of the thermal conductivity of electrically conducting liquids by the transient hot-wire method. Journal of Physics E: Scientific Instruments. ISSN 0022-3735. Vol. 14, n.º 12 (1981), p. 1435.

NAN, C. W.; SHI, Z.; LIN, Y. - A simple model for thermal conductivity of carbon nanotube-based composites. Chemical Physics Letters. ISSN 0009-2614. Vol. 375, n.º 5-6 (2003), p. 666-669.

NAN, C.W. - Physics of inhomogeneous inorganic materials. Progress in Materials Science. Vol. 37 (1993), p. 1-116.

NAN, CE-WEN [et al.] - Effective thermal conductivity of particulate composites with interfacial thermal resistance. Journal of Applied Physics. Vol. 81, n.º 10 (1997), p. 6692-6699.

NAN, CE-WEN [et al.] - Interface effect on thermal conductivity of carbon nanotube composites. Applied Physics Letters. Vol. 85, n.º 16 (2004), p. 3549-3551.

NASEH, MASOUD VESALI [et al.] - Fast and clean functionalization of carbon nanotubes by dielectric barrier discharge plasma in air compared to acid treatment. Carbon. ISSN 0008-6223. Vol. 48, n.º 5 (2010), p. 1369-1379.

NASIRI, AIDA [et al.] - Effect of dispersion method on thermal conductivity and stability of nanofluid. Experimental Thermal and Fluid Science. ISSN 0894-1777. Vol. 35, n.º 4 (2011), p. 717-723.

NGUYEN, C. T. [et al.] - Temperature and particle-size dependent viscosity data for water-based nanofluids - Hysteresis phenomenon. International Journal of Heat and Fluid Flow. ISSN 0142-727X. Vol. 28, n.º 6 (2007), p. 1492-1506.

OH, DONG-WOOK [et al.] - Thermal conductivity measurement and sedimentation detection of aluminum oxide nanofluids by using the 3[omega] method. International Journal of Heat and Fluid Flow. ISSN 0142-727X. Vol. 29, n.º 5 (2008), p. 1456-1461.

ORDONEZ-MIRANDA, J.; ALVARADO-GIL, J. J. - Thermal conductivity of nanocomposites with high volume fractions of particles. Composites Science and Technology. ISSN 0266-3538. Vol. 72, n.º 7 (2012a), p. 853-857.

ORDÓÑEZ-MIRANDA, J.; ALVARADO-GIL, J. J.; MEDINA-EZQUIVEL, R. - Generalized Bruggeman Formula for the Effective Thermal Conductivity of Particulate Composites with an Interface Layer. International Journal of Thermophysics. ISSN 0195-928X. Vol. 31, n.º 4-5 (2010), p. 975-986.

ORDONEZ-MIRANDA, J.; YANG, RONGGUI; ALVARADO-GIL, J. J. - A model for the effective thermal conductivity of metal-nonmetal particulate composites. Journal of Applied Physics. Vol. 111, n.º 4 (2012b), p. 044319-12.

ORDONEZ-MIRANDA, J.; YANG, RONGGUI; ALVARADO-GIL, J. J. - On the thermal conductivity of particulate nanocomposites. Applied Physics Letters. Vol. 98, n.º 23 (2011), p. -.

PATEL, HRISHIKESH E. [et al.] - Thermal conductivities of naked and monolayer protected metal nanoparticle based nanofluids: Manifestation of anomalous enhancement and chemical effects. Applied Physics Letters. Vol. 83, n.º 14 (2003), p. 2931-2933.

PATEL, HRISHIKESHE [et al.] - A micro-convection model for thermal conductivity of nanofluids. Pramana. ISSN 0304-4289. Vol. 65, n.º 5 (2005), p. 863-869.

PENAS, JOSE R. VAZQUEZ; ZARATE, JOSE M. ORTIZ DE; KHAYET, MOHAMED - Measurement of the thermal conductivity of nanofluids by the multicurrent hot-wire method. Journal of Applied Physics. Vol. 104, n.º 4 (2008), p. 044314.

PENG, HAIQING [et al.] - Sidewall Carboxylic Acid Functionalization of Single-Walled Carbon Nanotubes. Journal of the American Chemical Society. ISSN 0002-7863. Vol. 125, n.º 49 (2003), p. 15174-15182.

PERRIN, JEAN - Brownian Movement and Molecular Reality. Dover Publications, 2005. ISBN 0486442578.

PIKE, G. E.; SEAGER, C. H. - Percolation and conductivity: A computer study. I. Physical Review B. Vol. 10, n.º 4 (1974), p. 1421-1434.

POIRIER, D. R; GEIGER, GORDON H. (GORDON HAROLD) - Transport phenomena in materials processing / D.R. Poirier, G.H. Geiger. Minerals, Metals & Materials Society, 1994. ISBN 0873392728.

POLLACK, GERALD L. - Kapitza Resistance. Reviews of Modern Physics. Vol. 41, n.º 1 (1969), p. 48-81.

PONMOZHI, J. - Water based nanofluids development and characterization. Univeristy of Aveiro, 2009. 125 f.

PONMOZHI, J. [et al.] - Thermodynamic and transport properties of CNT- water based nanofluids. Journal of Nano Research. Vol. 11 (2009), p. 101-106.

POPA, IONEL [et al.] - Attractive and Repulsive Electrostatic Forces between Positively Charged Latex Particles in the Presence of Anionic Linear Polyelectrolytes. The Journal of Physical Chemistry B. ISSN 1520-6106. Vol. 114, n.º 9 (2010), p. 3170-3177.

PRASHER, RAVI; BHATTACHARYA, PRAJESH; PHELAN, PATRICK E. - Thermal Conductivity of Nanoscale Colloidal Solutions (Nanofluids). Physical Review Letters. Vol. 94, n.º Copyright (C) 2010 The American Physical Society (2005), p. 025901.

PRASHER, RAVI; PHELAN, PATRICK E.; BHATTACHARYA, PRAJESH - Effect of Aggregation Kinetics on the Thermal Conductivity of Nanoscale Colloidal Solutions (Nanofluid). Nano Letters. ISSN 1530-6984. Vol. 6, n.º 7 (2006), p. 1529-1534.

RAAB, CHRISTINA [et al.] - Production of nanoparticles and nanomaterials. Nanotrust dossiers. ISSN 1998-7293. Vol. 006en (2011).

RAHIMPOUR, AHMAD [et al.] - Novel functionalized carbon nanotubes for improving the surface properties and performance of polyethersulfone (PES) membrane. Desalination. ISSN 0011-9164. Vol. 286, n.º 0 (2012), p. 99-107.

REFRACTOMETER - Refractive index of ethylene glycol solutions [em linha]. [Consult. Disponível em:<URL:http://www.refractometer.pl/refraction-datasheet-ethylene-glycol>.

REIF, FEDERICK- Fundamentals of Statistical and Thermal Physics. International Edition 1985. Singapore: McGraw-Hill, 1965. ISBN/ISSN 0-07-085615-X.

RICHARDSON, J. F.; ZAKI, W. N. - Sedimentation and fluidisation: part I. Trans. Instn. Chem. Engrs. Vol. 32 (1954), p. -53.

RODER, HANS M. - A Transient Hot Wire Thermal Conductivity Apparatus for Fluids. Journal of Research of the National Bureau of Standards. Vol. 86, n.º 5 (1981).

RUSSEL, W.B.; SAVILLE, D.A.; SHOWALTER, W.R.- Colloidal Dispersions. Cambridge: Cambridge University Press, 1989. ISBN/ISSN 0521341884.

SABBAGHZADEH, JAMSHID; EBRAHIMI, SADOLLAH - Effective Thermal Conductivity of Nanofluids containing cylindrical nanoparticles. International Journal of Nanoscience. Vol. 06, n.º 01 (2007), p. 45-49.

SASTRY, N. N. VENKATA [et al.] - Predicting the effective thermal conductivity of carbon nanotube based nanofluids. Nanotechnology. ISSN 0957-4484. Vol. 19, n.º 5 (2008), p. 055704.

SCHNITZLER, MARIANEC; ZARBIN, ALDOJ G. - The effect of process variables on the characteristics of carbon nanotubes obtained by spray pyrolysis. Journal of Nanoparticle Research. ISSN 1388-0764. Vol. 10, n.º 4 (2008), p. 585-597.

SETARAM - Setsys Evolution [em linha]. [Consult. Disponível em:<URL:http://www.setaram.com/SETSYS-Evolution-TGA-DTA-DSC.htm>.

SHAFFER, M. S. P.; FAN, X.; WINDLE, A. H. - Dispersion and packing of carbon nanotubes. Carbon. ISSN 0008-6223. Vol. 36, n.º 11 (1998), p. 1603-1612.

SHENOGIN, S. [et al.] - Effect of chemical functionalization on thermal transport of carbon nanotube composites. AIP, 2004a.

SHENOGIN, SERGEI [et al.] - Role of thermal boundary resistance on the heat flow in carbon-nanotube composites. Journal of Applied Physics. ISSN 0021-8979. Vol. 95, n.º 12 (2004b), p. 8136-8144.

SHENOGINA, N. [et al.] - On the lack of thermal percolation in carbon nanotube composites. Applied Physics Letters. Vol. 87 (2005), p. 6-9.

SHIM, JAE-WOON; PARK, SOO-JIN; RYU, SEUNG-KON - Effect of modification with HNO3 and NaOH on metal adsorption by pitch-based activated carbon fibers. Carbon. ISSN 0008-6223. Vol. 39, n.º 11 (2001), p. 1635-1642.

SIDDIQUE, M. [et al.] - Recent Advances in Heat Transfer Enhancements: A Review Report. International Journal of Chemical Engineering. Vol. 2010 (2010).

SNOOK, IAN K.; HENDERSON, DOUGLAS - Monte Carlo study of a hard-sphere fluid near a hard wall. The Journal of Chemical Physics. Vol. 68, n.º 5 (1978), p. 2134-2139.

SONICS & MATERIALS, INC. - [em linha]. [Consult. Disponível em:<URL:http://www.sonics.biz/lp-accessories-large.htm>.

STAUFFER, D. - Scaling theory of percolation clusters. Physics Reports. ISSN 0370-1573. Vol. 54, n.º 1 (1979), p. 1-74.

STOKES, GEORGE GABRIEL - On the Effect of the Internal Friction of Fluids on the Motion of Pendulums Mathematical and Physical Papers. Cambridge University Press, 1850.

STONER, R. J.; MARIS, H. J. - Kapitza conductance and heat flow between solids at temperatures from 50 to 300 K. Physical Review B. Vol. 48, n.º 22 (1993), p. 16373-16387.

SWARTZ, E. T.; POHL, R. O. - Thermal boundary resistance. Reviews of Modern Physics. Vol. 61, n.º 3 (1989), p. 605-668.

TAGUCHI, G. - System of experimental design: engineering methods to optimize quality and minimize costs. UNIPUB/Kraus International Publications, 1987. ISBN 9780941243001.

TALAEI, ZEINAB [et al.] - The effect of functionalized group concentration on the stability and thermal conductivity of carbon nanotube fluid as heat transfer media. International Communications in Heat and Mass Transfer. ISSN 0735-1933. Vol. 38, n.º 4 (2011), p. 513-517.

TAYLOR, J.R. - An Introduction to Error Analysis: The Study of Uncertainties in Physical Measurements. University Science Books, 1997. ISBN 9780935702750.

TORQUATO, S. - Random Heterogeneous Materials: Microstructure and Macroscopic Properties. Springer, 2002. ISBN 9780387951676.

TURNEY, MICHAEL A. [et al.] - Hindered settling of rod-like particles measured with magnetic resonance imaging. AIChE Journal. ISSN 1547-5905. Vol. 41, n.º 2 (1995), p. 251-257.

VAISMAN, LINDA; WAGNER, H. DANIEL; MAROM, GAD - The role of surfactants in dispersion of carbon nanotubes. Advances in Colloid and Interface Science. ISSN 0001-8686. Vol. 128-130 (2006), p. 37-46.

VEINGNON, SOMJATE [et al.] - Development of Carbon Nanotube - Reinforced Silk and Cannabis Fibers by an Electrophoretic Deposition Method. Materials Science Forum. Vol. 695 (2011), p. 377-380.

VENERUS, DAVID C. [et al.] - Study of thermal transport in nanoparticle suspensions using forced Rayleigh scattering. Journal of Applied Physics. Vol. 100, n.º 9 (2006), p. 094310-5.

VERWEY, E.J.W.; OVERBEEK, J.T.G. - Theory of the Stability of Lyophobic Colloids. Dover Publications, 1999. ISBN 9780486409290.

WANG, BU-XUAN; ZHOU, LE-PING; PENG, XIAO-FENG - A fractal model for predicting the effective thermal conductivity of liquid with suspension of nanoparticles. International Journal of Heat and Mass Transfer. ISSN 0017-9310. Vol. 46, n.º 14 (2003a), p. 2665-2672.

WANG, CHENCHEN [et al.] - Chemical functionalization of carbon nanotubes by carboxyl groups on stone-wales defects: a density functional theory study. The Journal of Physical Chemistry B. ISSN 1520-6106. Vol. 110, n.º 21 (2006), p. 10266-10271.

WANG, XINWEI; XU, XIANFAN; CHOI, STEPHEN U. S. - Thermal conductivity of nanoparticle–fluid mixture. Journal of Thermophysics and Heat Transfer. Vol. 13 (1999), p. 474-480.

WANG, YAO; WU, JUN; WEI, FEI - A treatment method to give separated multi-walled carbon nanotubes with high purity, high crystallization and a large aspect ratio. Carbon. ISSN 0008-6223. Vol. 41, n.º 15 (2003b), p. 2939-2948.

WEBA-TECHNOLOGY- Glycol-Based Heat Transfer Fluid Technical Manual. 2003. [Consult. 04/11/2013]. Disponível em:<URL:http://www.webacorp.com/HTF-Manual.pdf>.

WEI, WANG [et al.] - A Comprehensive Model for the Enhanced Thermal Conductivity of Nanofluids. Journal of Advanced Research in Physics. Vol. 3, n.º 021209 (2012).

WEITING, JIANG; GUOLIANG, DING; HAO, PENG - Measurement and model on thermal conductivities of carbon nanotube nanorefrigerants. International Journal of Thermal Sciences. ISSN 1290-0729. Vol. 48, n.º 6 (2009), p. 1108-1115.

WEPASNICK, KEVINA [et al.] - Chemical and structural characterization of carbon nanotube surfaces. Analytical and Bioanalytical Chemistry. ISSN 1618-2642. Vol. 396, n.º 3 (2010), p. 1003-1014.

WHITE, FRANK M. - Fluid Mechanics. 6th. MC Graw Hill, 1998.

WILSON, ORLA M. [et al.] - Colloidal metal particles as probes of nanoscale thermal transport in fluids. Physical Review B. Vol. 66, n.º 22 (2002), p. 224301.

WONG, S. S.; BANERJEE, S. - Functionalization of carbon nanotubes with a metal-containing molecular complex. Nano Letters. ISSN 1530-6984. Vol. 2, n.º 1 (2002), p. 49-53.

XIAO, BOQI; YANG, YI; CHEN, LINGXIA - Developing a novel form of thermal conductivity of nanofluids with Brownian motion effect by means of fractal geometry. Powder Technology. ISSN 0032-5910. Vol. 239, n.º 0 (2013), p. 409-414.

XIE, HUAQING; CHEN, LIFEI - Adjustable thermal conductivity in carbon nanotube nanofluids. Physics Letters A. ISSN 0375-9601. Vol. 373, n.º 21 (2009), p. 1861-1864.

XIE, HUAQING; CHEN, LIFEI - Review on the Preparation and Thermal Performances of Carbon Nanotube Contained Nanofluids. Journal of Chemical & Engineering Data. ISSN 0021-9568. Vol. 56, n.º 4 (2011), p. 1030-1041.

XIE, HUAQING; FUJII, MOTOO; ZHANG, XING - Effect of interfacial nanolayer on the effective thermal conductivity of nanoparticle-fluid mixture. International Journal of Heat and Mass Transfer. ISSN 0017-9310. Vol. 48, n.º 14 (2005), p. 2926-2932.

XIE, HUAQING [et al.] - Nanofluids containing multiwalled carbon nanotubes and their enhanced thermal conductivities. Journal of Applied Physics. Vol. 94, n.º 8 (2003), p. 4967-4971.

XIE, HUAQING [et al.] - Thermal conductivity enhancement of suspensions containing nanosized alumina particles. Journal of Applied Physics. Vol. 91, n.º 7 (2002), p. 4568-4572.

XUAN, YIMIN; LI, QIANG - Heat transfer enhancement of nanofluids. International Journal of Heat and Fluid Flow. Vol. 21 (2000), p. 58-64.

XUAN, YIMIN; LI, QIANG; HU, WEIFENG - Aggregation structure and thermal conductivity of nanofluids. AIChE Journal. ISSN 1547-5905. Vol. 49, n.º 4 (2003), p. 1038-1043.

XUE, L. [et al.] - Effect of liquid layering at the liquid–solid interface on thermal transport. International Journal of Heat and Mass Transfer. ISSN 0017-9310. Vol. 47, n.º 19–20 (2004), p. 4277-4284.

XUE, L. [et al.] - Two regimes of thermal resistance at a liquid--solid interface. The Journal of Chemical Physics. Vol. 118, n.º 1 (2003), p. 337-339.

XUE, Q. Z. - Model for thermal conductivity of carbon nanotube-based composites. Physica B: Condensed Matter. ISSN 0921-4526. Vol. 368, n.º 1-4 (2005), p. 302-307.

XUE, QING-ZHONG - Model for effective thermal conductivity of nanofluids. Physics Letters A. ISSN 0375-9601. Vol. 307, n.º 5-6 (2003), p. 313-317.

YAJIE, REN; HUAQING, XIE; AN, CAI - Effective thermal conductivity of nanofluids containing spherical nanoparticles. Journal of Physics D: Applied Physics. ISSN 0022-3727. Vol. 38, n.º 21 (2005), p. 3958.

YAKOBSON, B. I.; BRABEC, C. J.; BERNHOLC, J. - Nanomechanics of Carbon Tubes: Instabilities beyond Linear Response. Physical Review Letters. Vol. 76, n.º 14 (1996), p. 2511.

YOO, DAE-HWANG; HONG, K. S.; YANG, HO-SOON - Study of thermal conductivity of nanofluids for the application of heat transfer fluids. Thermochimica Acta. ISSN 0040-6031. Vol. 455, n.º 1-2 (2007), p. 66-69.

YOUNG, D. A.; MARIS, H. J. - Lattice-dynamical calculation of the Kapitza resistance between fcc lattices. Physical Review B. Vol. 40, n.º 6 (1989), p. 3685-3693.

YU, W.; CHOI, S. U. S. - The role of interfacial layers in the enhanced thermal conductivity of nanofluids: A renovated Hamilton–Crosser model. Journal of Nanoparticle Research. Vol. 6, n.º 4 (2004), p. 355-361.

YU, W.; CHOI, S. U. S. - The Role of Interfacial Layers in the Enhanced Thermal Conductivity of Nanofluids: A Renovated Maxwell Model. Journal of Nanoparticle Research. ISSN 1388-0764. Vol. 5, n.º 1-2 (2003), p. 167-171.

YU, WEI [et al.] - Investigation on the thermal transport properties of ethylene glycol-based nanofluids containing copper nanoparticles. Powder Technology. ISSN 0032-5910. Vol. 197, n.º 3 (2010), p. 218-221.

YU, WEI [et al.] - Highly Efficient Method for Preparing Homogeneous and Stable Colloids Containing Graphene Oxide. Nanoscale Research Letters. ISSN 1931-7573. Vol. 6, n.º 1 (2011), p. 1-7.

YUDIANTI, RIKE [et al.] - Analysis of functional group sited on multi-wall carbon nanotube surface. The Open Materials Science Journal. Vol. 5 (2011), p. 242-247.

ZHANG, JIN [et al.] - Effect of Chemical Oxidation on the Structure of Single-Walled Carbon Nanotubes. The Journal of Physical Chemistry B. ISSN 1520-6106. Vol. 107, n.º 16 (2003), p. 3712-3718.

ZHANG, XING; GU, HUA; FUJII, MOTOO - Effective thermal conductivity and thermal diffusivity of nanofluids containing spherical and cylindrical nanoparticles. Journal of Applied Physics. Vol. 100, n.º 4 (2006), p. 044325-5.

ZHAO, XINYUAN; VANDERBILT, DAVID - Phonons and lattice dielectric properties of zirconia. Physical Review B. Vol. 65, n.º 7 (2002), p. 075105.

ZHONG, HONGLIANG; LUKES, JENNIFER R. - Interfacial thermal resistance between carbon nanotubes: Molecular dynamics simulations and analytical thermal modeling. Physical Review B. Vol. 74, n.º 12 (2006), p. 125403.

ZHOU, WEI; XU, JIANWEN; SHI, WENFANG - Surface modification of multi-wall carbon nanotube with ultraviolet-curable hyperbranched polymer. Thin Solid Films. ISSN 0040-6090. Vol. 516, n.º 12 (2008), p. 4076-4082.

ZHU, HAI-TAO; LIN, YU-SHENG; YIN, YAN-SHENG - A novel one-step chemical method for preparation of copper nanofluids. Journal of Colloid and Interface Science. ISSN 0021-9797. Vol. 277, n.º 1 (2004), p. 100-103.

# APPENDIX

## A. EXCLUDED VOLUME THEORY

The excluded volume of a particle is defined as the volume around a particle which the centre of another similar particle is not allowed to enter if overlapping of the two particles is to be avoided. This is an efficient concept to ascertain the degree of interparticle contacts on a dispersion (BALBERG et al., 1984a, BALBERG et al., 1984b). According to this theory, the excluded volume of a randomly oriented capped cylinder $\langle V \rangle$ can be expressed as:

$$\langle V \rangle = \frac{4\pi}{3} \cdot d_p^3 + 2\pi \cdot l_p \cdot d_p^{\,2} + 2 \cdot l_p^2 \cdot d_p \cdot \langle \sin\gamma \rangle \qquad \text{A.1}$$

where $\gamma$ is the average angle over all possible solid angles between two rigid cylinders. For an isotropic case $\langle \sin\gamma \rangle = \pi/4$.

This expression can be reduced to the excluded volume of a sphere when $l_p=0$. Such reduction is possible because the first term of the Equation A.1 represents the capped section of a cylinder. Furthermore, for high aspect ratio cylinders, $l_p^{\,2} \cdot d_p \cdot \pi/2 \gg 2\pi \cdot l_p \cdot d_p^{\,2}$, the excluded volume could be simplified for (BALBERG et al., 1984b):

$$\langle V \rangle \approx \frac{\pi}{2} \cdot l_p^{\,2} \cdot d_p \qquad \text{A.2}$$

The total excluded volume of the system $\langle V_{ex} \rangle$ is the excluded volume of one particle multiplied by the number of particles $n$. The average number of particles in contact to a given particle, $B$, is conceptually and numerically the same as the $\langle V_{ex} \rangle$, and could be expressed as:

$$\langle V_{ex} \rangle \equiv B = n \langle V \rangle \qquad \text{A.3}$$

where $n = \phi / (6\pi \cdot d_p^{\,3})$, for spherical particles and $n = 4 \cdot \phi / (\pi \cdot d_p^{\,2} \cdot l_p)$ for uncapped cylinders.

Through Monte Carlo simulations, it was found that $B$ at the percolation threshold, or $B_c$, is for ≈1.4 for uncapped rigid cylinders, and ≈2.8 for spherical particles. These results were in agreement with Pike *et al.* and Haan *et al.* (BALBERG et al., 1984a, HAAN et al., 1977, PIKE et al., 1974). Therefore, the critical volume fraction of monodispersed uncapped cylinders can be expressed as:

$$\phi_c \approx \frac{B_c}{2} \cdot \frac{d_p}{l_p} \qquad \text{A.4}$$

## B. BASE FLUID THERMO-PHYSICAL PROPERTIES

Table B.1: Thermo-physical properties of DW+30%EG (ASHRAE, 2005, WEBA-TECHNOLOGY, 2003).

| Temperature [K] | Thermal conductivity [W/mK] | Viscosity [Pa s] | Density [kg/m³] | Specific heat capacity [kJ/kg K] |
|---|---|---|---|---|
| 283.15 | 0.442 | 0.003 | 1050.0 | 3.617 |
| 293.15 | 0.453 | 0.002 | 1046.4 | 3.648 |
| 298.15 | 0.459 | 0.002 | 1044.5 | 3.663 |
| 303.15 | 0.464 | 0.002 | 1042.5 | 3.678 |
| 313.15 | 0.473 | 0.001 | 1037.9 | 3.704 |
| 323.15 | 0.481 | 0.001 | 1032.9 | 3.734 |

Table B.2: Thermo-physical properties of DW+60%EG (ASHRAE, 2005, WEBA-TECHNOLOGY, 2003).

| Aqueous solution of 60% ethylene glycol | | | | |
|---|---|---|---|---|
| Temperature [K] | Thermal conductivity [W/mK] | Viscosity [Pa s] | Density [kg/m³] | Specific heat capacity [kJ/kg K] |
| 283.15 | 0.340 | 0.008 | 1092.0 | 3.044 |
| 293.15 | 0.349 | 0.005 | 1087.5 | 3.085 |
| 298.15 | 0.352 | 0.005 | 1085.1 | 3.107 |
| 303.15 | 0.355 | 0.004 | 1082.6 | 3.130 |
| 313.15 | 0.360 | 0.003 | 1077.1 | 3.174 |
| 323.15 | 0.365 | 0.002 | 1071.3 | 3.216 |

## C. EFFECTIVE THERMAL CONDUCTIVITY EXPERIMENTAL LAYOUT

Table C.1: Effective thermal conductivity experimental layout.

| Run | MWCNTs | Base fluid | $\phi$ [%] | Temperature [K] |
|---|---|---|---|---|
| 1 to 6 | *d*50-80 /10-20 | DW+30%EG | 0.25% | 283.15 to 313.15 |
| 7 to 12 | | | 0.50% | |
| 13 to 18 | | | 0.75% | |
| 19 to 24 | | | 1.00% | |
| 25 to 30 | | | 1.50% | |
| 31 to 36 | | DW+60%EG | 0.25% | |
| 37 to 42 | | | 0.50% | |
| 43 to 48 | | | 0.75% | |
| 49 to 54 | | | 1.00% | |
| 55 to 60 | | | 1.50% | |
| 61 to 66 | *d*60-100 /5-15 | DW+30%EG | 0.25% | 283.15 to 313.15 |
| 67 to 72 | | | 0.50% | |
| 73 to 78 | | | 0.75% | |
| 79 to 84 | | | 1.00% | |
| 85 to 90 | | | 1.50% | |
| 91 to 96 | | DW+60%EG | 0.25% | |
| 97 to 102 | | | 0.50% | |
| 103 to 108 | | | 0.75% | |
| 109 to 114 | | | 1.00% | |
| 115 to 120 | | | 1.50% | |
| 121 to 126 | *d*60-100 /1-2 | DW+30%EG | 0.25% | 283.15 to 313.15 |
| 127 to 132 | | | 0.50% | |
| 133 to 138 | | | 0.75% | |
| 139 to 144 | | | 1.00% | |
| 145 to 150 | | | 1.50% | |
| 151 to 156 | | DW+60%EG | 0.25% | |
| 157 to 162 | | | 0.50% | |
| 163 to 168 | | | 0.75% | |
| 169 to 174 | | | 1.00% | |
| 175 to 180 | | | 1.50% | |
| 181 to 186 | *d*20-30 /10-30 | DW+30%EG | 0.25% | 283.15 to 313.15 |
| 187 to 192 | | | 0.50% | |
| 193 to 198 | | | 0.75% | |
| 199 to 204 | | | 1.00% | |
| 205 to 210 | | | 1.50% | |
| 211 to 216 | | DW+60%EG | 0.25% | |
| 217 to 222 | | | 0.50% | |
| 223 to 228 | | | 0.75% | |
| 229 to 234 | | | 1.00% | |

| Run | MWCNTs | Base fluid | $\phi$ [%] | Temperature [K] |
|---|---|---|---|---|
| 235 to 240 | | | 1.50% | |
| 241 to 246 | | | 0.25% | |
| 247 to 252 | | | 0.50% | |
| 253 to 258 | | DW+30%EG | 0.75% | |
| 259 to 264 | | | 1.00% | |
| 265 to 270 | | | 1.50% | |
| 271 to 276 | *d*20-30 *l*5-15 | | 0.25% | 283.15 to 313.1 |
| 277 to 282 | | | 0.50% | |
| 283 to 288 | | DW+60%EG | 0.75% | |
| 289 to 294 | | | 1.00% | |
| 295 to 300 | | | 1.50% | |
| 301 to 306 | | | 0.25% | |
| 307 to 312 | | | 0.50% | |
| 313 to 318 | | DW+30%EG | 0.75% | |
| 319 to 324 | | | 1.00% | |
| 325 to 330 | | | 1.50% | |
| 331 to 336 | *d*20-30 *l*1-2 | | 0.25% | 283.15 to 313.15 |
| 337 to 342 | | | 0.50% | |
| 343 to 348 | | DW+60%EG | 0.75% | |
| 349 to 354 | | | 1.00% | |
| 355 to 360 | | | 1.50% | |

# D. EXPERIMENTAL UNCERTAINTIES ANALYSIS

No physical quantity can be measured with perfect certainty, *i.e.* there are always errors, or uncertainties, in any experimental measurement. It is known that uncertainties are an unavoidable part of the experiments. In order to increase the confidence on the results it is, therefore, required the estimation of the uncertainty (BEVINGTON et al., 2003, TAYLOR, 1997).

## D.1 VOLUME FRACTION EXPERIMENTAL UNCERTAINTIES

As described in Equation 3.2, the measurement of the volume fraction depends on the both measurements of the carbon nanotubes mass and base fluid volume. Therefore, it is distinguishable that the uncertainty on the volume fractions developed has the propagation of the experimental errors of the mentioned quantities. This uncertainty propagation is given as (BEVINGTON et al., 2003, TAYLOR, 1997):

$$\Delta\phi=\sqrt{\left(\frac{\partial\phi}{\partial m_{CNT}}\right)^2\cdot\Delta m_{CNT}{}^2+\left(\frac{\partial\phi}{\partial V_{bf}}\right)^2\cdot\Delta V_{bf}{}^2} \quad \text{D.1}$$

Which, considering Equation 3.2 becomes:

$$\Delta\phi=\sqrt{\left(\frac{\rho_{CNT}\cdot V_{bf}}{\left(m_{CNT}\cdot\rho_{CNT}+V_{bf}\right)^2}\right)^2\cdot\Delta m_{CNT}{}^2+\left(\frac{-m_{CNT}\cdot\rho_{CNT}}{\left(m_{CNT}\cdot\rho_{CNT}+V_{bf}\right)^2}\right)^2\cdot\Delta V_{bf}{}^2} \quad \text{D.2}$$

where,

$$\Delta V_{bf}=\Delta V_{DW}+\Delta V_{EG}=2\cdot\Delta V=1\ ml \quad \text{D.3}$$

$$\Delta m_{CNT}=0.001\ g \quad \text{D.4}$$

## D.2 NANOPARTICLES SIZES DISTRIBUTIONS UNCERTAINTIES

The diameter and length distribution of the after dispersed MWCNTs were measured through SEM images analysis. However, it is known that these sizes were measured on a projection of the particles in a 2D plan, providing an uncertainty of difficulty to estimate. Even so, it was considered that these sizes comply within a normal distribution, enabling to estimate the 95% confidence interval of the samples, as well as the 95% confidence interval of the means considered for the reaming study.

However, the functionalized MWCNTs, presented a higher length reduction. This reduction developed a normal distribution that predicts negative lengths. Therefore, considering the nature of the nanoparticles, and the physical impossibility of such negative lengths, it was assumed that these comply within truncated normal distributions. These simple truncated normal distributions (truncated in 0 μm) requires the adjustment of the average and standard deviation of the lengths, which are provided ahead.

It was considered normal (and truncated) distributions, since the samples size is high (>100, see Table 3.6) and the t-student distribution converge to the normal distribution (see Table D.3, in Appendix D.6), despite the sample is a portion of the population.

In addition, the methodology to verify the goodness-of-fit of the distributions is also provided ahead.

### *D.2.1 DIAMETER DISTRIBUTION UNCERTAINTIES*

As mentioned, the diameters of the functionalized MWCNTs were considered to comply within normal distributions. Normal distributions have mean $\overline{d_p}$ and standard deviation $\sigma$ .The $\sigma$ of the diameters distributions mean can be expressed as:

$$\sigma=\sqrt{\frac{1}{N-1}\cdot\sum_{i=1}^{N}\left(d_{p_i}-\overline{d_p}\right)^2} \qquad \text{D.5}$$

where $N$ is the sample size (see Table 3.6).

The probability density function can be expressed as:

$$f\left(d_{p_i}\right)=\frac{1}{\sigma\sqrt{2\pi}}e^{-\frac{\left(d_{p_i}-\overline{d_p}\right)^2}{2\sigma^2}} \qquad \text{D.6}$$

From this, the 95% confidence interval of the diameter distribution, ranges from:

$$\left[\overline{d_p}-Z\sigma\,;\,\overline{d_p}+Z\sigma\right] \qquad \text{D.7}$$

where $Z$=1.96 (see Table D.3, in Appendix D.6) (BEVINGTON et al., 2003, TAYLOR, 1997).

The estimated 95% confidence interval for the expected mean size $\overline{d}_p$, is given by:

$$\overline{d}_{p_{expected}} = \overline{d}_p \pm \Delta\overline{d}_p \qquad \text{D.8}$$

where

$$\Delta\overline{d}_p = Z \cdot \frac{\sigma}{\sqrt{N}} \qquad \text{D.9}$$

where $N$ is given in Table 3.6 (BEVINGTON et al., 2003, TAYLOR, 1997).

### *D.2.2 LENGTH DISTRIBUTION UNCERTAINTIES*

As mentioned, the lengths distribution of the functionalized MWCNTs were very reduced, regarding the announced by the manufacturers to the pristine. As it will be seen, these produced an asymmetric distribution, with higher frequency to the left. Appling normal distributions to these results, led to part of the left tail of the distribution be on $\mathbb{R}^-$, an impossibility. As noticeable, this led to non-fitness of the results to the normal distributions.

Therefore, to improve the fitness of the results to the normal distributions, these were truncated in the interval ]0 ; +∞[, which describes the physical nature of the particles. The truncated normal distribution is a probability distribution from a normal distribution, were the values have, at least one bound (LAWLESS, 2006), in these case at the left, 0. Nevertheless, it should be noted that these are derived from a normal distribution, calculated in a similar way to the described in the previous Section.

The probability density function of the truncated normal distribution can be expressed as (LAWLESS, 2006):

$$f_{tru}(l_{p_i}) = \begin{cases} \dfrac{\dfrac{1}{\sigma\sqrt{2\pi}} e^{-\frac{\left(l_{p_i}-\overline{l}_p\right)^2}{2\sigma^2}}}{1-F(0)}, & \& \quad 0<l_p<+\infty \\ 0, & \& \quad l_p \leq 0 \end{cases} \qquad \text{D.10}$$

where $F(0)$ is the cumulative probability for the truncated bound, obtained from the original normal distributions.

Normal distributions have mean $\overline{l_p}$ and standard deviation $\sigma$ .Nevertheless, the truncated normal distributions provides variation in these quantities. The truncated mean $\overline{l_{p_{tru}}}$ can be estimated through the following expression:

$$\overline{l_{p_{tru}}} = \overline{l_p} + \frac{\varphi(\alpha)}{1-F(0)} \cdot \sigma \qquad \text{D.11}$$

where $\alpha = \left(a - \overline{l_p}\right)/\sigma$, and $a$ is the left bound of the truncated distribution, $a=0$, and $\varphi(\alpha)$ is the standard normal distribution of $\alpha$.

The truncated standard deviation $\sigma_{tru}$ of the truncated length distributions mean can be expressed as:

$$\sigma_{tru} = (1-\delta)\sqrt{\frac{1}{N-1} \cdot \sum_{i=1}^{N} \left(l_{p_i} - \overline{l_p}\right)^2} \qquad \text{D.12}$$

where $N$ is the sample size (see Table 3.6), and $\delta = \varphi(\alpha)/(1-F(0))$.

From this, the 95% confidence interval of the truncated length distributions, ranges from:

$$\left[\overline{l_{p_{tru}}} - Z\sigma_{tru} \; ; \overline{l_{p_{tru}}} + Z\sigma_{tru}\right] \qquad \text{D.13}$$

where $Z$=1.96 (see Table D.3, in Appendix D.6) (BEVINGTON et al., 2003, TAYLOR, 1997).

The estimated 95% confidence interval for the expected mean size $\overline{d_p}$, is given by:

$$\overline{l_{p_{tru}}}_{expected} = \overline{l_{p_{tru}}} \pm \Delta\overline{l_{p_{tru}}} \qquad \text{D.14}$$

where

$$\Delta\overline{l_{p_{tru}}} = Z \cdot \frac{\sigma_{tru}}{\sqrt{N}} \qquad \text{D.15}$$

where $N$ is given in Table 3.6 (BEVINGTON et al., 2003, TAYLOR, 1997).

### D.2.3 GOODNESS-OF-FIT FOR NORMAL DISTRIBUTION

It is important to demonstrate evidences on the fitness to the experimental measurements in the normal and truncated normal distributions predicted. There are several techniques to verify the goodness-of-fit of a distribution. Among these are the probability graphs and the $\chi^2$ test.

In Appendix F are provided comparisons of the cumulative probability graphs predicted through the respective normal and truncated normal distributions (for each MWCNTs geometry) with the cumulative frequency (in %) of the observed values. In these it seems that the frequency predicted by the normal or truncated normal distributions presents satisfactory fitness to the observed values.

In addition, evidences of the goodness-of-fit of the normal and truncated distributions where carried through $\chi^2$ test. In this, the $\chi^2$ of the estimated distribution through the following equation (TAYLOR, 1997):

$$\chi^2 = \sum \frac{O_X - E_X}{E_X} \qquad \text{D.16}$$

where $O_X$ is the frequency of observed values (diameter or length) and $E_X$ is the frequency of the expected ones. The later can be predicted through the respective distribution function multiplied by the sample size.

For simplicity, the $O_X$ and $E_X$ are transformed in categories through the following expression:

$$\Phi = \frac{O_{X_i} - \bar{\bar{O}_X}}{\sigma_{O_X}} \qquad \text{D.17}$$

where $\sigma$ is the standard deviation. This simplicity enables to categorize the problem in 4 groups, namely $\Phi < -1$, $-1 < \Phi < 0$, $0 < \Phi < 1$, and $\Phi > 1$.

Then the $\chi^2_{distribution}$ is compared with a theoretical one ($\chi^2_{theoretical}$), obtained from a table (TAYLOR, 1997). When $\chi^2_{distribution} > \chi^2_{theoretical}$ it could be considered that the normal and truncated normal distributions presents satisfactory fitness to the measurements. These results are summarized in Table D.1. In this, it is corroborated the results also obtained through the graphical approach.

Table D.1: Main results of the goodness-of-fit $\chi^2$ test to the normal distributions.

| | | diameter distribution | length distribution |
|---|---|---|---|
| | $\chi^2$ theoretical | $\chi^2$ distribution | $\chi^2$ distribution |
| *d*50-80 /10-20 | 7.815 | 1.686 | 5.223 |
| *d*60-100 /5-15 | 7.815 | 1.461 | 6.722 |
| *d*60-100 /1-2 | 7.815 | 2.683 | 7.512 |
| *d*20-40 /10-30 | 7.815 | 2.882 | 5.586 |
| *d*20-40 /5-15 | 7.815 | 2.629 | 5.450 |
| *d*20-40 /1-2 | 7.815 | 5.972 | 6.379 |

In the previous Table it was considered a p-value of 0.05 and 3 *degrees of freedom*, since the $\chi^2_{distribution}$ where grouped in 4 categories.

## D.3 EXPERIMENTAL ZETA POTENTIAL UNCERTAINTIES

As mentioned in Section 3.8.1, the *Malvern ZS Nano S* analyser was used to measure the Zeta potential of the dispersed MWCNTs. For each of the prepared samples, 5 independent runs were taken and the respective mean calculated. Nevertheless, in each of these runs, the *Malvern ZS Nano S* analyser performed several measurements, until converge to good quality criteria, such as good data distribution, among others. From these, the software of the instrument uses the Smoluchoski equation to estimate the zeta potential, and automatically calculate and provided the mean standard deviation and mean standard error. Therefore, in this case, the considered uncertainty of the measurements was the average of the 5 mean standard error estimated by the experimental apparatus. In Table D.2, is provided the mentioned mean standard error of each run and the overall mean uncertainty for each sample.

Table D.2: Standard error of the measurements, for each run, and respective overall mean uncertainty, predicted by Smoluchowski.

| MWCNTs | Base fluid | COV [%] | $\Delta\xi_1$ | $\Delta\xi_2$ | $\Delta\xi_3$ | $\Delta\xi_4$ | $\Delta\xi_5$ | $\overline{\Delta\xi}$ |
|---|---|---|---|---|---|---|---|---|
| *d*50-80 /10-20 | DW+30%EG | 2.03% | 3.50 | 3.87 | 3.47 | 3.50 | 3.60 | 3.50 |
| | DW+60%EG | 4.61% | 5.63 | 6.33 | 5.32 | 5.60 | 4.05 | 5.63 |
| *d*60-100 /5-15 | DW+30%EG | 1.73% | 4.67 | 4.30 | 4.60 | 4.57 | 5.63 | 4.67 |
| | DW+60%EG | 1.62% | 4.32 | 4.78 | 4.38 | 5.47 | 4.23 | 4.32 |
| *d*60-100 /1-2 | DW+30%EG | 3.15% | 4.30 | 3.67 | 4.17 | 3.93 | 3.93 | 4.30 |
| | DW+60%EG | 3.01% | 3.98 | 4.60 | 4.13 | 4.60 | 4.17 | 3.98 |
| *d*20-40 /10-30 | DW+30%EG | 1.23% | 3.29 | 3.60 | 3.77 | 3.90 | 3.60 | 3.29 |
| | DW+60%EG | 2.51% | 4.97 | 6.12 | 4.53 | 5.32 | 5.02 | 4.97 |
| *d*20-40 /5-15 | DW+30%EG | 1.42% | 5.90 | 5.17 | 4.53 | 5.17 | 5.00 | 5.90 |
| | DW+60%EG | 2.60% | 5.37 | 5.37 | 4.98 | 4.47 | 5.40 | 5.37 |
| *d*20-40 /1-2 | DW+30%EG | 1.84% | 5.13 | 5.00 | 5.33 | 4.57 | 4.90 | 5.13 |
| | DW+60%EG | 2.59% | 6.15 | 5.07 | 4.73 | 4.43 | 4.65 | 6.15 |

where COV is the coefficient of variance of the results.

## D.4 EXPERIMENTAL PHASE SEPARATION RATE UNCERTAINTIES

The *Stability Analyser LUMiSizer 6120* was used to assess the mean phase separation rate at high RCF, as explained in detail in 3.8.2. From these measurements, the standard deviation error of the mean phase separation rate at high RCF was automatically estimated by the instrument *LUMiSizer* during the readings, which were considered as the experimental uncertainties for the respective RCF.

Nevertheless, these readings are used to extrapolate the results for gravity conditions and, therefore, the uncertainty for these condition should be estimated. As mentioned, the extrapolation was performed, considering a linear correlation between the phase separation rate and the RCF, $y=m_c x$. Therefore, the mean standard deviation for gravity condition, i.e., RCF=1, was estimated through the following expression (TAYLOR, 1997):

$$\Delta y=\sqrt{\frac{\sum_{i=1}^{N}\left(y_i-m_c\cdot x_i\right)^2}{N-2}} \qquad \text{D.18}$$

## D.5 EXPERIMENTAL THERMAL CONDUCTIVITY UNCERTAINTIES

As envisaged in Section 4.2, the KD2-Pro has a declared accuracy of 5%. However, the experimental apparatus calibration for the base fluids presented repeatability of the measurements, with a maximum deviation of 1.2%. Even so, a t-Student distribution was considered to estimate the limits of the confidence interval of the experimental thermal conductivity mean. The t-Student distribution was selected since it was considered that the variance of the sample is an unknown parameter. As such, the standard deviation $\sigma$ of the effective thermal conductivity mean can be expressed as:

$$\sigma=\sqrt{\frac{1}{N-1}\cdot\sum_{i=1}^{N}(k_i-\bar{k})^2} \qquad \text{D.19}$$

where $\bar{k}$ is the thermal conductivity mean, and $N$ is the sample size ($N\geq10$, since the at least 10 consecutives data points are measured, for each run).

The estimated 95% confidence interval for the expected mean experimental thermal conductivity, for 9 degrees of freedom, is given by:

$$\bar{k}_{expected}=\bar{k}\pm\Delta\bar{k} \quad \text{D.20}$$

where

$$\Delta\bar{k}=t_{.975}.\frac{\sigma}{\sqrt{N}} \quad \text{D.21}$$

where $t_{.975}$ =2.262 (see Table D.3, in Appendix D.6) (BEVINGTON et al., 2003, TAYLOR, 1997).

## D.6 STANDARD TABLE OF STUDENT'S T AND NORMAL DISTRIBUTION

Table D.3: Standard table of student's t and normal distribution (TAYLOR, 1997).

| t table | | | | | | | | | | | | |
|---|---|---|---|---|---|---|---|---|---|---|---|---|
| | Probability | $t_{.50}$ | $t_{.75}$ | $t_{.80}$ | $t_{.85}$ | $t_{.90}$ | $t_{.95}$ | $t_{.975}$ | $t_{.99}$ | $t_{.995}$ | $t_{.999}$ | $t_{.9995}$ |
| *degrees of freedom* | 1 | 0 | 1.000 | 1.376 | 1.963 | 3.078 | 6.314 | 12.710 | 31.820 | 63.660 | 318.310 | 636.620 |
| | 2 | 0 | 0.816 | 1.061 | 1.386 | 1.886 | 2.92 | 4.303 | 6.965 | 9.925 | 22.327 | 31.599 |
| | 3 | 0 | 0.765 | 0.978 | 1.250 | 1.638 | 2.353 | 3.182 | 4.541 | 5.841 | 10.215 | 12.924 |
| | 4 | 0 | 0.741 | 0.941 | 1.190 | 1.533 | 2.132 | 2.776 | 3.747 | 4.604 | 7.173 | 8.610 |
| | 5 | 0 | 0.727 | 0.92 | 1.156 | 1.476 | 2.015 | 2.571 | 3.365 | 4.032 | 5.893 | 6.869 |
| | 6 | 0 | 0.718 | 0.906 | 1.134 | 1.440 | 1.943 | 2.447 | 3.143 | 3.707 | 5.208 | 5.959 |
| | 7 | 0 | 0.711 | 0.896 | 1.119 | 1.415 | 1.895 | 2.365 | 2.998 | 3.499 | 4.785 | 5.408 |
| | 8 | 0 | 0.706 | 0.889 | 1.108 | 1.397 | 1.860 | 2.306 | 2.896 | 3.355 | 4.501 | 5.041 |
| | 9 | 0 | 0.703 | 0.883 | 1.100 | 1.383 | 1.833 | ***2.262*** | 2.821 | 3.25 | 4.297 | 4.781 |
| | 10 | 0 | 0.700 | 0.879 | 1.093 | 1.372 | 1.812 | 2.228 | 2.764 | 3.169 | 4.144 | 4.587 |
| | 11 | 0 | 0.697 | 0.876 | 1.088 | 1.363 | 1.796 | 2.201 | 2.718 | 3.106 | 4.025 | 4.437 |
| | 12 | 0 | 0.695 | 0.873 | 1.083 | 1.356 | 1.782 | 2.179 | 2.681 | 3.055 | 3.930 | 4.318 |
| | 13 | 0 | 0.694 | 0.870 | 1.079 | 1.350 | 1.771 | 2.160 | 2.650 | 3.012 | 3.852 | 4.221 |
| | 14 | 0 | 0.692 | 0.868 | 1.076 | 1.345 | 1.761 | 2.145 | 2.624 | 2.977 | 3.787 | 4.140 |
| | 15 | 0 | 0.691 | 0.866 | 1.074 | 1.341 | 1.753 | 2.131 | 2.602 | 2.947 | 3.733 | 4.073 |
| | 16 | 0 | 0.69 | 0.865 | 1.071 | 1.337 | 1.746 | 2.120 | 2.583 | 2.921 | 3.686 | 4.015 |
| | 17 | 0 | 0.689 | 0.863 | 1.069 | 1.333 | 1.740 | 2.110 | 2.567 | 2.898 | 3.646 | 3.965 |
| | 18 | 0 | 0.688 | 0.862 | 1.067 | 1.33 | 1.734 | 2.101 | 2.552 | 2.878 | 3.610 | 3.922 |
| | 19 | 0 | 0.688 | 0.861 | 1.066 | 1.328 | 1.729 | 2.093 | 2.539 | 2.861 | 3.579 | 3.883 |
| | 20 | 0 | 0.687 | 0.86 | 1.064 | 1.325 | 1.725 | 2.086 | 2.528 | 2.845 | 3.552 | 3.850 |
| | 21 | 0 | 0.686 | 0.859 | 1.063 | 1.323 | 1.721 | 2.080 | 2.518 | 2.831 | 3.527 | 3.819 |
| | 22 | 0 | 0.686 | 0.858 | 1.061 | 1.321 | 1.717 | 2.074 | 2.508 | 2.819 | 3.505 | 3.792 |
| | 23 | 0 | 0.685 | 0.858 | 1.060 | 1.319 | 1.714 | 2.069 | 2.500 | 2.807 | 3.485 | 3.768 |
| | 24 | 0 | 0.685 | 0.857 | 1.059 | 1.318 | 1.711 | 2.064 | 2.492 | 2.797 | 3.467 | 3.745 |
| | 25 | 0 | 0.684 | 0.856 | 1.058 | 1.316 | 1.708 | 2.06 | 2.485 | 2.787 | 3.450 | 3.725 |
| | 26 | 0 | 0.684 | 0.856 | 1.058 | 1.315 | 1.706 | 2.056 | 2.479 | 2.779 | 3.435 | 3.707 |
| | 27 | 0 | 0.684 | 0.855 | 1.057 | 1.314 | 1.703 | 2.052 | 2.473 | 2.771 | 3.421 | 3.690 |
| | 28 | 0 | 0.683 | 0.855 | 1.056 | 1.313 | 1.701 | 2.048 | 2.467 | 2.763 | 3.408 | 3.674 |
| | 29 | 0 | 0.683 | 0.854 | 1.055 | 1.311 | 1.699 | 2.045 | 2.462 | 2.756 | 3.396 | 3.659 |
| | 30 | 0 | 0.683 | 0.854 | 1.055 | 1.31 | 1.697 | 2.042 | 2.457 | 2.750 | 3.385 | 3.646 |
| | 40 | 0 | 0.681 | 0.851 | 1.05 | 1.303 | 1.684 | 2.021 | 2.423 | 2.704 | 3.307 | 3.551 |
| | 60 | 0 | 0.679 | 0.848 | 1.045 | 1.296 | 1.671 | 2.000 | 2.390 | 2.660 | 3.232 | 3.460 |
| | 80 | 0 | 0.678 | 0.846 | 1.043 | 1.292 | 1.664 | 1.99 | 2.374 | 2.639 | 3.195 | 3.416 |
| | 100 | 0 | 0.677 | 0.845 | 1.042 | 1.290 | 1.660 | 1.984 | 2.364 | 2.626 | 3.174 | 3.390 |
| | ∞ | 0 | 0.675 | 0.842 | 1.037 | 1.282 | 1.646 | ***1.962*** | 2.330 | 2.581 | 3.098 | 3.300 |
| normal dist. | *Z* | 0 | 0.674 | 0.842 | 1.036 | 1.282 | 1.645 | ***1.960*** | 2.326 | 2.576 | 3.090 | 3.291 |
| | C.I. | 0% | 50% | 60% | 70% | 80% | 90% | 95% | 98% | 99% | 99.80% | 99.90% |

# E. Thermo-Gravimetric Analysis

## E.1 *d*50-80 /10-20

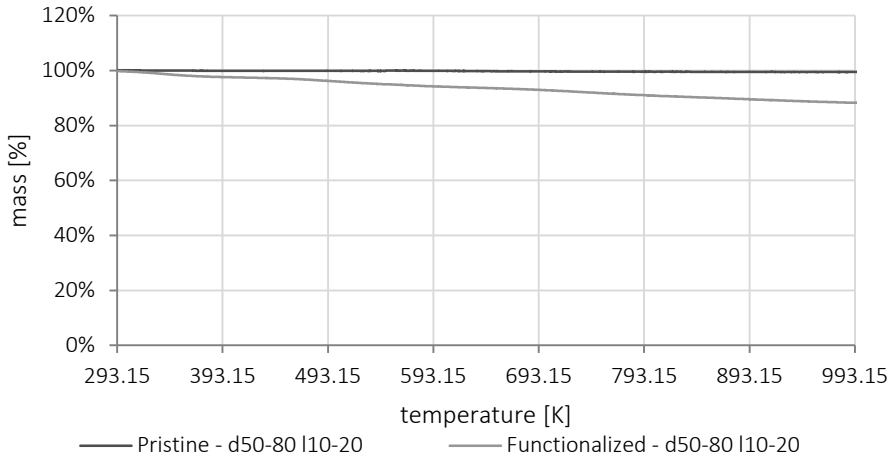


Figure E.1: TGA of functionalized and pristine MWCNTs (*d*50-80 /10-20).

## E.2 *d*60-100 /5-15

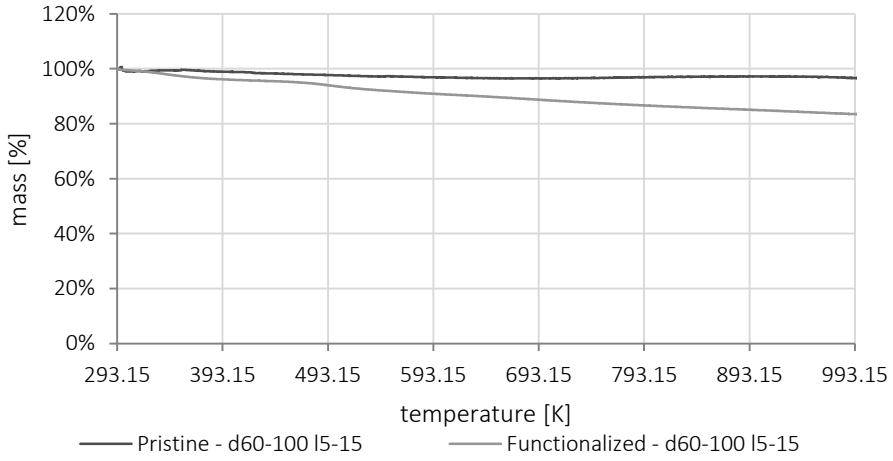


Figure E.2: TGA of functionalized and pristine MWCNTs (*d*60-100 /5-15).

## E.3 *d*60-100 *l*1-2

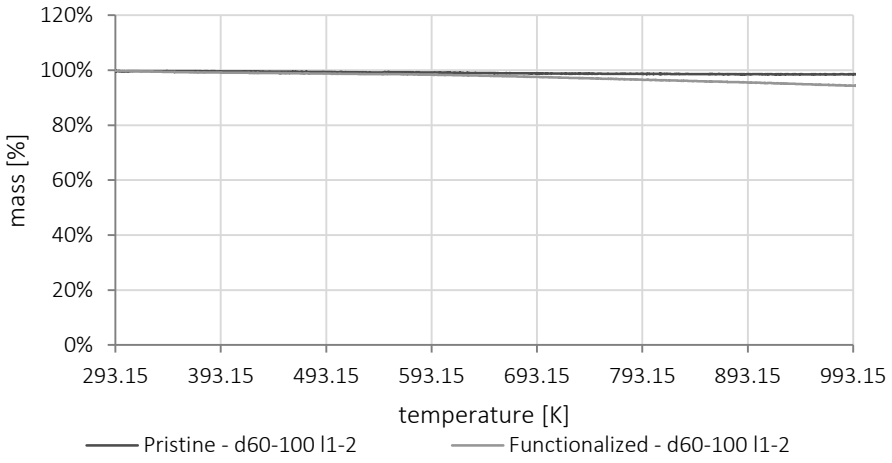


Figure E.3: TGA of functionalized and pristine MWCNTs (*d*60-100 *l*1-2).

## E.4 *d*20-40 *l*10-30

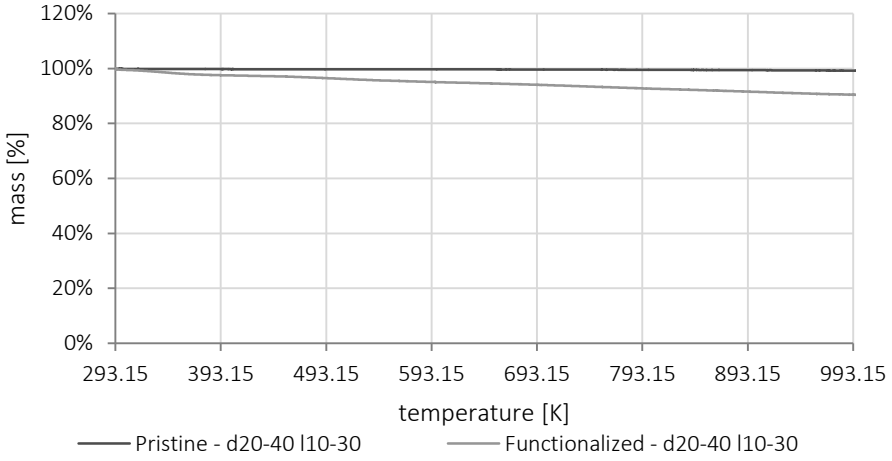


Figure E.4: TGA of functionalized and pristine MWCNTs (*d*20-40 *l*10-30).

## E.5 *d*20-40 *l*5-15

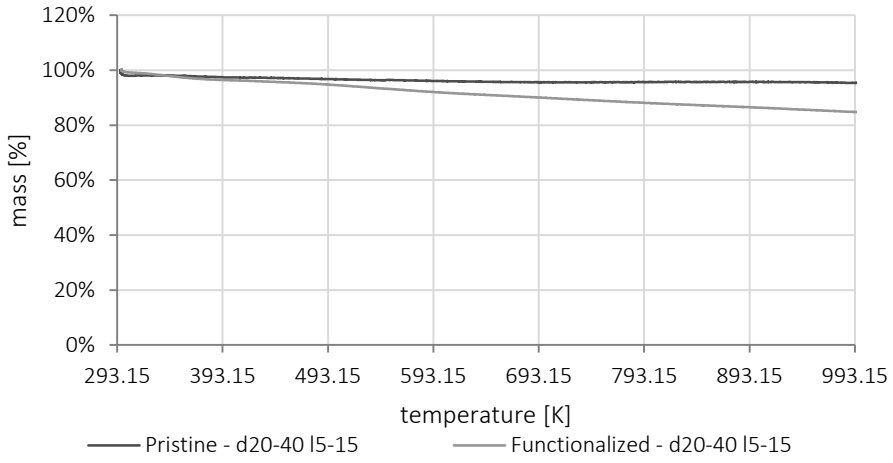


Figure E.5: TGA of functionalized and pristine MWCNTs (*d*20-40 *l*5-15).

## E.6 *d*20-40 *l*1-2

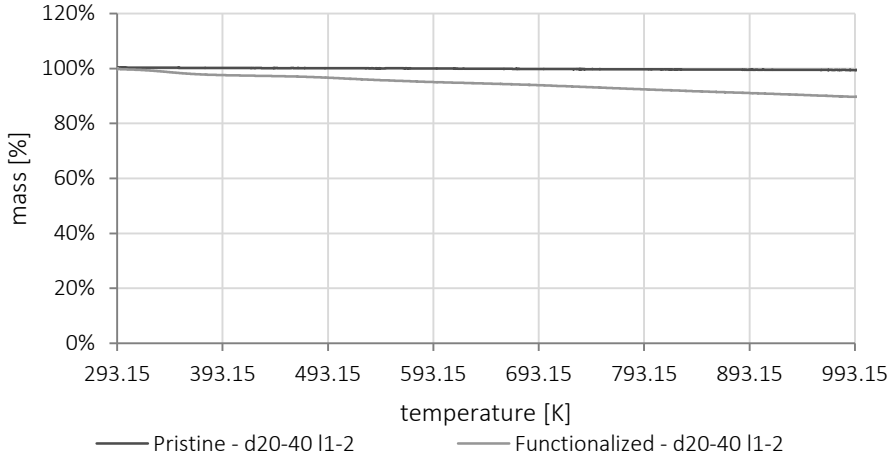


Figure E.6: TGA of functionalized and pristine MWCNTs (*d*20-40 *l*1-2).

# F. FUNCTIONALIZED MWCNTS SIZE DISTRIBUTIONS

## F.1 *d*50-80 /10-20

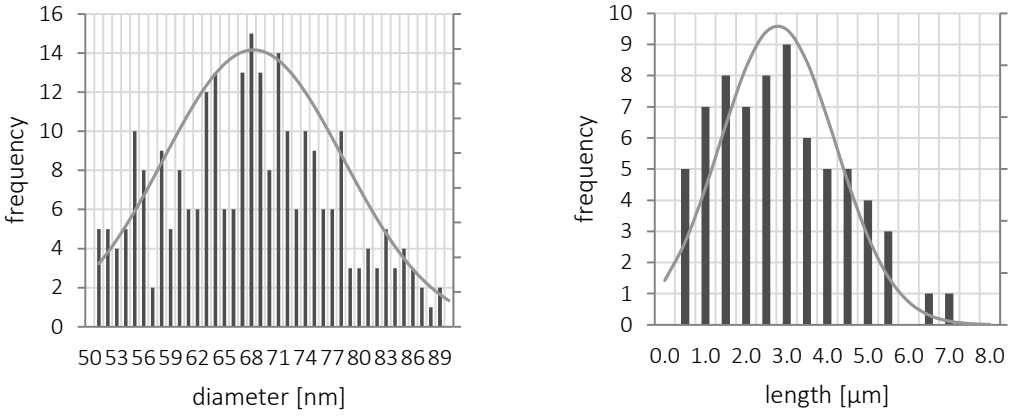


Figure F.1: Diameter and length distribution of the dispersed MWCNTs *d*50-80 /10-20.

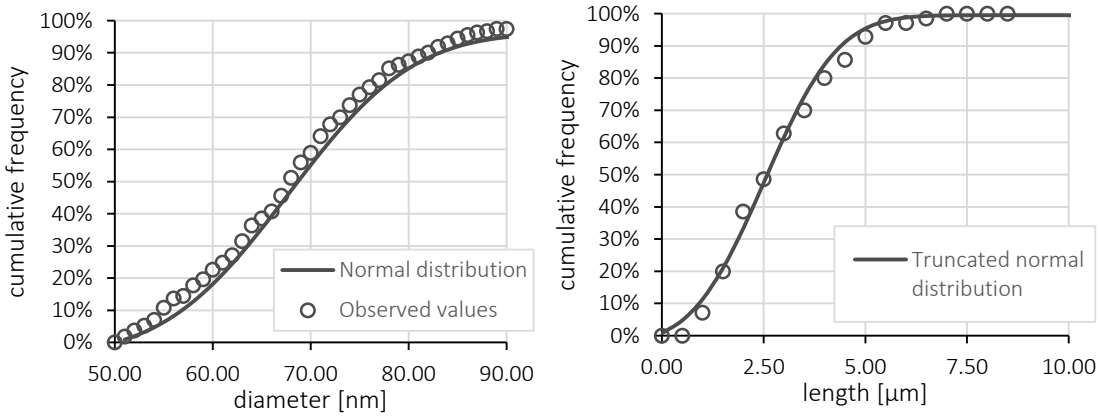


Figure F.2: Goodness-of-fit of the normal distribution to the observed values for the MWCNTs *d*50-80 /10-20.

## F.2 *d*60-100 *l*5-15

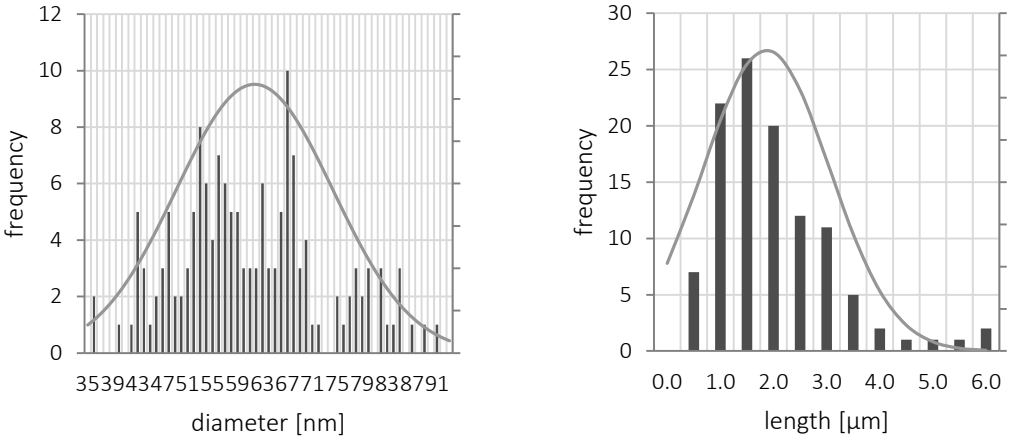


Figure F.3: Diameter and length distribution of the dispersed MWCNTs *d*60-100 *l*5-15.

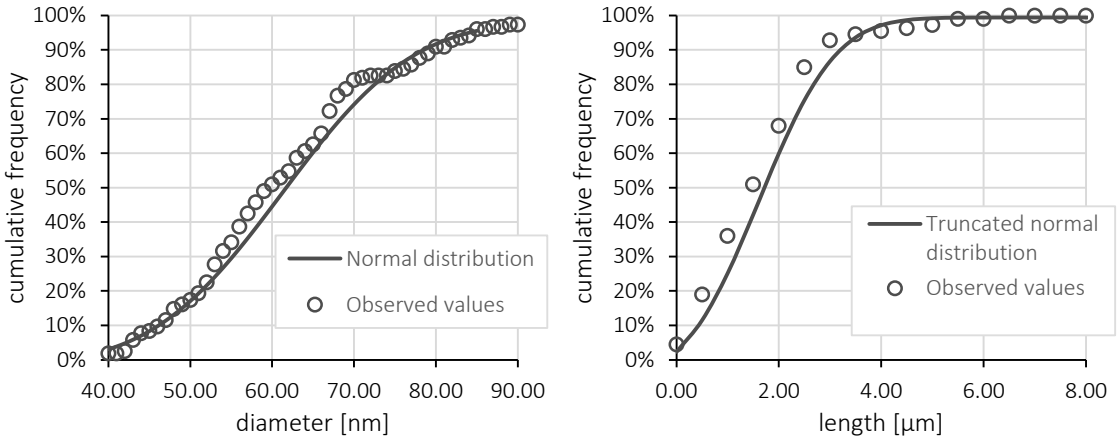


Figure F.4: Goodness-of-fit of the normal distribution to the observed values for the MWCNTs *d*60-100 *l*5-15

## F.3 *d*60-100 /1-2

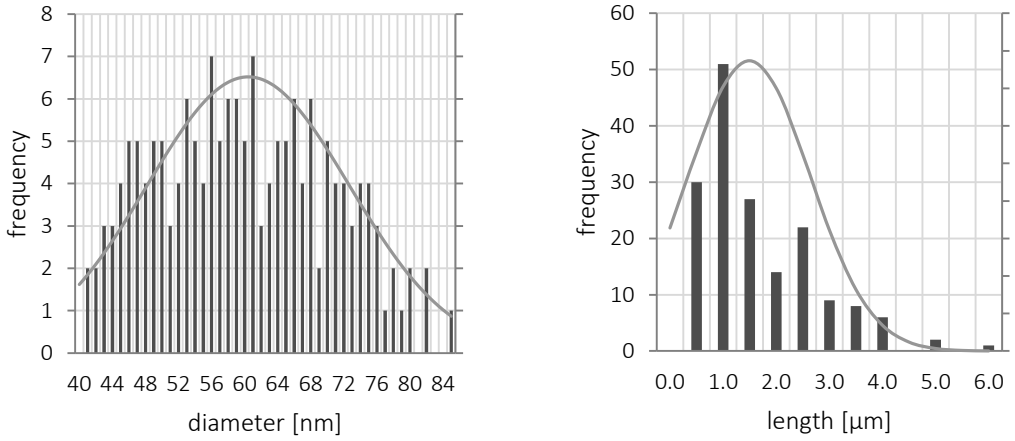


Figure F.5: Diameter and length distribution of the dispersed MWCNTs *d*60-100 /1-2.

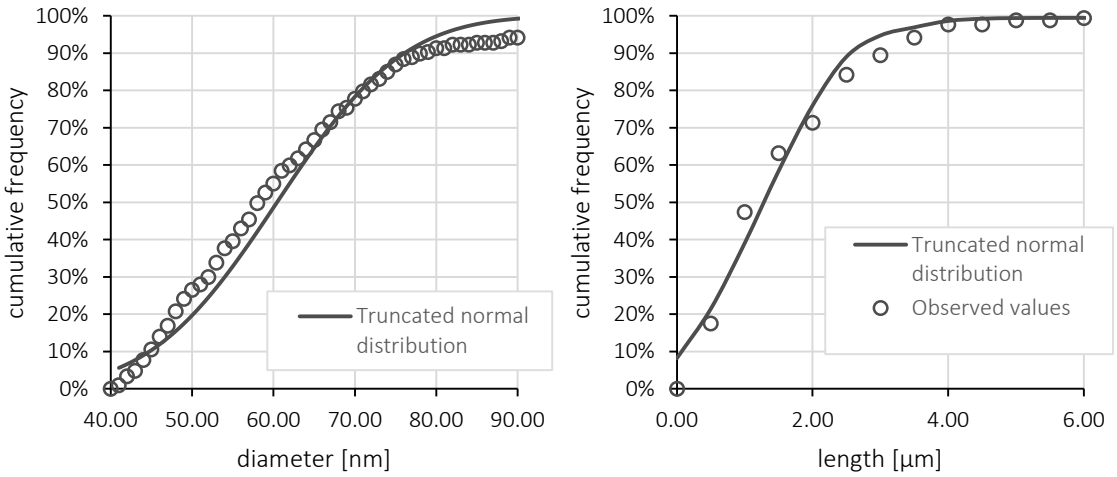


Figure F.6: Goodness-of-fit of the normal distribution to the observed values for the MWCNTs *d*60-100 /1-2

## F.4 *d*20-40 /10-30

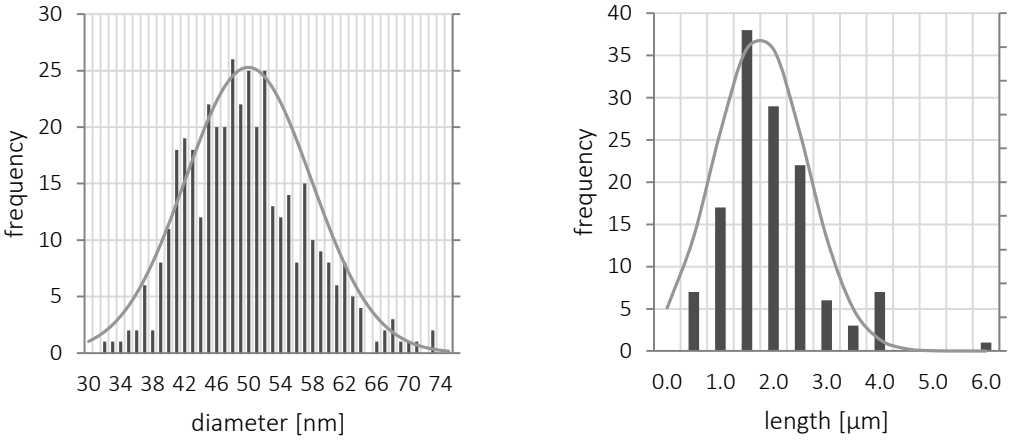


Figure F.7: Diameter and length distribution of the dispersed MWCNTs *d*20-40 /10-30.

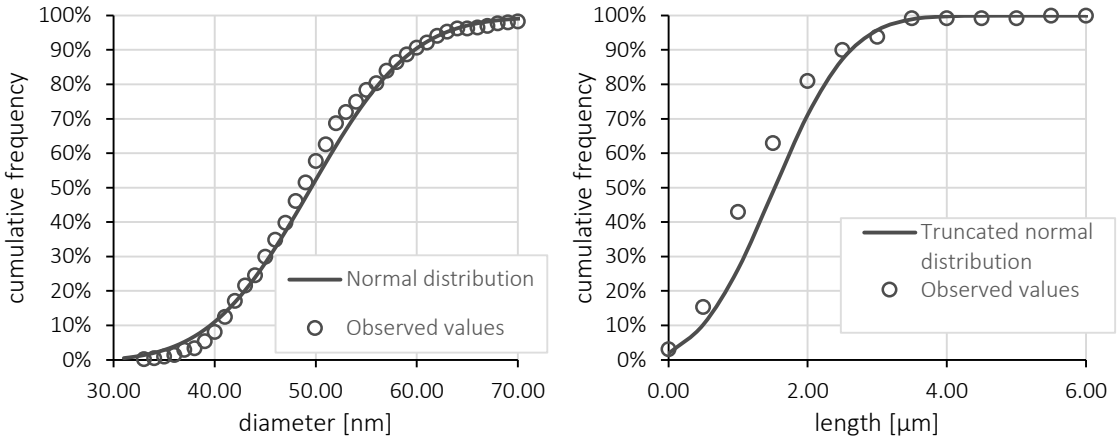


Figure F.8: Goodness-of-fit of the normal distribution to the observed values for the MWCNTs *d*20-40 /10-30

## F.5 *d*20-40 *l*5-15

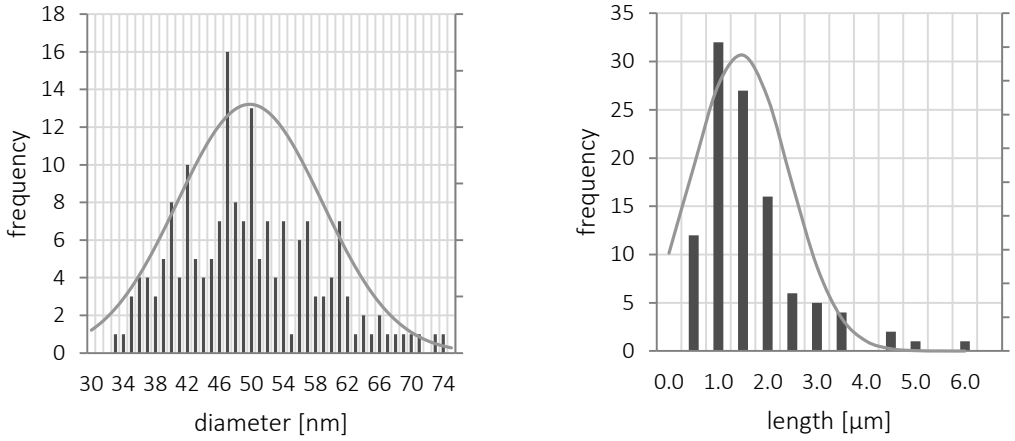


Figure F.9: Diameter and length distribution of the dispersed MWCNTs *d*20-40 *l*5-15.

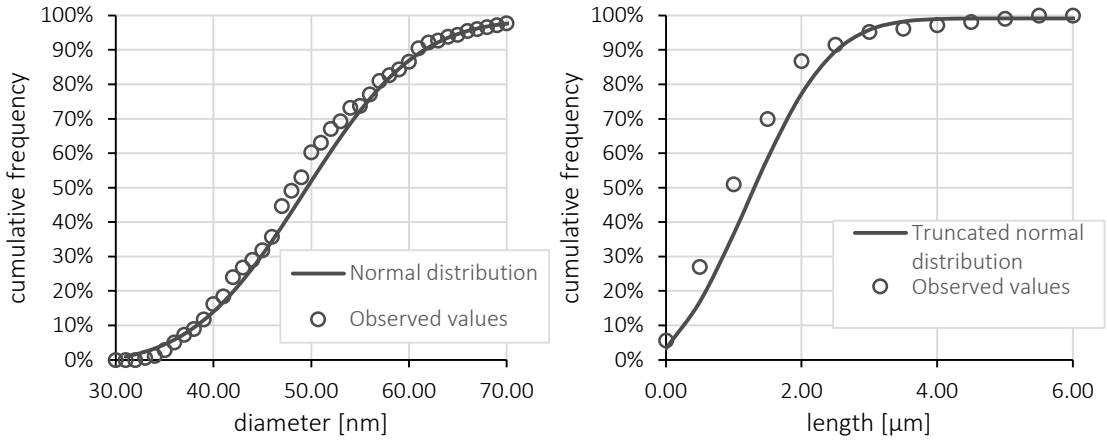


Figure F.10: Goodness-of-fit of the normal distribution to the observed values for the MWCNTs *d*20-40 *l*5-15

## F.6 *d*20-40 /1-2

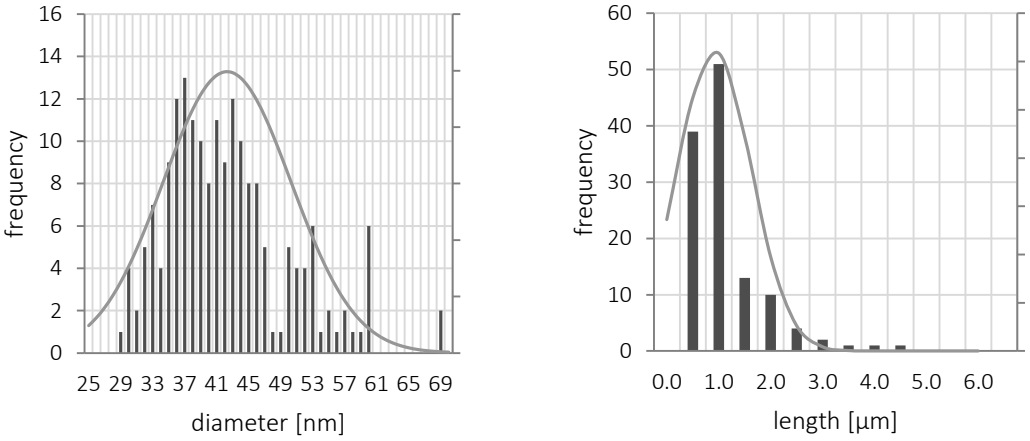


Figure F.11: Diameter and length distribution of the dispersed MWCNTs *d*20-40 /1-2.

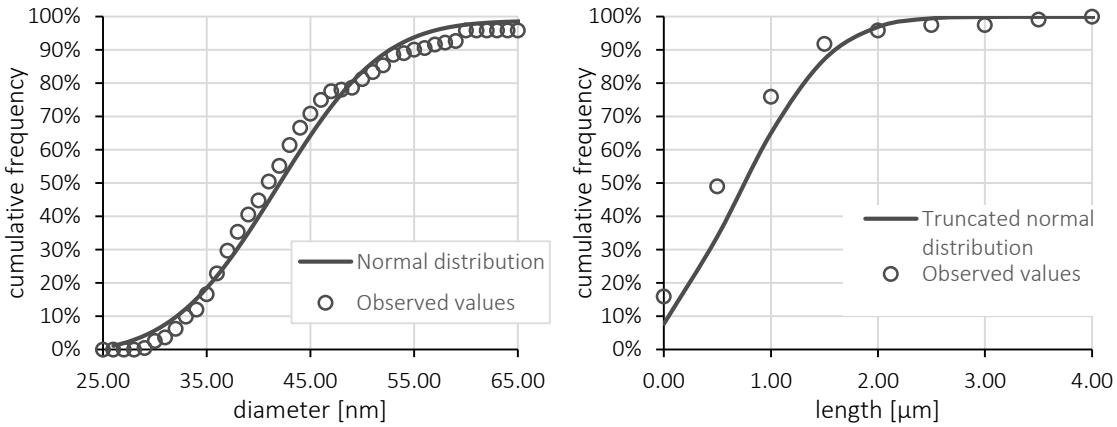


Figure F.12: Goodness-of-fit of the normal distribution to the observed values for the MWCNTs *d*20-40 /1-2

# G. PHASE SEPARATION RATE

## G.1 TRANSMISSION PROFILES

Figure G.1 shows the evolution of the transmission profiles for sample 1 at different RCF a) 500, b) 1000 and c) 2000 G.

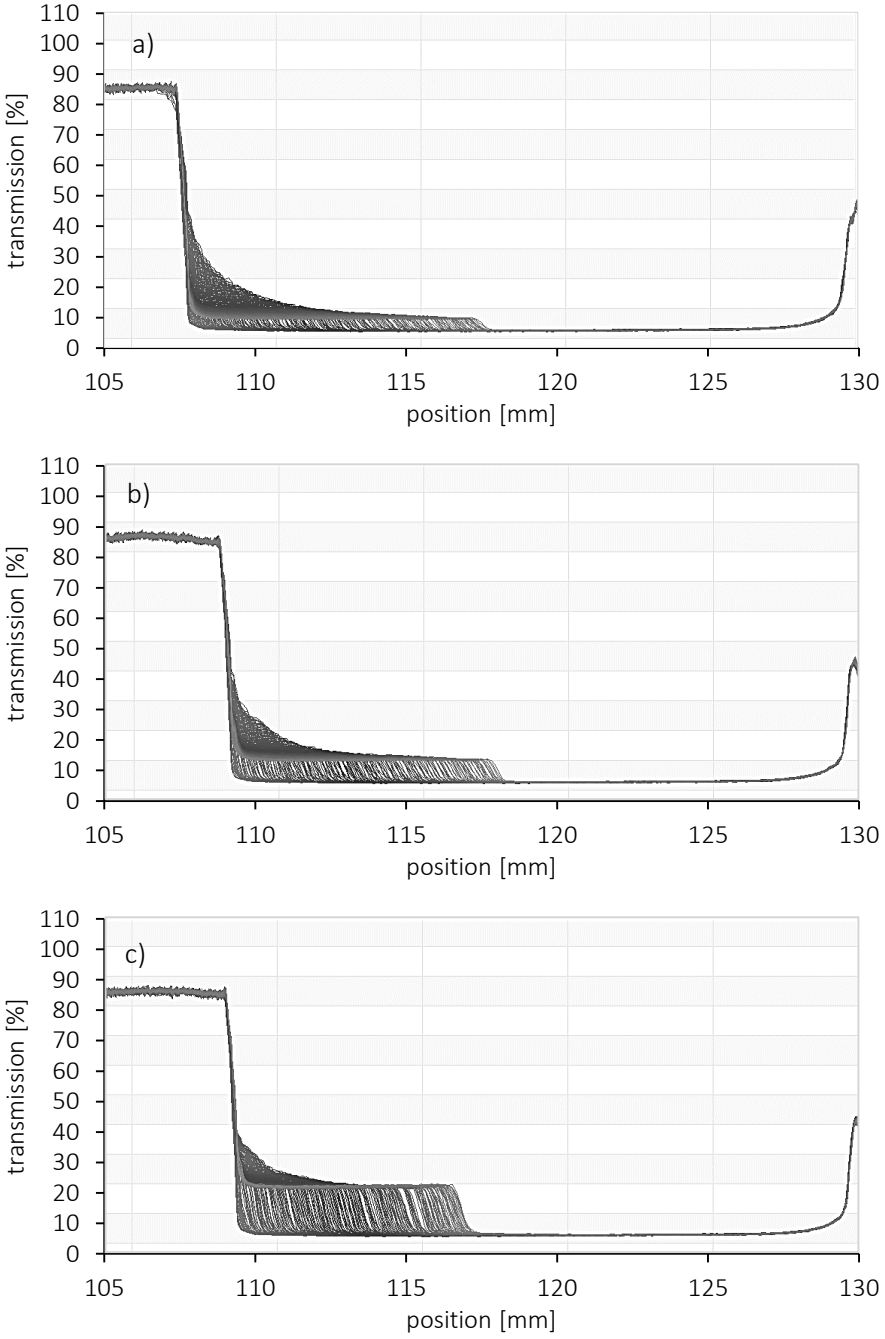


Figure G.1: Evolution of transmission profiles of sample 1 at different RCF (a) 500, (b) 1000 and (c) 2000 G.

When analysing Figure G.1, it can be stated that the light transmitted through the sample increases as the centrifugal forces rise. As it was expected, these results establish that the settling velocity increases with the rise of RCF. Furthermore, since each curve represents one measurement at a given time-step, it is found that there is a sedimentation constant profile over the whole sample. The behaviour described here for the sample 0.25%vol. *d*50-80 /10-20 in DW+30%EG was observed for all the remaining tested samples, which for simplicity are note provided in these document.

## G.2 PHASE SEPARATION RATE EVALUATION

Table G.1: Phase separation rate obtained at different RCF for the studied experimental layout.

| | | $\phi$ | Mean RCF [G] | Phase separation rate [mm/day] | Std. Dev. [mm/day] |
|---|---|---|---|---|---|
| *d*50-80 /10-20 | DW+30%EG | 0.25% | 480 | 10.8463 | 0.4477 |
| | | | 962 | 22.9743 | 1.0053 |
| | | | 1965 | 44.1845 | 1.6958 |
| | | 0.75% | 483 | 4.969 | 0.2888 |
| | | | 962 | 11.5598 | 0.5536 |
| | | | 1960 | 23.6596 | 1.0544 |
| | | 1.50% | 481 | 2.5326 | 0.2274 |
| | | | 959 | 7.7988 | 0.4839 |
| | | | 1940 | 16.6877 | 0.7701 |
| | DW+60%EG | 0.25% | 484 | 3.7888 | 0.121 |
| | | | 965 | 7.1122 | 0.4314 |
| | | | 1946 | 15.9486 | 0.228 |
| | | 0.75% | 483 | 1.6096 | 0.071 |
| | | | 956 | 3.4685 | 0.1339 |
| | | | 1934 | 7.5023 | 0.047 |
| | | 1.50% | 483 | 0.9903 | 0.0217 |
| | | | 958 | 2.5918 | 0.0675 |
| | | | 1944 | 6.546 | 0.0337 |
| *d*60-100 /5-15 | DW+30%EG | 0.25% | 490 | 20.0631 | 0.9753 |
| | | | 972 | 37.7338 | 1.6324 |
| | | | 1972 | 70.6327 | 2.0746 |
| | | 0.75% | 485 | 6.7054 | 0.4745 |
| | | | 961 | 13.5092 | 0.919 |
| | | | 1967 | 31.0144 | 1.4272 |
| | | 1.50% | 485 | 3.6989 | 0.2784 |
| | | | 963 | 7.9061 | 0.658 |
| | | | 1945 | 19.1574 | 1.2374 |
| | DW+60%EG | 0.25% | 487 | 6.2358 | 0.2942 |
| | | | 957 | 12.0562 | 0.7713 |

| | | $\phi$ | Mean RCF [G] | Phase separation rate [mm/day] | Std. Dev. [mm/day] |
|---|---|---|---|---|---|
| | | | 1964 | 25.8791 | 1.2327 |
| | | 0.75% | 485 | 1.8323 | 0.0726 |
| | | | 965 | 3.5213 | 0.2546 |
| | | | 1958 | 9.9146 | 0.2635 |
| | | 1.50% | 485 | 1.0955 | 0.0397 |
| | | | 955 | 2.0167 | 0.1201 |
| | | | 1991 | 5.8027 | 0.5761 |
| *d*60-100 *l*1-2 | DW+30%EG | 0.25% | 494 | 22.62 | 0.9207 |
| | | | 973 | 42.9807 | 1.5915 |
| | | | 1990 | 87.0119 | 1.7562 |
| | | 0.75% | 489 | 15.1711 | 0.6686 |
| | | | 970 | 29.5085 | 1.3347 |
| | | | 1966 | 60.161 | 1.7168 |
| | | 1.50% | 480 | 9.7444 | 0.5697 |
| | | | 963 | 20.2798 | 1.1789 |
| | | | 1968 | 42.9796 | 1.5992 |
| | DW+60%EG | 0.25% | 485 | 9.3639 | 0.3459 |
| | | | 962 | 18.0252 | 0.9792 |
| | | | 1977 | 27.0784 | 3.3977 |
| | | 0.75% | 484 | 4.8268 | 0.1728 |
| | | | 958 | 9.3956 | 0.4933 |
| | | | 1963 | 12.2537 | 1.4247 |
| | | 1.50% | 479 | 3.3753 | 0.1375 |
| | | | 953 | 6.1866 | 0.415 |
| | | | 1955 | 13.9818 | 0.5769 |
| *d*20-40 *l*10-30 | DW+30%EG | 0.25% | 486 | 5.2257 | 0.3081 |
| | | | 959 | 12.5428 | 0.423 |
| | | | 1970 | 33.8321 | 1.2404 |
| | | 0.75% | 519 | 1.4275 | 0.063 |
| | | | 1024 | 3.5403 | 0.1095 |
| | | | 2088 | 7.7897 | 0.2177 |
| | | 1.50% | 519 | 0.4444 | 0.0431 |
| | | | 1024 | 2.5195 | 0.0988 |
| | | | 2088 | 6.5669 | 0.1716 |
| | DW+60%EG | 0.25% | 519 | 1.6483 | 0.024 |
| | | | 1025 | 3.3722 | 0.0527 |
| | | | 2085 | 7.1297 | 0.074 |
| | | 0.75% | 519 | 0.3769 | 0.0386 |
| | | | 1025 | 1.4562 | 0.0606 |
| | | | 2085 | 4.0724 | 0.0919 |
| | | 1.50% | 519 | 0.1805 | 0.0196 |

| | | $\phi$ | Mean RCF [G] | Phase separation rate [mm/day] | Std. Dev. [mm/day] |
|---|---|---|---|---|---|
| | | | 1025 | 0.8249 | 0.0564 |
| | | | 2085 | 2.9041 | 0.1212 |
| *d*20-40 *l*5-15 | DW+30%EG | 0.25% | 484 | 5.7188 | 0.2684 |
| | | | 956 | 12.3536 | 0.5574 |
| | | | 1918 | 23.6873 | 1.3803 |
| | | 0.75% | 480 | 2.2587 | 0.1539 |
| | | | 956 | 5.2503 | 0.2909 |
| | | | 1947 | 12.1 | 0.2689 |
| | | 1.50% | 484 | 1.2614 | 0.1364 |
| | | | 950 | 3.7384 | 0.1956 |
| | | | 1945 | 9.2908 | 0.2164 |
| | DW+60%EG | 0.25% | 482 | 1.7614 | 0.1049 |
| | | | 962 | 3.7585 | 0.1346 |
| | | | 1954 | 13.0803 | 0.5775 |
| | | 0.75% | 484 | 0.2998 | 0.0598 |
| | | | 963 | 1.1879 | 0.0908 |
| | | | 1956 | 3.9072 | 0.3096 |
| | | 1.50% | 482 | 0.1542 | 0.0039 |
| | | | 961 | 0.6101 | 0.0319 |
| | | | 1954 | 2.8413 | 0.134 |
| *d*20-40 *l*1-2 | DW+30%EG | 0.25% | 488 | 4.6985 | 0.2563 |
| | | | 961 | 9.6532 | 0.4986 |
| | | | 1968 | 20.8652 | 0.9925 |
| | | 0.75% | 487 | 1.5073 | 0.1101 |
| | | | 956 | 3.1673 | 0.2472 |
| | | | 1939 | 8.4651 | 0.4323 |
| | | 1.50% | 480 | 0.5005 | 0.0173 |
| | | | 954 | 1.6277 | 0.1565 |
| | | | 1955 | 5.2228 | 0.3843 |
| | DW+60%EG | 0.25% | 482 | 1.3634 | 0.0757 |
| | | | 961 | 2.8817 | 0.1264 |
| | | | 1948 | 5.8256 | 0.3993 |
| | | 0.75% | 484 | 0.3296 | 0.0154 |
| | | | 957 | 0.9513 | 0.0895 |
| | | | 1954 | 4.2275 | 0.4269 |
| | | 1.50% | 482 | 0.1658 | 0.0169 |
| | | | 956 | 0.5295 | 0.0392 |
| | | | 1949 | 1.788 | 0.2627 |

Table G.2: Regression coefficients (*y=mx*) from the results obtained and the phase separation rate for RCF=1.

| Sample | $m_c$ | $r^2$ | Phase separation rate [mm/day] |
|---|---|---|---|
| 0.25% d50-80 l10-20 DW+30%EG | 0.0227 | 0.9974 | 0.023±0.0053 |
| 0.75% d50-80 l10-20 DW+30%EG | 0.0120 | 0.9961 | 0.012±0.0018 |
| 1.50% d50-80 l10-20 DW+30%EG | 0.0084 | 0.9757 | 0.008±0.0004 |
| 0.25% d50-80 l10-20 DW+60%EG | 0.0080 | 0.9934 | 0.008±0.0021 |
| 0.75% d50-80 l10-20 DW+60%EG | 0.0038 | 0.9944 | 0.004±0.0003 |
| 1.50% d50-80 l10-20 DW+60%EG | 0.0032 | 0.9611 | 0.003±0.0004 |
| 0.25% d60-100 l5-15 DW+30%EG | 0.0366 | 0.9912 | 0.037±0.0105 |
| 0.75% d60-100 l5-15 DW+30%EG | 0.0154 | 0.9912 | 0.015±0.0029 |
| 1.50% d60-100 l5-15 DW+30%EG | 0.0094 | 0.9780 | 0.009±0.0018 |
| 0.25% d60-100 l5-15 DW+60%EG | 0.0131 | 0.9987 | 0.013±0.0041 |
| 0.75% d60-100 l5-15 DW+60%EG | 0.0047 | 0.9525 | 0.005±0.0010 |
| 1.50% d60-100 l5-15 DW+60%EG | 0.0027 | 0.9570 | 0.003±0.0010 |
| 0.25% d60-100 l1-2 DW+30%EG | 0.0439 | 0.9995 | 0.044±0.0065 |
| 0.75% d60-100 l1-2 DW+30%EG | 0.0306 | 0.9999 | 0.031±0.0044 |
| 1.50% d60-100 l1-2 DW+30%EG | 0.0216 | 0.9985 | 0.022±0.0033 |
| 0.25% d60-100 l1-2 DW+60%EG | 0.0149 | 0.9634 | 0.015±0.0040 |
| 0.75% d60-100 l1-2 DW+60%EG | 0.0071 | 0.8909 | 0.007±0.0007 |
| 1.50% d60-100 l1-2 DW+60%EG | 0.0070 | 0.9947 | 0.007±0.0018 |
| 0.25% d20-40 l10-30 DW+30%EG | 0.0161 | 0.9556 | 0.016±0.0062 |
| 0.75% d20-40 l10-30 DW+30%EG | 0.0036 | 0.9865 | 0.004±0.0004 |
| 1.50% d20-40 l10-30 DW+30%EG | 0.0029 | 0.9181 | 0.003±0.0003 |
| 0.25% d20-40 l10-30 DW+60%EG | 0.0034 | 0.9983 | 0.003±0.0008 |
| 0.75% d20-40 l10-30 DW+60%EG | 0.0018 | 0.9219 | 0.002±0.0003 |
| 1.50% d20-40 l10-30 DW+60%EG | 0.0012 | 0.8730 | 0.001±0.0003 |
| 0.25% d20-40 l5-15 DW+30%EG | 0.0124 | 0.9980 | 0.012±0.0031 |
| 0.75% d20-40 l5-15 DW+30%EG | 0.0060 | 0.9844 | 0.006±0.0008 |
| 1.50% d20-40 l5-15 DW+30%EG | 0.0045 | 0.9581 | 0.005±0.0008 |
| 0.25% d20-40 l5-15 DW+60%EG | 0.0060 | 0.9102 | 0.006±0.0022 |
| 0.75% d20-40 l5-15 DW+60%EG | 0.0018 | 0.8906 | 0.002±0.0003 |
| 1.50% d20-40 l5-15 DW+60%EG | 0.0012 | 0.9729 | 0.001±0.0003 |
| 0.25% d20-40 l1-2 DW+30%EG | 0.0105 | 0.9971 | 0.011±0.0031 |
| 0.75% d20-40 l1-2 DW+30%EG | 0.0041 | 0.9595 | 0.004±0.0009 |
| 1.50% d20-40 l1-2 DW+30%EG | 0.0024 | 0.9061 | 0.002±0.0004 |
| 0.25% d20-40 l1-2 DW+60%EG | 0.0030 | 0.9994 | 0.003±0.0005 |
| 0.75% d20-40 l1-2 DW+60%EG | 0.0019 | 0.9708 | 0.002±0.0006 |
| 1.50% d20-40 l1-2 DW+60%EG | 0.0008 | 0.8942 | 0.001±0.0002 |

## H. APPARATUS FOR THE THERMAL CONDUCTIVITY MEASUREMENT

In Figure H.1, it is schematically represented the double jacketed bottled used for the effective thermal conductivity measurement. This enables to control the temperature of the samples through a recirculating bath, maintaining the temperature of the sample constant during the measurements. Maintaining a steady temperature is essential to the KD2-Pro measurement accuracy, the transient hot-wire, preventing free convention around the testing probe. The double jacketed bottled was fitted in a block cavity of a rigid polyurethane foam to decrease the vibrations provided by the laboratory environment.

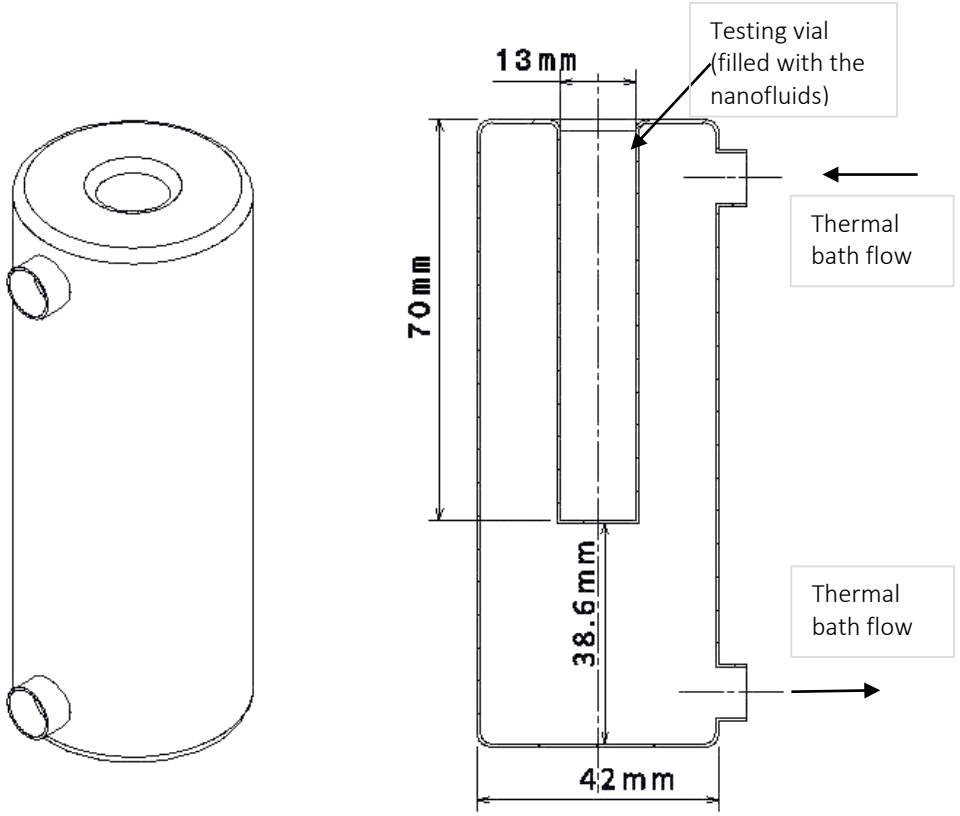


Figure H.1 Schematic illustration of the double jacketed bottled for the thermal conductivity.

# I. NANOFLUIDS EFFECTIVE THERMAL CONDUCTIVITY

## I.1 EXPERIMENTAL THERMAL CONDUCTIVITY TABLES

Table I.1: Experimental thermal conductivity of the MWCNTs based nanofluids studied. Note: the uncertainty represents the confidence interval of 95% of the mean value (Appendix D).

| MWCNTs | *d*50-80 /10-20 | | | | | |
|---|---|---|---|---|---|---|
| base fluid | DW+30%EG | | | | | |
| temp. [K] | 283.15 | 293.15 | 298.15 | 303.15 | 313.15 | 323.15 |
| 0.25% | 0.458 ± 0.004 | 0.468 ± 0.003 | 0.479 ± 0.001 | 0.477 ± 0.001 | 0.482 ± 0.002 | 0.494 ± 0.003 |
| 0.50% | 0.465 ± 0.009 | 0.473 ± 0.004 | 0.474 ± 0.001 | 0.484 ± 0.001 | 0.491 ± 0.005 | 0.501 ± 0.002 |
| 0.75% | 0.476 ± 0.005 | 0.482 ± 0.005 | 0.488 ± 0.001 | 0.491 ± 0.001 | 0.497 ± 0.002 | 0.506 ± 0.002 |
| 1.00% | 0.502 ± 0.009 | 0.501 ± 0.007 | 0.506 ± 0.002 | 0.510 ± 0.001 | 0.517 ± 0.002 | 0.525 ± 0.003 |
| 1.50% | 0.525 ± 0.001 | 0.534 ± 0.001 | 0.539 ± 0.001 | 0.543 ± 0.001 | 0.547 ± 0.001 | 0.552 ± 0.002 |

| MWCNTs | *d*50-80 /10-20 | | | | | |
|---|---|---|---|---|---|---|
| base fluid | DW+60%EG | | | | | |
| temp. [K] | 283.15 | 293.15 | 298.15 | 303.15 | 313.15 | 323.15 |
| 0.25% | 0.352 ± 0.005 | 0.353 ± 0.004 | 0.365 ± 0.001 | 0.354 ± 0.001 | 0.356 ± 0.001 | 0.357 ± 0.001 |
| 0.50% | 0.358 ± 0.005 | 0.364 ± 0.001 | 0.353 ± 0.003 | 0.367 ± 0.001 | 0.368 ± 0.001 | 0.372 ± 0.002 |
| 0.75% | 0.366 ± 0.001 | 0.373 ± 0.003 | 0.375 ± 0.001 | 0.377 ± 0.001 | 0.380 ± 0.001 | 0.382 ± 0.001 |
| 1.00% | 0.378 ± 0.005 | 0.384 ± 0.002 | 0.385 ± 0.001 | 0.387 ± 0.001 | 0.390 ± 0.001 | 0.393 ± 0.001 |
| 1.50% | 0.406 ± 0.004 | 0.409 ± 0.003 | 0.410 ± 0.004 | 0.412 ± 0.002 | 0.415 ± 0.001 | 0.419 ± 0.002 |

| MWCNTs | *d*60-100 /5-15 | | | | | |
|---|---|---|---|---|---|---|
| base fluid | DW+30%EG | | | | | |
| temp. [K] | 283.15 | 293.15 | 298.15 | 303.15 | 313.15 | 323.15 |
| 0.25% | 0.438 ± 0.003 | 0.456 ± 0.001 | 0.466 ± 0.001 | 0.462 ± 0.001 | 0.477 ± 0.002 | 0.499 ± 0.005 |
| 0.50% | 0.446 ± 0.001 | 0.459 ± 0.001 | 0.458 ± 0.002 | 0.470 ± 0.001 | 0.482 ± 0.001 | 0.499 ± 0.002 |
| 0.75% | 0.452 ± 0.001 | 0.468 ± 0.001 | 0.474 ± 0.001 | 0.477 ± 0.001 | 0.490 ± 0.002 | 0.515 ± 0.001 |
| 1.00% | 0.470 ± 0.004 | 0.479 ± 0.001 | 0.483 ± 0.002 | 0.487 ± 0.001 | 0.494 ± 0.002 | 0.505 ± 0.002 |
| 1.50% | 0.491 ± 0.005 | 0.500 ± 0.004 | 0.498 ± 0.006 | 0.501 ± 0.002 | 0.520 ± 0.001 | 0.535 ± 0.002 |

| MWCNTs | *d*60-100 /5-15 | | | | | |
|---|---|---|---|---|---|---|
| base fluid | DW+60%EG | | | | | |
| temp. [K] | 283.15 | 293.15 | 298.15 | 303.15 | 313.15 | 323.15 |
| 0.25% | 0.347 ± 0.002 | 0.353 ± 0.001 | 0.358 ± 0.001 | 0.356 ± 0.001 | 0.36 ± 0.001 | 0.364 ± 0.004 |
| 0.50% | 0.355 ± 0.009 | 0.357 ± 0.001 | 0.355 ± 0.001 | 0.361 ± 0.001 | 0.365 ± 0.001 | 0.369 ± 0.001 |
| 0.75% | 0.357 ± 0.001 | 0.362 ± 0.001 | 0.364 ± 0.001 | 0.365 ± 0.001 | 0.370 ± 0.001 | 0.376 ± 0.001 |
| 1.00% | 0.363 ± 0.005 | 0.367 ± 0.001 | 0.371 ± 0.001 | 0.371 ± 0.001 | 0.372 ± 0.001 | 0.377 ± 0.002 |
| 1.50% | 0.379 ± 0.002 | 0.383 ± 0.001 | 0.387 ± 0.001 | 0.388 ± 0.001 | 0.389 ± 0.001 | 0.393 ± 0.001 |

| MWCNTs | *d*60-100 /1-2 | | | | | |
|---|---|---|---|---|---|---|
| base fluid | DW+30%EG | | | | | |
| temp. [K] | 283.15 | 293.15 | 298.15 | 303.15 | 313.15 | 323.15 |
| 0.25% | 0.448 ± 0.012 | 0.457 ± 0.002 | 0.474 ± 0.001 | 0.470 ± 0.002 | 0.483 ± 0.002 | 0.499 ± 0.005 |
| 0.50% | 0.463 ± 0.003 | 0.470 ± 0.001 | 0.462 ± 0.001 | 0.478 ± 0.001 | 0.485 ± 0.001 | 0.492 ± 0.001 |
| 0.75% | 0.462 ± 0.001 | 0.472 ± 0.001 | 0.478 ± 0.001 | 0.482 ± 0.001 | 0.489 ± 0.001 | 0.496 ± 0.001 |
| 1.00% | 0.465 ± 0.003 | 0.471 ± 0.001 | 0.475 ± 0.001 | 0.478 ± 0.001 | 0.484 ± 0.001 | 0.493 ± 0.003 |
| 1.50% | 0.479 ± 0.001 | 0.489 ± 0.001 | 0.492 ± 0.001 | 0.496 ± 0.001 | 0.501 ± 0.001 | 0.511 ± 0.001 |

| MWCNTs | *d*60-100 /1-2 | | | | | |
|---|---|---|---|---|---|---|
| base fluid | DW+60%EG | | | | | |
| temp. [K] | 283.15 | 293.15 | 298.15 | 303.15 | 313.15 | 323.15 |
| 0.25% | 0.341 ± 0.001 | 0.351 ± 0.001 | 0.352 ± 0.001 | 0.355 ± 0.001 | 0.358 ± 0.001 | 0.365 ± 0.001 |
| 0.50% | 0.345 ± 0.001 | 0.351 ± 0.001 | 0.354 ± 0.001 | 0.353 ± 0.001 | 0.354 ± 0.001 | 0.361 ± 0.001 |
| 0.75% | 0.356 ± 0.001 | 0.361 ± 0.001 | 0.364 ± 0.001 | 0.366 ± 0.001 | 0.368 ± 0.001 | 0.378 ± 0.001 |
| 1.00% | 0.358 ± 0.001 | 0.366 ± 0.001 | 0.368 ± 0.001 | 0.370 ± 0.001 | 0.373 ± 0.001 | 0.378 ± 0.001 |
| 1.50% | 0.383 ± 0.003 | 0.387 ± 0.001 | 0.391 ± 0.001 | 0.392 ± 0.001 | 0.394 ± 0.001 | 0.398 ± 0.001 |

| MWCNTs | *d*20-40 /10-30 | | | | | |
|---|---|---|---|---|---|---|
| base fluid | DW+30%EG | | | | | |
| temp. [K] | 283.15 | 293.15 | 298.15 | 303.15 | 313.15 | 323.15 |
| 0.25% | 0.454 ± 0.002 | 0.463 ± 0.004 | 0.471 ± 0.001 | 0.47 ± 0.001 | 0.476 ± 0.001 | 0.487 ± 0.002 |
| 0.50% | 0.456 ± 0.002 | 0.464 ± 0.002 | 0.466 ± 0.002 | 0.474 ± 0.001 | 0.479 ± 0.001 | 0.490 ± 0.001 |
| 0.75% | 0.457 ± 0.002 | 0.466 ± 0.003 | 0.470 ± 0.001 | 0.474 ± 0.001 | 0.479 ± 0.001 | 0.494 ± 0.001 |
| 1.00% | 0.467 ± 0.005 | 0.479 ± 0.004 | 0.482 ± 0.001 | 0.487 ± 0.001 | 0.491 ± 0.001 | 0.502 ± 0.001 |
| 1.50% | 0.486 ± 0.005 | 0.495 ± 0.004 | 0.496 ± 0.002 | 0.502 ± 0.001 | 0.508 ± 0.001 | 0.515 ± 0.002 |

| MWCNTs | *d*20-40 /10-30 | | | | | |
|---|---|---|---|---|---|---|
| base fluid | DW+60%EG | | | | | |
| temp. [K] | 283.15 | 293.15 | 298.15 | 303.15 | 313.15 | 323.15 |
| 0.25% | 0.343 ± 0.002 | 0.346 ± 0.001 | 0.357 ± 0.001 | 0.351 ± 0.001 | 0.354 ± 0.001 | 0.363 ± 0.001 |
| 0.50% | 0.350 ± 0.006 | 0.355 ± 0.002 | 0.350 ± 0.001 | 0.359 ± 0.001 | 0.360 ± 0.001 | 0.365 ± 0.002 |
| 0.75% | 0.355 ± 0.005 | 0.359 ± 0.002 | 0.361 ± 0.002 | 0.363 ± 0.001 | 0.365 ± 0.001 | 0.368 ± 0.001 |
| 1.00% | 0.364 ± 0.002 | 0.370 ± 0.001 | 0.373 ± 0.001 | 0.374 ± 0.001 | 0.377 ± 0.001 | 0.383 ± 0.001 |
| 1.50% | 0.372 ± 0.009 | 0.379 ± 0.002 | 0.384 ± 0.002 | 0.389 ± 0.001 | 0.391 ± 0.001 | 0.394 ± 0.001 |

| MWCNTs | *d*20-40 /5-15 | | | | | |
|---|---|---|---|---|---|---|
| base fluid | DW+30%EG | | | | | |
| temp. [K] | 283.15 | 293.15 | 298.15 | 303.15 | 313.15 | 323.15 |
| 0.25% | 0.443 ± 0.003 | 0.455 ± 0.001 | 0.476 ± 0.002 | 0.464 ± 0.001 | 0.478 ± 0.001 | 0.498 ± 0.001 |
| 0.50% | 0.450 ± 0.013 | 0.473 ± 0.002 | 0.462 ± 0.001 | 0.478 ± 0.001 | 0.494 ± 0.002 | 0.506 ± 0.007 |
| 0.75% | 0.448 ± 0.007 | 0.470 ± 0.002 | 0.475 ± 0.002 | 0.481 ± 0.004 | 0.490 ± 0.003 | 0.513 ± 0.002 |
| 1.00% | 0.459 ± 0.001 | 0.477 ± 0.001 | 0.484 ± 0.001 | 0.487 ± 0.001 | 0.494 ± 0.001 | 0.51 ± 0.001 |
| 1.50% | 0.487 ± 0.002 | 0.498 ± 0.001 | 0.501 ± 0.001 | 0.508 ± 0.001 | 0.514 ± 0.001 | 0.532 ± 0.001 |

| MWCNTs | *d*20-40 /5-15 | | | | | |
|---|---|---|---|---|---|---|
| base fluid | DW+60%EG | | | | | |
| temp. [K] | 283.15 | 293.15 | 298.15 | 303.15 | 313.15 | 323.15 |
| 0.25% | 0.351 ± 0.004 | 0.353 ± 0.001 | 0.361 ± 0.001 | 0.356 ± 0.001 | 0.359 ± 0.001 | 0.368 ± 0.001 |
| 0.50% | 0.353 ± 0.003 | 0.357 ± 0.001 | 0.354 ± 0.001 | 0.363 ± 0.001 | 0.366 ± 0.001 | 0.371 ± 0.004 |
| 0.75% | 0.353 ± 0.002 | 0.360 ± 0.001 | 0.362 ± 0.001 | 0.363 ± 0.001 | 0.369 ± 0.001 | 0.379 ± 0.001 |
| 1.00% | 0.359 ± 0.001 | 0.364 ± 0.001 | 0.366 ± 0.001 | 0.367 ± 0.001 | 0.370 ± 0.001 | 0.376 ± 0.001 |
| 1.50% | 0.377 ± 0.002 | 0.381 ± 0.001 | 0.385 ± 0.001 | 0.385 ± 0.001 | 0.389 ± 0.001 | 0.398 ± 0.001 |

| MWCNTs | *d*20-40 /1-2 | | | | | |
|---|---|---|---|---|---|---|
| base fluid | DW+30%EG | | | | | |
| temp. [K] | 283.15 | 293.15 | 298.15 | 303.15 | 313.15 | 323.15 |
| 0.25% | 0.447 ± 0.002 | 0.457 ± 0.001 | 0.459 ± 0.001 | 0.464 ± 0.001 | 0.472 ± 0.001 | 0.494 ± 0.005 |
| 0.50% | 0.441 ± 0.002 | 0.455 ± 0.001 | 0.461 ± 0.001 | 0.461 ± 0.001 | 0.469 ± 0.001 | 0.489 ± 0.002 |
| 0.75% | 0.445 ± 0.003 | 0.459 ± 0.001 | 0.463 ± 0.001 | 0.466 ± 0.001 | 0.471 ± 0.001 | 0.496 ± 0.002 |
| 1.00% | 0.458 ± 0.002 | 0.470 ± 0.001 | 0.475 ± 0.001 | 0.479 ± 0.001 | 0.483 ± 0.001 | 0.501 ± 0.001 |
| 1.50% | 0.458 ± 0.004 | 0.467 ± 0.001 | 0.472 ± 0.001 | 0.476 ± 0.001 | 0.484 ± 0.001 | 0.499 ± 0.002 |

| MWCNTs | *d*20-40 /1-2 | | | | | |
|---|---|---|---|---|---|---|
| base fluid | DW+60%EG | | | | | |
| temp. [K] | 283.15 | 293.15 | 298.15 | 303.15 | 313.15 | 323.15 |
| 0.25% | 0.344 ± 0.003 | 0.350 ± 0.001 | 0.352 ± 0.001 | 0.354 ± 0.001 | 0.354 ± 0.001 | 0.360 ± 0.001 |
| 0.50% | 0.346 ± 0.001 | 0.350 ± 0.001 | 0.352 ± 0.001 | 0.353 ± 0.001 | 0.355 ± 0.001 | 0.360 ± 0.001 |
| 0.75% | 0.349 ± 0.002 | 0.351 ± 0.001 | 0.352 ± 0.001 | 0.355 ± 0.001 | 0.357 ± 0.001 | 0.362 ± 0.001 |
| 1.00% | 0.348 ± 0.001 | 0.353 ± 0.001 | 0.356 ± 0.001 | 0.358 ± 0.001 | 0.360 ± 0.001 | 0.361 ± 0.001 |
| 1.50% | 0.353 ± 0.003 | 0.354 ± 0.003 | 0.357 ± 0.003 | 0.359 ± 0.001 | 0.363 ± 0.001 | 0.369 ± 0.001 |

## I.2 Experimental thermal conductivity Figures

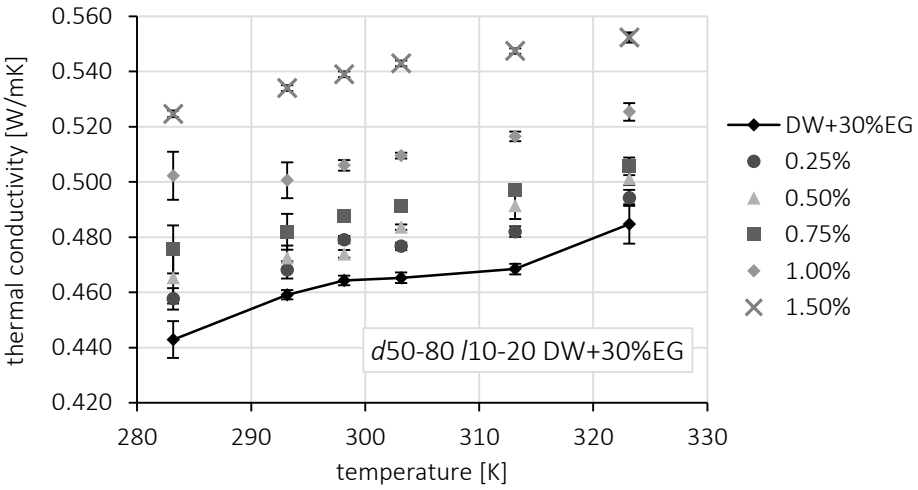


Figure I.1: Experimental thermal conductivity of the *d*50-80 /10-20 DW+30%EG.

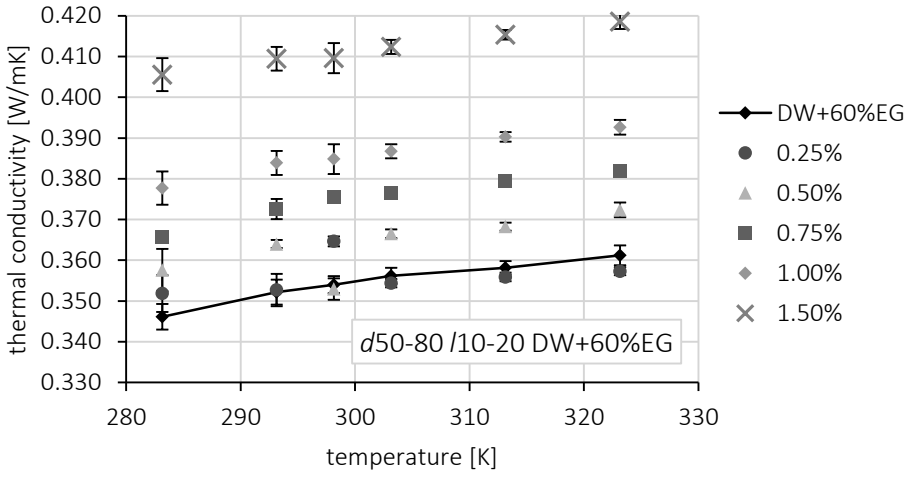


Figure I.2: Experimental thermal conductivity of the *d*50-80 /10-20 DW+60%EG.

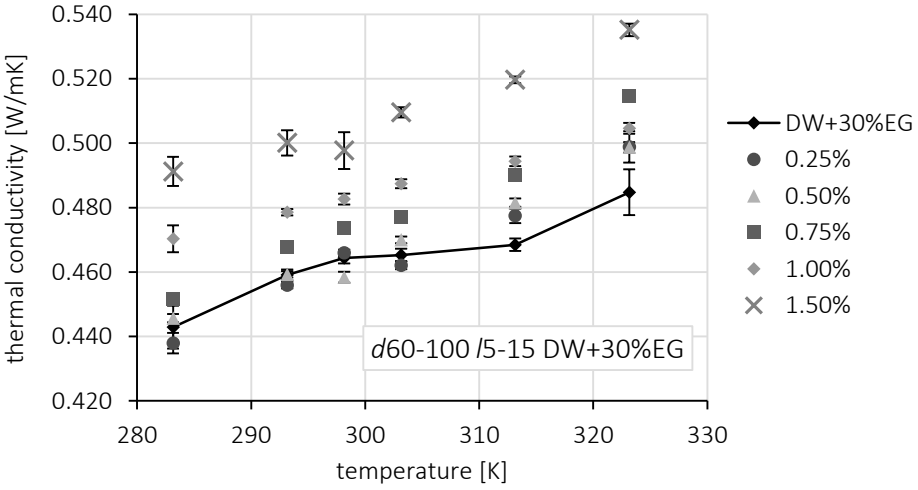

Figure I.3: Experimental thermal conductivity of the *d*60-100 /5-15 DW+30%EG.

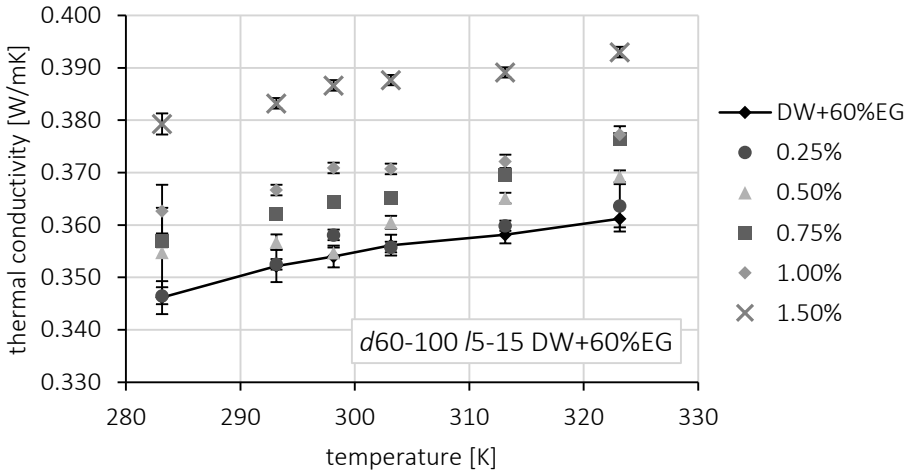


Figure I.4: Experimental thermal conductivity of the *d*60-100 /5-15 DW+60%EG.

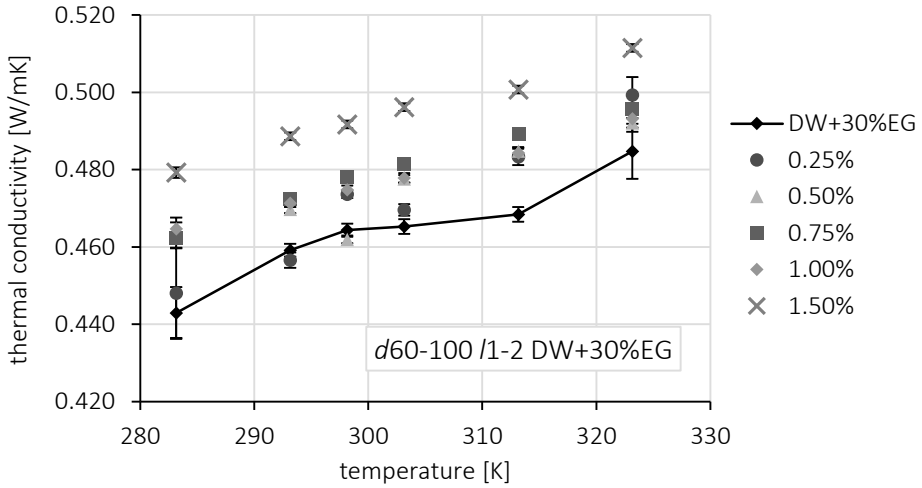


Figure I.5: Experimental thermal conductivity of the *d*60-100 /1-2 DW+30%EG.

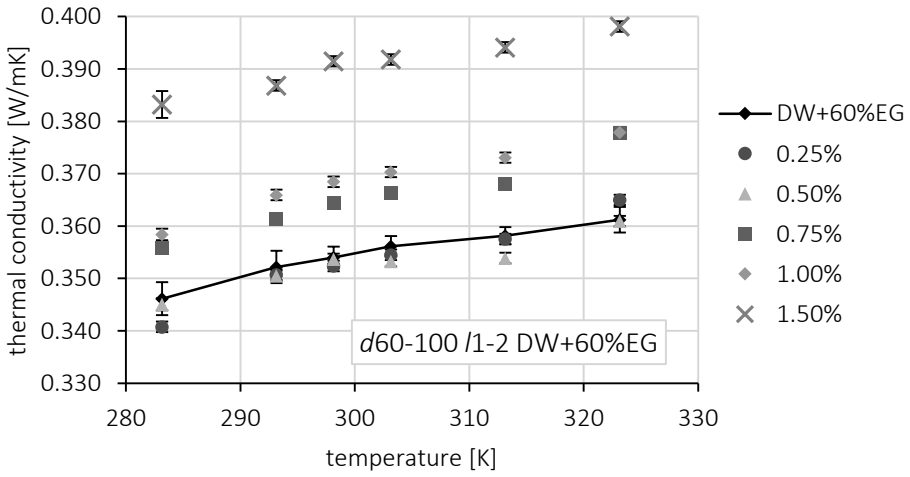


Figure I.6: Experimental thermal conductivity of the *d*60-100 /1-2 DW+60%EG.

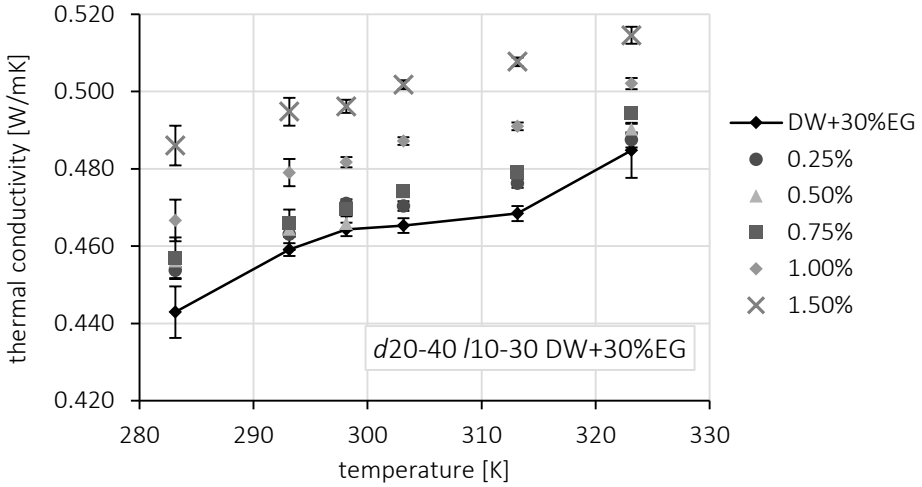


Figure I.7: Experimental thermal conductivity of the *d*20-40 /10-30 DW+30%EG.

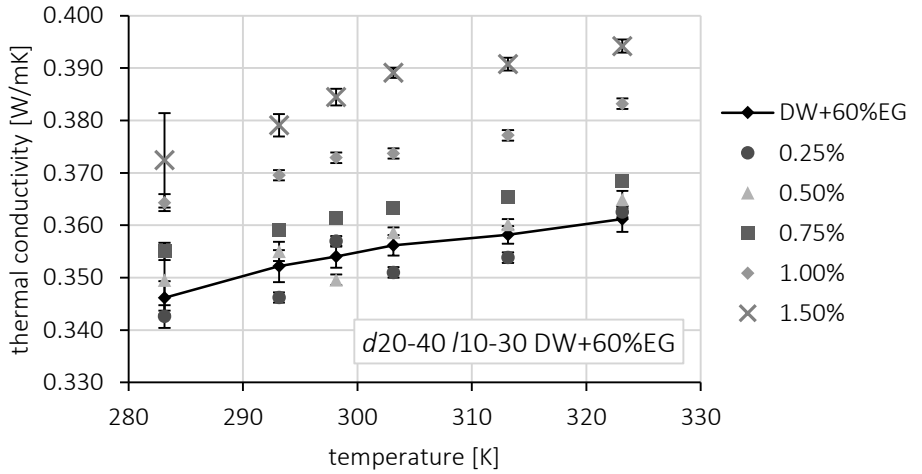


Figure I.8: Experimental thermal conductivity of the *d*20-40 /10-30 DW+60%EG.

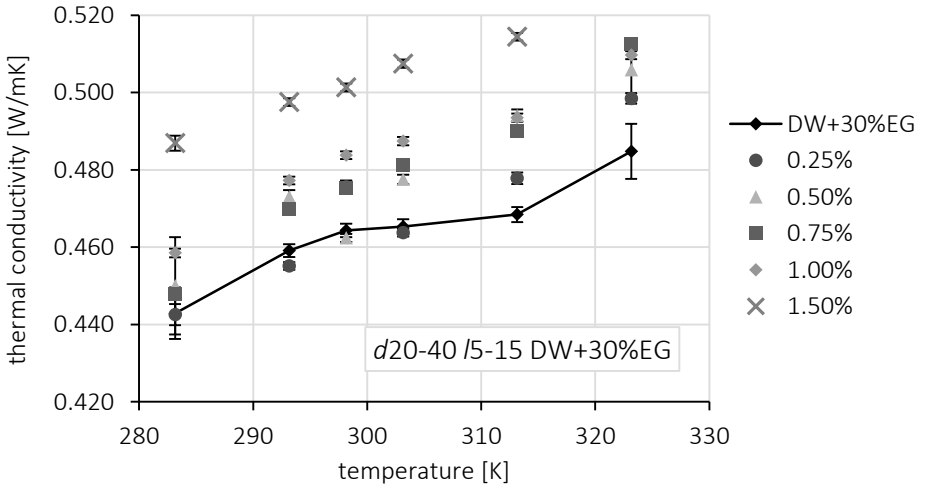


Figure I.9: Experimental thermal conductivity of the *d*20-40 /5-15 DW+30%EG.

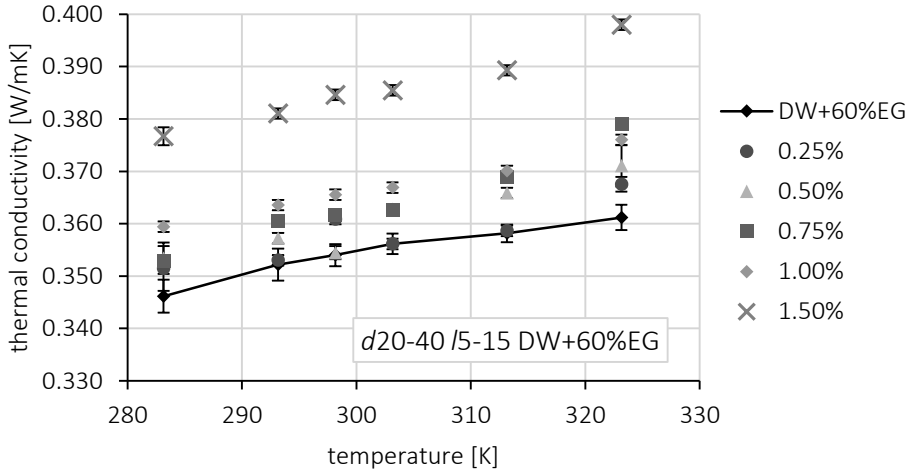


Figure I.10: Experimental thermal conductivity of the *d*20-40 /5-15 DW+60%EG.

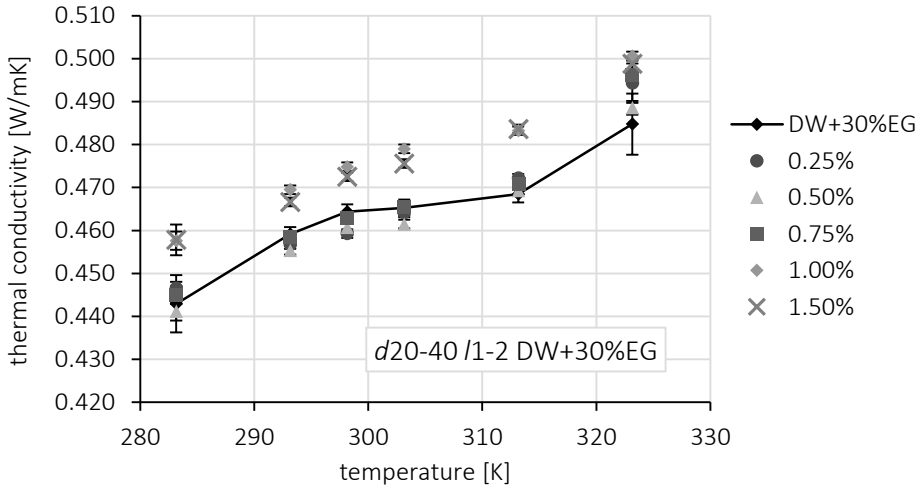


Figure I.11: Experimental thermal conductivity of the *d*20-40 /1-2 DW+30%EG.

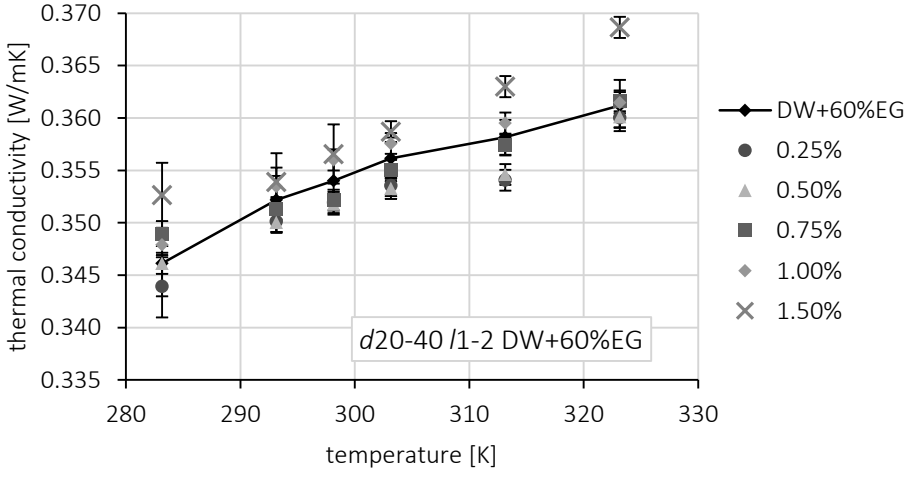


Figure I.12: Experimental thermal conductivity of the *d*20-40 /1-2 DW+60%EG.

# J. FIT TESTING OF PREDICTIVE MODELS

## J.1 PREDICTIVE MODELS CORRELATIONS

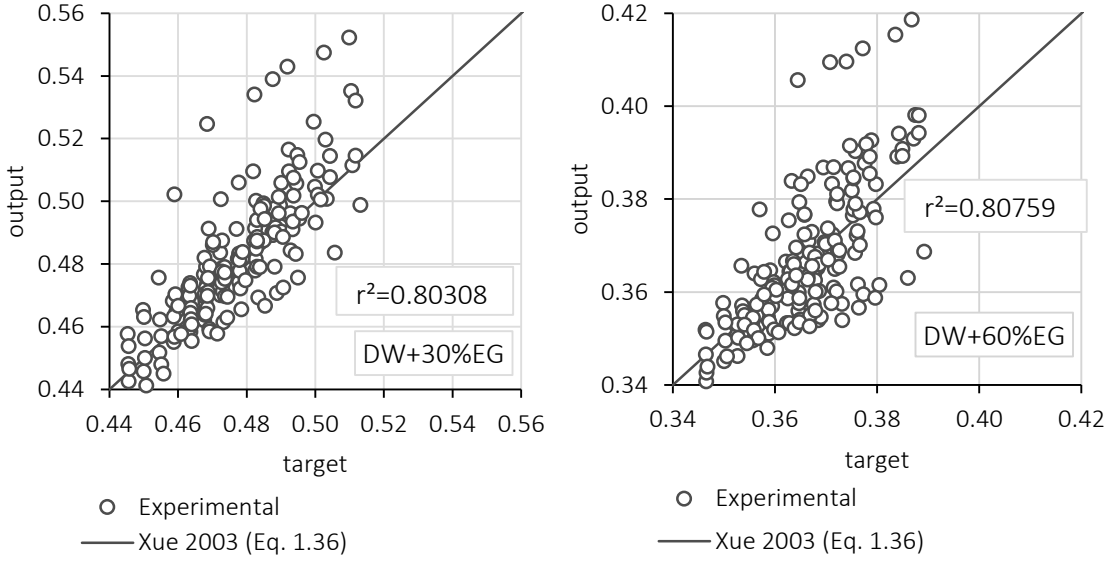


Figure J.1: Scatter chart of the Xue model and experimental data (in terms of $k_{eff}$) (XUE et al., 2003).

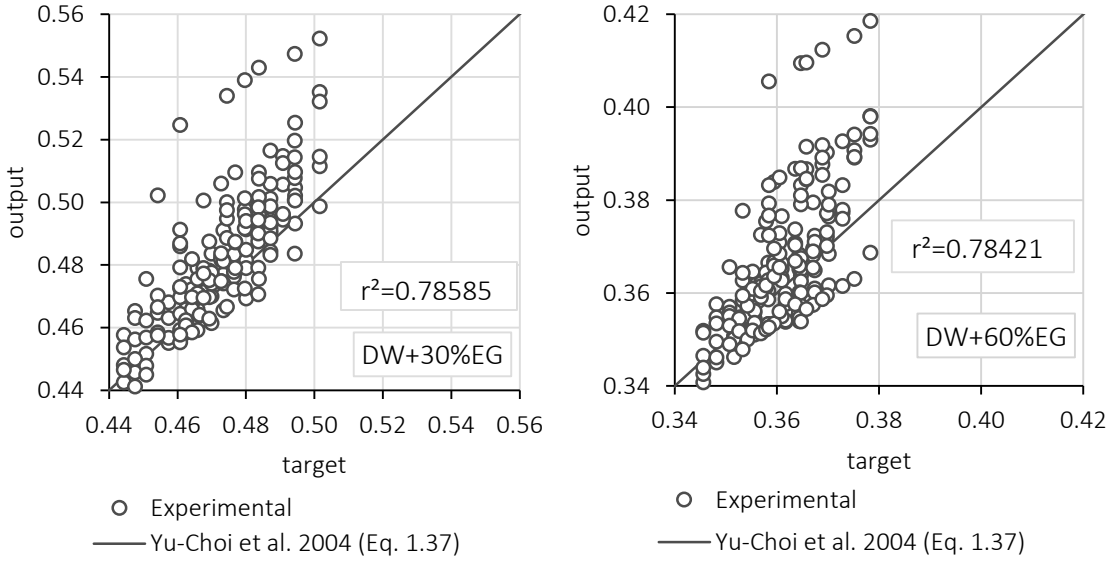


Figure J.2: Scatter chart of the Yu *et al.* model and experimental data (in terms of $k_{eff}$) (YU et al., 2004).

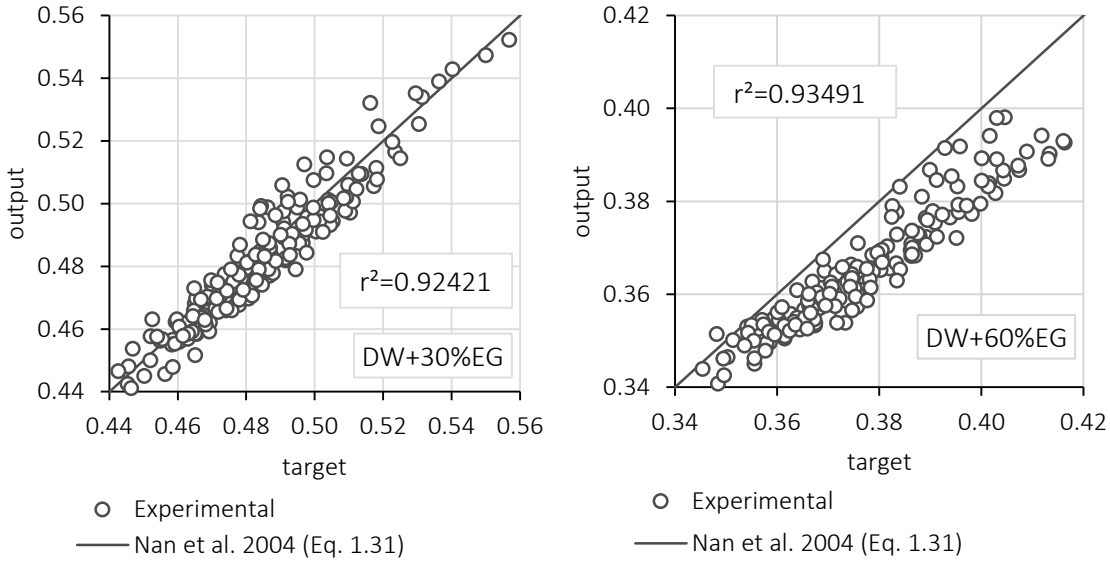


Figure J.3: Scatter chart of the Nan *et al.* model and experimental data (in terms of $k_{eff}$) (NAN et al., 2004).

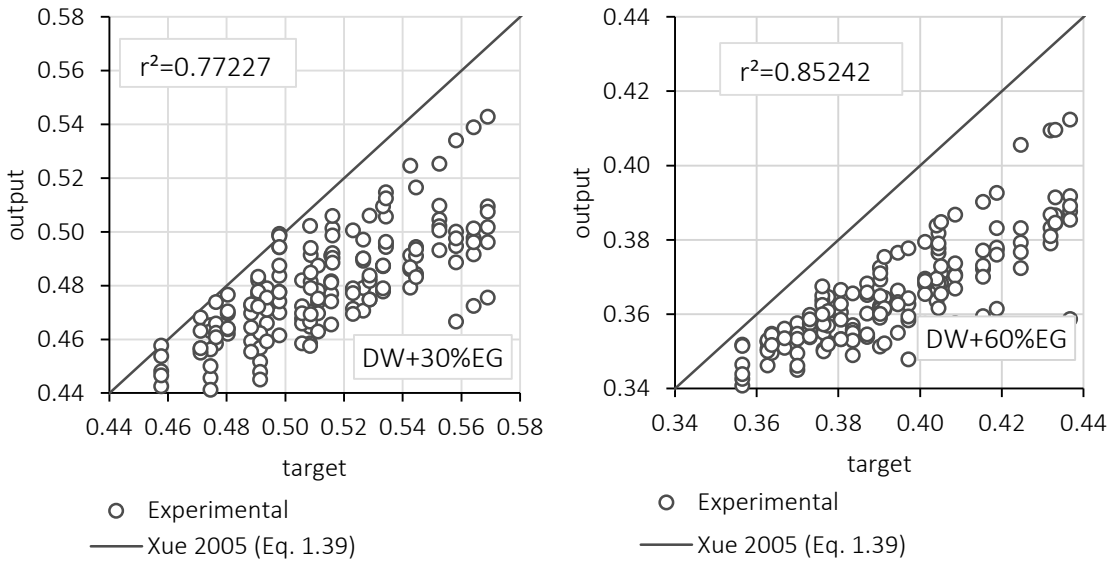


Figure J.4: Scatter chart of the Xue model and experimental data (in terms of $k_{eff}$) (XUE, 2005).

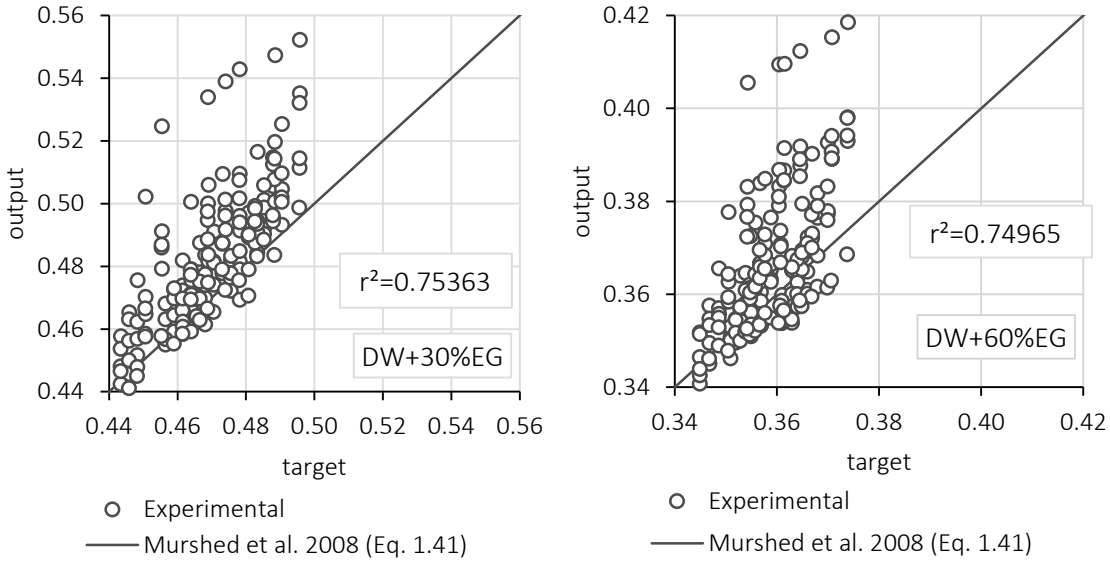


Figure J.5: Scatter chart of the Murshed *et al.* model and experimental data (in terms of $k_{eff}$) (MURSHED et al., 2008).

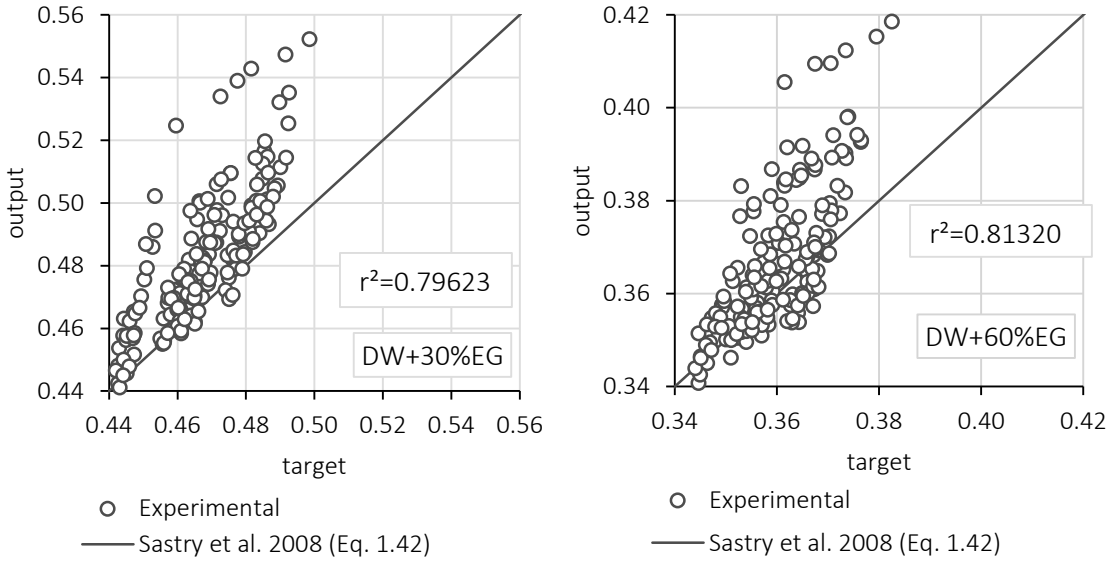


Figure J.6: Scatter chart of the Sastry *et al.* model and experimental data (in terms of $k_{eff}$) (SASTRY et al., 2008).

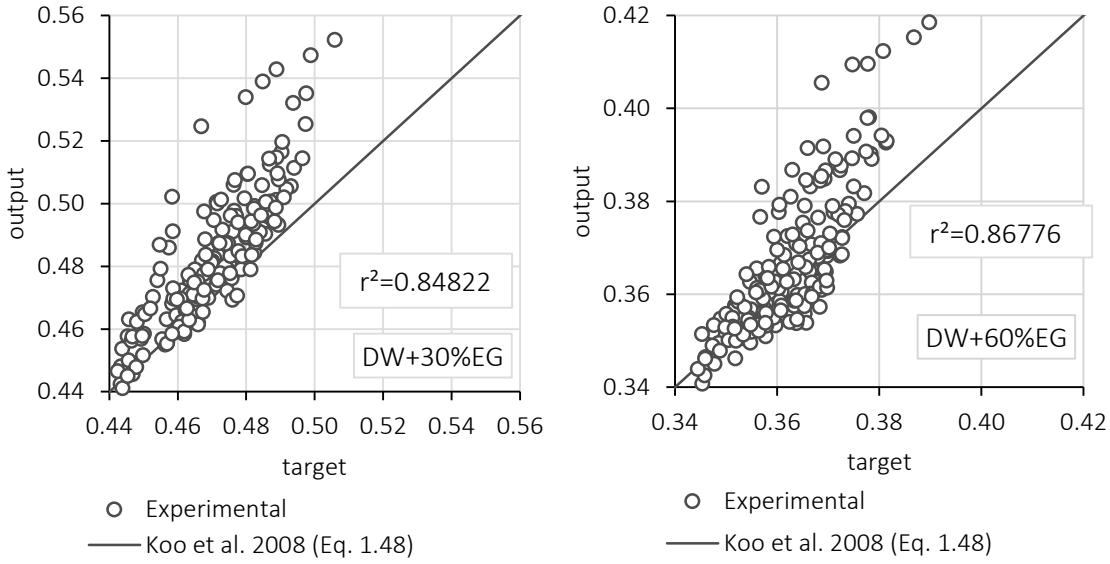


Figure J.7: Scatter chart of the Koo *et al.* model and experimental data (in terms of $k_{eff}$) (KOO et al., 2008).

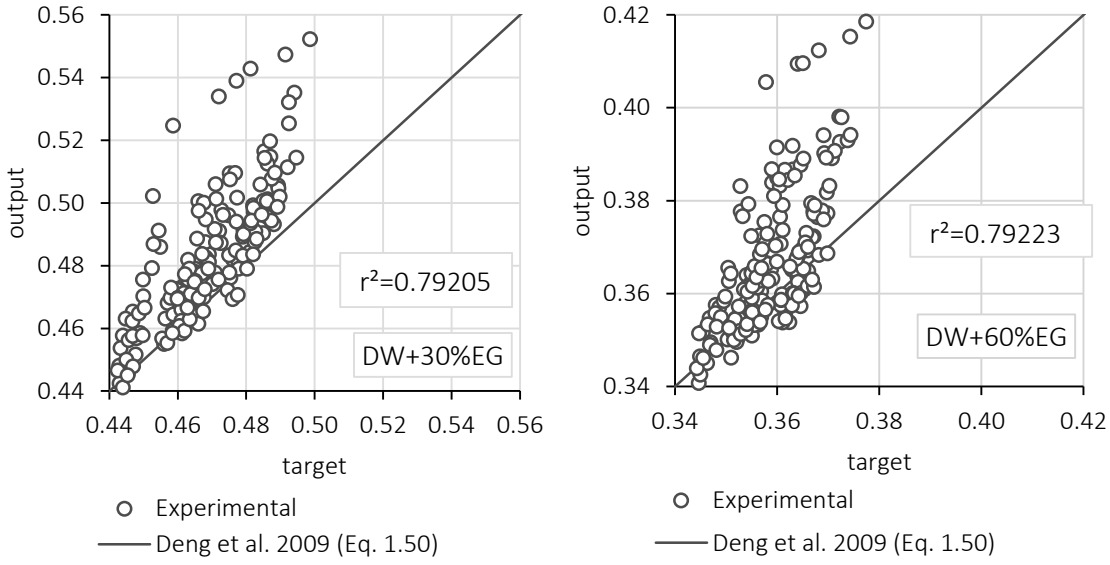


Figure J.8: Scatter chart of the Deng *et al.* model and experimental data (in terms of $k_{eff}$) (DENG et al., 2007, DENG et al., 2009).

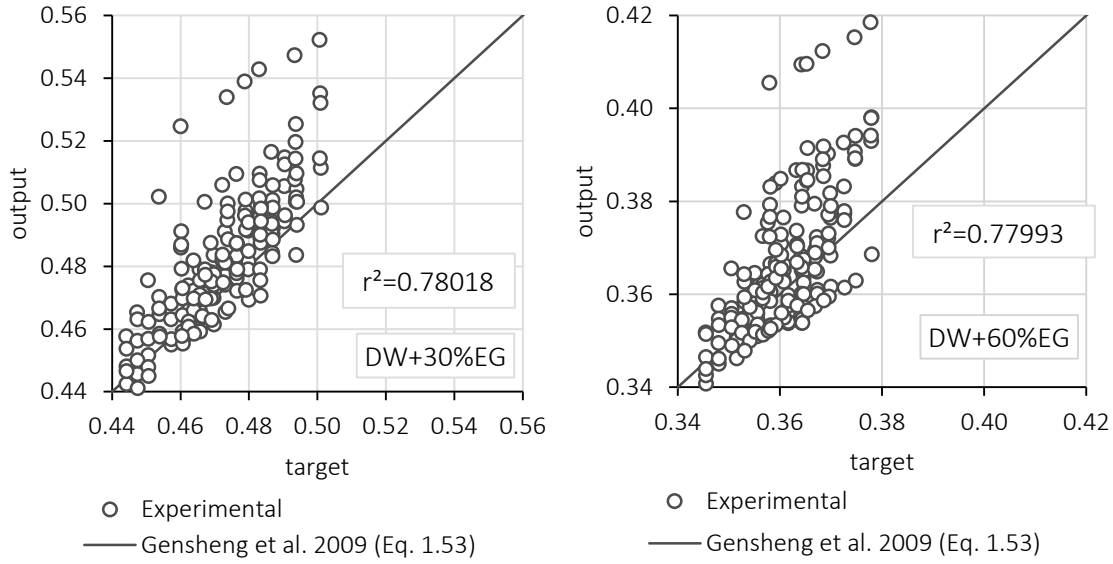


Figure J.9: Scatter chart of the Gensheng *et al.* model and experimental data (in terms of $k_{eff}$) (GENSHENG et al., 2009).

## J.2 CORRELATION ($r^2$) MATHEMATICAL FORMULATION

The correlation ($r^2$) of Pearson was used to verify the fitness of the predictive models in the Chapter 4 is given as (BEVINGTON et al., 2003, TAYLOR, 1997):

$$r^2 = \frac{\overline{xy} - \bar{x}\cdot\bar{y}}{\sqrt{\left(\overline{x^2} - \bar{x}^2\right)\left(\overline{y^2} - \bar{y}^2\right)}} \qquad \text{J.1}$$

where $x$ is the experimental thermal conductivity, and $y$ is the predicted thermal conductivity.

## J.3 FRACTIONAL ERROR MATHEMATICAL FORMULATION

A common central quantifying of the overall model performance is the measurement of the distance between the predicted value and the actual, or experimental, value $\left|y_{exp} - y_{the}\right|$. This concept is related to the "goodness-of-fit" of a model, with better models having smaller distances between predicted and observed values. However, since the values in question are very small, between 0 and 1, it is expected a very small difference for all the predictive models that difficult the readability of the performance parameters. Therefore, in a similar way to this concept, it was used the concept fractional error, a percentage variance between the predicted value and the experimental value. The fractional error ($f_{error}$), used to verify the fitness of the predictive models in the Chapter 4 is given as (BEVINGTON et al., 2003, TAYLOR, 1997):

$$f_{error} = \left| \frac{\frac{k_{eff_{exp}}}{k_{bf_{exp}}}}{\frac{k_{eff_{the}}}{k_{bf_{the}}}} - 1 \right| \quad \text{J.2}$$

where the subscripts *exp* and *the* refers to experimental and theoretical (predicted) results, respectively.

As revealed in Section 4.2,

Table 4.1, $k_{bf_{exp}} \approx k_{bf_{the}}$, with a maximum divergence of 1.2%. Taking this in consideration, the Equation J.2 can be simplified to:

$$f_{error} \approx \left| \frac{k_{eff_{exp}}}{k_{eff_{the}}} - 1 \right| \quad \text{J.3}$$

Nevertheless, Equation J.2 was used for the fraction error estimation.

## J.4 MEAN SQUARE ERROR MATHEMATICAL FORMULATION

The *mean square error* (*mse*) used also as an estimator of the accuracy of the predictive models can be expressed as (BEVINGTON et al., 2003, TAYLOR, 1997):

$$mse = \frac{1}{N} \cdot \sum_{i=1}^{N} \left( k_{eff_{exp}} - k_{eff_{the}} \right)^2 \quad \text{J.4}$$

where *N* are the number of data points (360 in this case).